MOUNTAIN-PLAINS CONSORTIUM

MPC 15-298 | R.I. Johnson and R.A. Atadero

Innovative and Economical Steel Bridge Design Alternatives for Colorado

MPC
MOUNTAIN-PLAINS CONSORTIUM

A University Transportation Center sponsored by the U.S. Department of Transportation serving the Mountain-Plains Region. Consortium members:

Colorado State University
North Dakota State University
South Dakota State University
University of Colorado Denver
University of Denver
University of Utah
Utah State University
University of Wyoming

Innovative and Economical Steel Bridge Design Alternatives for Colorado

Robert I. Johnson
Rebecca A. Atadero

Colorado State University

December 2015

Acknowledgements

The authors would like to thank the CDOT Applied Research and Innovation Branch, the Mountain Plains Consortium, and Colorado State University for providing funds that made this study possible. We are also grateful to the project study panel members: Mahmood Hasan, Trever Wang, Tawedrose Meshesha, Thomas Kozojed, and Matt Greer for their assistance with the project, and Aziz Khan for overseeing the project. We would like thank Hussam Mahmoud at CSU for his insights into steel construction and large scale laboratory tests. We wish to thank several graduate and undergraduate students at CSU who made important contributions to this project including Brianna Arthur, Omar Amini, Mehrdad Memari, Nathan Miller, and most especially Tyler Sobieck who went above and beyond in helping with the laboratory test. Finally, we would like to acknowledge the work that occurred on this project by its initial study team: John van de Lindt and Shiling Pei.

Dislcaimer

ABSTRACT

Simple-made-continuous (SMC) steel bridges are a relatively new innovation in steel bridge design. The SMC concept is a viable solution for steel bridges to recover market share of the bridges constructed in the United States. The majority of SMC bridges currently in use are constructed with concrete diaphragms. This work presents the results analysis and testing of this SMC connection scheme using steel diaphragms. A bridge of this type was constructed by the Colorado Department of Transportation in 2005 and its connections serve as the basis for the research presented herein. Preliminary numerical analysis was performed by hand; this analysis discovered potential design flaws in the current bridge connection. Subsequent numerical analysis using Abaqus finite element analysis software provided results that were indecisive in regard to the flaws found in the hand analysis. The finite element analysis did provide valuable insight into some of the connection behavior. Physical testing was subsequently performed on a full size model of the connection, which verified that there were design flaws in the original design. The results of analysis and physical testing provided information necessary to correct the design flaws and data required for the development of a design methodology for the connection type.

TABLE OF CONTENTS

LIST OF TABLES

LIST OF FIGURES

EXECUTIVE SUMMARY

This executive summary of the Innovative and Economical Steel Bridge Design Alternatives for Colorado report presents an overview of the project, which is an extension of previous work performed by researchers at Colorado State University investigating Simple-Made-Continuous (SMC) construction for steel bridges. The current work investigates the option of using steel-diaphragms at the SMC connection in place of concrete diaphragms, which are favored in other steel SMC research.

1. Introduction

Provides a summary of previous work performed for CDOT and an introduction to the SMC concept. The SMC concept involves placing simple span, cambered steel girders between piers, providing additional longitudinal top reinforcing for the slab over the support piers, and casting the composite deck slab. Once the concrete slab achieves strength, the additional top reinforcing allows the bridge girders to act as continuous for all superimposed loads, both dead and live.

2. Literature Review

Provides a review of literature related to the SMC concept, including summaries of steel SMC concepts presently in use and an inventory by type. Also presented are findings of other researchers regarding the SMC behavior of various connection compression and tension transfer mechanisms. The included research consists of both analytical analysis with finite element software and actual full scale physical testing.

3. Description of Study Bridge and Preliminary Calculations

The bridge carrying Colorado State Highway 36 over Box Elder Creek, an SMC bridge with steel diaphragms, is the subject of the study. In this section the bridge is described and preliminary hand and computer calculations are used to analyze the bridge. The computer calculations addressed the various AASHTO truck loadings and provided the final maximum ultimate design moments for the SMC bridge design. The SMC connection was then evaluated by simple hand calculations for its ability to carry the maximum SMC negative moment. During the hand analysis of the welds between the girder bottom flange and the sole plate, it was discovered that these welds were possibly inadequate for the AASHTO "Design Tandem" truck load.

4. Finite Element Modeling

In order to study the behavior of the selected bridge, the SMC connection was analyzed using Abaqus finite element analysis software. Prior to the analysis, a sensitivity analysis was performed to determine the most efficient element and material modeling of the various elements of the connection. While not an exact match to the physical test, the results of the analysis provided valuable insight into the behavior of various components of the connection, including the shear lag in the slab reinforcement and potentially high stresses in the sole plate.

5. Laboratory Testing of SMC Connection

A full scale physical test of the full connection and partial girders was performed in the structural lab at the Colorado State University Engineering Research Center. Loads were applied by the use of hydraulic actuators at the ends of two cantilever beams to simulate a negative moment at a center support. The test not only verified that the weld to the sole plate was below its required strength, but also that the sole plate

was inadequate for the applied axial load and its resulting moment. The results were compared to the finite element analysis and several aspects of the behavior compared well.

6. Parametric Study

A parametric study was performed to extend the range of the study to bridge girders with a span range of 80 feet to 140 feet, with girder spacing ranging from 7 feet 4 inches to 10 feet 4 inches and slab thicknesses varying from 8 inches to 9 inches. The results of this study were subsequently used in the development of a design methodology and design equations for the connection.

7. Design Recommendations for Future SMC Connections with Steel Diaphragms

In the original connection, the main elements resisting the SMC moment were the bottom flange, weld to the sole plate and sole plate for the compression component and the SMC top reinforcing steel for the tension component of the SMC moment. A simple method is developed to determine the required quantity of SMC reinforcing and subsequent equations to verify the capacity of the final connection. Also provided are cost comparisons showing conclusively that the subject connection not only creates a more economical steel bridge than similar schemes using concrete diaphragms, but that it is also more economical than conventional spliced fully continuous steel bridges.

8. Results of National Survey

At the request of CDOT, a survey of other states' DOTs was performed to investigate how they were using SMC construction. A total of 10 questions relating to SMC design were asked and the results of these surveys tabulated and discussed. Very few states are using steel SMC construction.

9. Conclusion

A summary of the benefits of the SMC concept and, in particular, the benefits of SMC bridges using steel diaphragms in lieu of concrete diaphragms are presented. It is readily apparent that SMC bridges are more economical and safer to construct; also, it is shown that SMC bridges with steel diaphragms are more economical and quicker to construct than those constructed with concrete diaphragms. Recommendations for further research into SMC behavior are presented. Based on the findings of the physical test, implementation steps are presented to address possible distress in the SH 36 bridge over Box Elder Creek.

1. INTRODUCTION

The popularity of pre-stressed concrete for bridge construction in comparison to steel may be largely attributed to the lower cost of pre-stressed concrete bridges. The impetus for the development of the Simple Made Continuous (SMC) concept came from the desire for steel bridges to be able to compete economically against precast/pre-stressed concrete bridges for medium to long girder spans.

Typically, continuous bridges are more economical than simple span bridges because they develop smaller positive interior span moments due to the negative moments at the continuous ends. Continuous bridges can also be attractive because they reduce the number of joints in a deck, which can have a positive impact on bridge durability. Conventional continuous steel bridges are non-competitive relative to continuous pre-stressed concrete bridges primarily due to the construction technique. The steel continuity connections must be made in the field, and these connections typically occur in portions of the spans over the bridged roadway, thus requiring shoring of the girders over the roadway until the continuity connection (welded or bolted) can be made. SMC steel bridge construction is able to overcome these limitations, and thus represents an innovation that may help make steel girder bridges competitive with precast concrete bridges, possibly increasing the economy of both construction techniques in Colorado.

In brief, SMC connections behave as simple or hinged connections for permanent dead load and as continuous connections for live loads and superimposed dead loads. The typical method of obtaining continuity involves placing steel girders and formwork for cast-in-place concrete slabs. Reinforcing steel for slabs, which spans perpendicular to the beams, is installed and additional top reinforcing oriented parallel to the girders is placed over the girder ends that are to act continuously. Once the concrete has set, negative moment continuity exists and is taken through the composite slab and various means of steel girder attachments. The overall concept results in lighter weight steel girders and a simplified construction process.

In the past 10-plus years, considerable research has gone into the development of details for SMC bridge connections for steel girder bridges. As described in the literature review of this report, extensive research has been conducted at the University of Nebraska, Lincoln on a concrete diaphragm-based design, and several bridges have been built using variations on that design in Nebraska and other states.

A past CDOT-funded research project on SMC construction (van de Lindt et al. 2008) was intended to provide designers a tool to rapidly estimate the cost of steel for a steel SMC bridge. This project focused on sizing of the girders and developed software that is able to output the lightest steel wide flange shape given various bridge dimensions such as span length, bridge width, and overhang. This project also developed design charts for one, two, and three span SMC bridges with various deck widths and calculated the cost of the structural steel per square foot of bridge deck.

The present study extends the work of the previous project to further develop steel SMC technology for use in Colorado and other states. As the continuity connection at the pier is a vital part of a successful SMC design, this report focuses on the findings of a numerical and experimental evaluation of an SMC connection using steel diaphragms rather than the concrete diaphragm that has been previously investigated at the University of Nebraska. This type of connection was used by CDOT for the SH 36 bridge over Box Elder Creek constructed in 2005 and 2006. The report includes the results of the evaluation, recommendations for enhancing the connections on the bridge over Box Elder Creek, and design guidance for future connections of this type. The report also provides findings from a survey about steel SMC construction that was completed in 2010.

1.1 Report Organization

The content of this report is organized as follows:

Section 2. Literature review focusing on continuity connection details for steel SMC bridge construction

Section 3. Description of the Box Elder Creek bridge, evaluation objectives, and preliminary analysis of the steel diaphragm SMC connection used on this bridge

Section 4. Finite element modeling of the steel diaphragm SMC connection

Section 5. Experimental testing of the steel diaphragm SMC connection

Section 6. Parametric study considering the steel diaphragm SMC connection for different bridge configurations

Section 7. Design recommendations for future steel diaphragm SMC connections

Section 8. Findings from survey on SMC construction

Section 9. Conclusion

2. LITERATURE REVIEW

Literature related to SMC construction and the continuity connection at the pier in particular was reviewed and is summarized here as it relates to 1) the concept of simple made continuous, 2) general research to develop the SMC concept, 3) findings at University of Nebraska – Lincoln, including details of finite element analysis (FEA) modeling and physical testing performed in the lab, 4) existing code requirements for design of affected elements, 5) previous physical testing performed in the field on completed structures, and 6) a review of bridge deck structures known to have been constructed with the SMC concept.

2.1 Simple Made Continuous Concept for Steel Bridges

The earliest mention of the idea of SMC found was in a paper that discussed the integral construction of steel girders into concrete piers to achieve continuity after the concrete had attained its design strength (set). The reasons for the continuity, however, were not for using smaller steel sections but for increased seismic strength of the completed structure. The details of this methodology were extremely complex and correspondingly expensive to construct and it is therefore only mentioned in a historic context (Nakamura, 2002).

While not in widely distributed literature, a master's thesis (Lampe, 2001) presented a study of steel bridge economics and presented a preliminary analysis and physical testing of a simple made continuous bridge girder connection. Based on this research, it is believed that steel bridges made with the SMC concept could be competitive with precast concrete bridges. Details of the testing will be discussed in Section 2.3.2.

The earliest publicly published relevant mention of the SMC concept as used in the United States was in, appropriately enough, "Roads and Bridges" (Azizimanini & Vander Veen, 2004) , in which the following benefits of the SMC concept were presented:

- Negative moments at piers are less for SMC than for beams continuous for all loads, dead and live.
- Mid-span moments will be larger due to locked-in dead load moment from simple beam action; however, this balances positive and negative moments better than standard continuous beams in which negative moments may be significantly larger than positive moments.
- Eliminates welded and/or bolted field splices altogether.
- Moment of inertia of the beam is increased after composite action is invoked for both positive and negative bending.

The same article also points out the following improvements in the fabrication and erection processes of the SMC concept:

- Shop detailing of the bridge girders is simplified as no flange holes are necessary for splice plates, and no detailing of the splice plates themselves is required.
- Smaller and hence cheaper cranes will be required for bridge erection since they won't be required to reach over the roadway to support partial span girders.
- Time savings in overall erection compared to conventional continuous girders, which are typically constructed with bolted field splices. These splices are generally made at low stress locations close to the points of inflection of the continuous girders.
- Significantly less disruption of traffic on existing roadways since splices are constructed over the bridge piers.

2.2 Research to Develop Steel SMC Connections

This work was done at the University of Nebraska - Lincoln and is described in a series of theses and reports Lampe (2001), Farimani (2006), and Niroumand (2009). The goals of this research were to:

- Work toward the development of an economically competitive concept for steel bridges to compete against pre-stressed concrete bridges.
- Comprehend the force transfer mechanism at the SMC girder connection
- Develop a mechanistic model to predict the behavior of the connection under design loads and a design methodology.

All specimens considered had concrete diaphragms at the supports based on the thought that since these were specified in NDOR standards (NDOR, 1996) for SMC bridges constructed with precast/pre-stressed girders, they should also be used on steel girder bridges.

Research started with Lampe (2001) who modeled and tested the connection shown in Figure 2.1. Lampe started with SAP2000 modeling of the connection shown along with two other variations (Lampe N. J., 2001). The results of the SAP2000 analysis were very approximate and will not be discussed further except to say:

- This was a quick way to obtain preliminary results and fine tune an analytical model before going into a full finite element analysis with more complex software such as ANSYS or ABAQUS
- A full span analysis was performed in order to determine initial rotations induced by the dead load on the simple spans, which were then used in the physical model.

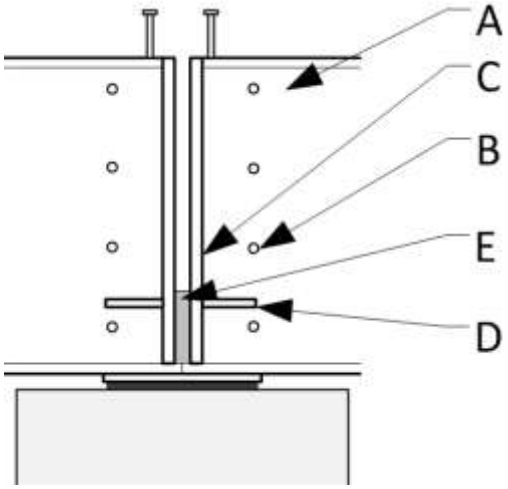

Legend:
A = Girder
B = Web openings for reinforcing
C = End vertical stiffener plate
D = Horizontal stiffener plate
E = Concrete compression block

Figure 2.1 Girder connection specimen modeled at University of Nebraska – Lincoln (Lampe N.J., 2001)

Of the three variations investigated, that shown in Figure 2.1 was chosen for physical testing primarily because the computer analysis showed that the contact of the bottom flanges resulted in ductile behavior of the connection. For the physical testing of the connection, the configuration consisted of first initiating end rotation in the beam ends to simulate the initial dead load end rotation by adjusting the slab support shoring in stages. This involved the lowering of the temporary supports and taking potentiometer readings of the girder end displacements. Based on an increase in horizontal separation of the girders, the end rotation could be calculated. Once the theoretical rotation was achieved, shores would remain in place until the concrete had attained its design strength. Of all of the literature reviewed on the subject of SMC

connections testing, this is the only work that mentioned applying the simple span end rotation prior to testing.

The completed model was then subjected to fatigue testing prior to ultimate strength testing. The fatigue testing resulted in the largest cracks occurring in the slab at the edges of the concrete diaphragm, which was attributed to an abrupt change in rigidity from the slab over the diaphragm to the slab alone. In over two million cycles, the stress in the reinforcing steel varied less than 0.5 ksi and remained in the elastic range. Although there were several pump failures before failure load was achieved, failure of the specimen occurred at a load of 350 kips, which induced a moment at the SMC connection of 4200 ft-kips. The failure was due to yielding of the top tension reinforcing bars, a ductile failure.

Farimani (2006) considered three specimens as described below and shown in Figure 2.2.

Specimen 1: Two girders with abutting bottom flanges to directly transfer compression and thick end compression stiffeners that develop a portion of the interstitial concrete in compression.

Specimen 2: Two girders separated by a gap and no stiffeners, so that compression in the girder and webs must be transferred by only a small region of the concrete.

Specimen 3: Two girders with a gap and thick end compression stiffeners that develop the interstitial concrete in compression.

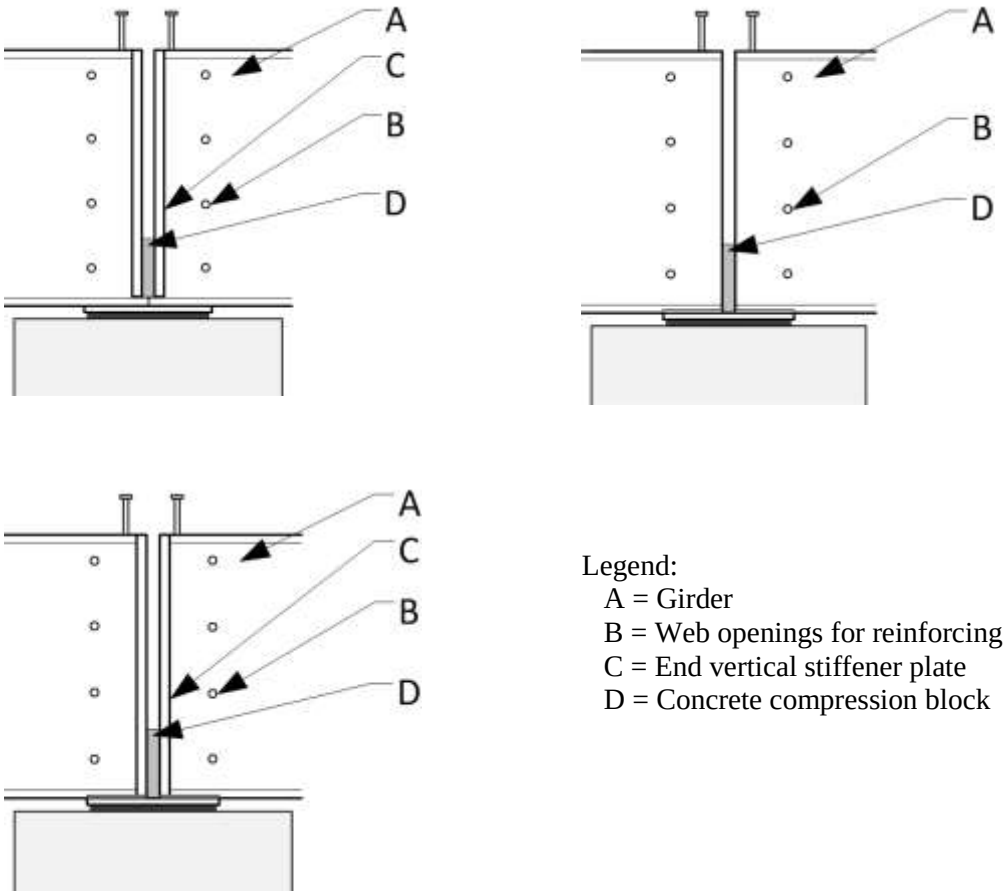

Figure 2.2 Girder Connection Specimens Tested at University of Nebraska-Lincoln (Farimani M., 2006)

All the specimens evaluated had holes either punched or drilled through the girder webs to allow the longitudinal reinforcing of the diaphragm to pass through in order to behave continuously. It's noteworthy that this is not the case in the NDOR standards for precast concrete girders in which the longitudinal diaphragm reinforcing is terminated on either side of the girder. The girders with the diaphragm and composite slab installed are shown in Figure 2.3.

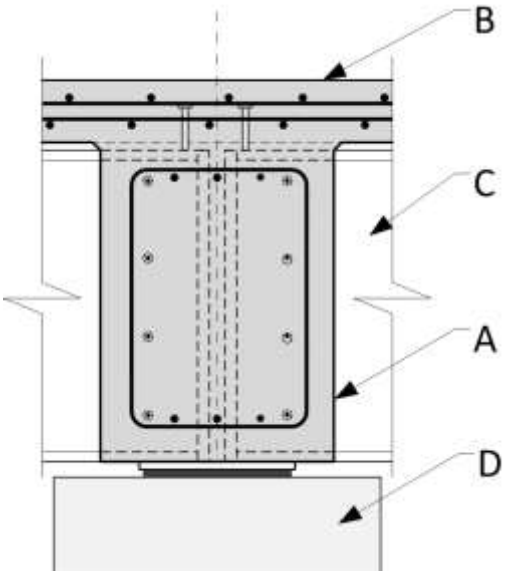

Legend:
A = Concrete diaphragm
B = Composite concrete slab
C = Steel girder
D = Concrete pier

Figure 2.3 Connection with diaphragm and slab in place

In this case, physical testing was conducted prior to the FE analysis. Fatigue testing was performed on all three specimens. The appropriate number of cycles for the testing was determined to be 135,000,000, which was based on AASHTO and the S-N curves for the girder material; this number of cycles was deemed to be excessive for testing. It was decided to alternatively increase the applied load and reduce the number of cycles using AASHTO equation (6.6.1.2.5-2) (AASHTO, 2012) in an attempt to achieve the same effect. Following 2,780,000 cycles in fatigue, ultimate load tests were performed on the same specimens. Faults in the loading due to failing load pumps required unloading and reloading of the specimens during pump replacement. Due to instrumentation failures, values for the many strains in the second and third specimens were unavailable.

Based on the test results, composite action was verified to be effective in all of the tests as there was virtually no slip measured between the top girder flange and the bottom of the concrete slab. This was discussed as being the result of bond between the concrete and the headed shear studs; bond seems unlikely to be stronger than the actual contact bearing between the slab concrete and the stud heads and shafts. In the test of the second specimen, excessive deformation/movement of the bottom flanges occurred due to failure of the interstitial concrete; it was enough such that the diaphragm bars through the girder web failed or were sheared through. In the test of the third specimen, an increase in concrete compressive stresses was noted between the girder end stiffeners; this is obviously due to the bottom flanges not being connected as they were in the first specimen and thus the specimen failed due to concrete crushing.

Based on the physical testing, the following is a summary of what were determined to be the modes of failure of the specimens:

Specimen 1: Yielding of top reinforcing steel (ductile failure)

Specimen 2: Crushing of diaphragm concrete at the girder bottom flange (crushing or brittle failure)

Specimen 3: Crushing of concrete between the end stiffener plates (crushing or brittle failure)

The finite element analysis was performed using ANSYS software to obtain more information about the connection behavior beyond that of the physical test. By exploiting symmetry, only half the model was required and necessary constraints were placed at the center of the SMC connection. The analysis used a static non-linear analysis due to the low rate of load application.

Investigation of the load displacement curves of the physical tests and FEA analysis indicated they compared well. Numerical instabilities occurred in some of the results for the second specimen, which also performed poorly in the physical tests. Otherwise, these results corresponded well with the results of the physical test specimen's results.

Another study by Niroumand (2009) was performed at the University of Nebraska–Lincoln to evaluate an SMC connection intended for accelerated construction and to look at SMC connections for skew bridges; the portion specific to skew bridges will not be discussed herein. A distinguishing feature of the connection intended for accelerated construction is that the top flanges are coped so that the longitudinal slab reinforcing may be hooked into the diaphragm at the location of the girders, Figure 2.4 and Figure 2.5. Neither the compression plate sizes nor their attachment method was given. The compression plate is used in lieu of the full height end girder stiffeners and actually abuts the compression plate of the adjacent girder, thus taking the concrete compression block out of the connection behavior. From examination of Figure 2.4, it may be seen that the compression blocks (C) at the end of the beam are stiffened toward their outside edges by vertical stiffeners (F) and at the center by the web of the girder (A). Erection of this type of connection in the field will require very tight fabrication tolerances in the shop. If a girder is too short, there will be a gap between the compression plates; whereas, if a girder is too long, the girders will not be able to be set since portions of the compression plates will try to occupy the same space.

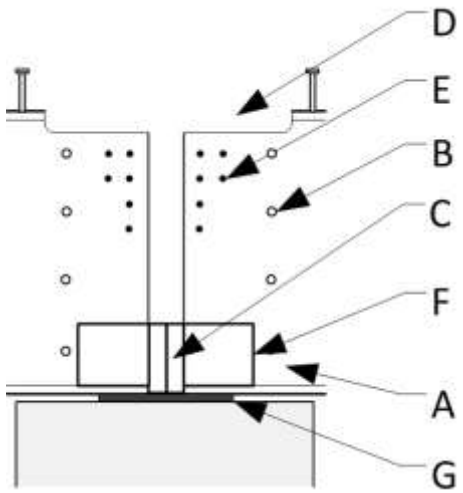

Legend:
A = Girder
B = Web openings for reinforcing
C = End abutting compression plates
D = Coped top flange
E = Bolts through web
F = Vertical edge stiffener each side
G = Elastomeric bearing pad

Figure 2.4 Accelerated connection detail modeled at University of Nebraska–Lincoln (Niroumand, 2009)

The accelerated idea in this detail is that the SMC (lower) layer of top slab reinforcing is to be placed in two pieces; each has a hooked lap bar placed into the far end of the diaphragm, Figure 2.5, thus also lapping nearly the full width of the diaphragm.

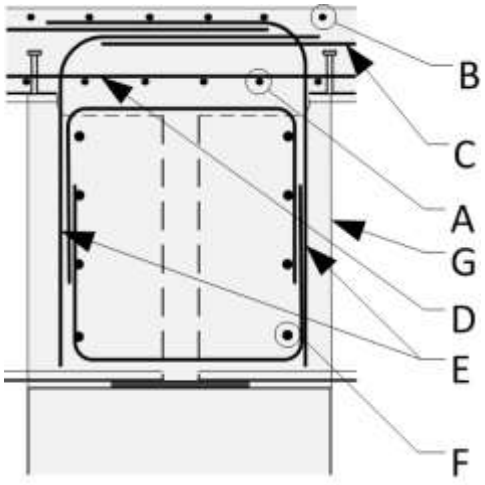

Legend: A = Slab bottom moment reinforcing
B = Slab top moment reinforcing
C = Top SMC bars
D = Bottom slab bars
E = Hooked lap bars for top SMC bars
F = Diaphragm bars through girder web
G = Concrete diaphragm

Figure 2.5 Detail at SMC Connection showing reinforcing layout in diaphragm and slab

Physical testing was again conducted prior to the FE analysis. Fatigue testing of the model preceded ultimate load testing and, as in the previous University of Nebraska–Lincoln study, the number of cycles was reduced from 135,000,000 to 4,000,000 through the use of AASHTO equation (6.6.1.2.5-2). By use of this method, the applied fatigue moment had to be increased from 532 foot-kips to 1137 foot-kips or approximately double the load to reduce the number of cycles to 1/34 of the original number.

Subsequent to the fatigue testing, the ultimate load test was performed. Due to load application issues, the test was stopped, corrections made, and then started all over. When loaded the second time, there was evidence of some nonlinear behavior at a load that had previously behaved linearly during the stopped first test; no explanation was provided for this phenomenon, but it was likely due to crack initiation in the tension zone of the slab.

In addition to the physical model testing, material tests were performed on the various materials, i.e., structural steel, reinforcing steel, concrete, and elastomeric material to obtain their engineering properties for later validation of results with a finite element analysis of the connection.

Significant conclusions drawn at the end of the ultimate load testing and evaluation of instrumentation results are summarized below:

- The strain profile at the end of the girder was linear.
- The cantilever end of the girder had considerable displacements, up to 13 in. vertically without concrete failure and thus exhibited significant ductility.
- The strain profile of the longitudinal reinforcing bars at the diaphragm dropped significantly at the face of the diaphragm; this was likely due to the increase in the amount of reinforcing in this area.
- While the concrete in the vicinity of the steel blocks had the highest compressive strains, these strains were lower than those that would cause cracking or crushing.

The finite element analysis of this scheme was performed using ABAQUS finite element software and was conducted subsequent to the physical testing of the model. Material properties based on the previously discussed material tests were used in the model. The verification process was considered complete when the load-displacement curves for the FEA and physical test were in agreement. Once the finite element analysis was verified with the physical test, it would give the ability to evaluate different scenarios. As ABAQUS was the finite element analysis software selected for use in the research project described in this report, additional details of this analysis is provided in section 2.3.1.

2.3 Findings of Nebraska Experimental Program

In total, the University of Nebraska–Lincoln studies investigated five different connection types. All had the similarity of being encased in concrete pier diaphragms, with holes drilled through the girder webs so that the diaphragm reinforcing could pass through the web and act continuously. Three of the six specimens, Figure 2.1 (Lampe), Figure 2.2a (Farimani) and Figure 2.4 (Niroumand), had the benefit of some sort of interconnection between the bottom (compression) flanges of the girders at the center of the SMC connection; these connections failed by steel yielding, a ductile failure. The remaining specimens had no connection between the girders in the compression area and failed in concrete compression, a brittle failure. It is evident that connection details involving the interconnection of the bottom flanges had a more desirable failure mode and the authors did not hesitate to point this out.

Of the three ductile connections, the most economical and likely quickest to construct was that investigated by Lampe, which was subsequently the basis of the work by Farimani. This connection had the simplest reinforcing steel details and a straightforward steel compression transfer mechanism between the steel girders. However, this connection still has complexities and unknowns, specifically:

- The diaphragm steel passing through the girder webs, which require that holes be punched, drilled, or flame cut through the webs.
- The concrete diaphragm is cast prior to the bridge slab and thus will engage the girder ends prior to the slab concrete; this could cause changes between the behavior in the lab and the field.
- By the girders being embedded in the concrete diaphragms, they are susceptible to moisture seepage due to gaps caused by concrete shrinkage that will occur at their perimeters.

The previous work at University of Nebraska–Lincoln also provided valuable insight in terms of finite element modeling and physical testing.

2.3.1 Details of Finite Element Modeling

Of the SMC connections studied for which FEA was performed, three types of FEA software were used, specifically, SAP2000 (Lampe, 2001), ANSYS version 5.7 (Farimani, 2006), and ABAQUS 6.9 (Niroumand, 2009). Only details related to the use of ABAQUS are presented here, as ABAQUS was the finite element software used to evaluate the steel diaphragm SMC connection.

In the third study (Niroumand, 2009), prior to the complete finite element analysis of the model, ABAQUS was used to obtain true stress-strain curves for the reinforcing bars; the ABAQUS analysis included the effects of necking of the bars under stress. Furthermore, in this study (Niroumand, 2009), two methods to model concrete in both tension and compression available in ABAQUS were considered, specifically, Concrete Smeared Cracking and Concrete Damaged Plasticity. For the subject model, Concrete Damaged Plasticity was chosen as it models the nonlinear behavior of concrete in both tension and compression more accurately than Concrete Smeared Cracking, although at the cost of significantly more processing time. Five different tension failure models were discussed for concrete in uniaxial tension and, in the end, the Barros et al. (2002) method was selected; this method is somewhat complex as

it involves the evaluation of more than six equations. Three different compression failure models were considered for concrete in uniaxial compression. The Carreirra and Chu (1985) method was selected as its peak value matches the ultimate compressive strength of the concrete under, unlike the other methods considered.

The study's (Niroumand, 2009) discussion on element type selection was fairly brief in comparison with the material selection discussion. The steel girder was modeled using shell elements as this provided not only nodal displacements, but also nodal rotations. Nodal rotations cannot be obtained by the use of first order solid elements, but can be provided by second order solid elements at the cost of additional processing time. Timoshenko beam elements were chosen to model the shear studs as these would also provide shear deformation results. Three dimensional two node truss elements were selected to model the slab reinforcing. The slabs were modeled as first order eight node brick elements; no explanation was given as to why a second order element was not required.

Constraints consisted of embedding the reinforcing bars and studs in the slab; while this method simplifies analysis, modeling the stud as an embedded beam may not capture the effect of the head of the stud locking the slab down since the beam is only a line type element. However, this should not have a significant effect on the overall results. The lower nodes of the studs were tied to the girder top flange. Although not very clear, it appears that lateral constraints were applied to the bottom flanges of the girders and the vertical load was carried through part contact with the elastomeric bearing. Additional contacts were modeled between the end steel compression plates. No mention of contact between the interstitial concrete and the ends of the girders was mentioned.

Sensitivity analyses were carried out on variations of mesh size, omitting studs and tying the slab to the girder, load application methodology, etc. A summary of the findings of this analysis follows:

- While a finer overall mesh was no better than a coarse mesh for the entire model, more accurate results were obtained using a finer mesh in the vicinity of the concrete diaphragm.
- The load application applied to the top of the slab vs. the bottom flange of the girder gave better correlation to the actual physical test results.
- The girder connected directly to the deck in lieu of being tied with studs caused considerable elongation in the slab reinforcing bars over the girder, thus shear studs should be used to correctly model this interaction.

2.3.2 Lab Testing of SMC Bridge Connections

Lab testing of physical models involved construction of the model simultaneous with the placement of embedded and surface mounted instrumentation; the instrumentation is subsequently wired to a data acquisition device. Lampe (2001) went into great detail about instrumentation types, their use, and their placement. The types of monitoring instrumentation used, their mounting locations, and other details of their installation are given in Table 2.1.

Table 2.1 Summary of Instrumentation Type and Placement

Gage Type	Placement
Steel surface electrical strain gages	mounted to the surface on the top and sides of the girder flanges, mounted to embedded reinforcing bars
Concrete embedment vibrating wire strain gages	placed in the composite slab and the concrete pier and diaphragm
Steel embedded electrical strain gages	placed on girder flanges and web outside of the concrete diaphragm and slab
Concrete surface electrical strain gages	measure strain on the surface of the concrete slab and diaphragm, mounted on the concrete surface
Potentiometers (linear transducers)	positioned at the girder ends to determine and set initial simple beam end rotation and at the location of load application to measure beam deflection

Farimani (2006) provided instrumentation to obtain results for the two load stages tested, cyclic fatigue loading, and ultimate loading. Instrumentation used included electrical strain gages, vibrating wire embedment gages, and potentiometers. Electrical strain gages were mounted to the steel girder webs and flanges and the steel reinforcing bars, vibrating wire embedment gages were positioned and mounted within the concrete slab and diaphragm. These gages were also attached to the reinforcing steel in the diaphragm between the girder ends. Potentiometers were used to measure the vertical deflection of the beam ends and in the test of the third specimen, Figure 2.2.a, they were used to measure the movement of the girder bottom flanges into the concrete diaphragm. For the cyclic fatigue loading, two 220 kip MTS actuators were used, one at the cantilever end of each girder. The load was applied to a spreader beam so as not to subject the bridge deck to a concentrated load. The load range of 2 kips to 106 kips was then applied by means of displacement control. After a cyclic fatigue test, it was found that the stiffness of the specimen had decreased such that the load for the specified displacement had decreased to 74 kips from 106 kips. At the conclusion of the fatigue test, it was noted that there was a reduction in stiffness of approximately 12%.

Niroumand (2009) provided instrumentation to monitor both the fatigue and ultimate load tests. The types of gages and their utilization were similar to those listed in Table 2.1, with the addition of a crack meter between the girder webs at the top flange at the center of the connection. The cyclic fatigue loading was applied in the same manner as the tests conducted by Farimani (2006). The stiffness of the system was again observed to decrease during the test, thus it may have been better to use load control over displacement control.

For the ultimate strength test (Niroumand, 2009), the MTS actuators were replaced by four 300-ton hydraulic rams placed at locations where they would provide the correct moment based on the applied load, which would correspond to the beam end shear. The rams applied the load to the slab by means of a spreader beam with a rod from each ram at the ends. The test load was increased gradually in load steps that varied from 10 kips to 25 kips during the test.

2.4 Field Testing of Bridges Constructed with SMC Connections

Several bridges designed and constructed with the SMC concept have been tested in the field to verify their efficacy in continuous behavior for live load. Of the bridges tested, there was no evidence found of any previous specific lab testing or finite element analysis as in the Nebraska bridges.

The earliest published field test information was by Lin (2004); this work investigated/verified the AASHTO specification live load distribution factors for two different bridges. However, also in this study, the author investigated the live load continuity of one of the bridges, Ohio State Highway 56 over the Scioto River (2003), constructed with the SMC concept to verify its SMC behavior.

The SMC detail of this bridge is shown in Figure 2.6 and Figure 2.7 and bears a strong resemblance to the Nebraska detail shown in Figure 2.8. The bridge was instrumented with four pairs of strain gages on two adjacent girders, two feet from the support pier. Based on information from the strain gages, the bending moments from a known truck as a function of position along the bridge were able to be calculated. Upon review of the bending moments, the bridge was indeed found be acting continuously for the live load of the truck.

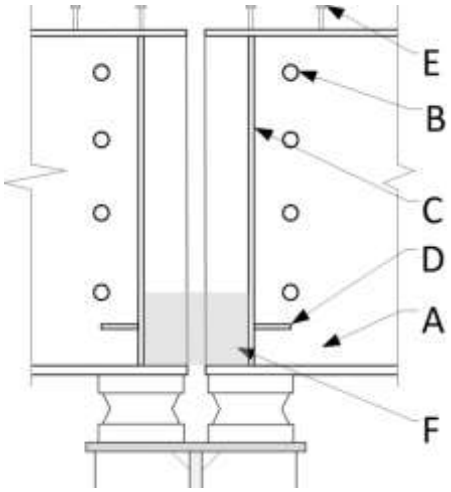

Legend:
A = Girder
B = Web openings for reinforcing
C = End vertical stiffener plate
D = Horizontal stiffener plate
E = Headed studs
F = Concrete compression block

Figure 2.6 Bridge over the Scioto River SMC detail

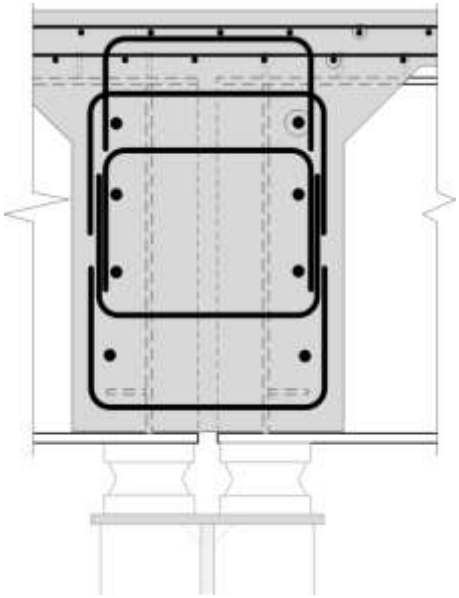

Figure 2.7 Bridge over the Scioto River pier detail

Subsequent field evaluation (Solis A.J., 2007) on a bridge on U.S. 70 over Sonoma Ranch Road (2004) in Las Cruces, New Mexico, was performed to verify SMC behavior at the interior bridge piers. As shown in Figure 2.8, this bridge appears to be a variation of the Nebraska detail shown in Figure 2.1, with the main difference being the addition of a bolted splice plate connecting the top flanges and more web openings. From review of the construction documents, the procedure for fastening the top plates involves tightening the bolts after the concrete has fully cured; this, along with the concrete compression block being ineffective until it has attained design strength, insures that the connection will not resist any dead load moment. In addition to the top flange splice plate, the composite slab has additional reinforcing in the negative moment zone over the pier. The top flange splice plate also has shear studs, which have been omitted from the figure for clarity.

The field study involved the installation of 56 strain transducers at select locations along the bridge where they were attached to the center of the web and either the top of the bottom flange or the underside of the top girder flange, depending upon location in the span. For the test, a truck with a total weight of approximately 56,000 lbs. was positioned along the bridge at eight different locations. Based on strain readings, the neutral axes of the girder were determined and compared to the assumed theoretical values. The evaluation of the experimental vs. the theoretical showed that the results compared well and also showed that the actual composite action included the effects of the longitudinal reinforcing steel and the concrete haunch being effective.

Additional study was done by comparing the experimental results with those obtained with an SAP 2000 model. The model in SAP 2000 was calibrated as much as possible to agree with the behavior of the actual bridge. Based on the experimental and the SAP 2000 results, the bridge behavior was found to be simple for dead load and continuous for live load. Also, the studies showed that although there was a top flange splice plate, in order for the bridge to behave as it had, the top reinforcing steel was also necessary to resist the negative moments over the supports.

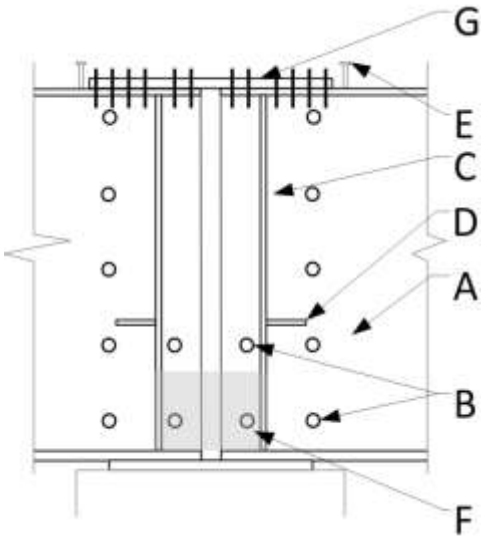

Legend:
A = Girder
B = Web openings for reinforcing
C = End vertical stiffener plate
D = Horizontal stiffener plate
E = Headed studs
F = Concrete compression block
G = Bolted splice plate

Figure 2.8 U.S. 70 over Sonoma Ranch Road SMC detail

Another bridge on which field studies were performed is the DuPont Access Road Bridge in Humphreys County, Tennessee, shown in Figure 2.9 and Figure 2.10 (Chapman, 2008). This bridge is somewhat of a hybrid due to the following variations in its construction:

- The top flange has no studs in the negative moment tension zone
- The bottom flange has a lower reinforcing plate in the negative moment compression zone
- Wedge compression plates are field welded between the bottom flanges prior to placement of the concrete diaphragm

This bridge does not actually meet the definition of having SMC connections; however, it is noted in this literature review because it does have an interesting feature in that the continuous connection of this bridge is developed by the use of field installed and welded wedge plates between the bottom girder flanges, Figure 2.11. This is a novel approach to connecting the bottom flanges for continuity as it allows for adjustment in the field and does not require the tight tolerances as would be required in the Nebraska details. Also, while not studied in the work (Chapman, 2008), the behavior of the wedge plates would be the same as the abutting end plates of the Nebraska detail and thus would most likely result in more ductile behavior in the connection.

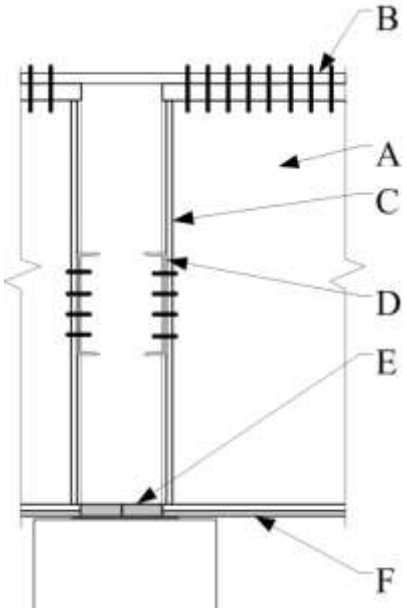

Legend:
A = Girder
B = Splice plate and bolts
C = End vertical stiffener/comp. plate
D = Horizontal channel stabilizers
E = Wedge compression plates
F = Bottom flange reinforcing plate

Figure 2.9 DuPont Access bridge SMC detail

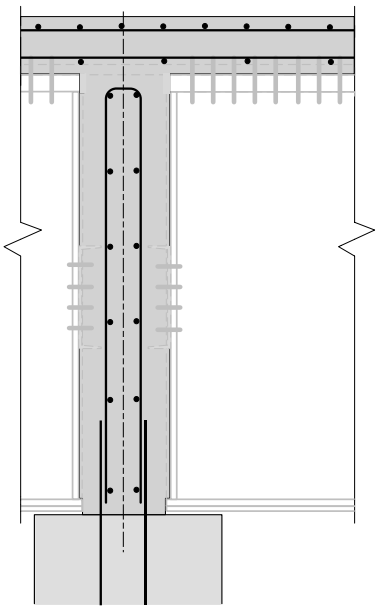

Figure 2.10 DuPont Access bridge slab and diaphragm

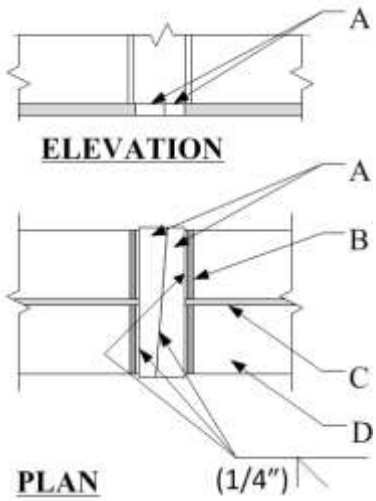

Legend:
A = Wedge plates
B = End stiffener
C = Girder web
D = Girder bottom flange

Figure 2.11 Wedge plate detail

2.5 Summary of Bridges Constructed with the SMC Concept

At the time of this writing, there were at least twelve known constructed and operational steel girder bridges found in the United States that have used the SMC concept or variations thereof; there are quite possibly more in design and planning or construction stages, which are not considered. These operating bridges and relevant points about their SMC details/behavior are summarized in chronological order below; dates provided are the dates that the drawings were issued for construction. Detailed information about each bridge is provided in Appendix A.

Massman Drive over Interstate 40, Davidson County, Tennessee – November, 2001
This is a two-span, two-lane composite rolled girder bridge with concrete diaphragms at interior supports; maximum span is 145'-6". Continuity is achieved by steel compression blocks between bottom flanges and a steel top flange splice plate, which is fastened prior to concrete placement; thus this bridge is actually simple for only the girder self-weight and continuous for all other loads.

State Highway N-2 over Interstate 80, Hamilton County, Nebraska – November, 2002
This is a tub (box) girder bridge and is not directly within the scope of this study but it is noted that it uses the SMC concept at its interior piers.

U.S. 70 over Sonoma Ranch Blvd. – Las Cruces, New Mexico – August, 2002
This structure consists of two nearly identical bridges one in each direction. Each is a three-span, two-lane, composite plate girder bridge with concrete diaphragms and a tension flange splice plate, which is bolted subsequent to the concrete setting; maximum span is 119'-9". Continuity is achieved by girder bearing stiffeners compressing the diaphragm concrete and tension in the top flange splice plate, which also has headed studs and top slab reinforcing steel. The top splice plate is unique to this bridge and it takes the place of providing additional reinforcing steel in the top of the slab to develop the SMC behavior.

Dupont Access Road over State Route 1, Humphrey's County, Tennessee – December, 2002
This is a two-span, two-lane composite rolled girder bridge with concrete diaphragms at interior supports, maximum span is 87'-0". Continuity is achieved in the same manner as the Massman Drive bridge.

Sprague St. over Interstate 680, Omaha, Nebraska – May, 2003
This is a two-span, two-lane bridge with composite rolled steel girders with concrete diaphragms at interior supports; maximum span is 97'-0". Continuity is achieved by end bearing plates on the girder compressing the diaphragm concrete and top tension steel in the deck slab.

Ohio S.H. 56 over the Scioto River – Circleville, Ohio – June 2003
This is a six-span, two-lane bridge with composite plate girders with concrete diaphragms at interior supports, maximum span is 112'-8". Continuity is achieved by girder bearing stiffeners compressing the diaphragm concrete and tension in the top flange splice plate.

State Highway No. 16 over US 85, Fountain, Colorado – February, 2004
This is a four-span, two-lane bridge with composite steel plate girders embedded in concrete diaphragms at the interior supports, maximum span is 128'-2". Continuity is achieved by end bearing plates on the girder compressing the diaphragm concrete and top tension steel in the deck slab.

New Mexico 187 over Rio Grande River – Arrey/Derry, New Mexico – June, 2004
This is a five-span, two-lane composite plate girder bridge with concrete diaphragms and a top flange tension splice plate, which is bolted subsequent to the concrete setting; maximum span is 105'-0". Continuity is achieved by girder bearing stiffeners compressing the diaphragm concrete and tension in the top flange splice plate, which also has headed studs and top slab reinforcing steel.

State Route 210 over Pond Creek, Dyer County, Tennessee – June, 2004
This is a five-span, two-lane composite rolled girder bridge with concrete diaphragms at interior supports; maximum span is 132'-2". Continuity is achieved in the same manner as the Massman Drive bridge. Three of the five spans of this bridge also have full mid-span bolted plate splices.

Church Ave. over Central Ave., Knox County, Tennessee – January, 2005
This is a six-span, three-lane, composite rolled girder bridge with concrete diaphragms at interior supports, maximum span is 100'-0". Continuity is achieved in the same manner as the Massman Drive bridge.

State Highway No. 36 over Box Elder Creek, Watkins, Colorado – June, 2005
This is a six-span, two-lane bridge with composite rolled steel girders with steel diaphragms at the interior supports; maximum span is 77'-10". Continuity is achieved by compression being transferred between girders by connection to a common sole plate and top tension steel in the deck slab. This is the only completely SMC bridge to not use a concrete diaphragm.

US 75 over North Blackbird Creek – Macy, Nebraska – May 2010 and US 75 over South Blackbird Creek – Macy, Nebraska – May 2010
These are almost identical three-span, two-lane bridges with composite rolled steel girders with concrete diaphragms at interior supports, maximum spans are 65'-8" and 73'-6", respectively. Continuity is achieved by end bearing plates on the girder compressing the diaphragm concrete and top tension steel in the deck slab.

The behavior of these bridges may be summarized as being in one of the following four categories:

1. Simple made continuous with an integral concrete diaphragm and abutting bottom flanges, as shown in Figure 2.2a or similar
   - State Highway No. 16 over US 85, Fountain, Colorado
   - Sprague St. over Interstate 680, Omaha, Nebraska
   - State Highway N-2 over Interstate 80, Hamilton County, Nebraska
   - US 75 over North Blackbird Creek – Macy, Nebraska
   - US 75 over South Blackbird Creek – Macy, Nebraska
   - Ohio S.H. 56 over the Scioto River – Circleville, Ohio
2. Simple made continuous for all superimposed loads with flange interconnections, i.e., simple for girder dead load only, Figure 2.9
   - Church Ave. over Central Ave., Knox County, Tennessee
   - Dupont Access Road over State Route 1, Humphrey's County, Tennessee
   - Massman Drive over Interstate 40, Davidson County, Tennessee
   - State Route 210 over Pond Creek, Dyer County, Tennessee
3. Simple made continuous for live loads with post connected flange interconnection(s), Figure 2.8
   - New Mexico 187 over Rio Grande River – Arrey/Derry, New Mexico
   - U.S. 70 over Sonoma Ranch Blvd. – Las Cruces, New Mexico

4. Simple made continuous with steel diaphragms and exposed ends, Figure 2.12
   State Highway No. 36 over Box Elder Creek, Watkins, Colorado

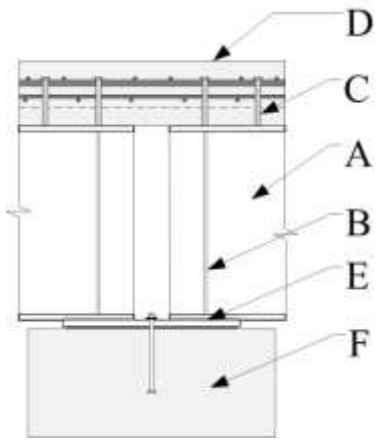

Legend:
A = Bridge Girder welded to bearing plate
B = End stiffener (diaphragm beam not shown)
C = Shear studs
D = Composite slab
E = Steel bearing plate
F = Support pier

Figure 2.12 SMC Detail with a Steel Diaphragm

3. DESCRIPTION OF STUDY BRIDGE AND PRELIMINARY CALCULATIONS

3.1 Bridge over Box Elder Creek

The previously constructed steel SMC bridges described at the end of Section 2 generally make use of a concrete diaphragm that must, in most cases, help resist compression developed due to the negative moment over the pier in order for the SMC behavior to develop. By far, the most unique of the SMC concepts currently in use is that on the S.H. 36 bridge over Box Elder Creek in Colorado, shown in Figure 3.1.

Figure 3.1 SH 36 Over Box Elder Creek (reprinted courtesy of AISC)

This bridge develops its SMC continuity through tension in the composite slab top reinforcing steel and compression in welds to a sole (base) plate on top of the pier that is common with the adjacent girder, as shown in Figure 3.2. This connection works without the need for a concrete diaphragm for compression and thus has steel diaphragm beams connected to the bearing stiffener at the pier, as shown in Figure 3.3.

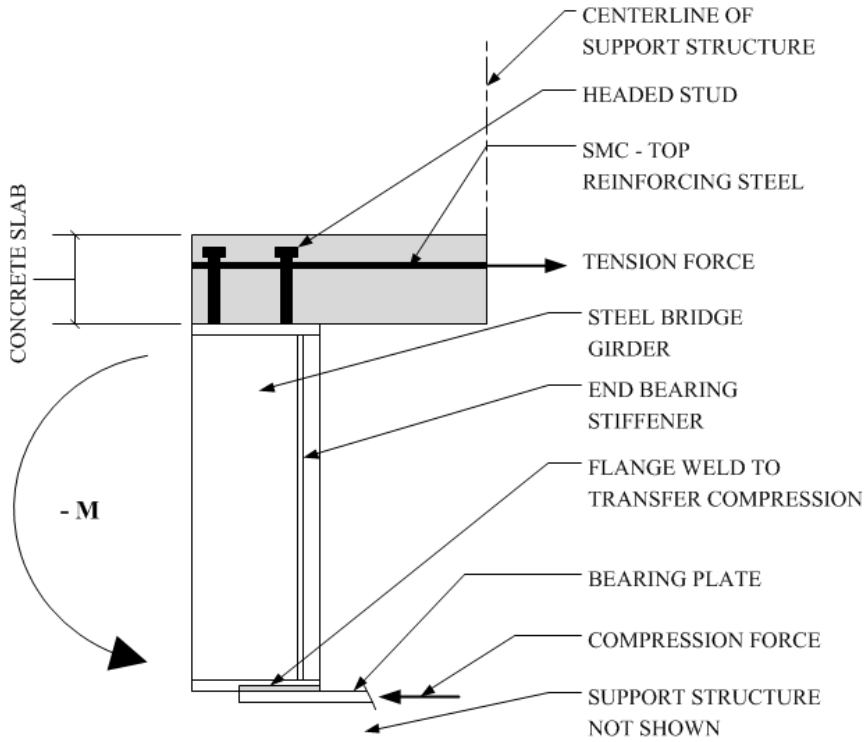

Figure 3.2 Steel SMC Connection Elements without Concrete Diaphragm

Figure 3.3 SH 36 Over Box Elder Creek – Girder Details (reprinted courtesy of AISC)

The behavior and design of this steel diaphragm SMC connection is the primary subject of this report for the following reasons:

1. It is a unique concept that hasn't been analytically investigated nor experimentally tested before.
2. No concrete diaphragm is required to transfer the SMC compressive forces, which means:
    a. No need to wait for the diaphragm concrete to set up to cast the deck slabs, which will result in time savings and accelerated construction
    b. Absence of the concrete diaphragm makes the connection accessible for future inspection and allows the steel girder to properly weather for corrosion protection
    c. All compression is transferred by steel elements, which means both the tensile and compressive forces at the connection are transferred by a ductile material, implying ductile connection behavior
    d. No need to rely on the additional concrete strength afforded by confinement, which is a necessity with some of the Nebraska schemes
3. It is simple and straightforward in both its design and construction.
    a. The use of a common base plate allows for slight deviations in longitudinal girder dimensions without the accuracy required for exact fit-up as in the other steel-to-steel details.
4. Due to its simplicity, it appears to be more economical than other previously studied schemes.
5. Design of this type of connection is not well addressed by existing AASHTO provisions, thus making it a desirable subject for analysis and testing.
6. This connection involves field welding of the bottom girder flanges to a common sole plate to transfer the compression component of the SMC connection forces as opposed to direct bearing connections in most of the other SMC schemes.

3.2 Scope of Evaluation

The evaluation efforts on this connection included the use of analytical models and experimental testing to understand the behavior/performance of this SMC connection with rolled girders with loading representative of bridges with spans in the range of 80-160 feet. The investigation of the connection also aims to develop complete design provisions for this type of connection, including:

- Consideration of the effect of shear lag in the top deck reinforcement and development of design procedures to specify the rebar placement
- Investigation of the transfer of load through the girder such that all forces are capable of being transferred through only a bottom flange connection
- Understanding of the interaction between the bottom girder flange and the sole plate and identification of all design parameters required
- Determination of calculations necessary for the welds between the sole plate and girder flange
- If weld sizes and/or lengths become excessive, development of formulations and design criteria for steel wedge bearing plates to transfer bottom flange compression across the joint
- If wedge plates are required, consideration of details to prevent lateral movement of the SMC girders

Throughout the investigation and the development of a design methodology, the economy and constructability of the connection has been a primary consideration.
The limitations of the evaluation described by this report include:

- Only gravity loads due to typical roadway loading have been considered. No lateral loads such as vehicular centrifugal force, vehicular braking force, wind, earthquake, soil pressure, etc. were included in any analysis or design check.

- The analysis considers only the effects of the applied maximum moment and corresponding shear. Thermal effects such as temperature gradient or thermal expansion forces due to environmental temperature changes were not considered in any analysis or design check.
- Other incidental forces such as effects due to shrinkage or down drag were not considered.

3.3 Preliminary Calculations

3.3.1 Bridge and Connection Loading

3.3.1.1 AASHTO Requirements

Loading on the study bridge (and its SMC connections) was determined in accordance with the AASHTO LRFD Bridge Design Specification (AASHTO, 2012). The bridge is subjected to both dead and live loads. Of the dead loads, there are permanent loads that will cause only simple moments in the girders. Permanent dead loads include the self-weight of the steel framing, the concrete slab, and anything cast into the slab such as drain grates, hangers, etc. Then there are superimposed dead loads, which are installed after the SMC connection has become effective. Superimposed dead loads would include wearing course pavement, downspouts, signage, railings, etc.

The code-required live loads on bridges, designated as HL-93, consist of a lane load along with any of three specified truck loadings. The lane loading is 0.64 klf over a 10-foot-wide lane or 0.064 ksf. The truck loadings consist of: (1) the design truck with 6'-0"-wide axles and front axle spacing, L1, of 14'-0" and rear axle spacing, L2, of 14'-0" through 30'-0", at one-foot increments, this would create a total of 19 possible trucks, Figure 3.4; (2) the design tandem truck as shown in Figure 3.5; and (3) the dual trucks as shown in Figure 3.6.

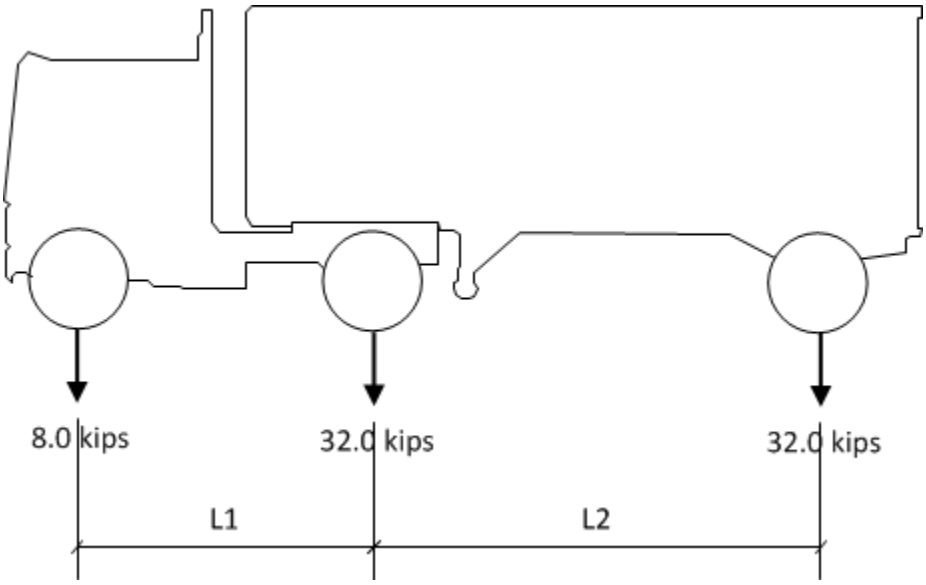

Figure 3.4 AASHTO Design Truck

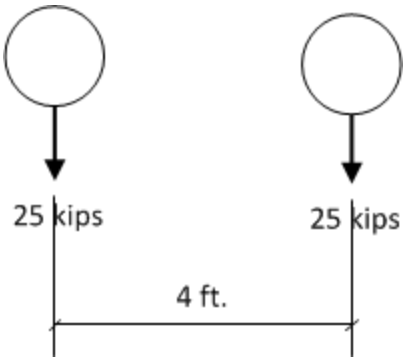

Figure 3.5 AASHTO Dual Tandem

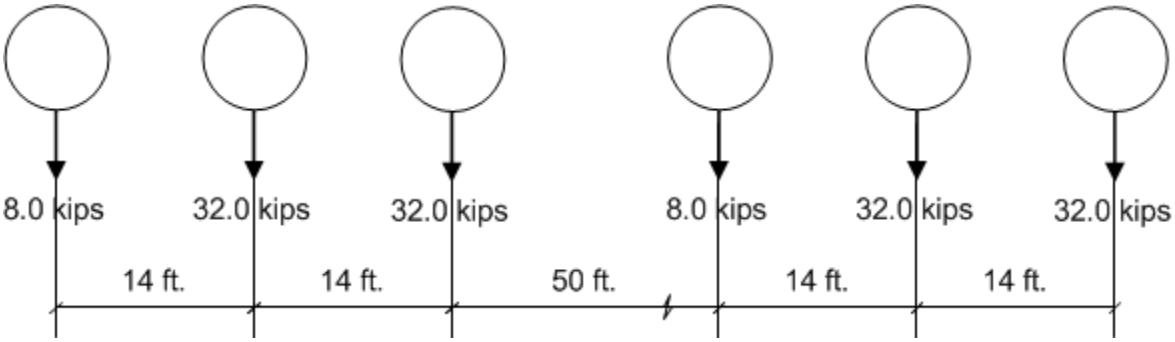

Figure 3.6 AASHTO Dual Truck

For the type of bridge selected, AASHTO specifies four applicable load combinations, which are shown in Table 3.1. Once the appropriate combination has been selected, applicable load factors, γ's, based on the combination are used (Table 3.2). For the purpose of this study, the "Strength I" combination will be used since it will create the largest wheel loads and, consequently, the largest absolute internal moments and shears.

Table 3.1 Applicable Load Combinations

Combination Name	Description
Strength I	Basic load combination relating to the normal vehicular use of the bridge without wind.
Service II	Load combination intended to control yielding of steel structures due to vehicular live load.
Fatigue I	Fatigue and fracture load combination related to infinite load-induced fatigue life.
Fatigue II	Fatigue and fracture load combination related to finite load-induced fatigue life.

Table 3.2 AASHTO Load Factors, γ's

Combination Name	Dead(DC)	Vehicular Live(LL)	Pedestrian Live(PL)	Vehicular Dynamic Load Allowance (IM)
Strength I	1.25	1.75	1.75	33%
Service II	1.00	1.30	1.30	33%
Fatigue I	--	1.50	--	15%
Fatigue II	--	0.75	--	15%

The vehicular dynamic load allowance (AASHTO Table 3.6.2.1.1) is determined in accordance with Equation 1. The IM shall only be applied to the truck wheel loads and not to the uniform lane loading. The IM shall be applied as an additional load factor to the static loads in combination with the values for IM in

$$1.0 + IM/100 \qquad \textbf{Equation 1}$$

The final form of the load equation is $Q = \Sigma \eta_i \gamma_i Q_i$, where for the bridge considered,

η_i = Load modifiers as follows:

η_D = factor relating to ductility $= 1.00$

η_R = factor relating to redundancy $= 1.00$

η_I = factor relating to operational classification $= 1.00$

Q_i = the various loadings

γ_i = the applicable load factor for the load under consideration

While the η values are all 1.00 for this particular bridge, this is not always the case.

Distribution of live loads for moments to interior and exterior beams is determined based on bridge supporting component (girder) type and deck type. In this study, the girders are steel beams and the deck type is a cast-in-place concrete slab, which according to AASHTO Table 4.6.2.2.1-1 is a cross-section type (a). Thus, in accordance with AASHTO Table 4.6.2.2.2b-1, the design loads shall be determined based on Equation 2 for one design lane loaded and on Equation 3 for two or more design lanes loaded. It should be noted that the distribution factors are to be applied to the axle loads, not the wheel loads, which are one-half of the axle loads.

$$0.06 + \left(\frac{S}{14}\right)^{0.4} \left(\frac{S}{L}\right)^{0.3} \left(\frac{K_g}{12.0Lt_s^3}\right)^{0.1} \qquad \textbf{Equation 2}$$

$$0.075 + \left(\frac{S}{9.5}\right)^{0.6} \left(\frac{S}{L}\right)^{0.2} \left(\frac{K_g}{12.0Lt_s^3}\right)^{0.1} \qquad \textbf{Equation 3}$$

In these equations, the variables used are defined as shown on the following page.

$$K_g = n\left(I_g + Ae_g^2\right) \qquad (4.6.2.2.1\text{-}1)$$

$$n = \frac{E_B}{E_C} \qquad (4.6.2.2.1\text{-}2)$$

$I_g =$ moment of inertia of girder (in.^{4})

$A =$ girder area (in.^{2})

$E_B =$ modulus of elasticity of girder (ksi)

$E_C =$ modulus of elasticity of concrete (ksi)

$S =$ spacing of beams or webs (ft.)

$t_s =$ depth of concrete slab (in.)

$L =$ span of beam (ft.)

$N_b =$ number of beams, stringers or girders

$S =$ spacing of beams or webs (ft.)

$t_s =$ depth of concrete slab (in.)

$L =$ span of beam (ft.)

$N_b =$ number of beams, stringers or girders

$e_g =$ distance between the centers of gravity of the basic beam and deck (in.)

And the limits of applicability are:

$$3.5 \le S \le 16.0$$

$$4.5 \le t_s \le 12.0$$

$$20 \le L \le 240$$

$$N_b \ge 4$$

$$10,000 \le K_g \le 7,000,000$$

In addition, the variable *L* may vary depending on the desired force effect and is defined in AASHTO Table C4.6.2.1.1-1. Should all the girder spans be the same, then *L* would be the same for all force effects such as minimum/maximum moments, shears and reactions.

Alternatively, AASHTO allows another methodology, the lever method, which provides more conservative (Barker, 2007) loads than the distribution factor method and thus was not considered.

3.3.1.2 Determination of Bridge and Connection Loading

For the study bridge, load determination for the girder was made with a computer analysis of the effects of the design trucks, Figure 3.4, Figure 3.5, and Figure 3.6. The Excel-based software tool developed for this study provides the maximum positive/negative moments in the spans and at each support as well as the maximum/minimum reactions at the each support for all 19 trucks. The software also provides the position of the first wheel of the truck that produces these maximum effects. The user can then select the case for the desired result (minimum or maximum moment, shear, etc.) and request a detailed analysis of that truck and its first wheel location. Results of the detailed analysis include shear and moment diagrams for the entire bridge based on the critical load position. The diagrams for S.H. 36 over Box Elder Creek for the truck position producing maximum negative moment at a support are shown in Figure 3.7 (shear) and Figure 3.8 (moment). The blue (dashed) line indicates the loading due to the superimposed wheel, lane and wearing course loads and the red (solid) line indicates the sum of the superimposed loads and the simple dead load.

The load condition shown in these figures (corresponding to the maximum negative moment the SMC connections on the bridge must resist) is the condition caused by the dual truck (Figure 3.6) with its first wheel 136 feet from the beginning of the bridge. The dead load moments used in the total were based on the weight of the bridge girder, steel diaphragms, and concrete slab. The shear and moment determined here were used throughout this evaluation effort, including the preliminary assessment of connection performance and for the loading in the finite element model and experimental test of the connection.

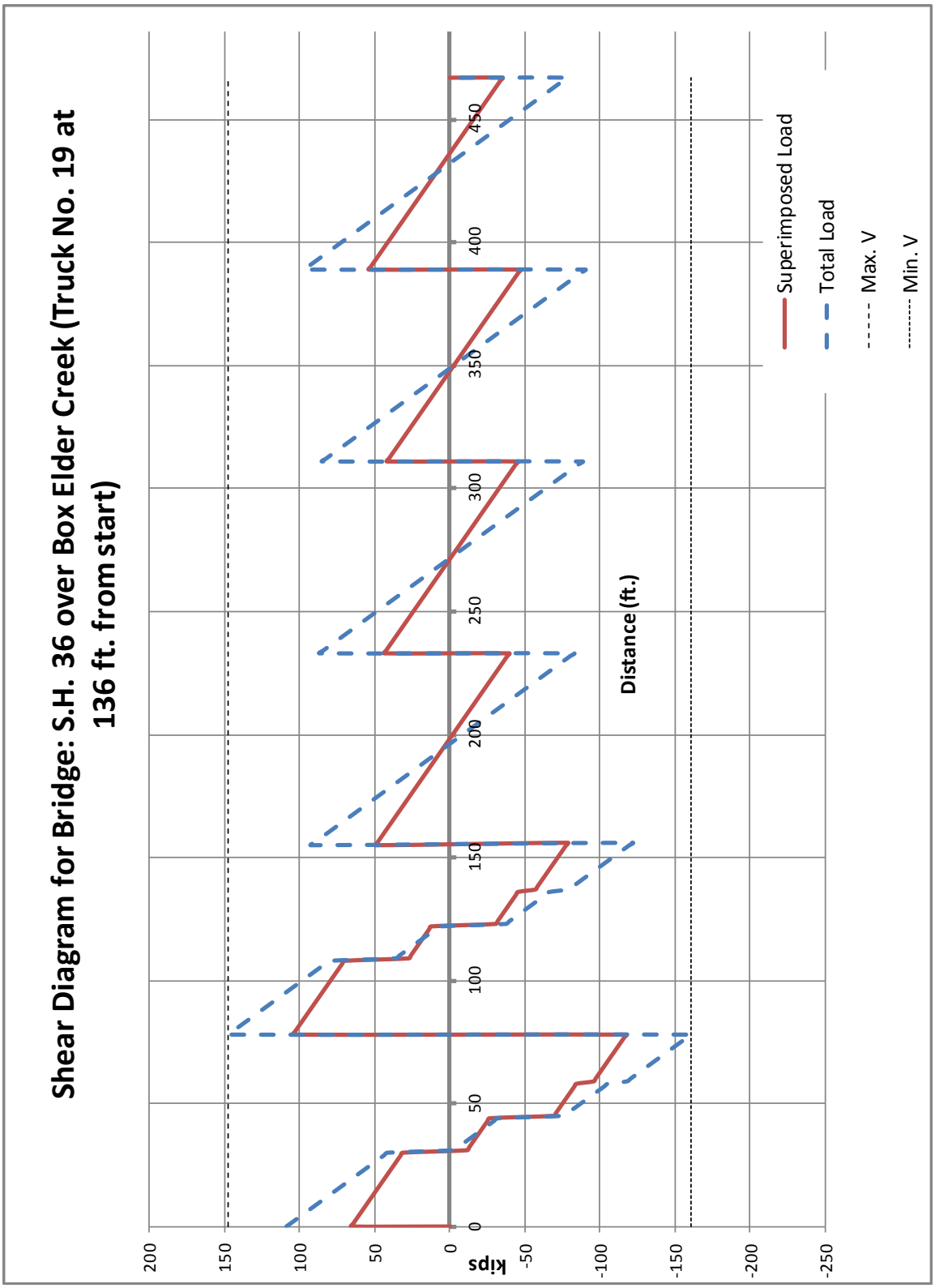

Figure 3.7 Shear Diagram

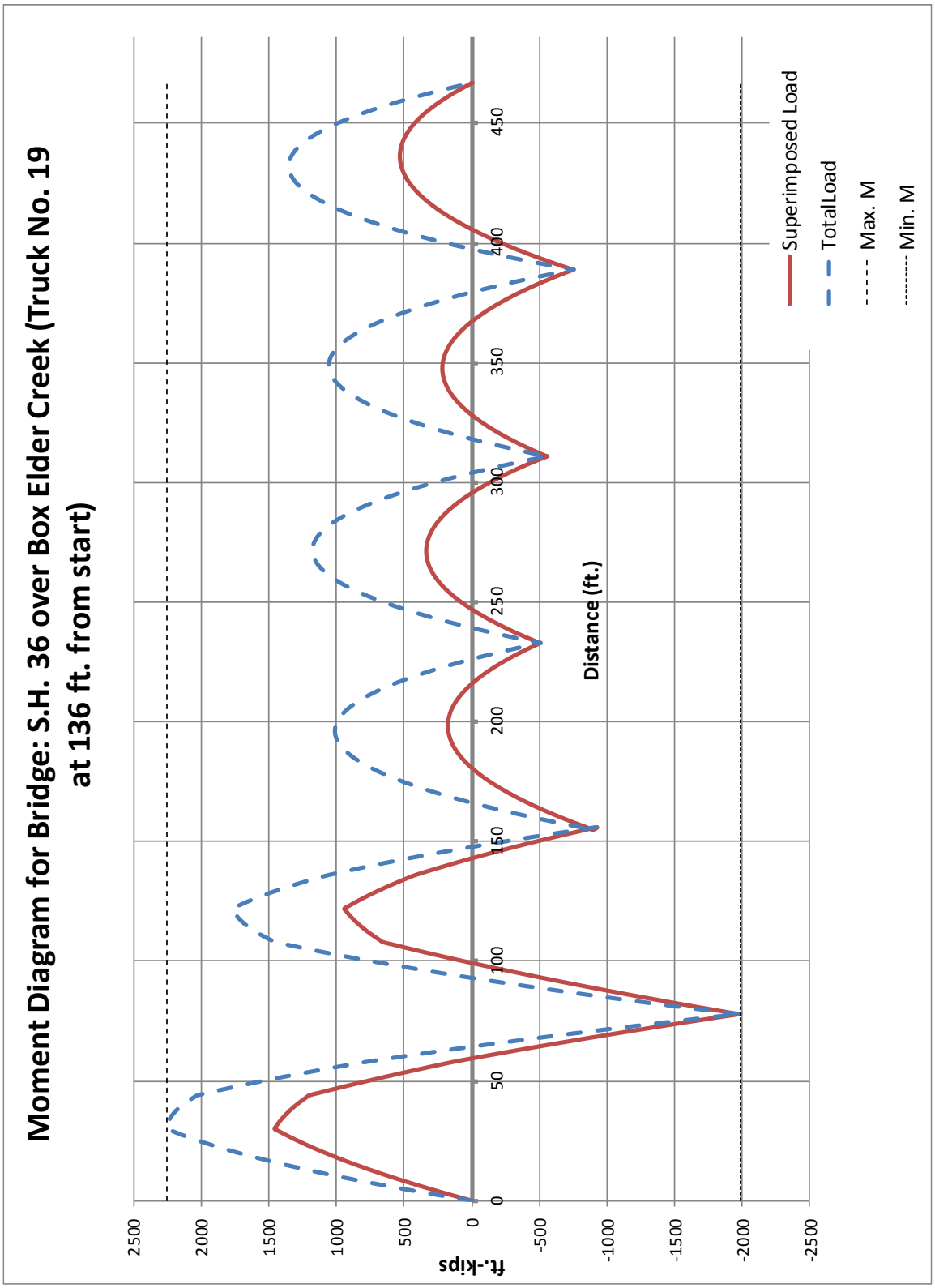

Figure 3.8 Moment Diagram

3.3.2 Bridge Limit States and Resistance Requirements

AASHTO (2012) provides the formulations and methodology to determine the structural capacities of elements subject to different components of force and the applicable resistance factors for the specific limit states involved.

Specific materials considered in the study were:

- Structural steel for girders and plates
- Reinforcing steel
- Steel for headed studs
- Filler metal for welds
- Concrete for the slab, haunch, and support pier

Detailed ultimate capacity or ultimate stress requirements based on AASHTO (2012) are presented in Table 3.3. These values were used in hand calculations for approximate determination of the ultimate moment and shear capacity of the connection as detailed. The hand calculations followed the standard practice of ignoring the tensile capacity of the concrete.

Table 3.3 AASHTO Ultimate Capacity Calculations

Material	Stress/Load Description	Formula for Determination	Source (AASHTO eqn. number unless noted)
Structural Steel	Nominal Flexural Resistance $D_p \le 0.1D_t$	$M_n = M_p$	(6.10.7.1.2-1)
Structural Steel	Nominal Flexural Resistance $D_p > 0.1D_t$	$M_n = M_p\left(1.07 - 0.7\frac{D_p}{D_t}\right)$	(6.10.7.1.2-2)
Structural Steel	Nominal Flexural Resistance (continuous span limitation)	$M_n \le 1.3R_hM_y$	(6.10.7.1.2-3)
Structural Steel	Nominal Shear Resistance of Stiffened Webs	$V_n = V_p\left[C + \frac{0.87(1-C)}{\sqrt{1+\left(\frac{d_0}{D}\right)^2}}\right]$	(6.10.9.2-1)
Structural Steel	Nominal Shear Resistance of Unstiffened Webs	$V_n = V_{cr} = CV_p$ and $V_p = 0.58F_{yw}Dt_w$	(6.10.9.2-1)
Structural Steel - Bearing Stiffeners	Nominal Axial Load Capacity	$P_e = \frac{\pi^2 E}{\left(\frac{Kl}{r_s}\right)^2}A_g$	(6.9.4.1.2-1)
Fillet Welds	Nominal Shear Resistance	$R_r = 0.6F_{exx}$	(6.13.3.2.4b-1)
Shear Connectors	Nominal Shear Resistance	$Q_r = Q_n$	(6.10.10.4.1-1)
Concrete	Modulus of Elasticity	$E_c = 1{,}820\sqrt{f_c'}$	(C5.4.2.4-1)
Concrete	Modulus of Rupture	$0.24\sqrt{f_c'}$	(Sect. 5.4.2.6)
Concrete	Tensile Strength	$0.23\sqrt{f_c'}$	(Sect. C5.4.2.7)

Variable definitions:

C = ratio of the shear-buckling resistance to the shear yield strength from Eqs. 6.10.9.3.2-4,-5 or -6 as applicable, with $k_v = 5.0$

D = clear distance between the flanges less the inside corner radius on each side

D_p = distance from the top of the concrete deck to the neutral axis of the composite section at the plastic moment (in.)

D_t = total depth of the composite section (in.)

M_p = plastic moment capacity of the composite section (kip-in.) per AASHTO D6.1

M_u = ultimate moment at the strength limit state (kip-in.)

R_h = hybrid factor per AASHTO article 6.10.1.10.1 (1.0 for rolled girders and girders with constant F_y)

Once the nominal strength values for the various limit states are determined, resistance factors in accordance with Table 3.4 are applied to determine the design strength.

Table 3.4 AASHTO resistance factors

Limit State	Resistance Factor and Value
Flexure (structural steel)	$\phi_f = 1.00$
Compression (structural steel only)	$\phi_c = 0.90$
Tension in gross section (structural steel)	$\phi_y = 0.95$
Tension (reinforcing steel)	$\phi_y = 0.90$
Shear (structural steel)	$\phi_v = 1.00$
Shear (concrete)	$\phi_v = 0.90$
Shear Connectors in Shear	$\phi_{sc} = 0.85$
Shear Connectors in Tension	$\phi_{st} = 0.85$
Web Crippling	$\phi_w = 0.80$
Weld metal in fillet welds with tension or compression parallel to axis of weld	$\phi_{e1} = 1.00$ (same as base metal)
Weld metal in fillet welds with shear in throat of weld metal	$\phi_{e2} = 0.80$

3.3.3 Preliminary Connection Evaluation

The study connection was analyzed by hand (Appendix B) to determine the controlling moment capacity of the various components. Moment capacities were determined by calculating the nominal axial capacities of the various components, applying their respective resistance factors and multiplying by their moment arms. The moment results of these calculations are presented in Table 3.4. The applied maximum moment from the analysis, as shown in Figure 3.8 is 1,968 kip-feet.

Table 3.5 Comparison of SMC Moment Capacities of Study Connection

Component	ϕP_n	Moment Arm	ϕM_n Moment Capacity
Slab Reinforcing #8+#5	1129 kips	41.375 inches	3890 kip-feet
W33 Bottom Flange	615 kips	40.345 inches	2070 kip-feet
Welds to Sole Plate	421 kips	40.875 inches	732 kip-feet
Sole Plate	700 kips	41.375 inches	2414 kip-feet

As shown in the table, the moment capacity of the welds to the sole plate (1,434 kip-feet) is over 25% less than the required moment capacity of 1,968 kip-feet for the worst case truck load. The anticipated actual ultimate axial load to the welds is 578 kips (compared with a calculated capacity of 421 kips). This preliminary finding influenced the experimental test. As described in Section 4, the connection that was built for testing was modified from the exiting connection on the Box Elder Creek Bridge. The connection was built with two different weld sizes on the two girders, one weld was the size specified on the plans and one was the larger weld calculated to provide adequate moment capacity. A safety device was also installed to allow the connection to continue taking load even after failure of the small weld.

4. FINITE ELEMENT MODELING OF SMC CONNECTION

This section discusses modeling of the study connection in ABAQUS finite element software. Material modeling methods are discussed and the material properties to be used are developed. The first finite element analysis (FEA) performed was a sensitivity analysis of a double cantilever girder to optimize the meshing, element selection, element order, contact and constraint types to be used, boundary conditions, and load application methodology. Finally, the study girder connection was modeled and analyzed using ABAQUS. The final ABAQUS results were then used for monitoring of and comparison with the physical model test.

4.1 Material Modeling

Materials modeled were steel for beams, steel for stiffener plates, steel for sole (bearing) plates, weld metal for welds, steel for reinforcing bars, steel for headed stud anchors, concrete for slabs, and concrete for support piers. Steel members were expected for the most part to remain in the elastic range; however, some areas, particularly in the area of the welded connection, might extend into the plastic range. The same material model was used for both tension and compression for the structural steel. Concrete is brittle and has very low tensile capacity, thus its properties were defined on the basis of both tensile failure and compressive failure.

Steel beams: No damage of beams was anticipated except for the possibility of some plastic behavior, thus the beam material was modeled in ABAQUS as follows:
General=>Density = 2.935×10^{-4} kips/inch^3 (use gravity value of -1)
Mechanical=>Elasticity=>Elastic Young's Modulus = 29,000 ksi, Poisson's Ratio = 0.30
Mechanical=>Plasticity=> per Table 4.1

Table 4.1 Steel stress-strain curve values for F_y = 50 ksi (Salmon, 2009)

No.	Yield Stress (ksi)	Plastic Strain (in/in)
1	52	0
2	54	0.0193
3	69	0.0283

Steel stiffeners and sole (bearing) plates: No yielding of the stiffener plates or the bearing plates was anticipated; however, the stiffener and bearing plate material will be modeled as follows:
General=>Density = 2.935×10^{-4} kips/inch^3 (use gravity value of -1)
Mechanical=>Elasticity=>Elastic Young's Modulus = 29,000 ksi; Poisson's Ratio = 0.3
Mechanical=>Plasticity=> per Table 4.2

The elasticity properties were used until yield and then the plasticity properties were used for all of the plates modeled.

Table 4.2 Steel stress-strain curve values for F_y = 50 ksi (Salmon, 2009)

No.	Yield Stress (ksi)	Plastic Strain (in/in)
1	50	0
2	54	0.0193
3	69	0.0283

Steel reinforcing bars: Damage might have occurred to the reinforcing bars over the support at the location of the SMC action and therefore the material was modeled as follows:
General=>Density = 2.935×10^{-4} kips/inch^3 (use gravity value of -1)
Mechanical=>Elasticity=>Elastic Young's Modulus = 29,000 ksi; Poisson's Ratio = 0.3
Mechanical=>Plasticity=> per Table 4.3.

Table 4.3 Steel Reinforcing Stress-Strain Curve Values for F_y = 60 ksi (Grook, 2010)

No.	Stress (ksi)	Plastic Strain (in/in)
1	60	0
2	63.9	0.0155 (0.0175-0.002)
3	74.9	0.0380
4	88.0	0.0780
5	91.6	0.1180
6	86.8	0.1580
7	81.9	0.1830

Weld Metal: E70XX electrodes were used on both the actual bridge and the physical model. Stress-strain information about welds was difficult to find and many times was found to be specious at best. The selected reference, Ricles (Ricles, 2000), appears to have been used in a considerable amount of studies up until the present. The weld material information presented therein was based upon coupon testing of samples welded with E70 electrodes. The weld metal was anticipated to yield and most likely fail prior to the final total moment.
General=>Density = 2.935×10^{-4} kips/inch^3 (use gravity value of -1)
Mechanical=>Elasticity=>Elastic Young's Modulus = 29,000 ksi; Poisson's Ratio = 0.3
Mechanical=>Plasticity=> per Table 4.4 and Figure 4.1.

Table 4.4 Weld Stress-Strain Properties for E70 Electrodes

No.	Stress (ksi)	Plastic Strain (in/in)
1	71.0 (yield)	0.0000
2	78.0	0.0205
3	80.0	0.0206
4	86.6	0.0455
5	89.0	0.0955
6	90.0	0.1205
7	89.0	0.1455
8	86.6	0.1955
9	75.0	0.2455
10	53.0	0.2955
11	1.0	0.2956

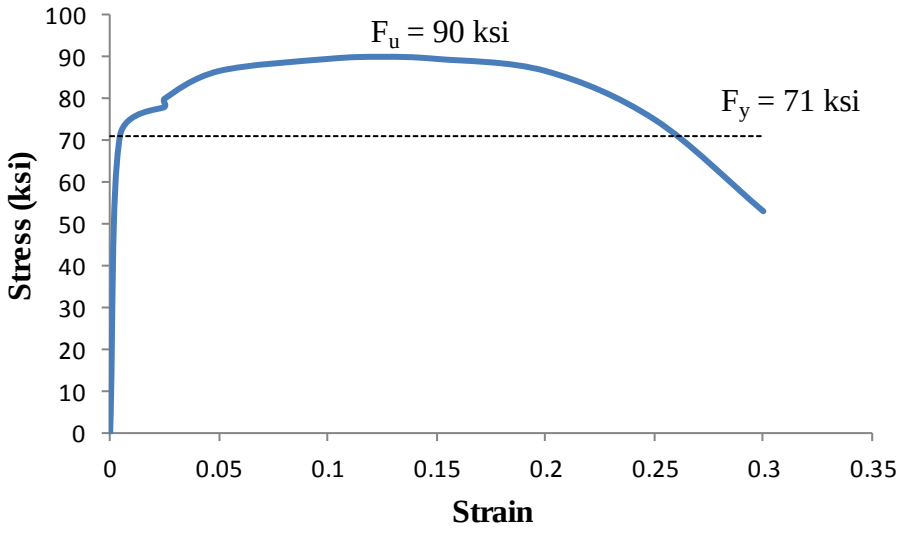

Figure 4.1 Stress-Strain Diagram for Weld Metal (Ricles, 2000)

Shear Studs: No yielding of the shear studs was anticipated; nonetheless, the material was modeled as follows:
General=>Density = 2.935×10^{-4} kips/inch^3 (use gravity value of -1)
Mechanical=>Elasticity=>Elastic Young's Modulus = 29,000 ksi; Poisson's Ratio = 0.3
Mechanical=>Plasticity=> per Table 4.5.

Mechanical properties for headed studs were given in the Nelson Stud Welding Catalog (Nelson, 2011). These studs conform to ASTM A-108 specifications for 1010 through 1020 mild steels. A graph of their stress-strain diagram is presented in Figure 4.2. It should be noted that the locations of strain hardening and ultimate strain were estimated as 25 times and 40 times yield strain, respectively, based on review of the behavior of other similar steels; these did not have an effect on the analysis since their interaction with the concrete did not cause significant strains nor plastic strains in the studs.

Table 4.5 Steel Stud Material Properties for Stress-Strain Diagram

Minimum Values	Mild Steel Shear and Concrete Anchors
Yield, 0.2% offset (ksi), R_e	51
Ultimate Tensile (ksi), R_m	65
% Elongation, A_s, in 2" gage length	20
% Area Reduction	50 (ICC, 2012)

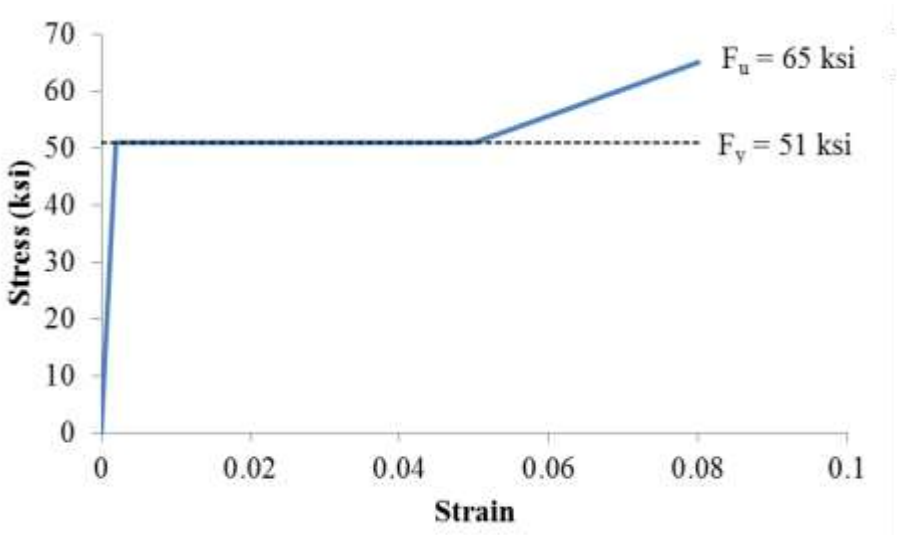

Figure 4.2 Stress-strain diagram for stud shear connectors

Concrete: It was anticipated that for the SMC action to be invoked, there would be cracking in the upper concrete when it was subjected to tensile loads from the negative moment over the support. The concrete material model that modeled this effect most properly was "CONCRETE DAMAGED PLASTICITY." Characteristics of this model are two failure mechanisms, tensile cracking of the concrete, and compressive crushing of the concrete. A suitable concrete response curve and formulation for concrete subject to uniaxial tension was presented by Godalaratnam (1985). This formulation provides a peak at the determined tensile strength and then a curved softening response after tensile failure, which accurately models the effects of widening cracks, Figure 4.3. This response occurs due to tension from bending action on the concrete causing micro cracking over the support. The tensile damage behavior became effective initially over the supports and then extended further into the slab as more load was applied at the girder ends.

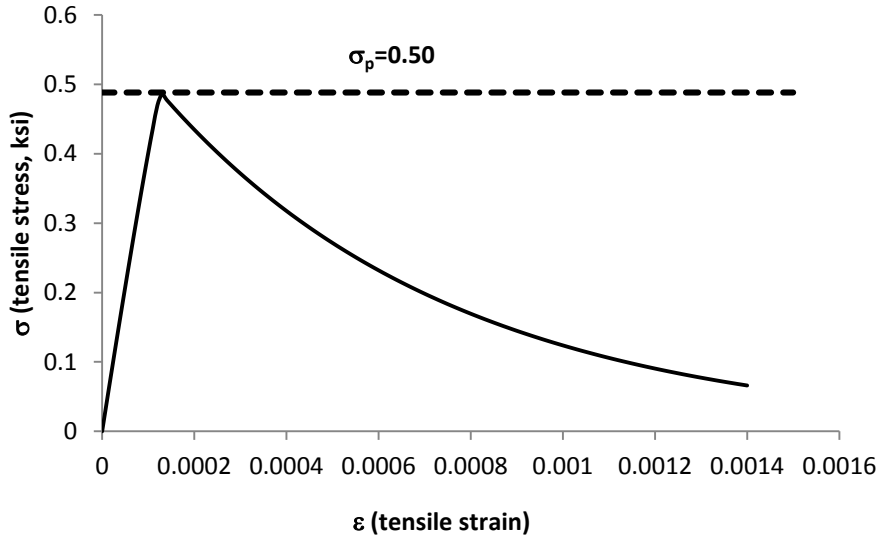

Figure 4.3 Softening Response to Uniaxial Loading Based on Plain Concrete Tensile Damage (Gopalaratnam, 1985)

Where:

For the ascending portion:

$$\sigma = \sigma_p \left[1 - \left(1 - \frac{\varepsilon}{\varepsilon_p} \right)^A \right]$$

Where:

$\sigma =$ tensile stress

$\sigma_p =$ peak value of σ

$\varepsilon =$ tensile strain

$\varepsilon_p =$ value of ε at σ_p

$A = E_t \varepsilon_p / \sigma_p$

$E_t =$ initial tangent modulus

For the descending portion:

$$\sigma = \sigma_p \left(e^{-k\omega\lambda} \right)$$

Where:

$\omega =$ crack width (μin)

$\lambda =$ 1.01 a factor

$k = 1.554x10^{-3}$ a factor

The values used in the model are summarized in Table 4.6; these values were determined using f'$_c$ = 4712 psi for the actual physical model concrete, which came from the concrete cylinder tests.

Table 4.6 Damaged stress/strain values for 4712 psi concrete in uniaxial tension

Stress (ksi)	Strain	Plastic Strain
0	0	0
0.500	0.00013	0
0.481	0.00015	0.00002
0.459	0.00018	0.00005
0.431	0.00022	0.00009
0.325	0.00040	0.00027
0.305	0.00044	0.00031
0.255	0.00058	0.00045
0.173	0.0008	0.00067
0.067	0.0014	0.00127

Niroumand (2009) considered several models for damage of concrete under uniaxial compression loading. The study compared the work of three sources and settled on a reasonably simple approach (Carreira & Chu, 1985); this model uses only concrete ultimate compressive strength, strain at ultimate strength, and strains to determine the values of useable compressive strength (f_c'). In addition, it was the only model investigated, which allowed the concrete to reach its ultimate compressive strength before failure; all others peaked at values less than the ultimate strength. The basic formula for this model is given in Equation 4. This equation uses a factor β, which is determined by using Equation 5. However, Equation 5 is dependent upon f_c' in units of MPa; this was converted for ksi in Equation 6. For verification purposes, the Carreira & Chu study was compared against an older, frequently used (Simula, 2011) method (Karsan, 1969), which somewhat conservatively underestimates the compressive strength of the concrete. Comparisons of both methodologies for 4712 psi concrete are presented in the chart in Figure 4.4. Corresponding tabular values, based on Carreira and Chu were used in the analysis are presented in Table 4.7.

Another, more recent concrete uniaxial compressive damage model was found that showed promise (Lu, 2010). However, on evaluation of the formulations, the values for this model could not be reproduced by the author using the formulations presented. Additionally, the formulation depended primarily on the initial tangent modulus of the concrete being considered; this is not a value that is normally provided for concrete mixes, thus this model was considered unusable for multiple reasons.

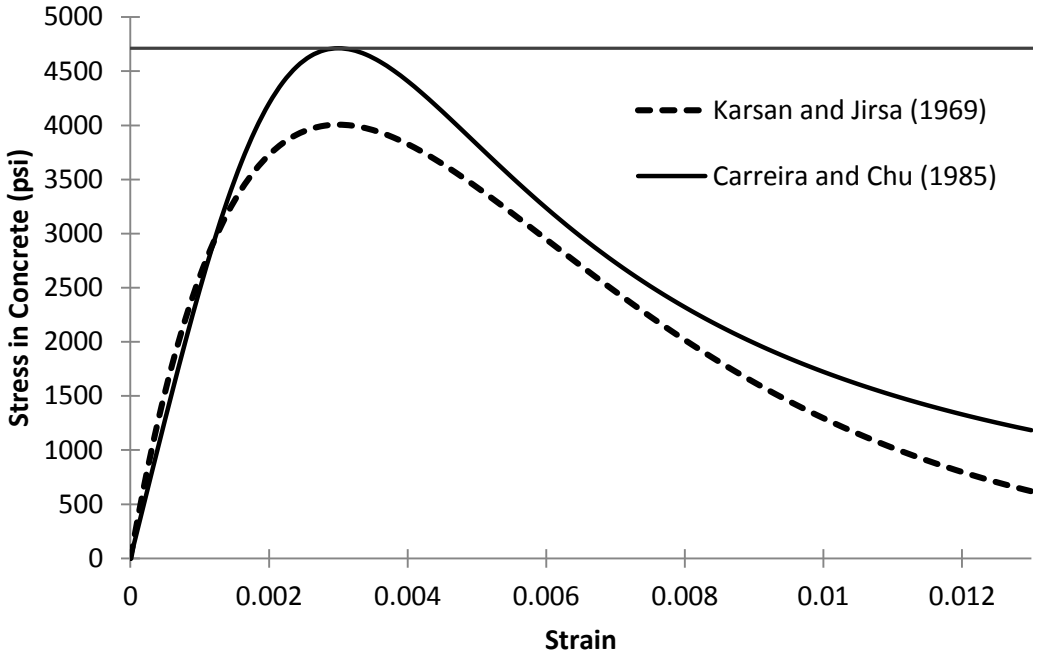

Figure 4.4 Damage Model for Concrete in Uniaxial Compression for f'$_c$ = 4712 psi

$$f_c = \frac{f_c' \beta \left(\frac{\varepsilon}{\varepsilon_c'} \right)}{\beta - 1 + \left(\frac{\varepsilon}{\varepsilon_c'} \right)^{\beta}}$$

Equation 4

$$\beta = \left[\frac{f_c'}{32.4} \right]^3 + 1.55$$

Equation 5

$$\beta = \left[\frac{f_c'}{4.7} \right]^3 + 1.55$$

Equation 6

Where:

ε = strain in concrete ($< \varepsilon_u$)

ε_c' = strain corresponding to the maximum stress, f_c'

f_c' = maximum compression stress (*ksi*)

Table 4.7 Damaged stress/strain values for 4712 psi concrete in uniaxial compression

Stress (ksi)	Strain	Plastic Strain
0	0	0
3.66	0.0016	0
4.20	0.0020	0.0004
4.63	0.0026	0.0010
4.71	0.0030	0.0014
4.70	0.0032	0.0016
4.65	0.0034	0.0018
4.41	0.0040	0.0024
3.95	0.0050	0.0034
3.24	0.0060	0.0044
2.73	0.0070	0.0054

In addition to tension and compression failure curves, the "CONCRETE DAMAGED PLASTICITY" model also requires several variables to fully model the behavior of the concrete; the values used are presented in Table 4.8.

Table 4.8 Additional variables to effectively model "CONCRETE DAMAGED PLASTICITY"

Variable	Symbol	Value	Source
Dilatation angle	ψ (degrees)	31° (based on a concrete friction angle of 37°)	(Malm, 2009)
Eccentricity	ε	0.1	Default value (Simula, 2011)
$\frac{\text{Equibiaxial}}{\text{Uniaxial}}$ compressive yield stress	$\frac{\sigma_{b0}}{\sigma_{c0}}$	1.16	(Lubliner, 1989)
Ratio of tensile meridian stress to compressive meridian stress without Hydrostatic pressure	$K_c = \bar{q}_{(TM)} / \bar{q}_{(CM)}$	2/3	Default value (Simula, 2011)
Viscosity parameter	μ	0	Default Value (Simula, 2011)

4.2 Element Selection and Modeling

Element types: ABAQUS offers a substantial number of element types when all the standard elements and their variations are considered. Selection of the appropriate element type for a given structural part and material can decrease processing time as well as provide more accurate results. The element types, which were anticipated to be used in this study, are presented in Table 4.9.

Table 4.9 Possible element types and their descriptions

Element Name	Description	Possible Use	Notes
S4R	4-node doubly curved thin or thick shell, reduced integration, hourglass control, finite membrane strains.	Girder Flanges Girder Web Girder Stiffeners	1
S8R	8-node doubly curved thick shell, reduced integration with 5 or 6 degrees of freedom per node		
C3D8R	8-node linear brick with reduced integration and hourglass control (only provides nodal displacements)	Solid Girder Steel Plates Welds Shear Connectors Concrete Slab Concrete Haunch Concrete Pier	
C3D20R	20-node linear brick with reduced integration (provides both nodal rotations and displacements)		2
T3D2	2-node linear 3D truss element	Reinforcing Steel	
T3D3	3-node quadratic 3D truss element	Reinforcing Steel	
B31	2-node linear 3D beam element (shear flexible)	Shear Connectors Reinforcing Steel	
B32	3-node quadratic 3D beam element (shear flexible)		

Notes:

1. Shell elements do not provide output of internal forces for comparison to the moments calculated by hand. Extracting and assembling the nodal forces and resultant moments from a beam created with shell elements is a major task.
2. Quadratic brick elements for the slab become severely distorted when modeled with elements embedded within them.

Structural steel: Structural steel shapes and stiffener plates were modeled as either shell or solid elements. The shell elements had the advantage of not only providing the three components of displacement, but also providing the three components of rotation at nodes, which were not provided by first order solid elements, Figure 4.5. The final determination of the element type was based on the results of the sensitivity analysis, Section 4.4.

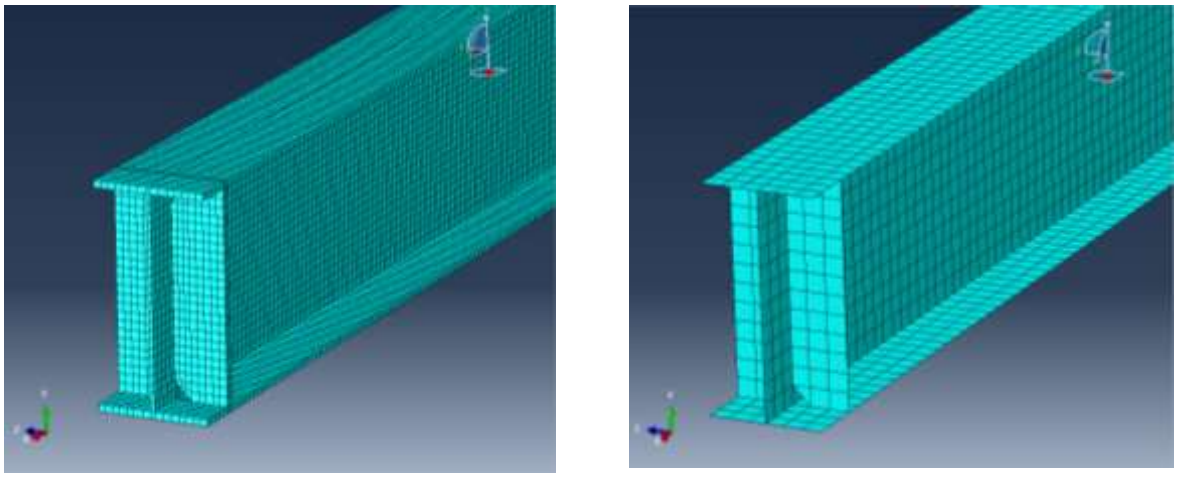

Figure 4.5 Meshed Girders - Solid Brick Elements (left) and Shell Elements (right)

Steel Sole plate: Due to its simplicity, structural steel for the sole plate was modeled using linear brick elements, Figure 4.6.

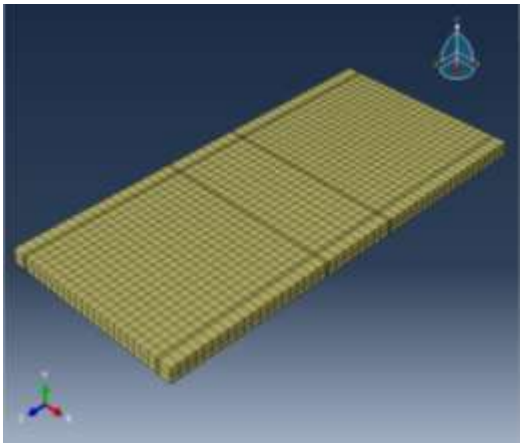

Figure 4.6 Meshed Sole Plate

Headed studs (shear connectors): Headed stud anchors for composite action were modeled as either linear brick elements, linear beam elements, or quadratic beam elements. Dimensional information for modeling of the shear stud and the connector as modeled and meshed are shown in Figure 4.7.

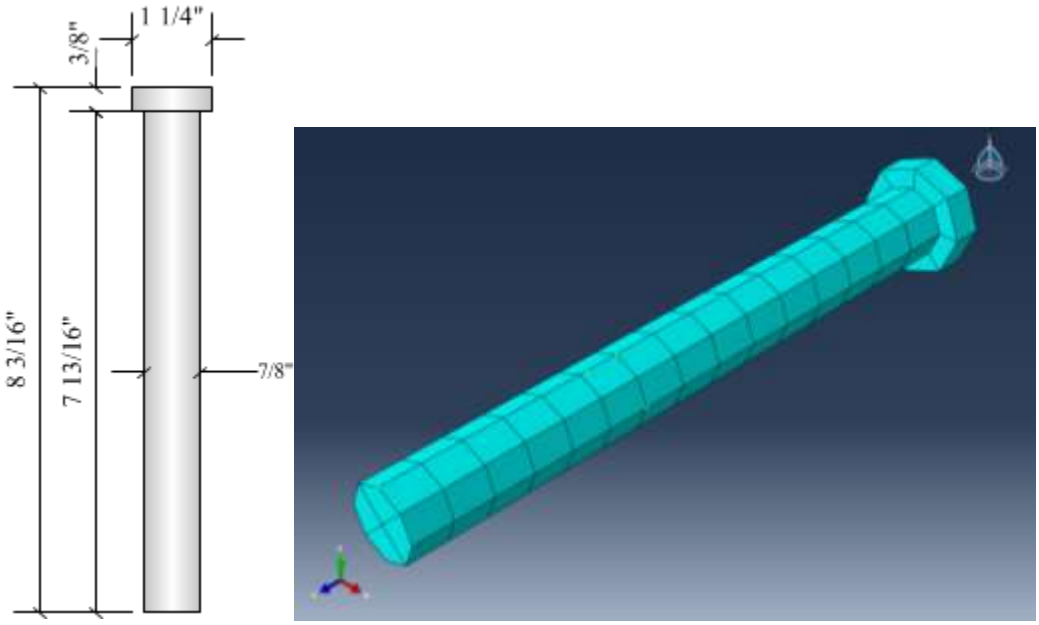

Figure 4.7 Shear Stud Connector Dimensions and as Modeled (brick elements)

Welds: Welds were modeled as either linear or quadratic brick elements, Figure 4.8.

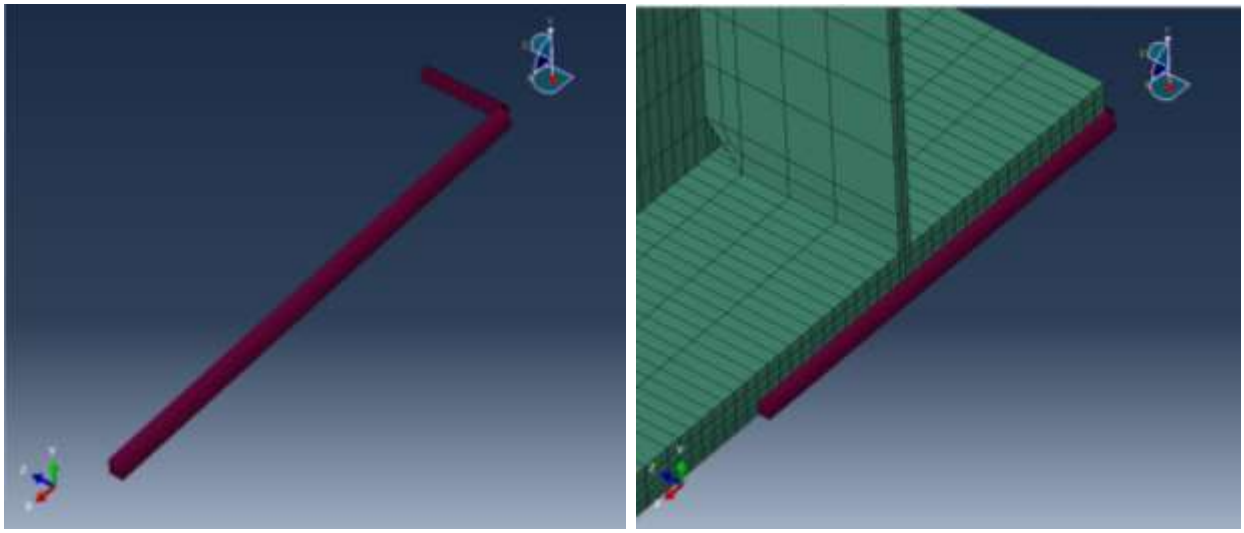

Figure 4.8 Weld (left), Weld and Girder (right)

Reinforcing Steel: Reinforcing steel was modeled as either two or three node truss elements, linear beam elements, or solid linear brick elements. Linear beam elements would include shear deformations.

Concrete Slab and Haunch: These members were created as a single member to allow common meshing and material definition. The combined section was modeled with either linear or quadratic brick elements, Figure 4.9.

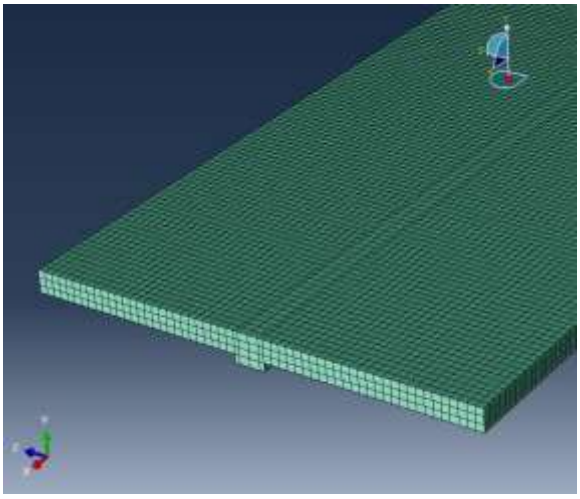

Figure 4.9 Meshed Slab and Haunch

Concrete Support Pier: The pier, Figure 4.10, was modeled with linear brick elements as variations in element selection for this part would have little effect on the SMC behavior and the pier is only acting as a support.

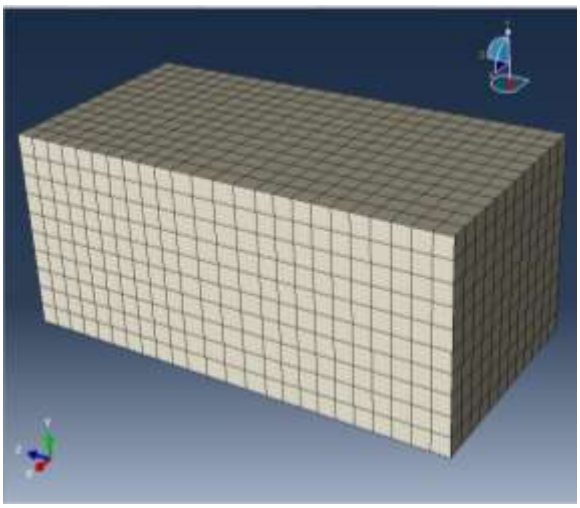

Figure 4.10 Meshed Pier

4.3 Constraints and Contacts

Constraints consist of boundary conditions such as rigid supports and springs to restrain the structure from displacing or rotating depending upon actual support conditions and the anticipated behaviors. However, constraints can provide much more than just boundary conditions; they may specify tied behavior between dissimilar parts or materials so they behave as a unit. Ties may also indicate to the software that one part is partially in another and tie the two together at the intruding portion, such as shear studs tied to the top of the girder and extending into the concrete. They may also be used to specify parts embedded in other parts, such as reinforcing steel in concrete slabs.

Boundary condition constraints are available for all nodal displacements and rotations. When using linear brick elements, rotational constraints may cause errors since only displacement constraints are necessary to develop fixity. Boundary condition constraints were used on the base of the pier for only translational displacements since the pier was modeled with linear brick elements.

The embedded region or the tie constraint may be used for the interaction between the reinforcing steel and the slab concrete; the final selection is based on the results of the sensitivity analysis. The embedded region or the tie constraint may also be used for the interaction between the shear studs and the slab. The shear studs were in effect tied to the girder by making the two a combined shape and, thus, no constraint was necessary; this is discussed in detail in Section 4.4.

Contacts allow the definition of interactions between two parts. If contacts are not defined or improperly defined, ABAQUS does not have the ability to determine interactions and the contacting parts will just move through each other as the model displaces. By defining contacts, the user is able to control the behavior of the interaction between parts in order to achieve correct results.

The interaction type “Surface to Surface contact” was chosen for all the possible interactions between adjacent parts, which were not interconnected. The contact types available include tangential behavior, normal behavior, damping, damage, fracture criterion, and cohesive behavior; for this study, only tangential and normal behaviors were considered. Tangential behavior is defined by the friction between the two surfaces, which is selected by using the “Penalty” option and entering a coefficient of friction between the two materials or zero for no friction. For steel on concrete and concrete on steel, the coefficient chosen was 0.40; this interaction occurred between the load application girders and the top of the slab, between the bottom of the concrete haunch and the top of the girder and between the bottom of

the sole plate and the top of the concrete support pier. For steel on steel, a coefficient of 0.5 was used; this condition occurred between the bottom of the girder and the top of the sole plate. It is unlikely that any movement between the girder and the sole plate occurred since the two are also tied together with welds.

4.4 Sensitivity Analysis

A sensitivity analysis was conducted to determine the most accurate and best performing element types for use in the finite element analysis of the final model. The basic scheme of the girder used in the sensitivity analysis was similar, but significantly simplified from the final model and is as shown in Figure 4.11 and Figure 4.12. The girder as modeled in ABAQUS is shown and annotated in Figure 4.13.

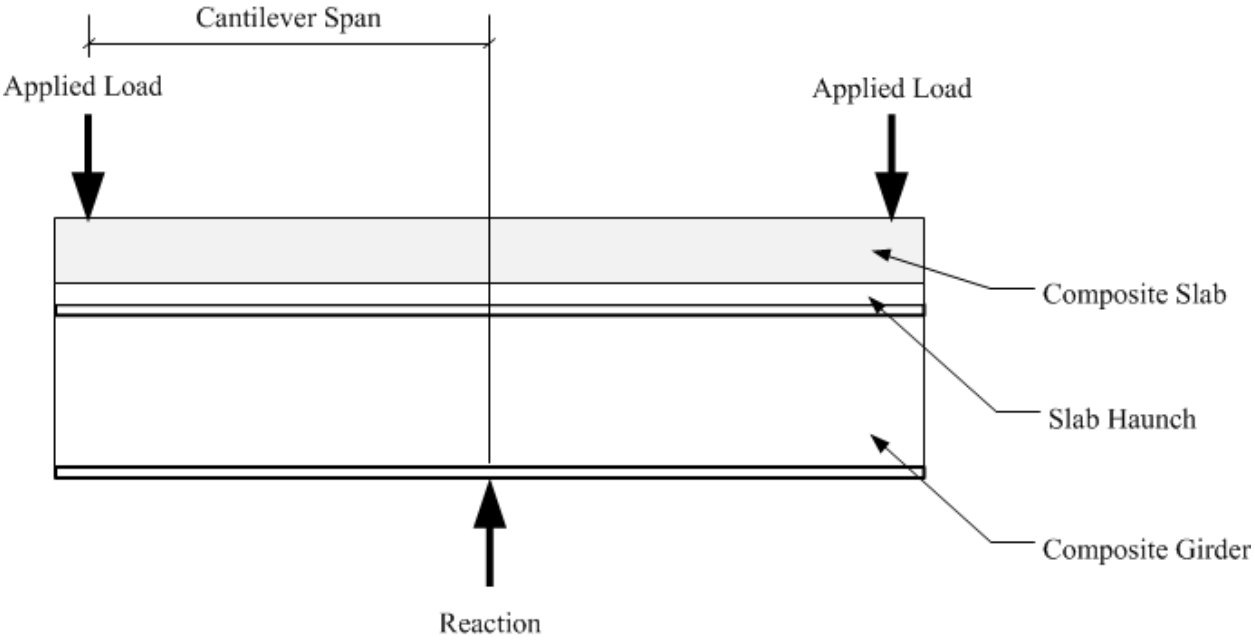

Figure 4.11 Sensitivity Analysis Composite Girder - Elevation

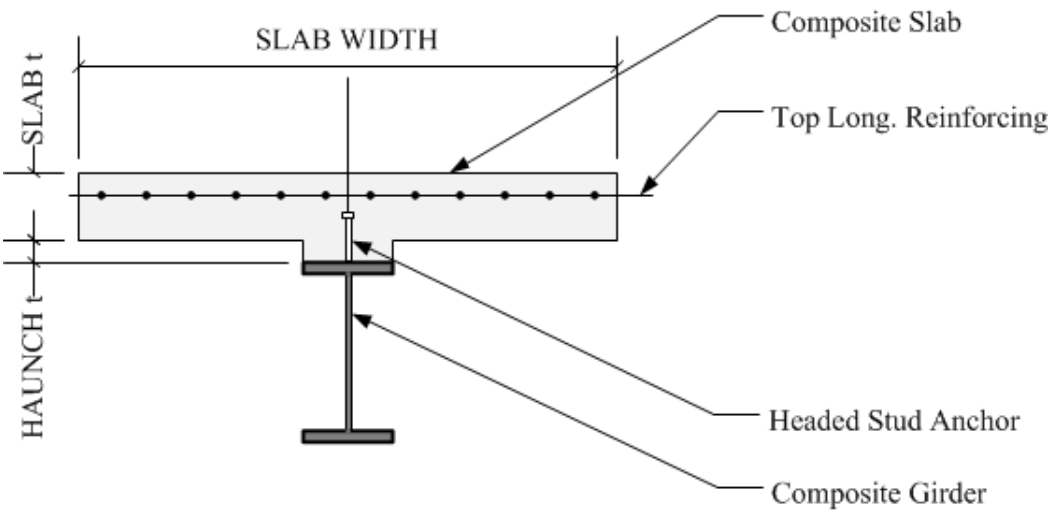

Figure 4.12 Sensitivity Analysis Composite Girder – Section

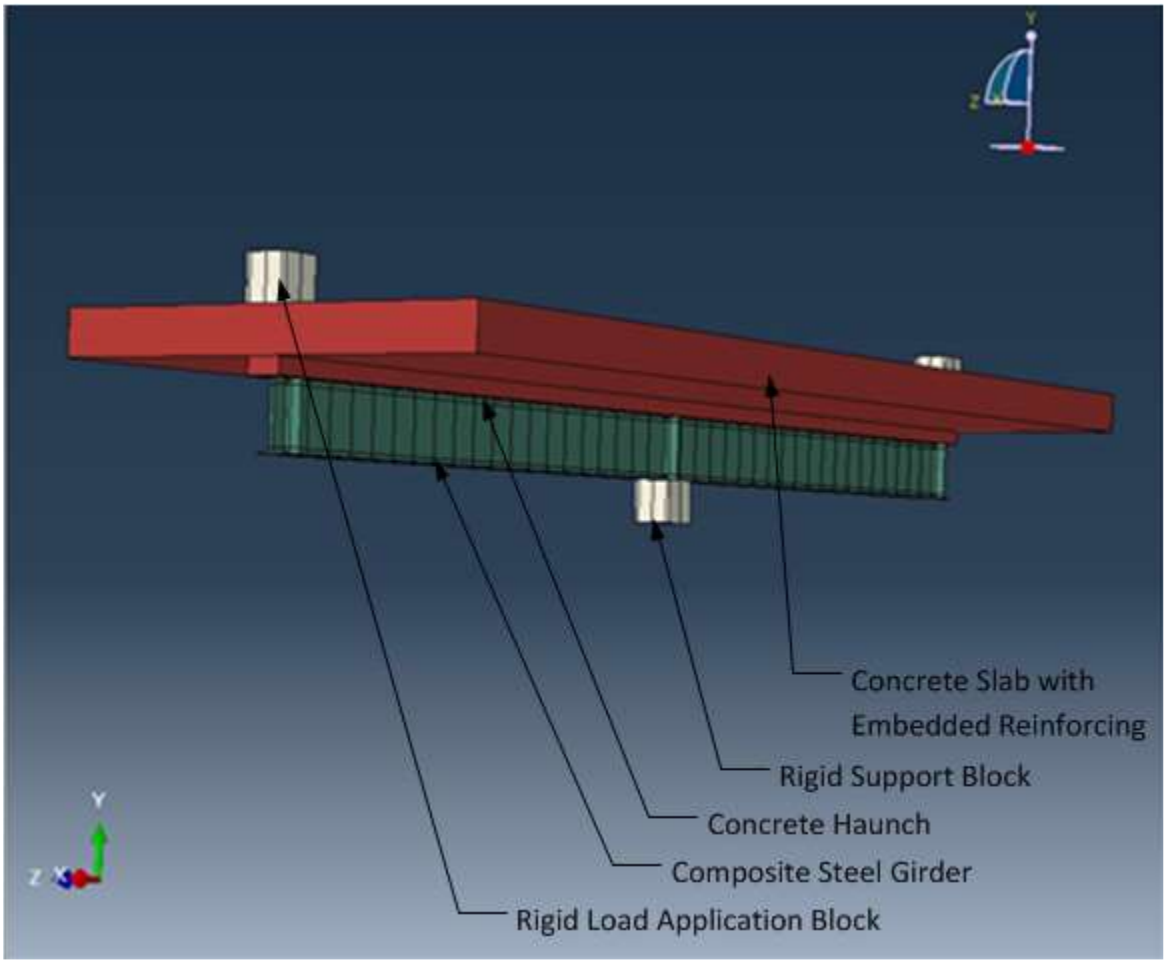

Figure 4.13 Sensitivity Girder - ABAQUS Model

Of equal importance to the selection of element types were the constraint and contact methodologies and properties. Constraints for boundary conditions were constant throughout the sensitivity analysis, consisting of the base of the support block constrained in all three component directions. Additional constraints involved how the reinforcing interacted with the slab and how the beam with studs was connected to the slab. Both the tie and embedded region methods were evaluated in the sensitivity analysis with mixed results. These same two methodologies were also applied to the studs on the beam and the slab, also with mixed results.

Contacts involved telling the program that two or more parts may contact each other and provided the ability to define what happens when that contact occurs. Contacts used in the sensitivity analysis were between the bottom of the haunch and the top of the girder, between the bottom of the rigid load application blocks and the top of the slab, and between the bottom of the girder and the top of the rigid support block.

Prior to the start of the sensitivity analysis, hand calculations were prepared to determine values of displacements based on various numbers of bars effective in composite action and moments along the span up to the support. The total span of the beam from point of load application to the face of the support is 118 inches. The calculated values were used for validation/comparison of the different FE models to the predicted calculated values. The deflections used for the validation/comparison are given in Table 4.10.

Table 4.10 Deflections in Inches for Various Combinations of #6 Bars Effective

Bars Effective	I_x (in^4)	Distance from the Support (inches)									
		0	**11**	**33**	**55**	**66**	**77**	**88**	**99**	**110**	**118**
0	204	0	0.009	0.123	0.345	0.488	0.648	0.821	1.005	1.195	1.389
1	287	0	0.007	0.088	0.246	0.347	0.461	0.584	0.715	0.850	0.988
2	361	0	0.005	0.070	0.195	0.276	0.366	0.464	0.568	0.675	0.785
3	428	0	0.004	0.059	0.165	0.233	0.309	0.392	0.479	0.570	0.662
4	488	0	0.004	0.051	0.144	0.204	0.271	0.343	0.420	0.499	0.580
5	544	0	0.004	0.046	0.129	0.183	0.243	0.308	0.377	0.448	0.521
6	594	0	0.003	0.042	0.118	0.168	0.222	0.282	0.345	0.410	0.477
7	641	0	0.003	0.039	0.110	0.155	0.206	0.262	0.320	0.381	0.442
8	683	0	0.003	0.037	0.103	0.146	0.193	0.245	0.300	0.357	0.415
9	723	0	0.003	0.035	0.097	0.138	0.183	0.232	0.284	0.337	0.392
10	759	0	0.003	0.033	0.093	0.131	0.174	0.221	0.270	0.321	0.373
11	793	0	0.002	0.032	0.089	0.126	0.167	0.211	0.258	0.307	0.357
M (k-in)	----------	2360	2140	1700	1260	1040	820	600	380	160	0

The sensitivity analysis stepped through variations in element types and constraints to consider the 36 different models summarized in Table 4.11.

Table 4.11 Sensitivity Analysis Matrix (Shaded areas indicate the choices being analyzed)

	Girder				Slab & Haunch			Loads	Reinforcing			Studs	Constraints				Contacts			
Case	Shell Elements	Solid Linear Elements	Solid Quadratic Elements	Second Order Accuracy	Solid Linear Elements	Second Order Accuracy	Solid Quadratic Elements	SMC Live Load	Truss Elements	Solid Linear Elements	Beam Elements	Linear Beam Elements	Embedded Reinforcing	Tied Reinforcing	Embedded Studs	Tied Studs	No contact slab to girder	Contact slab to girder	Run name using 10 processors	Total run Time (min.)
1		1"			3"				3"			1"							CT1	26
2		1"			3"				3"			1"							CT2	26
3		1"			3"				3"			1"							CT3	26
4		1"					3"		3"			1"							CT4	208
5			1"		3"				3"			1'							CT5	43
6		1"			3"				3"			1"							CT6	21
7		1"					3"		3"			1"							CT7	222
8			1"		3"				3"			1"							CT8	48
9		1"			3"				3"			1"							CT9	21
10		1"					3"		3"			1"							CT10	123
11			1"		3"				3"			1"							CT11	38
12		1"			2"				3"			1"							CT12	27
13		1"					2"		3"			1"							CT13	1505
14			1"		2"				3"			1"							CT14	174
15		1"			3"				3"			1"							CT15	26
16		1"					3"		3"			1"							CT16	191
17			1"		3"				3"			1"							CT17	50
18		1"			3"				3"			1"							CT18	19
19		1"					3"		3"			1"							CT19	134
20			1"		3"				3"			1"							CT20	30

Table 4.11 Sensitivity analysis matrix (continued)

	Girder				Slab & Haunch			Loads	Reinforcing			Studs	Constraints				Contacts			
Case	Shell Elements	Solid Linear Elements	Solid Quadratic Elements	Second Order Accuracy	Solid Linear Elements	Second Order Accuracy	Solid Quadratic Elements	SMC Live Load	Truss Elements	Solid Linear Elements	Beam Elements	Linear Beam Elements	Embedded Reinforcing	Tied Reinforcing	Embedded Studs	Tied Studs	No contact slab to girder	Contact slab to girder	Run name using 10 processors	Total run Time (min.)
21		1"			3"						3"-Q	1"							CT21	32
22		1"					3"				3"-Q	1"							CT22	732
23			1"		3"						3"-Q	1"							CT23	66
24	1"				3"						3"-Q	1"							CT24	17
25	Q				3"						3"-Q	1"							CT25	28
26	1"						3"				3"-Q	1"							CT26	194
27	1"				3"						3"-Q	1"							CT27	11
28	Q				3"						3"-Q	1"							CT28	31
29	1"				3"						3"-Q	1"							CT29	14
30	Q				3"						3"-Q	1"							CT30	23
31	1"				3"						3"-Q	1"							CT31	N/A
32	Q				3"						3"-Q	1"							CT32	N/A
33		1"			3"				3"-3D			1"							CT33	348
34		1"					3"		3"-3D			1"							CT34	183
35			1"		3"				3"-3D			1"							CT35	57
36		1"			3"					3"		1"							CT36	34

1" = 1" element size, etc.

Q = Quadratic elements

The results of the sensitivity analysis provided information on the correctness of the internal forces and deflections, run times, and quantity of increments required to complete the analysis. Also discovered during the sensitivity analysis were schemes of element type combinations, which failed to produce useable results or, much less, run at all.

Internal forces were the primary measure of acceptability of a particular run or runs. Deflections were unlikely to correspond to a simple hand analysis due to the severe indeterminacy of the girder-slab-reinforcing behavior, so while tabulated for comparison, these were not considered except to identify abnormal behavior, which may have invalidated a particular modeling scheme. Due to the inability to use the deflection values, the additional measures used were the run time and quantity of increments since these two don't necessarily increase together. A large number of increments indicate convergence issues, which were to be expected when using higher order elements; however, convergence issues also occurred with contact interactions. If contacts had no effect on the overall behavior of a model, they were omitted and run time decreased, sometimes considerably. A large number of increments also meant large output files, another good reason to improve convergence.

Since the cantilever section of the model is statically determinate, the moments at various points along these sections must be correct if calculated by hand using statics. Based on comparison of moments along the span for the various sensitivity models to the moments based on hand calculations, the models that compared well were numbers 4, 7, 16, 19, 22, 33, 34, and 36 as shown in the plot in Figure 4.14. A summary of the runs, execution times, and number of increments for these models is shown in Table 4.12.

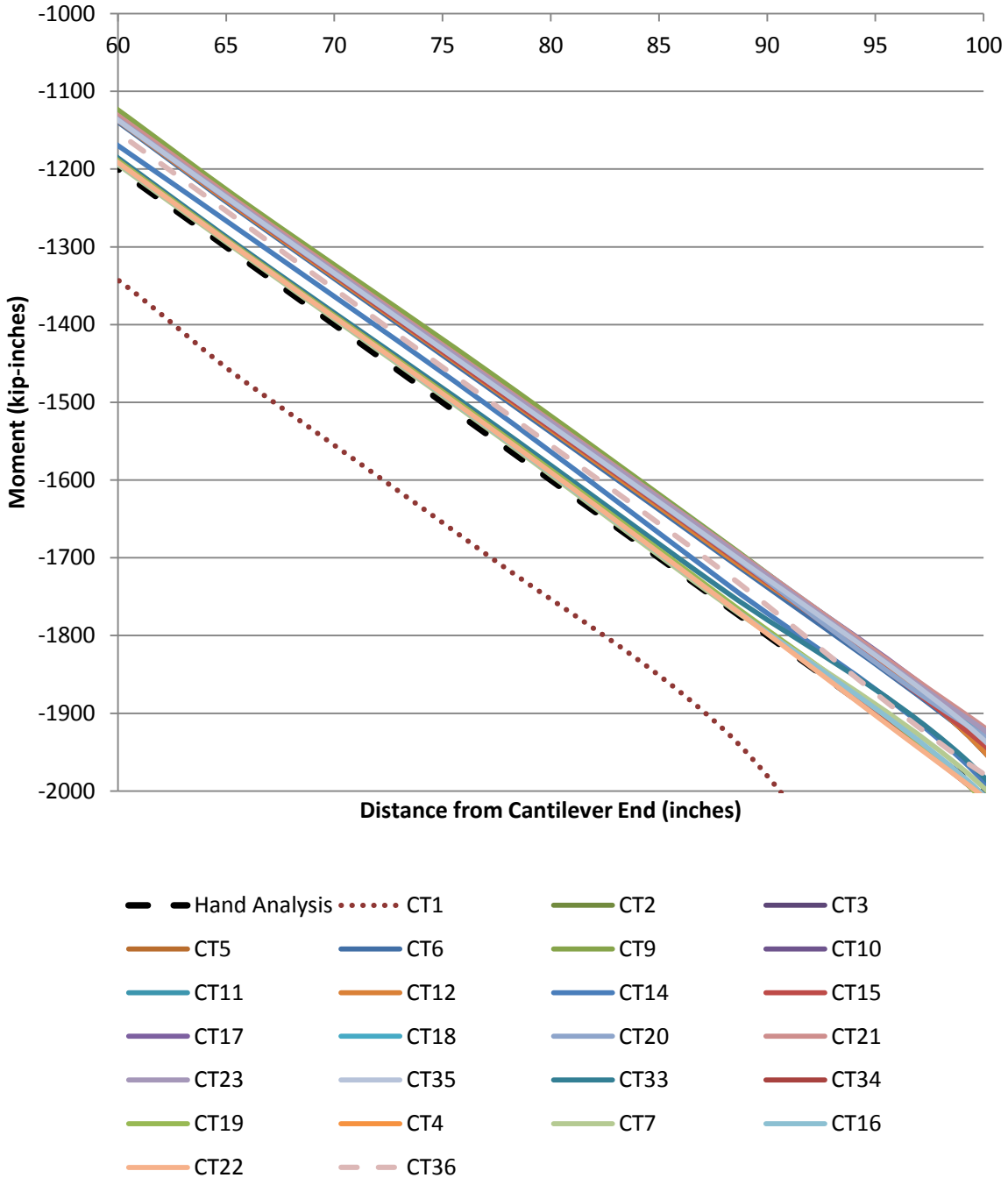

Figure 4.14 Comparison of Bending Moments from Sensitivity Analysis

Table 4.12 Sensitivity Analysis - Comparison of Increments and Run Times

Sensitivity Model Number	Execution Time (minutes)	Number of Increments
4	208	556
7	222	611
16	191	471
22	732	577
33	348	989
34	183	678
36	34	354

Reviewing Table 4.12, the run with the shortest execution time is number 36; this was the only run to use solid linear elements for the reinforcing bars in lieu of the supposedly simpler truss and beam elements. It's interesting to note that none of the runs that used smaller meshing for the slab (12, 13, and 14, where the element size is noted in the shaded box) provided any more accurate results than the runs with the coarser meshing of the slab. The finer meshed slabs also had the highest run times, between four and eight times longer than for the coarser meshed slabs.

4.5 Finite Element Analysis of the Study Girder Connection

4.5.1 Basic Finite Element Modeling

Based on the results of the sensitivity analysis, the finite element model of the study connection was created. From the sensitivity analysis, the element types and sizes given in Table 4.13 were selected for the respective parts.

Table 4.13 Final Part Element Types

Part	Element Type	Element Size
Girder and Stiffeners	Linear brick elements	1 inch
Shear Studs	Beam elements	1 inch
Slab and Haunch	Linear brick elements	3 inches
Reinforcing Steel	Linear brick element	3 inches
Sole Plate	Linear brick elements	1 inch
Concrete Support Pier	Linear brick elements	3 inches

The constraint types selected for use between the given parts are presented in Table 4.14.

Table 4.14 Final Constraint Types

Master	Slave	Constraint Type
Slab and Haunch	Reinforcing Steel	Embed
Slab and Haunch	Shear Studs	Embed
Steel Girder	Welds to Sole Plate	Tie
Sole Plate	Welds to Steel Girder	Tie

The interaction types selected for use between the given parts are given in Table 4.15.

Table 4.15 Final Interaction Types

Master	Slave	Interaction Type
Load Application Beams	Slab and Haunch	Hard Contact – μ = 0.4
Sole Plate	Steel Girder	Hard Contact – μ = 0
Concrete Support Pier	Sole Plate	Hard Contact – μ = 0.4
Steel Girder	Slab and Haunch	None

Notes on interactions:

1. μ is the coefficient of static friction.
2. A value of μ = 0 was used for contact between the bottom of the steel girder and sole plate to ensure that the total axial load component of the SMC behavior is transferred through the welds to the sole plate. Although somewhat unrealistic, it would also have been un-conservative to consider friction as resisting part of a load that may possibly overload the connection.
3. No interaction was necessary between the girder and slab since the two are constrained by the studs being embedded in the slab.

The final model was used to help predict and anticipate the behavior of the physical test. The model was then verified with the final test results and calibrated as necessary. This verified model was then used in a parametric study to develop design equations. The initial finite element model of the study connection is shown in Figure 4.15.

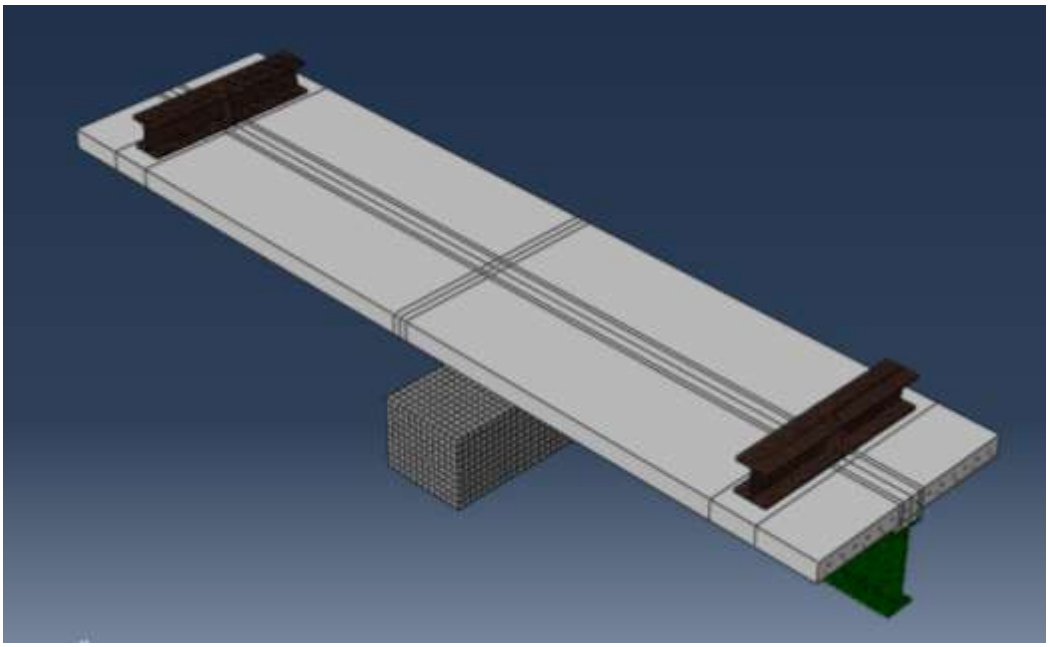

Figure 4.15 Modeling of Study Connection

4.5.2 Loads and boundary conditions

The FEA loads were applied in two steps. In the first step, the dead load of the structure was applied. The second step induced a moment in each girder to simulate the effects of the controlling design truck. In order to correctly represent the physical test model, the dead loads of model elements had to be considered in ABAQUS. The dead loads of the model consisted of the self-weight of the load application

beams, slab and haunch, reinforcing bars, steel girders, and steel studs. In lieu of using mass densities, unit weights were used with a gravity acceleration of -1 inch/second.^{2} The truck loading to be applied was a 90.0-kip concentrated load acting on each of the load application beams.

Boundary conditions consisted only of x, y, and z support reactions at the bottom of the pier. Since all elements of the FEA model were tied together and all loads were concentric and symmetric, no stabilizing boundary conditions were necessary. While the physical model had bottom flange stabilizers at the ends of the cantilevers, no such supports were necessary in the FEA model as it did not buckle laterally.

4.5.3 Contacts and Constraints

Contacts on the model of the SMC connection were created between the anchor bolts and the holes in the sole plate, the anchor bolt nuts and the top of the sole plate, the bottom of the steel girders and the top of the sole plate, and the bottom of the sole plate and the top of the pier (Figure 4.16). Contact was also created between the bottom of the load application beam and the top of the slab.

Tie constraints were used between the girder bottom flanges and the welds and between the welds and the sole plates (Figure 4.16). Tie constraints were also used between the headed studs on the top of the girder and the concrete slab, thus enforcing the composite behavior of the girder and slab (Figure 4.17). Embedded region constraints were used to define the top SMC reinforcing and the bending/shrinkage reinforcing in the slab (Figure 4.17).

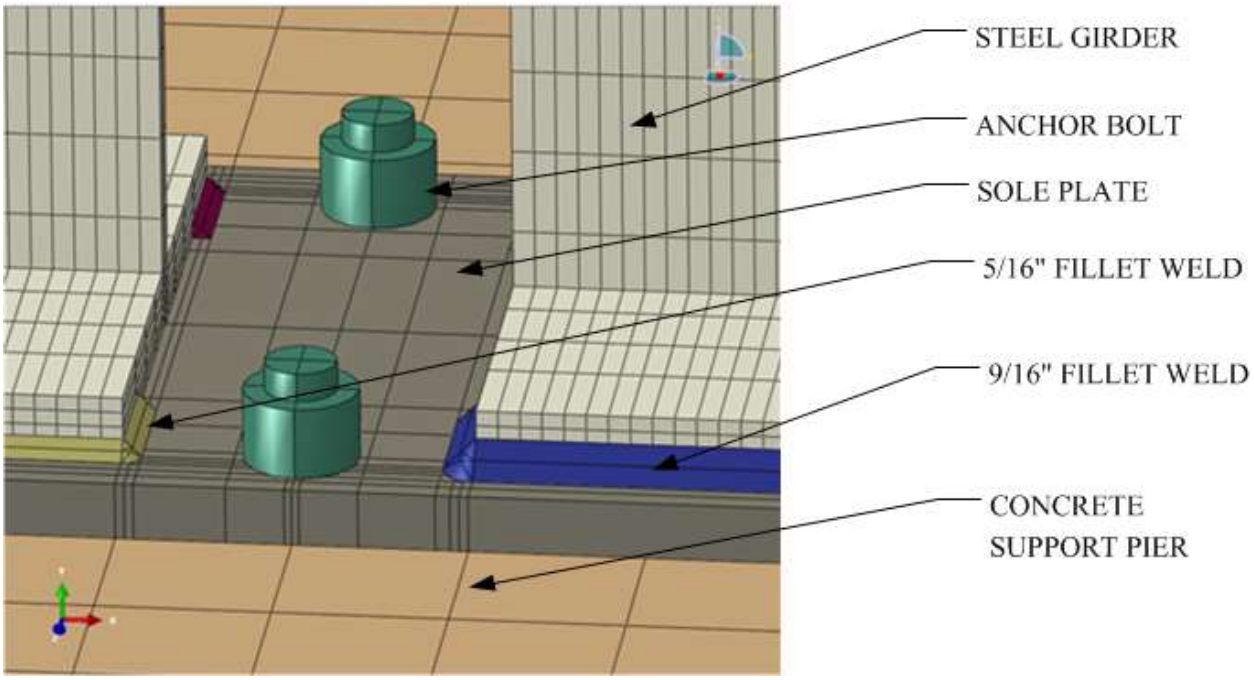

Figure 4.16 Contacts and Constraints at Support Pier

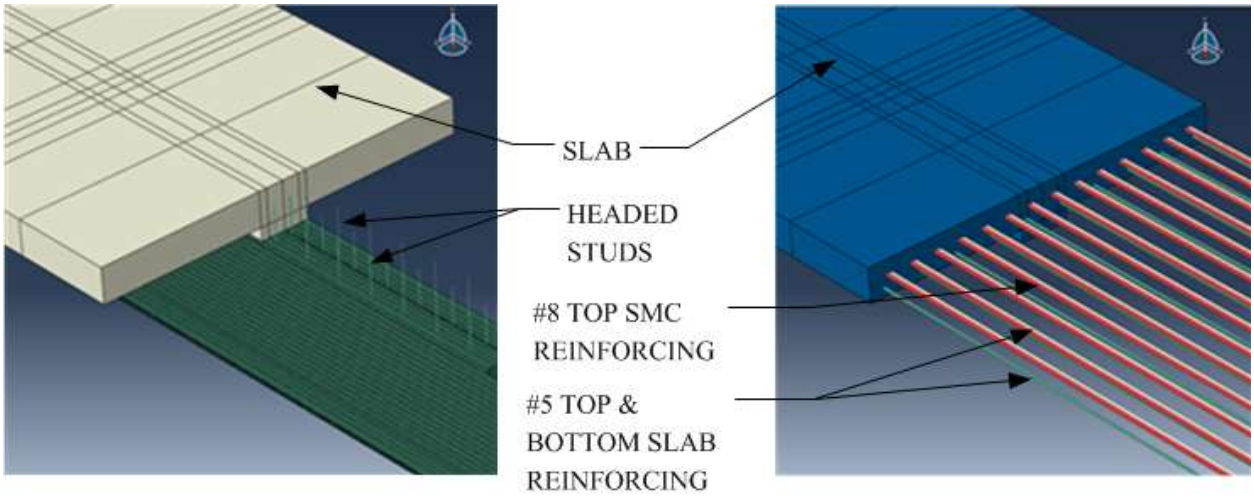

Figure 4.17 Slab, Studs, and Reinforcing Constraints

4.5.4 Load Steps and Convergence Criteria

Loads in Abaqus are applied in steps, which usually define a particular event in the life and behavior of the structure. Two steps were used in the subject analysis, one for considering the effects of the dead load gravity effects of the modeled structure and another to apply the concentrated load to the double cantilever structure to develop the remainder of the full SMC moment at the support. Each step was assigned a duration of one second and then the software attempted to solve each step in a single increment. For simple steps such as the application of the self-weight of the structure, one increment would usually do the job as the load is relatively small and unlikely to create any non-linear behavior. Convergence in Abaqus is a function of solution method, convergence tolerances, number of equilibrium iterations allowed before time cutbacks are made, and factors for time cutbacks. The solution method chosen for the analysis was the direct method instead of iterative since the structure will have a sparse stiffness matrix due to its geometry and creation technique, which went through multiple revisions and modifications. The direct solver uses a "multi-front" technique, which may have reduced computational time. The matrix storage method was chosen as the solver default, which is the unsymmetric method; the unsymmetric method enforces the use of Newton's method as the numerical technique for solving nonlinear equations.

Convergence tolerances were "loosened" to account for the nonlinear behavior of the slab and its interaction with the shear studs and reinforcing. Additionally, numbers of increments available for each particular step were modified depending on the magnitude of load to be applied in the step. The larger the load, the more likely that the time increment would require reduction to converge; and if enough increments were not allowed, the run would have terminated prematurely.

4.5.5 Discussion of Results

The model completed successfully with a combination of the model dead load and a simulation service level load of 90 kips at each end. The run required a total of 137 increments, one for the gravity effects of the dead load of the model and the remaining 136 for analysis of the effects of the two symmetrically placed 90-kip loads.

4.5.5.1 Internal Force Results

The FEA moment induced at the center of the support was 13,560 inch-kips or 1,130 ft-kips (Figure 4.18), which agrees very well with 1,172 ft-kips determined in section 3.3.3. It is reasonable that the moment from the FEA would be smaller than from conventional analysis since in reality the shear in the girders diminishes as the girder begins to be supported by the sole plate, whereas the conventional analysis considers the girders to be point supported at the center of the support.

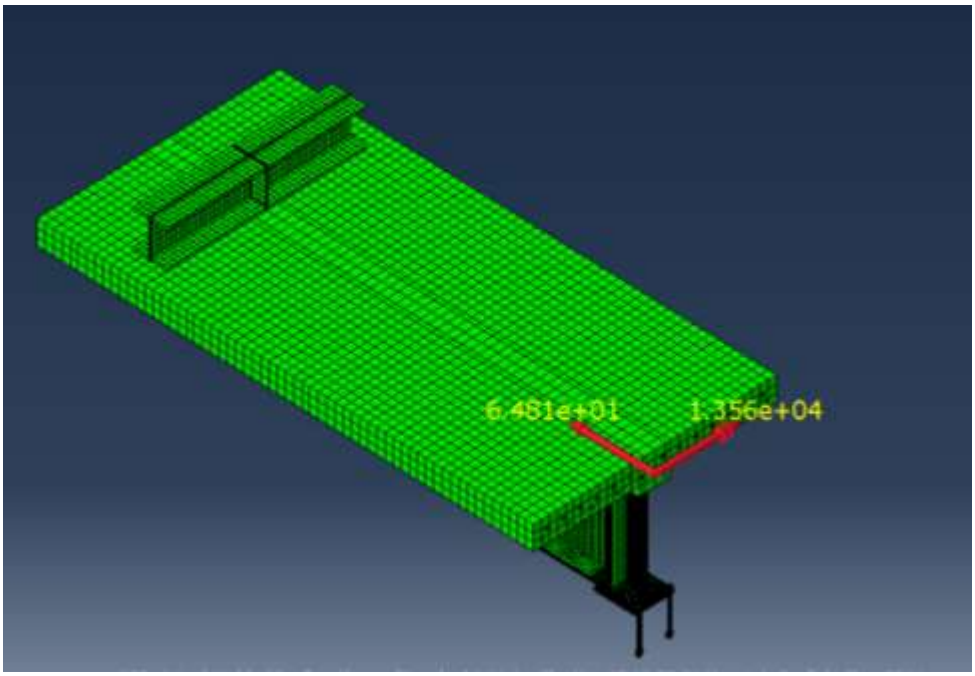

Figure 4.18 Centerline Negative Moment at SMC Connection

The axial load, which is transferred by a combination of compression in the sole plate (Figure 4.20) and friction between the sole plate to the pier (Figure 4.19), is approximately 567 kips (ultimate load). Reviewing the moment arms in Section 3.3.3, the moment arm for the weld is 40.875 inches, which combined with ultimate weld load determined above corresponds to an ultimate moment of 1,931 ft-kips, which compares well with the ultimate moment of 1,978 ft-kips obtained in the aforementioned section. Again, this moment would be less than that calculated by hand for the reasons discussed in the preceding paragraph.

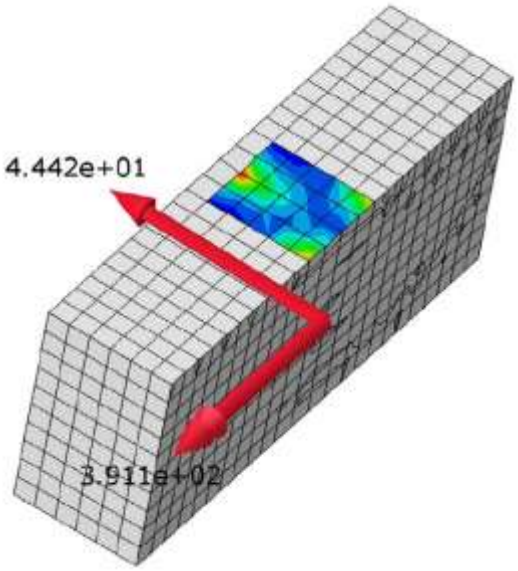

Figure 4.19 Axial Force at Pier

Figure 4.20 Axial Force at Sole Plate

An alternative FEA was performed on a nearly identical model, the only exception being that the slab was constructed in two parts, which abutted at the center and transferred load only through contact, and thus would take only compression at the center. In this run, the moment induced at the center of the support was somewhat less, 1,011 ft-kips versus the solid slab case where it was 1,130 ft-kips. However, the combined compression and frictional axial loads at the center of the connection were 324 kips, exactly the same; this implies that whether or not the concrete is capable of transferring any tension over the support, the force in the welds will be the same.

4.5.5.2 Material Behavior

Behavior of the material models used was verified by using Abaqus stress plots at various stages in the analysis.

The stresses in the top of the concrete slab are shown in Figure 4.21, Figure 4.22, and Figure 4.23 at dead load application, 75% of concentrated load application, and 100% of concentrated load application, respectively. Based on the "Damaged Plasticity" model, the maximum tensile stress that the slab may take is 0.50 ksi (Figure 4.3); once the tensile stress has reached 0.50 ksi and more load is applied, the stress decreases and redistributes elsewhere in the slab or goes to the reinforcing steel; the decrease in tensile stress in apparent in the latter two figures.

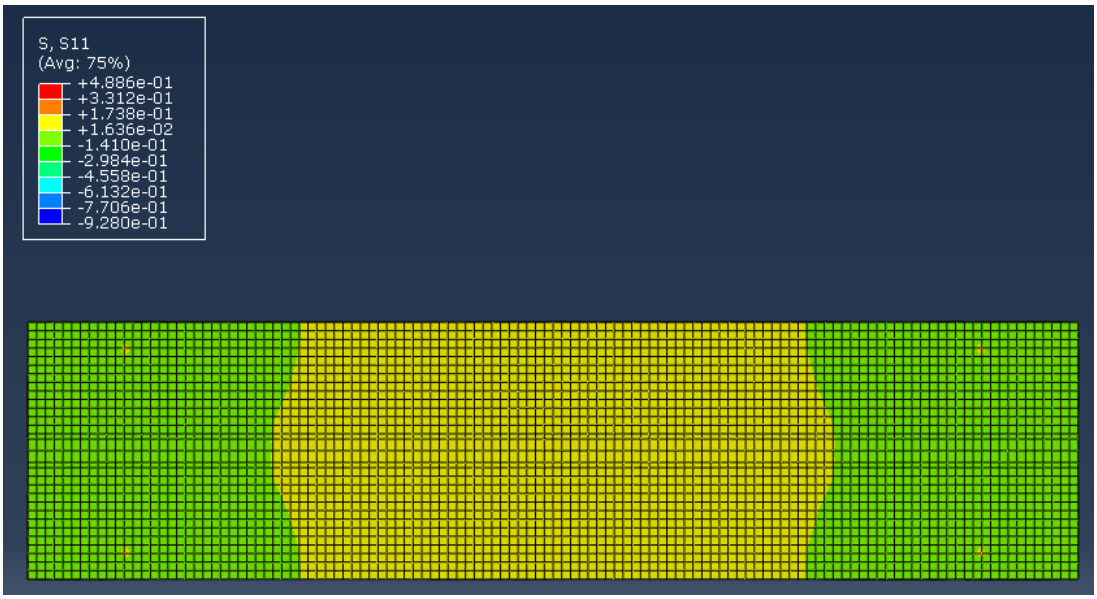

Figure 4.21 Concrete Surface Axial Stress after Dead Load Application

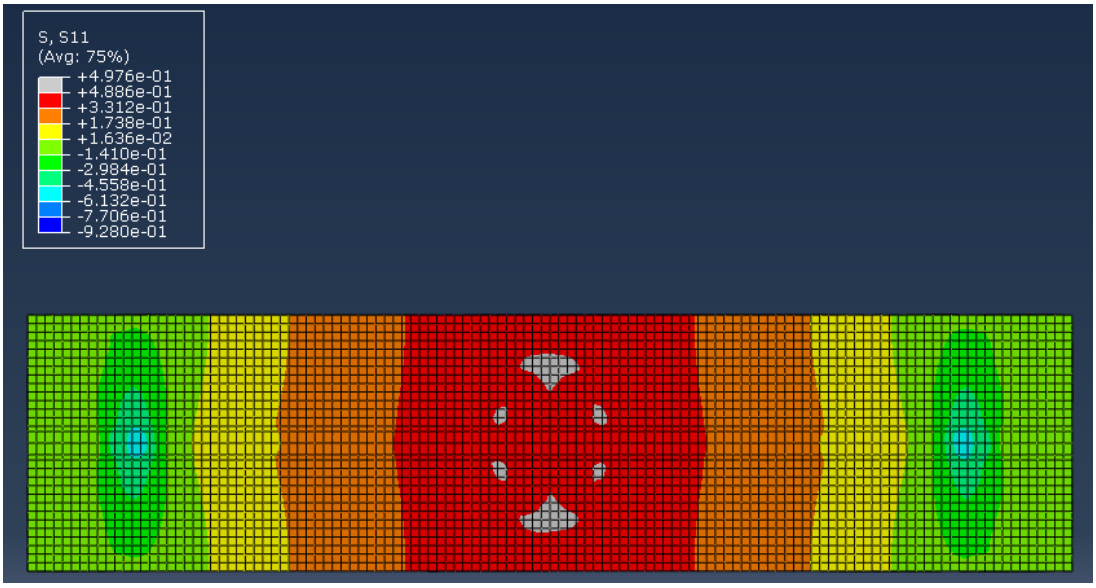

Figure 4.22 Concrete Surface Axial Stress after 75% of Concentrated Load Application

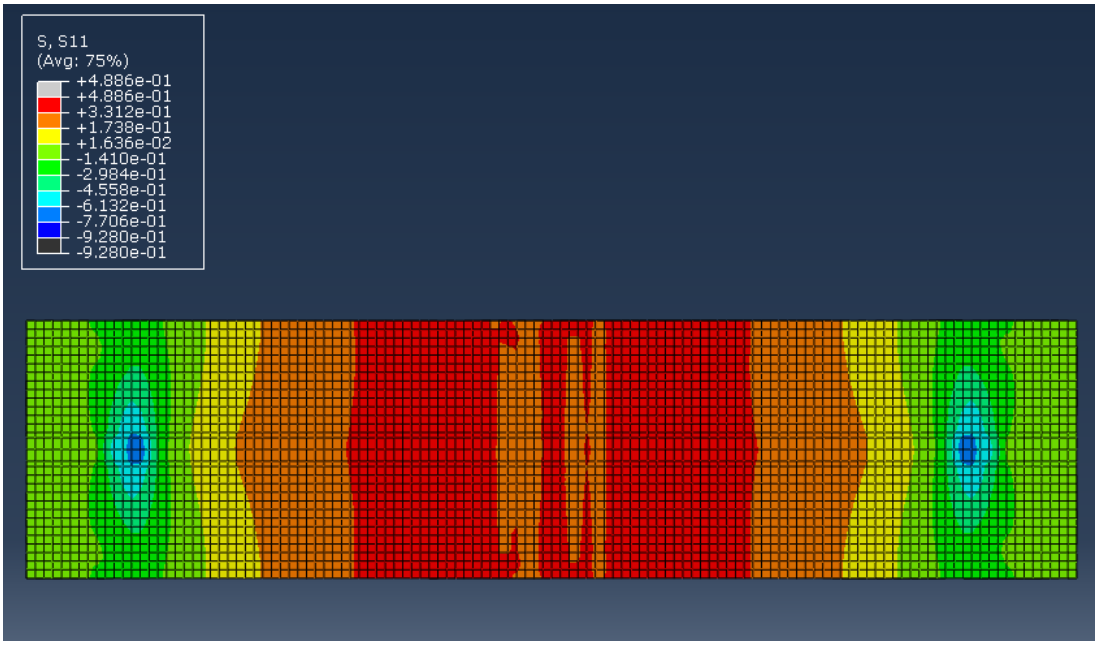

Figure 4.23 Concrete Surface Axial Stress after 100% of Concentrated Load Application

The fillet welds to the sole plate, which are the critical element in the SMC behavior, were evaluated for von Mises stress at various stages of the analysis. Specific stages selected were the end of the dead load application (Figure 4.24), at 75% of the concentrated load application (Figure 4.25), and 100% of the concentrated load application (Figure 4.26). None of the von Mises stresses exceeded the ultimate weld stress, F_u = 70 ksi, although several exceeded the AWS yield stress, F_y = 58 ksi, but by less than 10%.

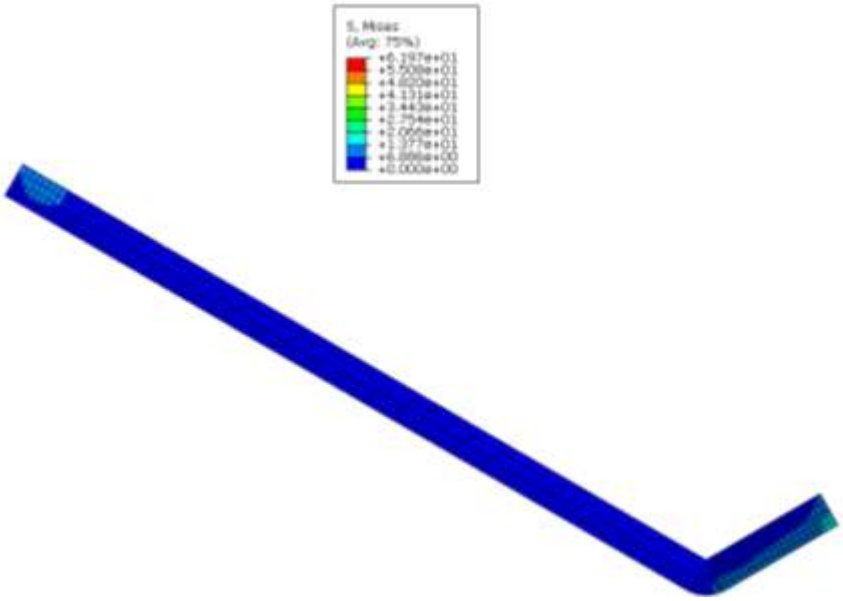

`

Figure 4.24 von Mises Stress in Weld after Dead Load Application

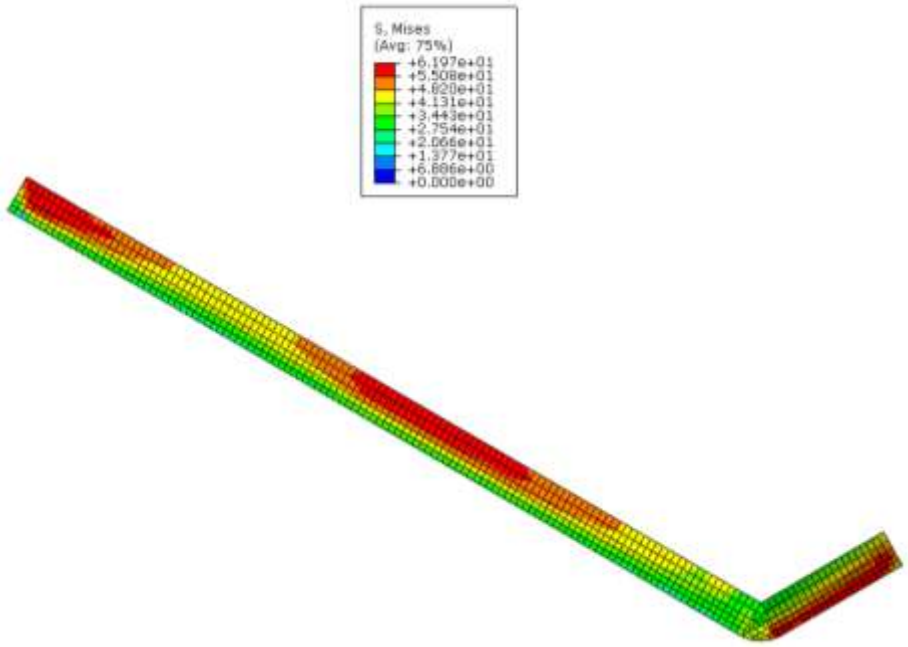

Figure 4.25 von Mises Stress in Weld after 75% of Concentrated Load Application

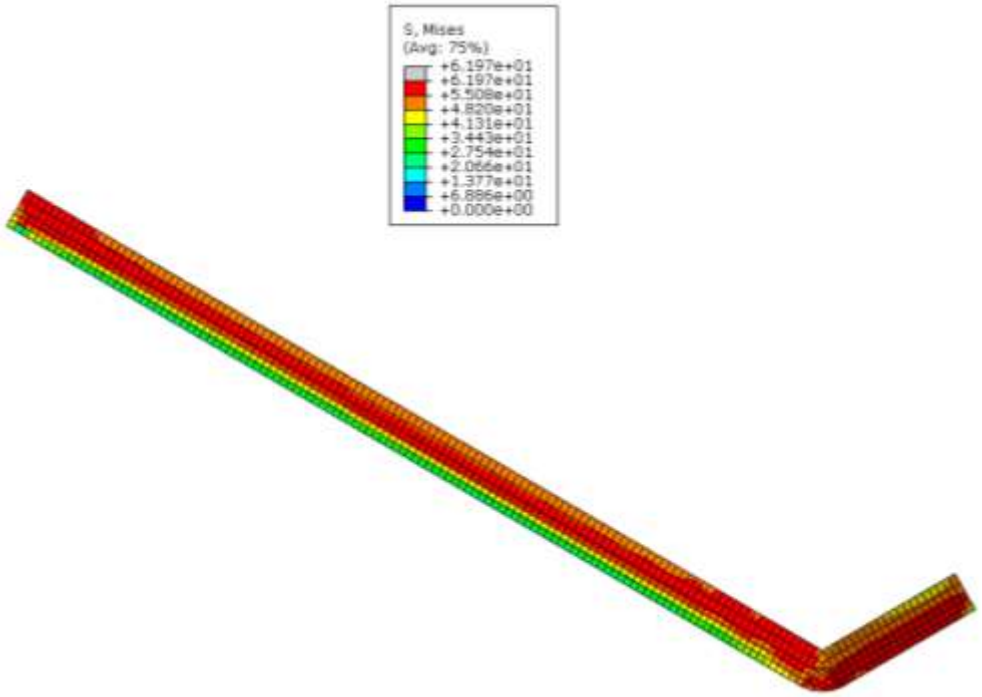

Figure 4.26 von Mises Stress in Weld after 100% of Concentrated Load Application

4.5.5.3 Results for Test Reference

Load, displacement, and strain data were gathered from the FEA in order to correlate the analysis with the physical test model. However, when compared with the final physical test results, the displacements, stresses, and forces determined from the FEA did not correspond well at all; this is discussed further in 5.6.4 Correlation/Comparison with Abaqus Results.

5. LABORATORY TESTING OF SMC CONNECTION

5.1 Loading Facilities

Testing was conducted at the CSU Engineering Research Center.A self-reacting load frame was constructed in the laboratory to facilitate this large scale test. The self-reacting frame was designed to support a total test load of 440 kips in order to match the capacities of the largest available actuators in the CSU lab. Construction photos of the frame show the concrete center support pier reinforcing, Figure 5.1, and the completed concrete pier, Figure 5.2.

Figure 5.1 Self-Reacting Load Frame - Concrete Support Pier Reinforcing

Figure 5.2 Self-Reacting Load Frame - Finished Concrete Support Pier

5.2 Test Specimen Description

The test specimen consisted of a reinforced concrete pier supporting an anchored steel sole plate with a neoprene bearing between. The bridge girders were two cantilevered W33x152 steel beams (**Figure**Figure 5.3), both of which were welded to the sole plate. Welds to the sole plate were different for each girder; the north girder was welded in accordance with the original bridge design, 14 inches of 5/16-inch fillet weld on each side. The 5/16-inch fillet weld was anticipated to fail at a test load of 90 to 100 kips. The south girder was welded with 14 inches of 5/8-inch fillet weld on each side, which was determined to be adequate for the bridge test and actual design loads. A partial W27x84 diaphragm beam (Figure 5.5) was installed on the west side of the girder for stability; the beam size chosen is the same as in the actual bridge. Additionally, due to the potential for damage and injury of personnel when the 5/16" fillet welds failed, a safety device (Figure 5.3) was installed between the beam ends to limit the movement of the beam at failure. The safety device, when engaged, would transfer the axial compression component directly between the girder bottom flanges. During the time that the safety device would be active, no horizontal loads would be transferred to the welds or the sole plate.

The top flanges of the girders had welded headed stud anchors in rows of three at nine inches on center (Figure 5.4). The concrete slab was reinforced top and bottom in both directions as in the actual bridge slab (Figure 5.7). The slab width was 7'-4", the same as the effective slab width allowed per AASHTO (2012), one-half of the spacing between girders on each side (Figure 5.6). Load application beams were installed and anchored near the ends of both cantilevers to accept the actuator and load cell arrangements. The load application beams were anchored to the slab with a total of six half-inch-diameter wedge anchors each to keep them from displacing horizontally. The load application beams were sized to uniformly distribute the load from the actuator over a width of 72 inches of slab. The loads were applied by a 220-kip actuator at the north end (Figure 5.8) and two 110=kip actuators at the south end (Figure 5.9).

The dimensions of the final physical test model of the study girder connection were set to match those of the finite element analysis. The selected connection also matched that built in the field, but with shortened girder lengths and load magnitude and application points calculated to create the same resultant moments and reaction at the pier. A plan of the tested model is shown in Figure 5.10. The entire set of drawings for the construction of the test specimen is provided in Appendix C.

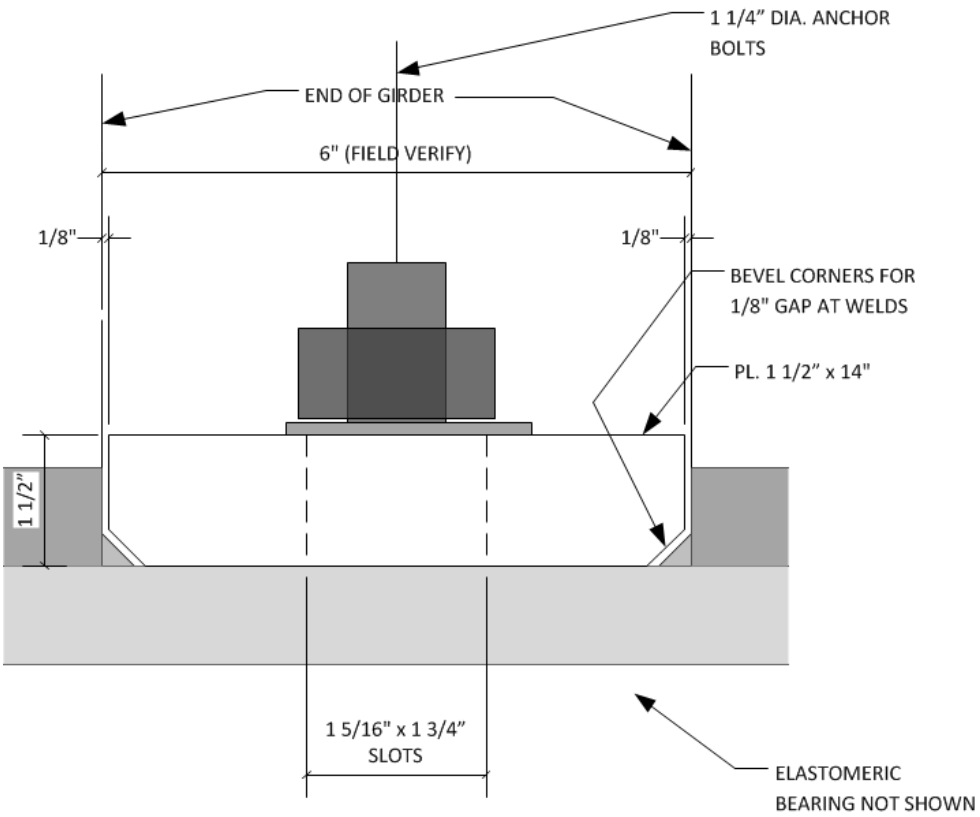

Figure 5.3 Safety Device Details

Figure 5.4 Bridge Girders with Studs

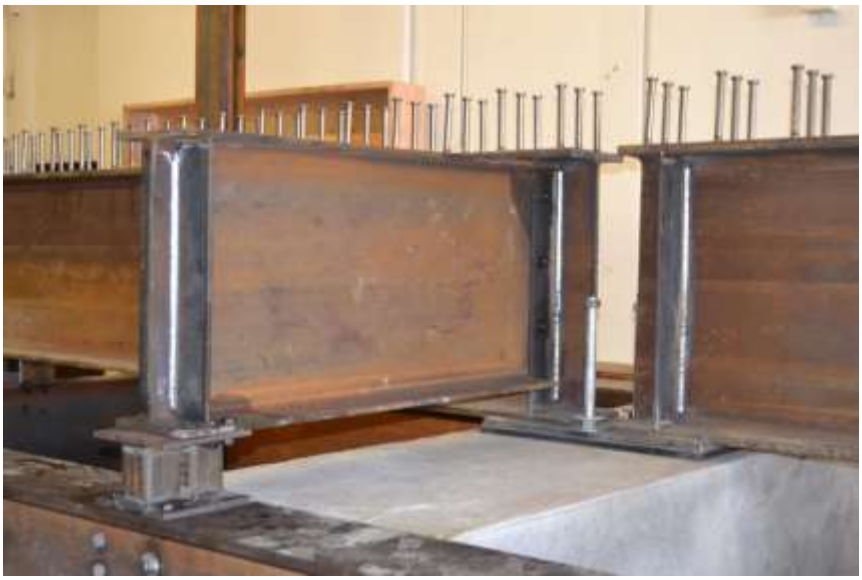

Figure 5.5 Steel Diaphragm Beam

Figure 5.6 Concrete Deck Slab

Figure 5.7 Slab Reinforcing Placement

Figure 5.8 220-kip Actuator and Load Application Beam

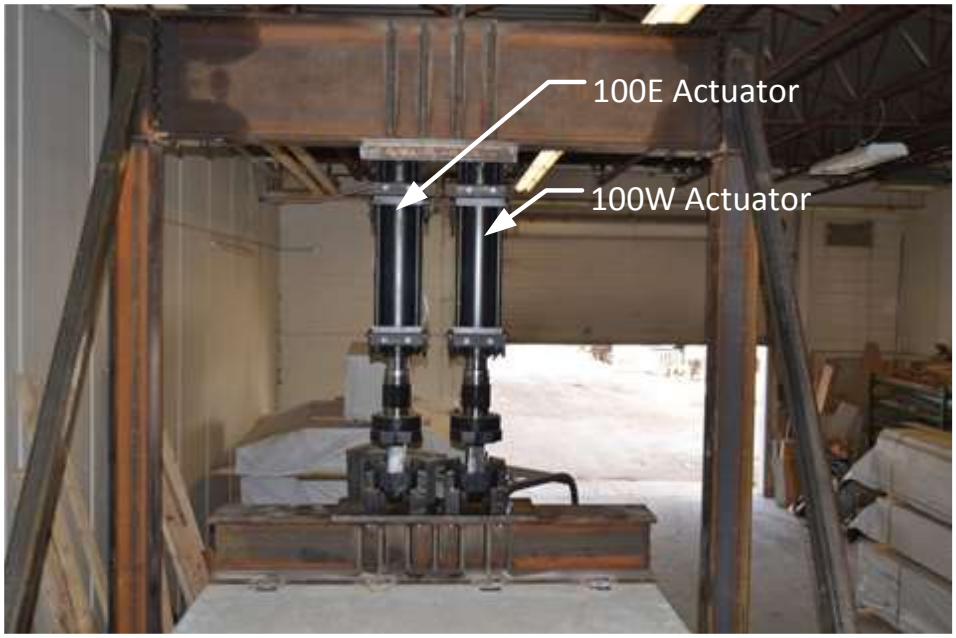

Figure 5.9 (2) 110-kip Actuators and Load Application Beam

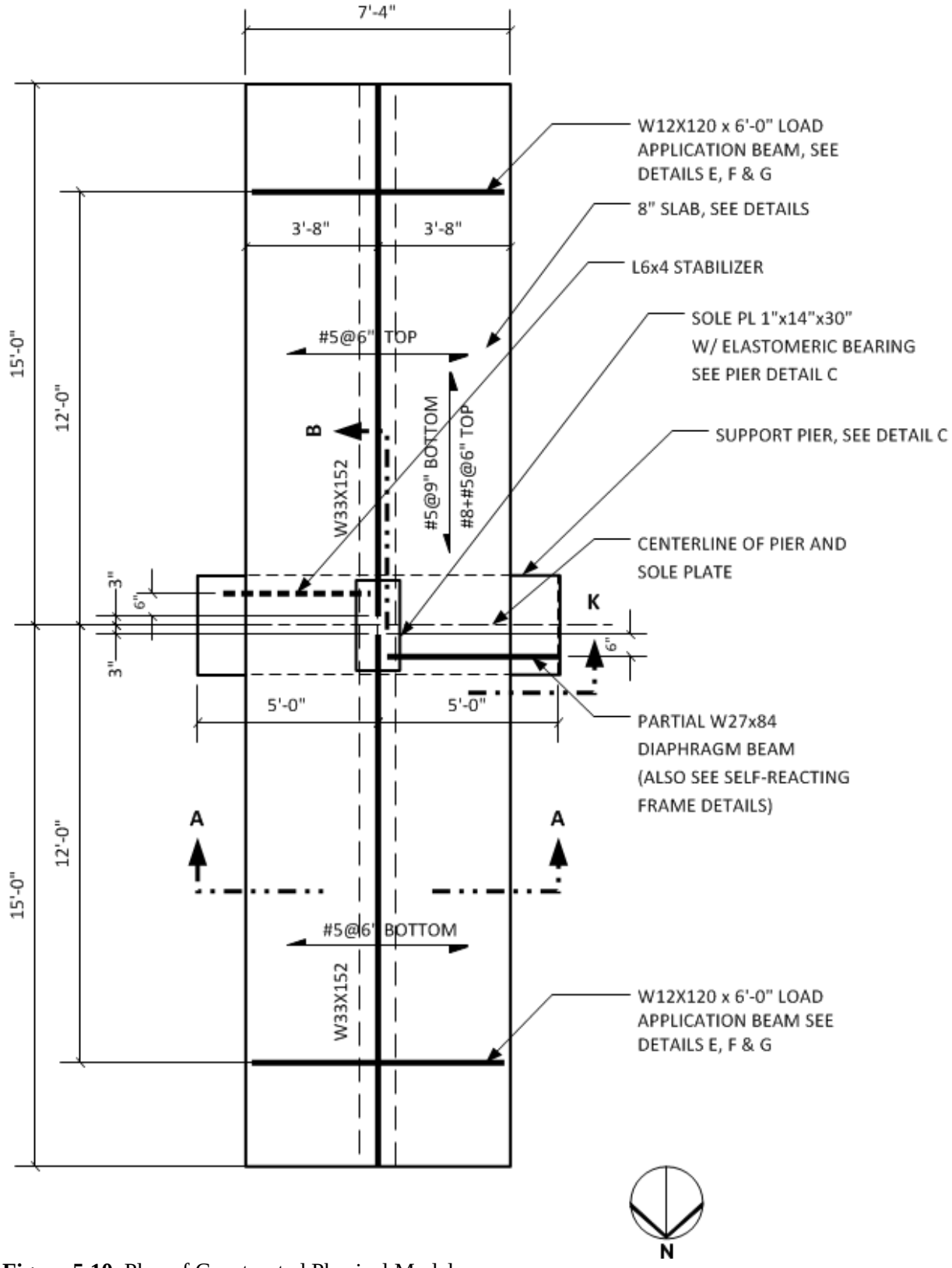

Figure 5.10 Plan of Constructed Physical Model

5.3 Test Specimen Instrumentation

The physical test specimen was instrumented at key locations based on results of the finite element analysis for later validation of the finite element model. The physical model was instrumented with electrical surface mounted strain gages and string and linear potentiometers. The various devices were positioned as shown in Figure 5.12 through Figure 5.19; a legend is given in Figure 5.11. Rationale for the placement of gages is given below the figures. The numbers shown in ovals are the gage numbers and the numbers shown in rectangles are the corresponding channel numbers for the DAQ.

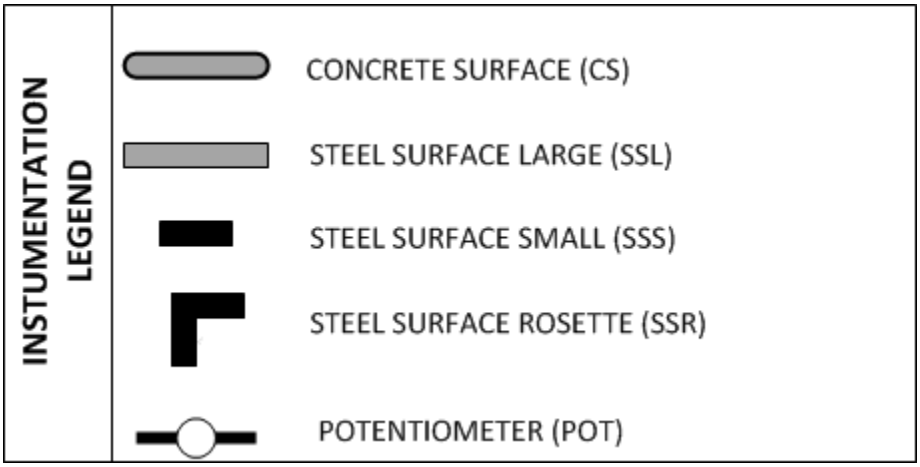

Figure 5.11 Legend for Instrumentation Layouts

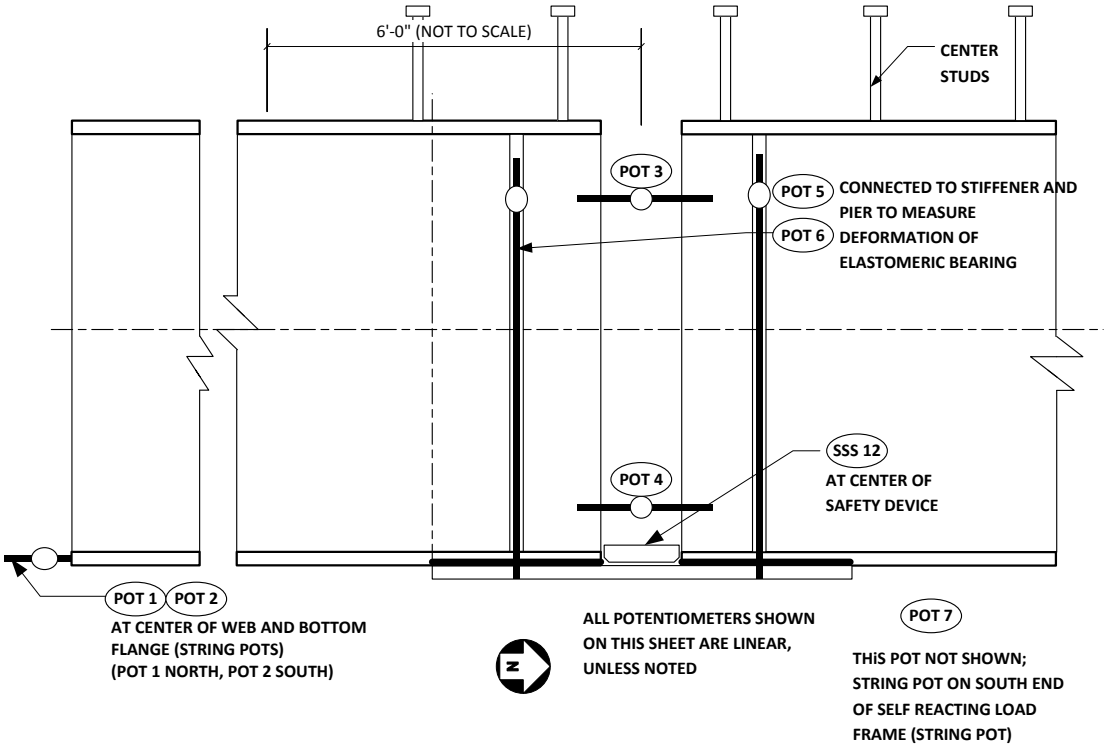

Figure 5.12 Instrumentation Layout at the Girder Ends – 1

Figure 5.13 Pots 3, 4, 5, and 6 in Position During Testing

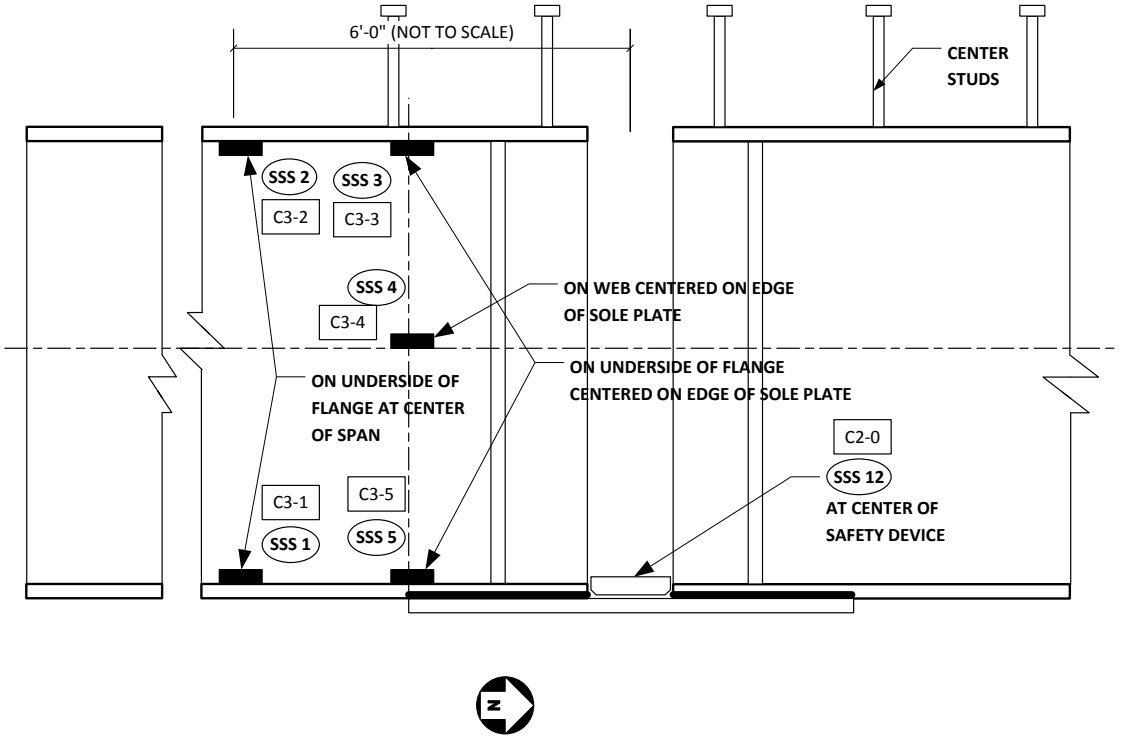

Figure 5.14 Instrumentation at the Girder Ends -2

Steel girder: The areas instrumented with strain gages were to provide the strains near the connection to determine the flow of stresses in the girder in the area where the load was anticipated to transfer through the web to the bottom flange and finally to the welds.

Pot 1 and Pot 2 were connected to girder ends to measure the total cantilever deflection of the bridge girders. Pot 8 was to measure the upward deflection of one of the self-reacting girders, which was in effect a cantilever beam. Pot 3 and Pot 4 were connected to the girder web near the top and bottom to determine the rotation of the girder ends. Pot 5 and Pot 6 were connected between the stiffeners and the top of the concrete pier to measure the deflection of the elastomeric bearing.

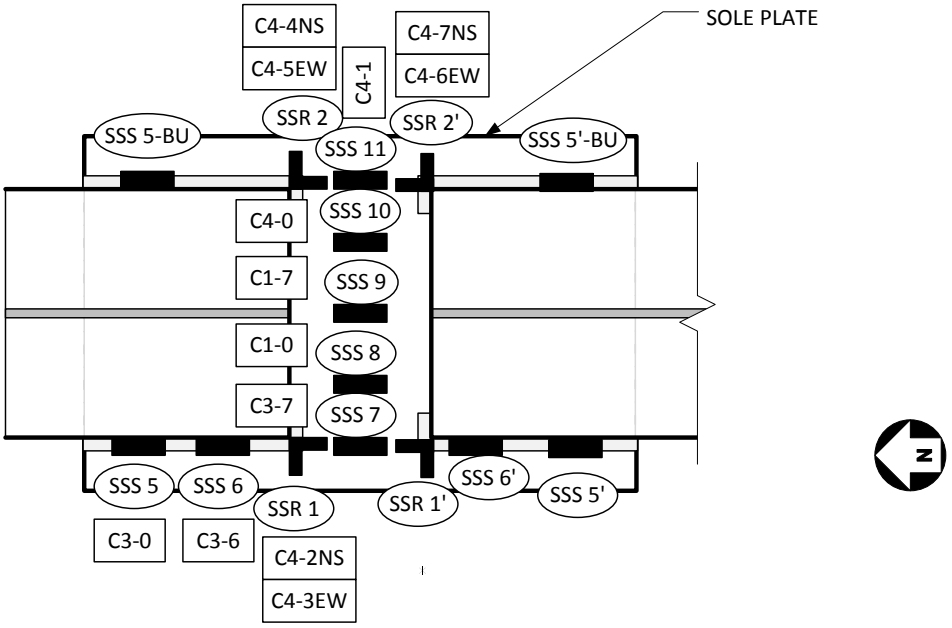

Figure 5.15 Instrumentation Layout at the Sole Plate

Sole plate: The sole plate instrumentation was set up to measure the strains going through the sole plate where the compression load transfer is occurring between the girders and, particularly, to measure the strains at the welds (Figure 5.16). As previously mentioned, the welds were believed to be the most critical parts of the SMC connection. An additional strain gage was positioned at the center of the safety device (Figure 5.14) to determine its loading once it became active.

Figure 5.16 Gage Placement at 5/8" Sole Plate Fillet Weld

Figure 5.17 Strain Gage Attached to Top of Slab

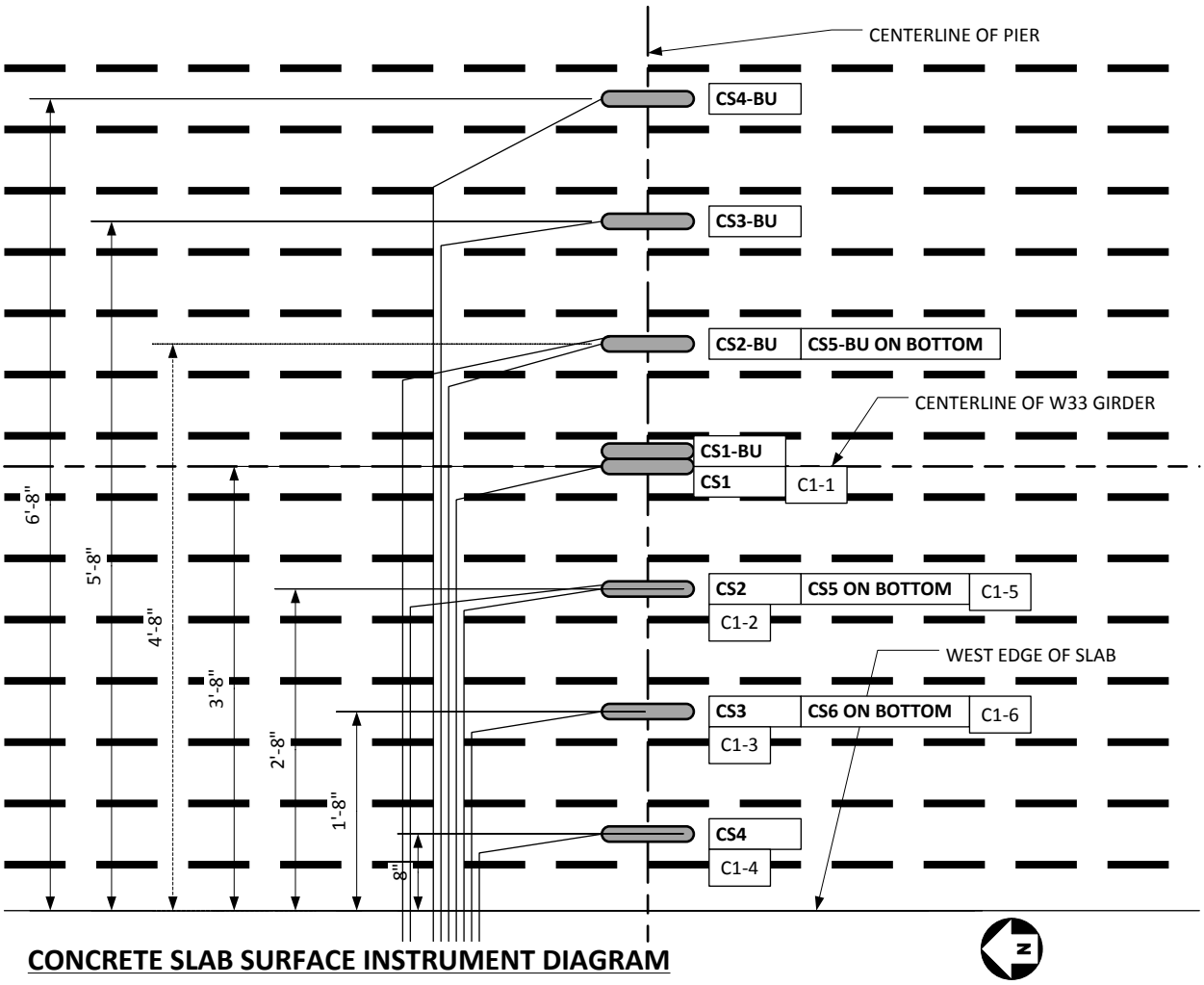

Figure 5.18 Instrumentation Layout on the Top and Bottom of Slab

Top of slab: This area is instrumented to determine strains and corresponding stresses to verify the concrete failure model used and to see the effects of shear lag in the top of the slab (Figure 5.18 and Figure 5.17).

Bottom of slab: This area is instrumented to determine the direction of strain, compressive or tensile, in order to create an accurate force balance in the end connection and for verification of the FE model.

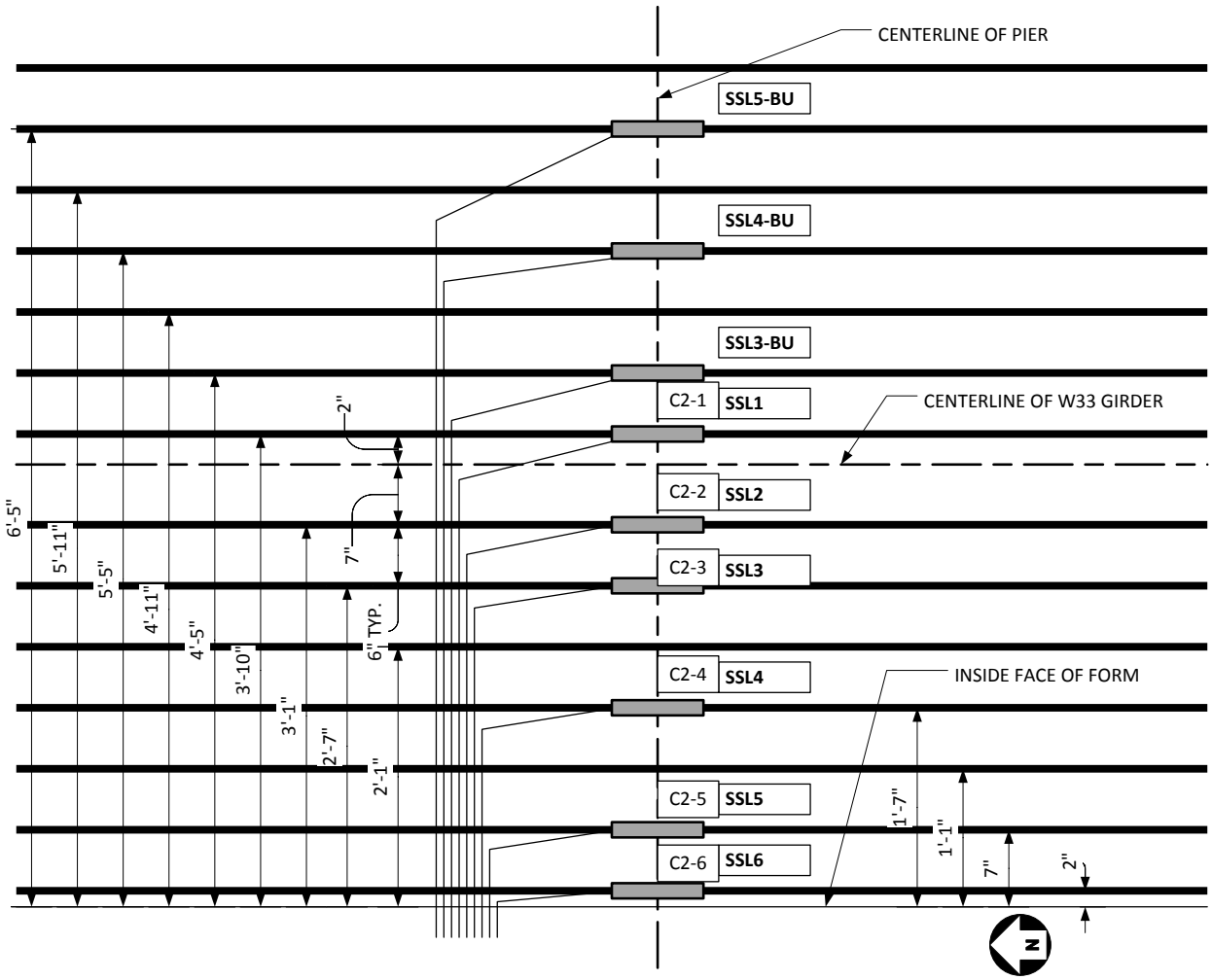

Figure 5.19 Instrumentation Layout on the Slab Reinforcing

Top reinforcing bars: These bars are instrumented for strains to determine tension forces in bars and then, based on their relative locations, to observe the shear lag effects in the SMC top reinforcing and the slab (Figure 5.19 and Figure 5.20). Due to the location of shear studs on the bridge girder, the reinforcing bars could not be placed symmetrically.

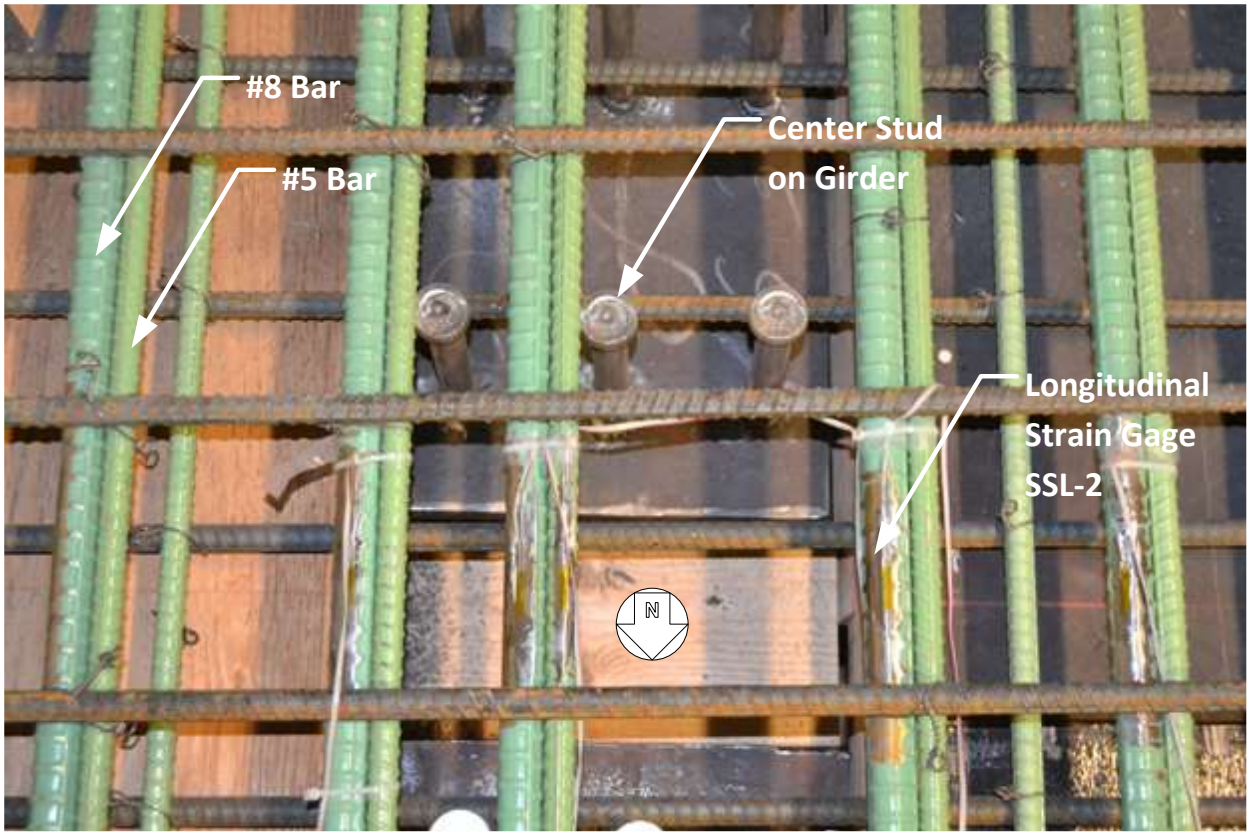

Figure 5.20 Strain Gages Attached to Reinforcing Steel

5.4 Physical Test

The test specimen was constructed with temporary shoring supports for each girder at center and end points. Once the concrete had attained its design strength, the shores were to be removed; and during this process, the instrumentation would be tested to verify functionality and to measure strains from the dead load of the model being active. However, due to concrete shrinkage from drying and reaction with mix water, the slabs actually lifted not only themselves but also the steel girders slightly off of the temporary supports. Due to the upward shrinkage displacement it was not possible to verify the gage functionality prior to the load test.

During testing, load was applied via displacement control using an MTS Flextest unit to control all three actuators. The actuators were given a specified displacement rate of 0.5 mm/second, and applied this displacement to the load application beams. The control program was written such that user intervention was required after every load application, which in effect required the operator to push a button after each five minutes. The operator intervention acted as an additional safety mechanism in the event of a sudden malfunction or failure. The Flextest unit simultaneously recorded the actuator displacement, the applied force, and the time. The unit was set up to record at 10 Hz, but it internally set the time increment value to 0.0996 seconds vs. the specified 0.100 seconds.

Additional data were collected with a National Instruments NI PXIe-1082 Data Acquisition Unit (DAQ). The DAQ was able to capture data from up to 32 channels for strain gages and eight channels for linear potentiometers. The locations of the gages and potentiometers were discussed in Section 5.3 Test Specimen Instrumentation.

The test began on Tuesday, July 22, 2014, and concluded on Wednesday, July 23, 2014. Initially, a shakedown load of 10 kips was applied at each end of the model to verify all equipment was functioning properly. The test equipment was verified to be working properly; however, several gages gave questionable data; fortunately, redundant gages were already active for the suspect gages. The structure was then unloaded and the test begun.

Load was gradually applied via displacement to develop an increasing negative moment at the center of the pier. Originally, the maximum anticipated load to be applied was 90 kips at each cantilevered end in order to develop the negative moment due to the design truck (1,172 kip-feet) although the load predicted to fail the smaller 5/16-inch welds to the sole plate would be considerably less (approximately 61 kips). Thus, failure was anticipated to most likely occur prior to the full load application. A 90-kip concentrated load applied to the load application beam in combination with the dead load moment of the structure was anticipated to develop a total moment of 1,172 kip-feet at the SMC connection. However, due to the lack of dead load deflection and dead load stresses due to concrete shrinkage, it was estimated that a load of 98 kips with a moment arm of 12 feet would be required in order to develop the design moment of 1,172 kip-feet. At an applied load of about 85 kips, a sudden bang was heard and it appeared that the safety device had been engaged. The loading was temporarily stopped. A visual examination of the welds indicated that no weld cracking failure had occurred and review of the strain gage data confirmed this. The decision was made to continue applying load to the model in an attempt to fail the north (smaller) weld.

The test continued on until a load of approximately 132 kips was applied at each end and no signs of failure or distress were evident. The load was removed from the model and the decision was made to recommence testing the following day. That evening, it occurred to the author that the sole plate may have compressed enough that the safety device became engaged; this would require a total shortening of the sole plate of 1/8 inch for which the corresponding strain would be 0.0208. A strain of 0.0208 indicates that that the sole plate had somehow entered the plastic range. Upon review of the calculations for the sole plate capacity given in Table 3.5, the plate appeared to have enough capacity. However, from review of Figure 3.2 and Appendix B, it was noted that the sole plate is also subjected to a moment as shown in the free body diagram in Figure 5.21. Due to a combination of normal stresses from the axial compression and moment, the sole plate had an applied stress of 99.3 ksi, which results in axial and bending deformation of the plate. The applied stress was well in excess of the yield stress of the sole plate, F_y = 50 ksi, thus the sudden failure and activation of the safety device.

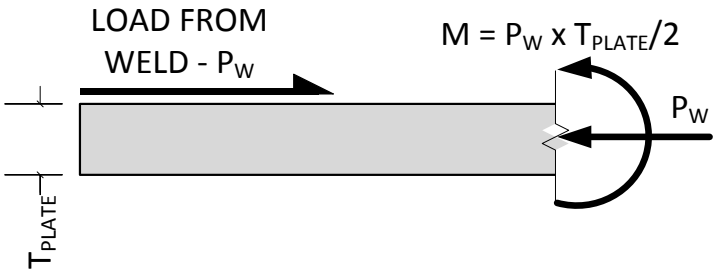

Figure 5.21 Free Body Diagram of Sole Plate

The additional loading applied on the first day after the load bang, was basically moot as far as the welds to the sole plate were concerned since the safety device was active and, thus, the axial load was transferred directly between the girder bottom flanges. This test did, however, demonstrate the effectiveness of the safety plate in transferring load between the girders and maintaining the integrity of the SMC connection.

The following morning, knowing the cause of the safety plate activation, the girders were jacked up to their horizontal position and the safety device was removed. The safety device was modified by machining an additional 1/16 inch from each side. The safety device was subsequently reinstalled between the girder ends and bolted down.

A new load test was begun in which the displacement was applied at a rate of 1 mm/second, again with operator control for each step. This test was to run until either the maximum test load of 200 kips was reached or some anomaly occurred, whichever came first. At an applied load of approximately 120 kips, there was loud bang and the loading was stopped. An examination of the girder ends indicated that again the safety device had been activated and that the welds on the south end of the north girder had failed in several places. The damage was photographically documented and the strain and displacement data stored. The cracked welds are shown in Figure 5.22 and Figure 5.23. It is also interesting to note the extreme displacement of the elastomeric bearing in Figure 5.22.

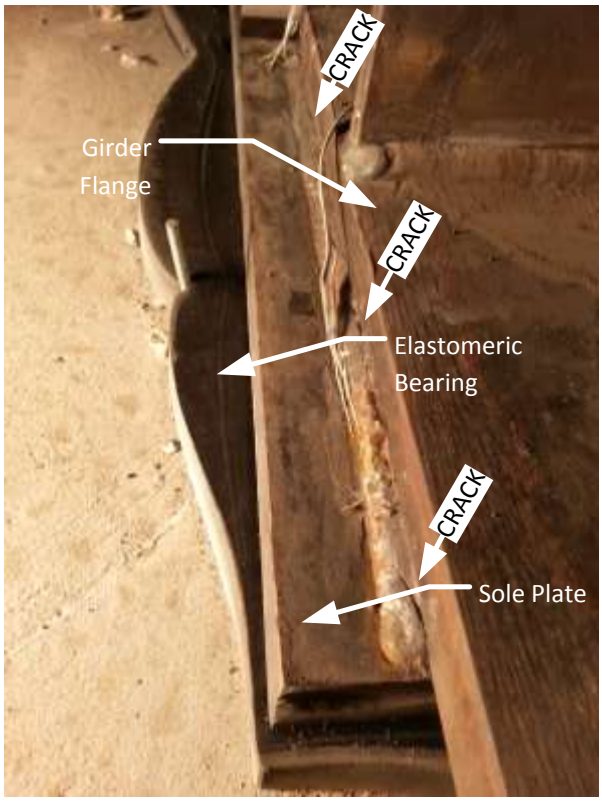

Figure 5.22 Failed Weld on East Side of North Girder

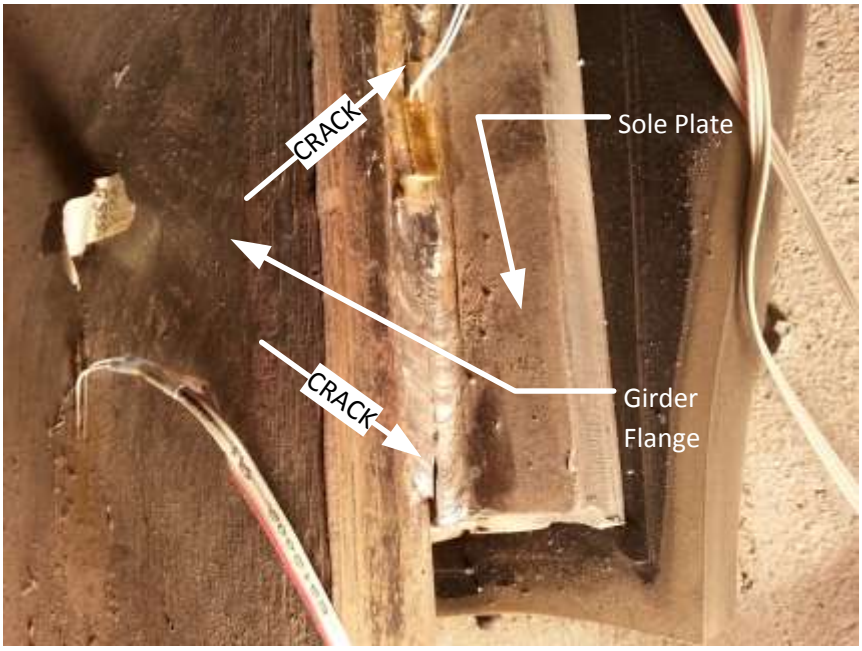

Figure 5.23 Failed Weld on West Side of North Girder

The test was recommenced at the same displacement rate and was continued until a load of 198 kips was applied. No signs of additional failure were evident after the load was removed and the model closely examined. As previously mentioned, once the safety device became active, load was transferred directly between the girder bottom flanges and, thus, the welds and the sole plate were no longer loaded by any of the forces in the SMC connection.

5.5 Test Results

The test data consisted of sets of readings from strain gages, potentiometers, load cells, and actuator displacement gages. Additionally, photographic evidence of model behavior was collected. The strain gage and potentiometer data were recorded as strain or displacement values vs. time intervals of 0.10 second. The load cell and actuator displacement readings were taken vs. time intervals of 0.0996 seconds as mentioned previously. In order to correlate the strain/model displacement data to the load/displacement data, the load/actuator displacement data were recalibrated to a time set at 0.10 seconds.

Two completely different sets of data were collected, the first for the testing performed on July 22, 2014, and the second for the testing performed on July 23, 2014; these will be referred to as the Day 1 Test and Day 2 Test, respectively.

5.5.1 Day 1 Test Results

Actuator data for Force vs. Displacement for the Day 1 Test are shown in Figure 5.24. From review of this chart, it is evident when the safety device became activated at approximately 85 kips of applied load. Aside from the point at which activation of the safety device occurred, the load vs. displacement curves are relatively linear for both the north and south sets of actuators.

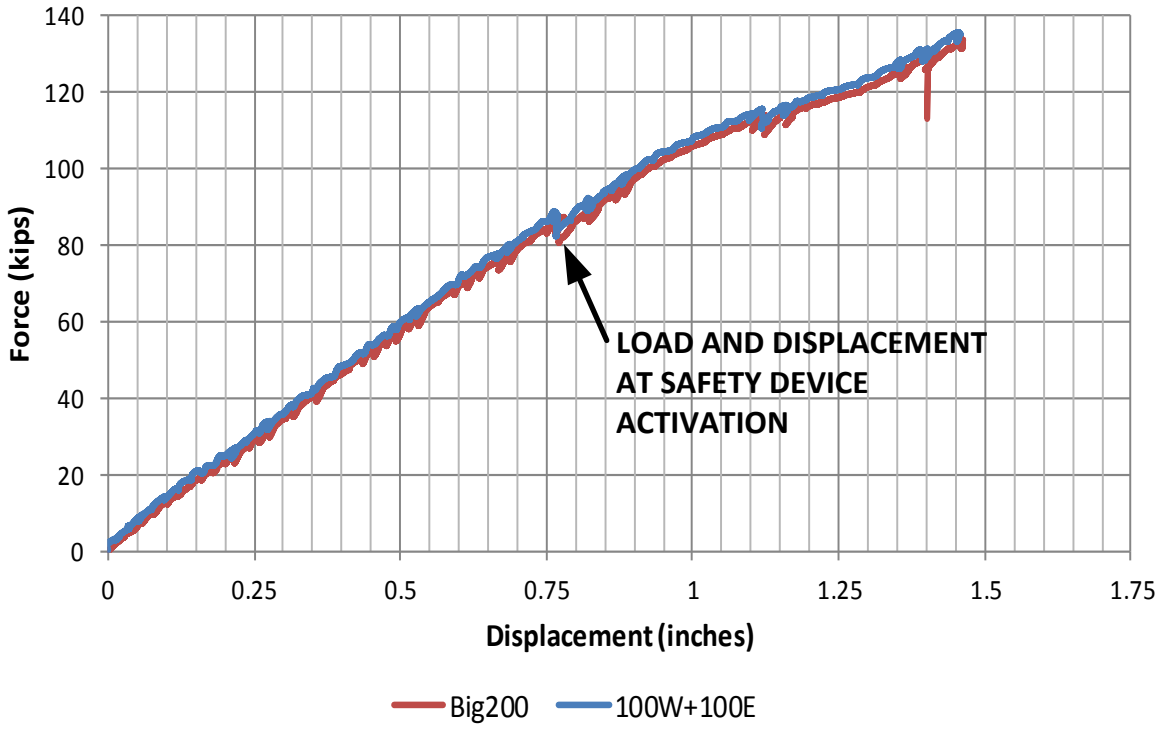

Figure 5.24 Actuator Force vs. Displacement – Day 1 Test

The final strains for the Day 1 Test in the top SMC reinforcing bars were converted to forces and a plot of these force values is presented in Figure 5.25. While only the #8 bars were instrumented, each #8 bar had a #5 bar adjacent to and centered on it, so force values for the #8's alone and the #8's in combination with the #5's are plotted. From review of the forces in the reinforcing bars, there is a significant drop in the load taken by the bar near the edge of the slab as well as the center bar (SSL-1, refer to Figure 5.19 for gage locations). The position of the center bar, directly over the girder, consistently showed lower force in other reports where similar testing was performed (Azizinamini A. , 2005). The Abaqus analysis results also showed this same behavior. The force decrease in the bar near the edge of the slab is most likely due to shear lag in the slab and its proximity to the edge of the slab, which is two inches away. The ultimate capacity of a #8 plus a #5 reinforcing bar is 66.0 kips, whereas, the factored ultimate capacity is 59.4 kips, the most highly loaded set of bars is that at gage SSL-2, which has a calculated load of 55.3 kips. The load of 55.3 kips is less than the ultimate capacity of 59.4 kips, thus, based on these data no yielding of the SMC reinforcing bars occurred.

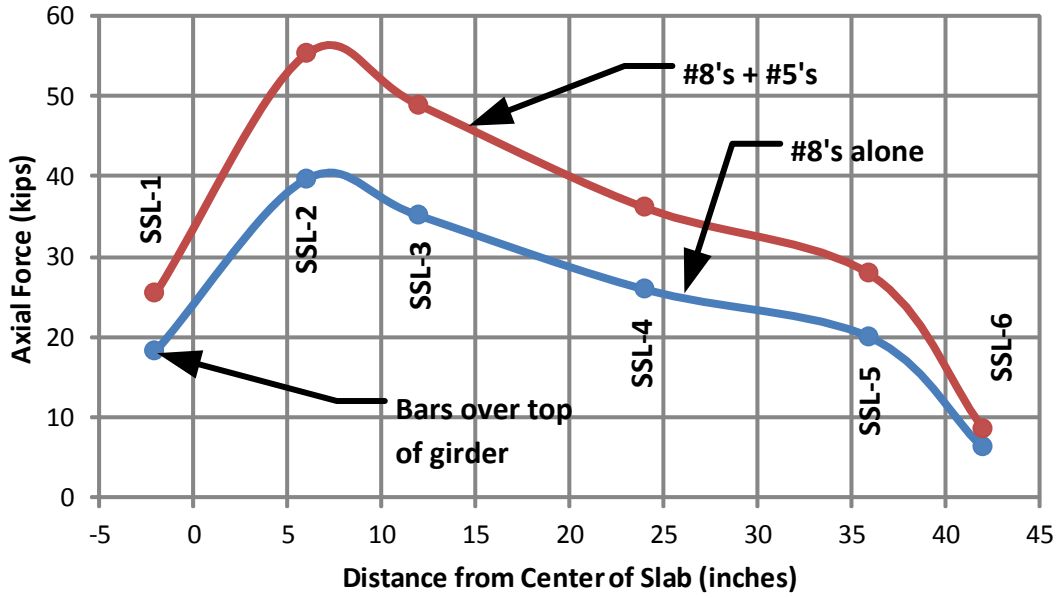

Figure 5.25 Shear Lag in Top SMC Bars - Day 1 Test

Concrete top surface strain gage values were plotted vs. load and are shown in Figure 5.26. At an applied actuator load of 50 kips, all the gages with the exception of CS1 (refer to Figure 5.18 for locations of gages), which is at the center, were no longer functioning properly. Gage CS1 eventually malfunctioned at an actuator force of 57 kips. The gages most likely malfunctioned due to excessive cracking or loss of bond between the gage epoxy and the concrete surface.

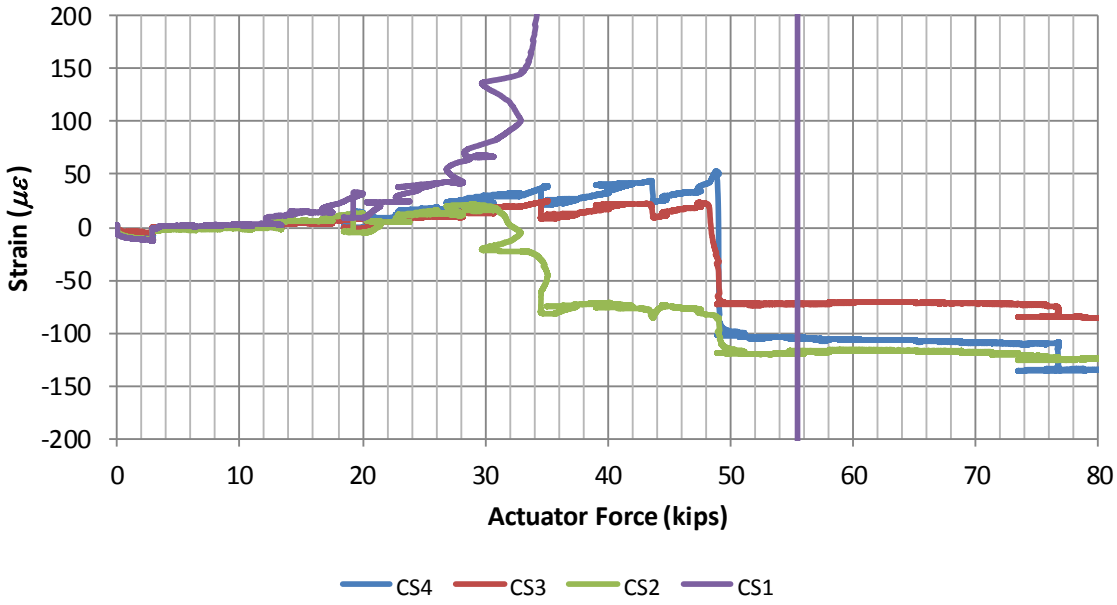

Figure 5.26 Concrete Top Surface Strains

Concrete bottom surface strain gage values are shown in Figure 5.27. Gage CS6 is in tension for a short time and then follows the trend of CS5 when it goes into compression. Both gages have a drop in strain at a load of nearly 80 kips, which is near the load at which the safety device becomes activated. After the activation, the strains at CS5, which are closer to the center of the girder, decrease and approach the values of CS6. Both gages trend toward less negative stress as the girder is loaded, which is reasonable as the neutral axis should be moving downward.

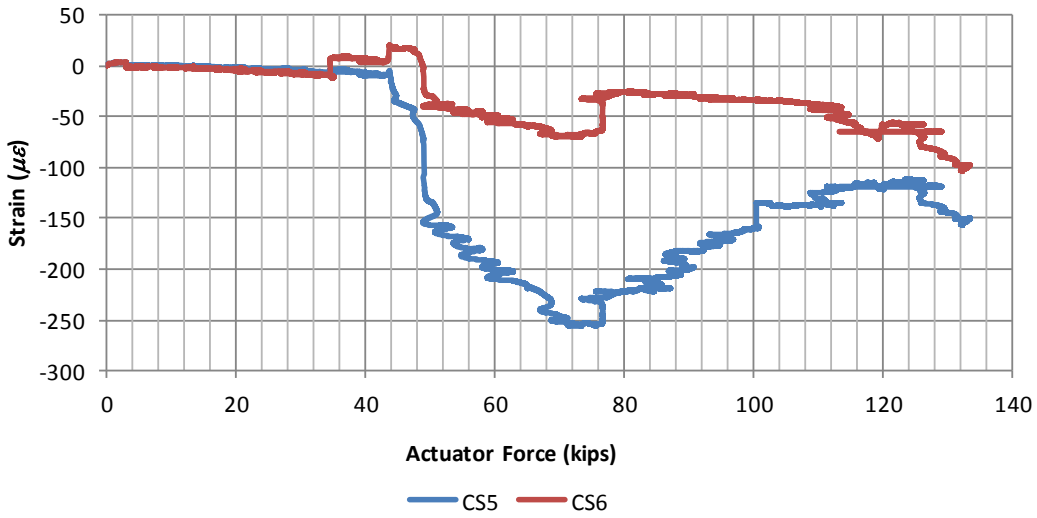

Figure 5.27 Concrete Bottom Surface Strains

Upon review of the concrete strain gage data at the locations where there are gages on both the top and bottom of the slab at the end of day 1, all four gages had readings of between -100 $\mu\varepsilon$ and -150 $\mu\varepsilon$, which would indicate there is compression throughout the full depth of the slab. This cannot be true since the top of the concrete slab must be in tension because the top SMC reinforcing steel was in tension. It is likely that the top of the concrete slab gages began to malfunction after the concrete cracked and, thus, their readings after the point of cracking will be ignored. The presence of compression in the bottom of the slab would mean there would be a compressive component of force from the slab to partially counteract the tensile forces in the top SMC reinforcing bars and tension in the concrete above the neutral axis (see further discussion in Section 5.7).

Final strains in the sole plate were determined from strains at gages SSS7, SSS 9, SSS 10, and SSS 11. Gage SSS 8 malfunctioned, thus the value for the symmetric gage SSS10 was substituted. A plot of the sole plate strains measured at the end of the Day 1 Test and their corresponding stresses is shown in Figure 5.28. The strains are significantly higher at the locations of the welds, one inch from either side vs. the center of the plate.

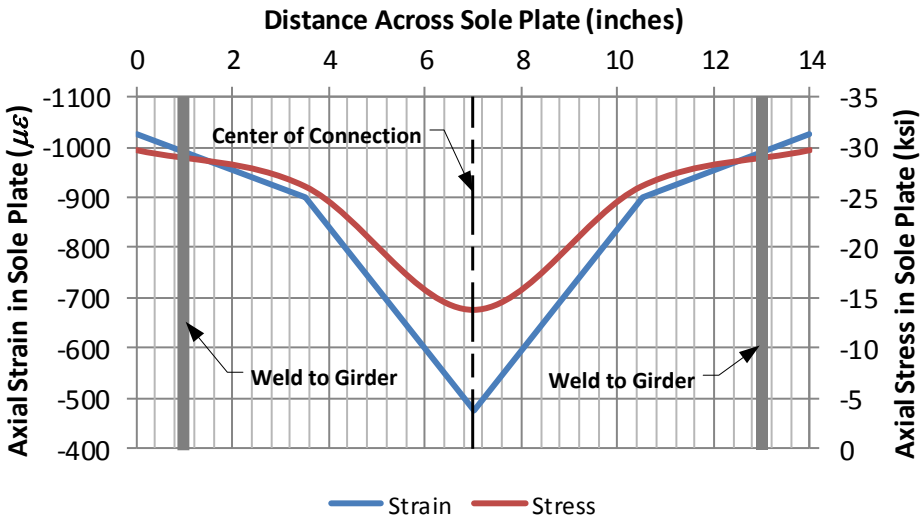

Figure 5.28 Sole Plate Strains and Stresses - Day 1 (Note that strains and stresses are compressive and thus negative)

Although the safety device became activated, its gage recorded no appreciable strain and thus no plot is provided herein. The only gage on the device was at the center of the plate and based on the strains in the sole plate, it's likely that the higher strains were near the extremities where no gages were present. The ends of the girders were manually flame cut during fabrication; whereas, the safety device edges were precisely machined, thus there was not a perfect fit up when the safety device became engaged. It was noted that the device was not in contact with the girder web and most likely the bottom flange at that location due to roughness in the cut of the girder end. Contact was noted to be occurring at either end of the girder bottom flange, which is also the location of the welds to the sole plate.

Displacements of the girder ends are shown in Figure 5.29 and Figure 5.30. Reviewing the displacement at the north girder, the jump in displacement at activation of the safety device is quite evident, whereas in the south girder there is only a subtle dip in the displacement. Also evident is the relatively linear decreasing behavior of the displacement at the south girder, while the north girder is almost a straight line until a load of about 65 kips is applied. The difference in the behavior of the two girder ends is likely due to various internal interactions between all of the dissimilar materials achieving composite action.

Along with differences in behavior under load, there is also a significant difference in displacement at the ends of about 0.30 inches. The reason for this appears to be the variation in displacements of the elastomeric bearing at the center of the connection; the elastomeric bearing displacements are shown in Figure 6.29 and Figure 6.30, which show the displacements at the north and south potentiometer locations, respectively (Pot 1 and Pot 2). The north end's displacement at the end of testing was 0.14 inches, while at the south end the displacement was 0.17 inch. The differential between the readings is -0.03 inches toward the south end and over 18 inches (1.5 feet) between gages; this corresponds to a total differential of -0.30 inches from end to end over the 30-foot total span of the girders. Accordingly, both end displacements may be adjusted to reflect this slope effect and the corrected displacement at each end is 0.95 inches.

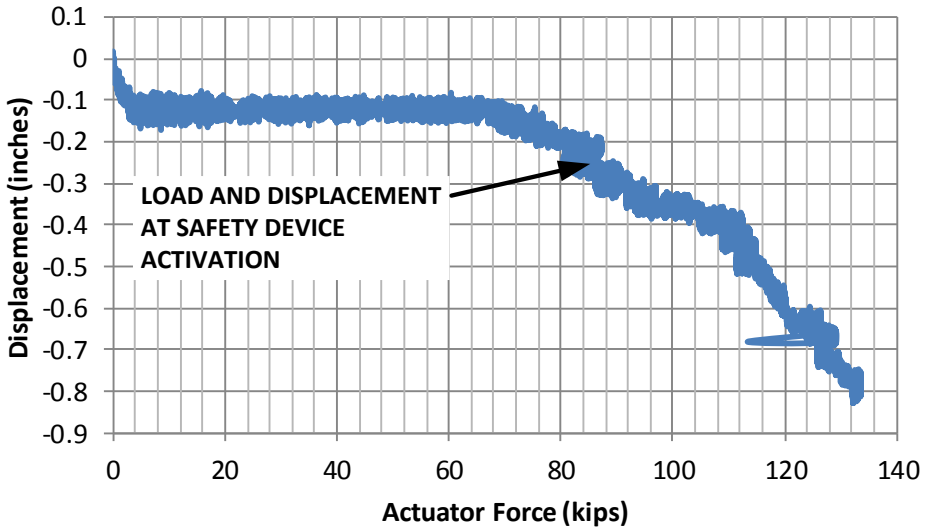

Figure 5.29 Displacement at North Girder vs. Actuator Force –Day 1

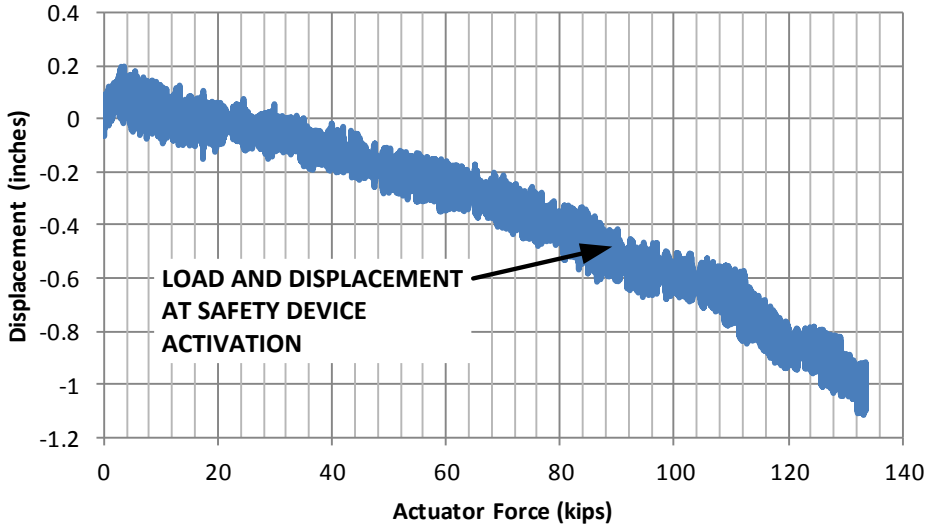

Figure 5.30 Displacement at South Girder vs. Actuator Force – Day 1

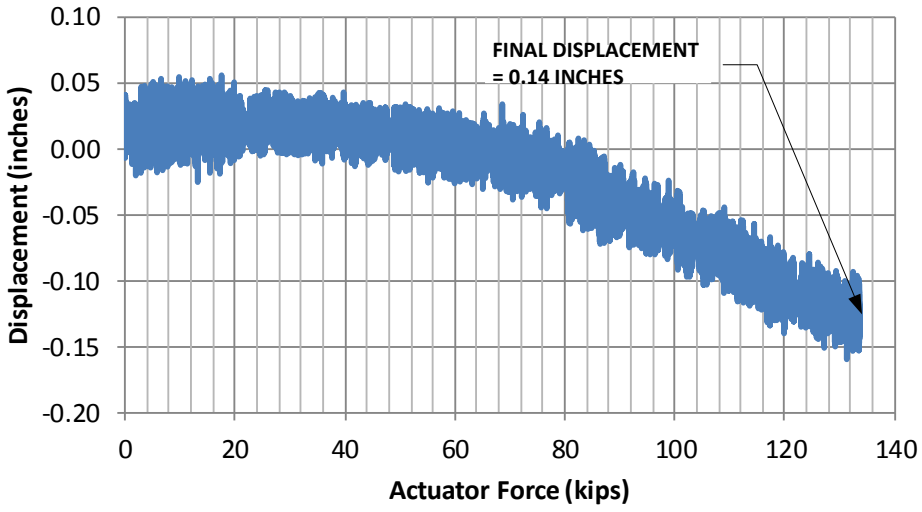

Figure 5.31 Displacement of North Elastomeric Bearing – Day 1

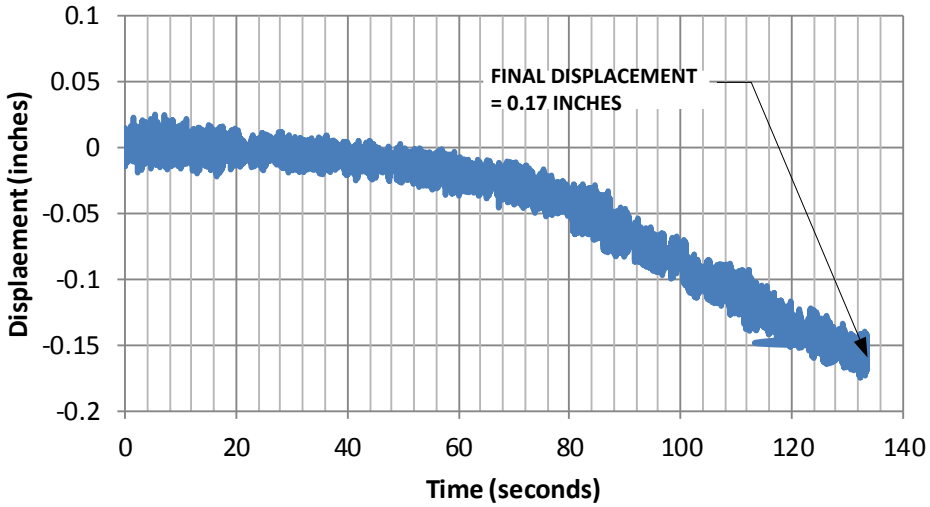

Figure 5.32 Displacement of South Elastomeric Bearing – Day 1

5.5.2 Day 2 Test Results

Actuator data for force vs. displacement for the Day 2 Test are shown in Figure 5.33. From review of this chart, it is evident when the safety device became activated at approximately 120 kips of applied load. Aside from the point at which activation of the safety device occurred, the load vs. displacement curves are relatively linear for both the north and south sets of actuators with just slight curvature of both sets after activation of the safety device.

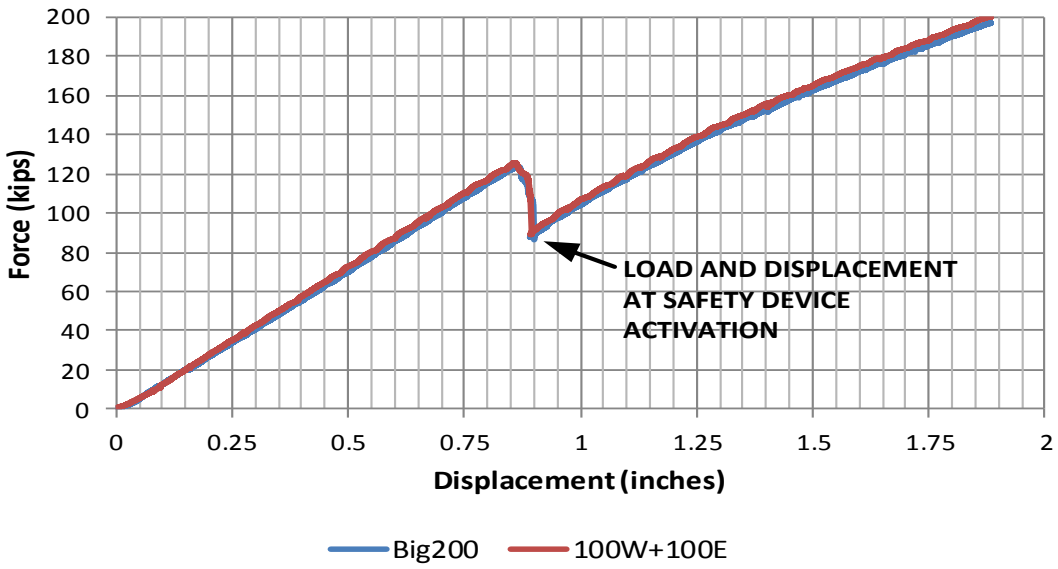

Figure 5.33 Actuator Force vs. Displacement - Day 2 Test

The top SMC reinforcing bar strains for the Day 2 Test were examined for consistency with the Day 1 Test values for the same bars and some anomalies were discovered. As may be seen in Figure 81, the strain at the end of the Day 2 Test for the subject bar, instrumented with gage SSL-1, was nearly equal to the strain at the end of the Day 1 Test. The end load for the Day 1 Test was 132 kips, while the end load for the Day 2 Test was 198 kips. Considering that this test specimen is statically determinate, a difference in end loading of 60 kips should not produce the same strains in the subject reinforcing bar. Upon further review, the initial strain in the bar varied between the two tests. There are many likely reasons for the difference in initial strain, such as effects of concrete cracking causing the aggregate to interlock and not allow the cracked concrete to fully close back up, relief of initial concrete shrinkage stresses, etc.

The original initial unloaded strain for gage SSL-1 was +660 $\mu\varepsilon$ for the Day 1 Test, while the unloaded strain was +320 $\mu\varepsilon$ for the Day 2 Test. Somehow the difference between these two initial strains must be incorporated into the Day 2 Test strain vs. actuator load charts. There are two possible methods; the first would be to start the Day 2 Test strain at the difference in the two strains, 340 $\mu\varepsilon$ as shown in

Figure. This scheme is not logical and the slopes of the two lines should be relatively parallel, at least until the Day 2 Test weld break. The second possible method would be to proportion the difference in strain to the measured strain in the reinforcing bar linearly along the chart. This method uses the following formulation:

$$\varepsilon_{revised} = \varepsilon + \frac{\varepsilon}{\varepsilon_{\max}} \Delta\varepsilon$$

Where:

$\varepsilon_{revised}$ = the modified strain

ε = the original strain reading

$\varepsilon_{\max}$ = the maximum unmodified (original) strain

$\Delta\varepsilon$ = the difference between the Day 1 Test and Day 2 Test initial strains

Using this formulation yielded the results shown in Figure 5.35; these results appear to be very reasonable, considering that both lines are nearly parallel and almost overlap up until their respective safety device activations. Also, the reinforcing steel strains remained linear, which reflects the fact that the strains and resulting forces in the top SMC reinforcing steel must increase if load is increased. On the basis of this analysis, the scheme 2 methodology will be used to modify the strain curves of the instrumented structural elements from the Day 2 Test. Subsequent internal force analysis should support or refute the validity of this selection.

The reinforcing force results vs. the applied actuator load with the aforementioned adjusted strain values are shown in Figure 5.37 and Figure 5.38 or the Day 2 Test at the activation of the safety device and at the end of the test, respectively. The analysis of the reinforcing forces and corresponding internal moments are discussed in Section 5.6.1 Internal Forces and Model Equilibrium. Based on that analysis, the results of the modified load, the proposed modification to the curve provided consistently reasonable results.

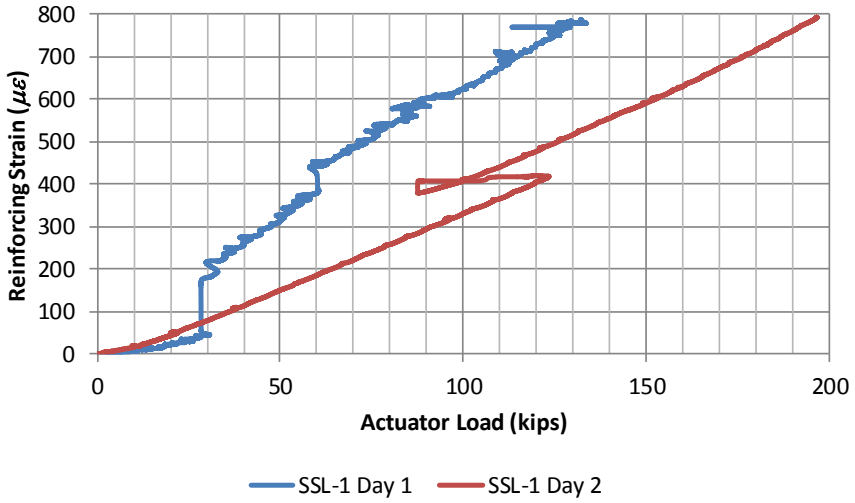

Figure 5.34 Comparison of Days 1 and 2 Actuator Load and Reinforcing Strain

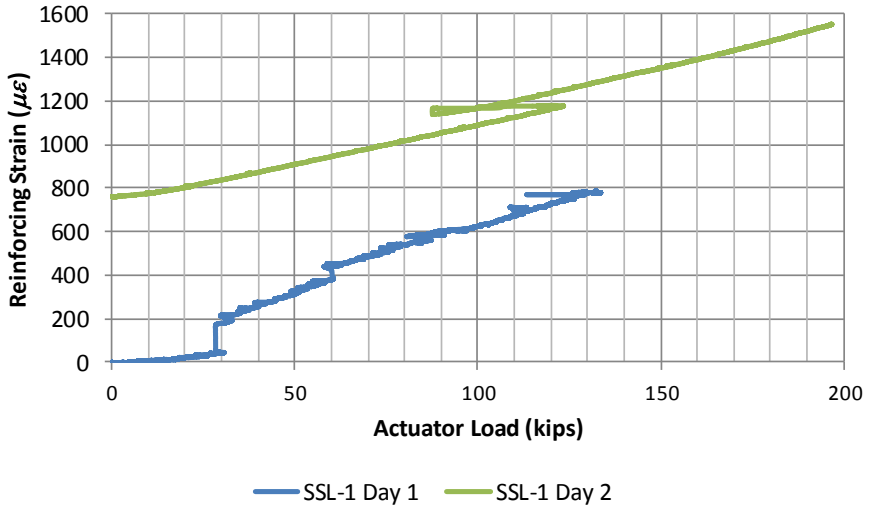

Figure 5.35 Comparison of Days 1 and 2 Actuator Load and Reinforcing Strain - Scheme 1

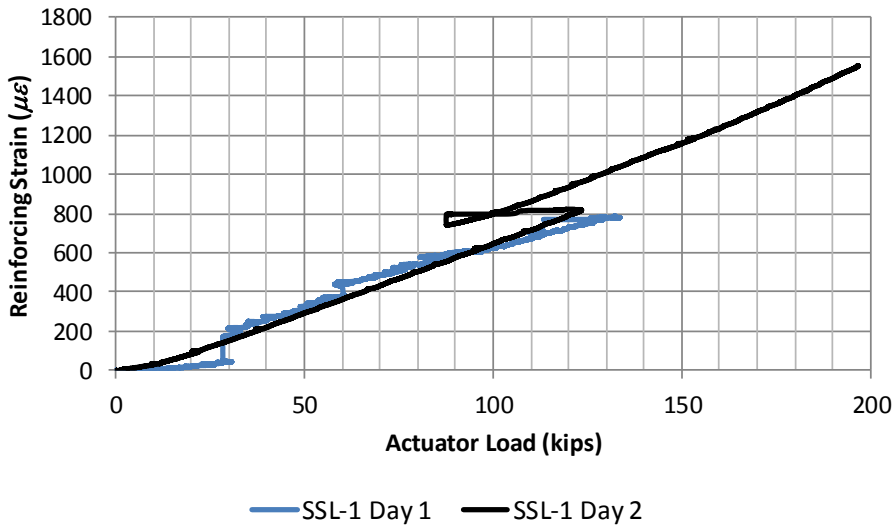

Figure 5.36 Comparison of Days 1 and 2 Actuator Load and Reinforcing Strain - Scheme 2

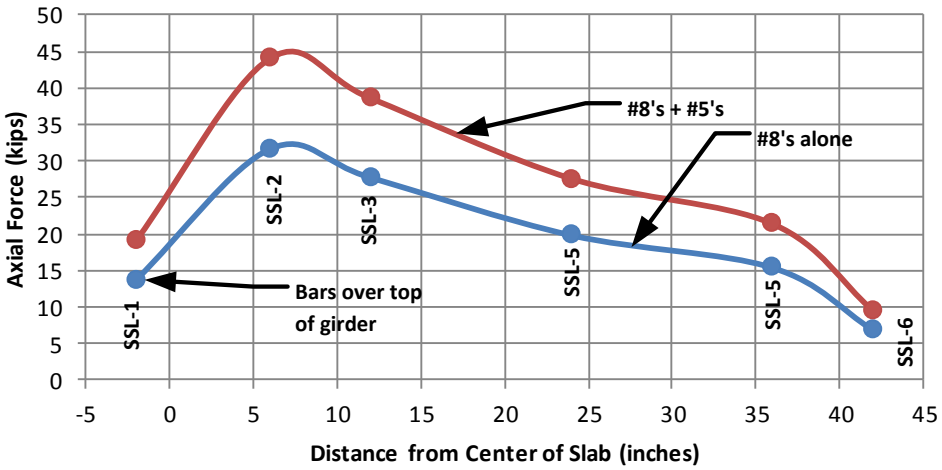

Figure 5.37 Shear Lag in Top SMC Bars - Day 2 Test - Safety Device Activation

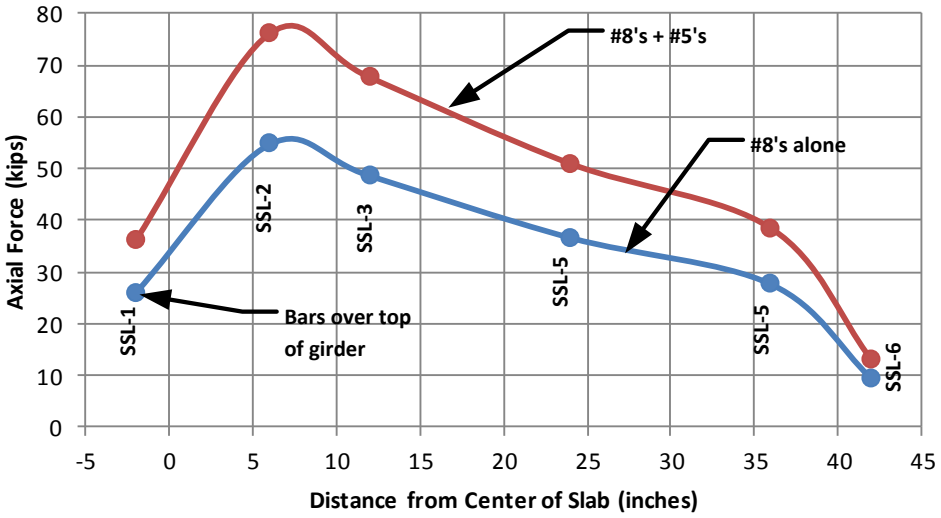

Figure 5.38 Shear Lag in Top SMC Bars - Day 2 Test - End of Test

Concrete top strain gage values were unreliable due to cracking damage from the Day 1 Test and additional cracking from the Day 2 Test, thus no data from these gages will be presented.
Concrete bottom strain gage values are presented in Figure 6.39. It can be seen that up until about 120 kips, the bottom of the slab is in tension. The location of the safety device activation is shown; at this location there is a decrease in strain along with a corresponding decrease in load. This is due to the rapid displacement at the center connections when the south weld cracked/failed and the actuators had to reapply the load lost in the sudden displacement. Once load was reapplied, the strains turned positive again indicating tension in the bottom of the slab, although, just slightly in the case of CS6.

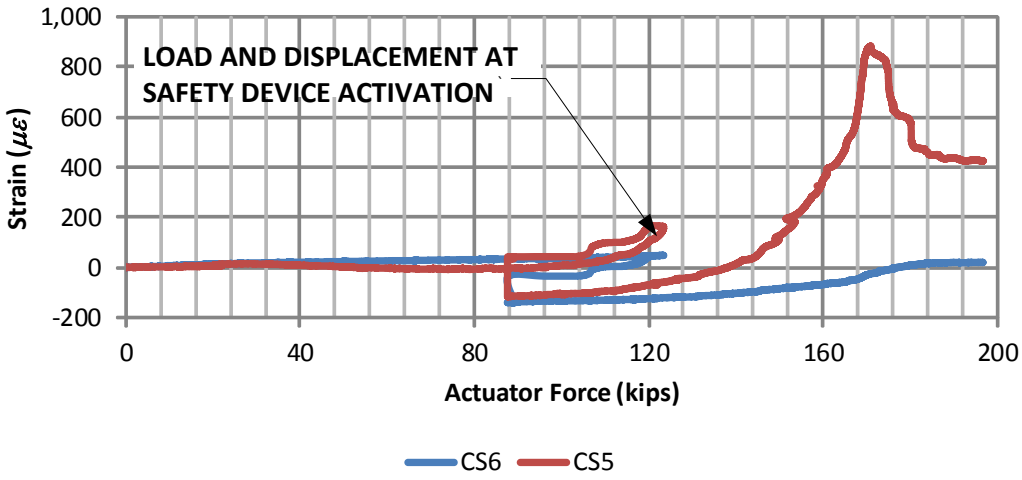

Figure 5.39 Bottom Concrete Strain Gages - Day 2

The strains at the center of the sole plate are shown in Figure 5.40. Based on review of the strain diagram, the sole plate is in compression as expected until the activation of the safety device. At activation, the strain starts increasing and eventually turns into tensile strain; this may be due the behavior of the bottom flanges bowing slightly since they are only partially in contact with the safety device due to bevels shown in Figure 5.43, to accommodate for the welds to the sole plate. Strains in the sole plate were determined from the gages SSS7, SSS9, SSS10, and SSS11. A plot of the sole plate strains measured and

corresponding stresses at the point of the activation of the safety device for the Day 2 Test are shown in Figure 5.28. The strains are significantly higher at the locations of the welds, one inch from either side vs. the center of the plate, which is similar to the previous results. Due to machining additional material off of the safety device, it was possible to put more load into the sole plate; in this instance, the load was increased by roughly 40 kips over the Day 1 Test, a 50% increase. Also, the high stresses near the welds have almost reached the factored ultimate capacity of the plate. The unloading path of the sole plate follows the loading path very well. Once load begins to be reapplied, there is a straight decrease in the negative strain in the plate. Subsequently, the strain goes from negative to positive strain until the end of the Day 2 Test.

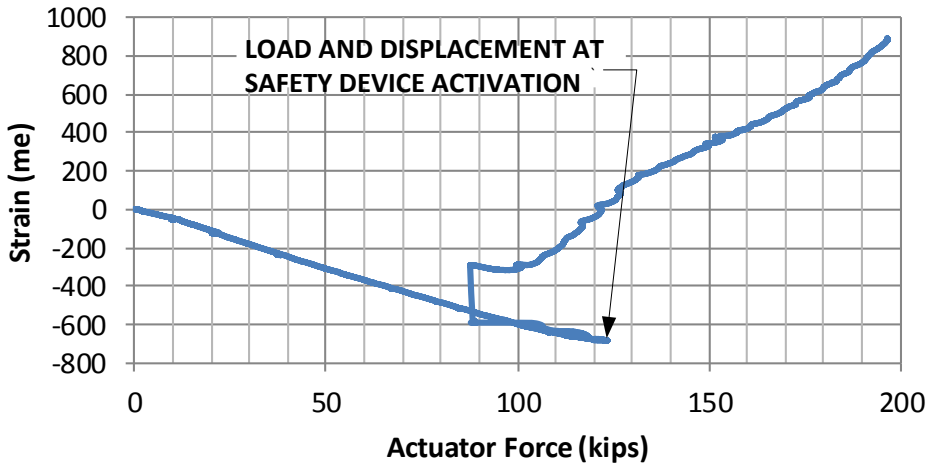

Figure 5.40 Strains at Center of Sole Plate

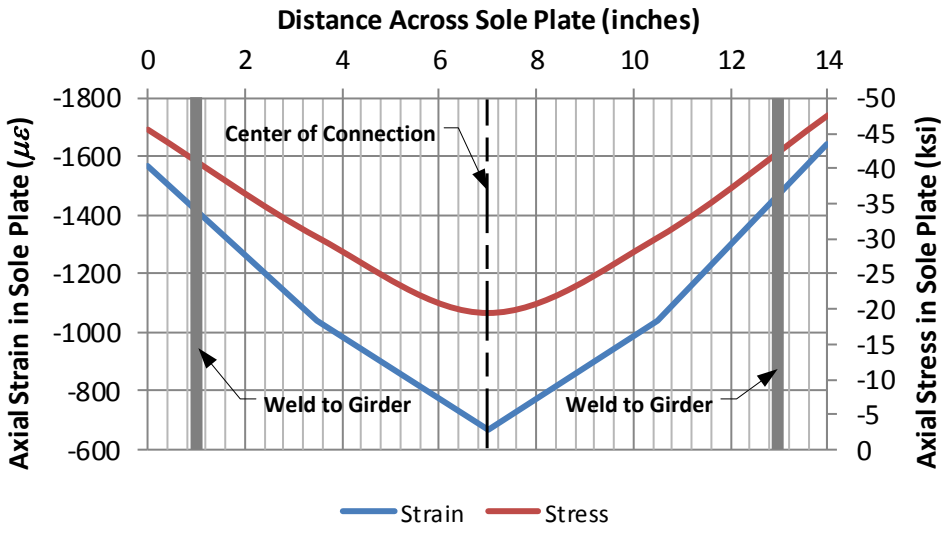

Figure 5.41 Sole Plate Strains and Stress at Safety Device Activation - Day 2

The strains for the entire Day 2 Test are shown in Figure 5.42. The location where the safety device becomes activated is obvious, and as shown in the previous charts, the loading reduces and then, begins again. The reason for the tension may be due to the top of the safety device being ½-inch higher than the top of the bottom flange and possibly some negative bending occurring in the top of the device until the

load in the device equalizes. Following the tensile strains, the plate has a non-linear increase in negative strain to a maximum value of 1490 $\mu\varepsilon$.

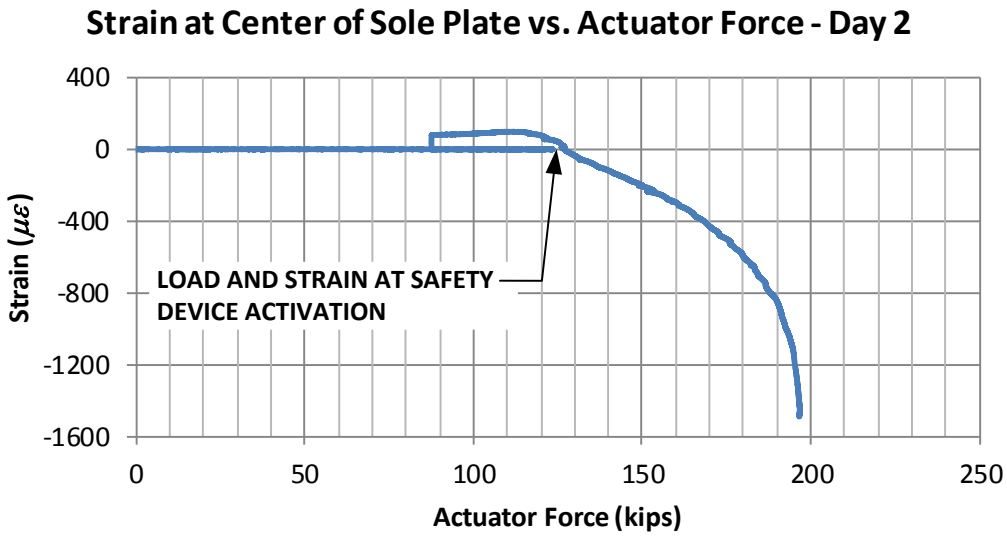

Figure 5.42 Strains at Center of Safety Device - Day 2

Figure 5.43 Detail of Sole Plate Showing Bevel at Weld

Vertical displacements at the girder ends are shown in Figure 5.44 and Figure 5.45. The north end displacement vs. force is not quite linear up an applied load of 123 kips, whereas the curve is very linear for the south end displacement vs. force. The most likely reason for the behavior is the more excessive deformation of the elastomeric bearing at the north end of the sole plate, Figure 5.46. The location at which the safety device became activated is noted on both charts and it is obvious that a large displacement occurred along with a 25% decrease in applied load. Subsequently, the load was increased

and displacement became fairly linear for both ends. The difference in the total readings is again an effect of the non-uniform compression of the elastomeric bearing. However, during this test, the displacements for the girder mounted potentiometers became somewhat unreliable because the deformation of the bearing was so extreme that it actually deformed enough laterally to distort the anchors for the potentiometers (Figure 5.46).

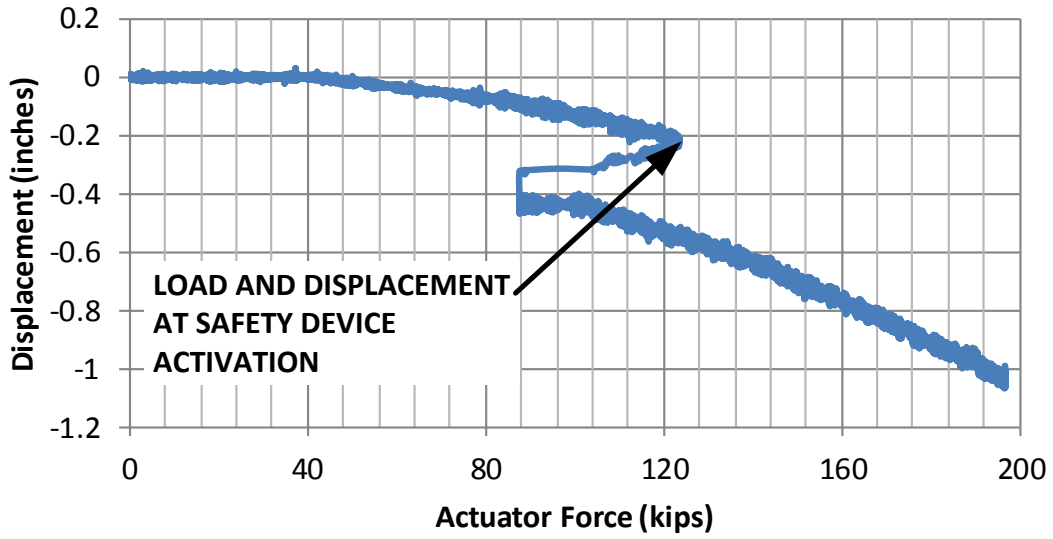

Figure 5.44 Displacement at North Girder vs. Actuator Force - Day 2

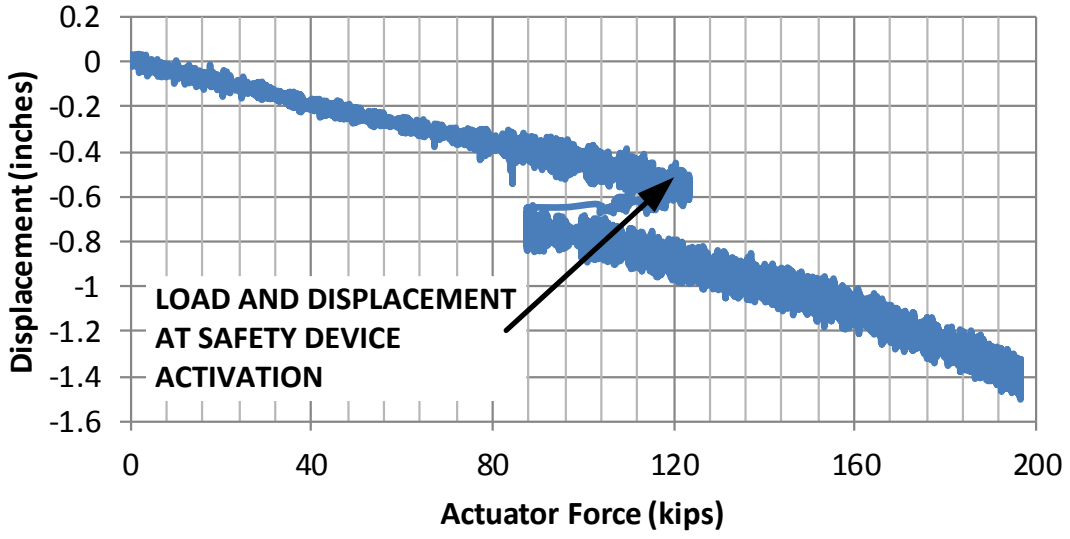

Figure 5.45 Displacement at South Girder vs. Actuator Force - Day 2

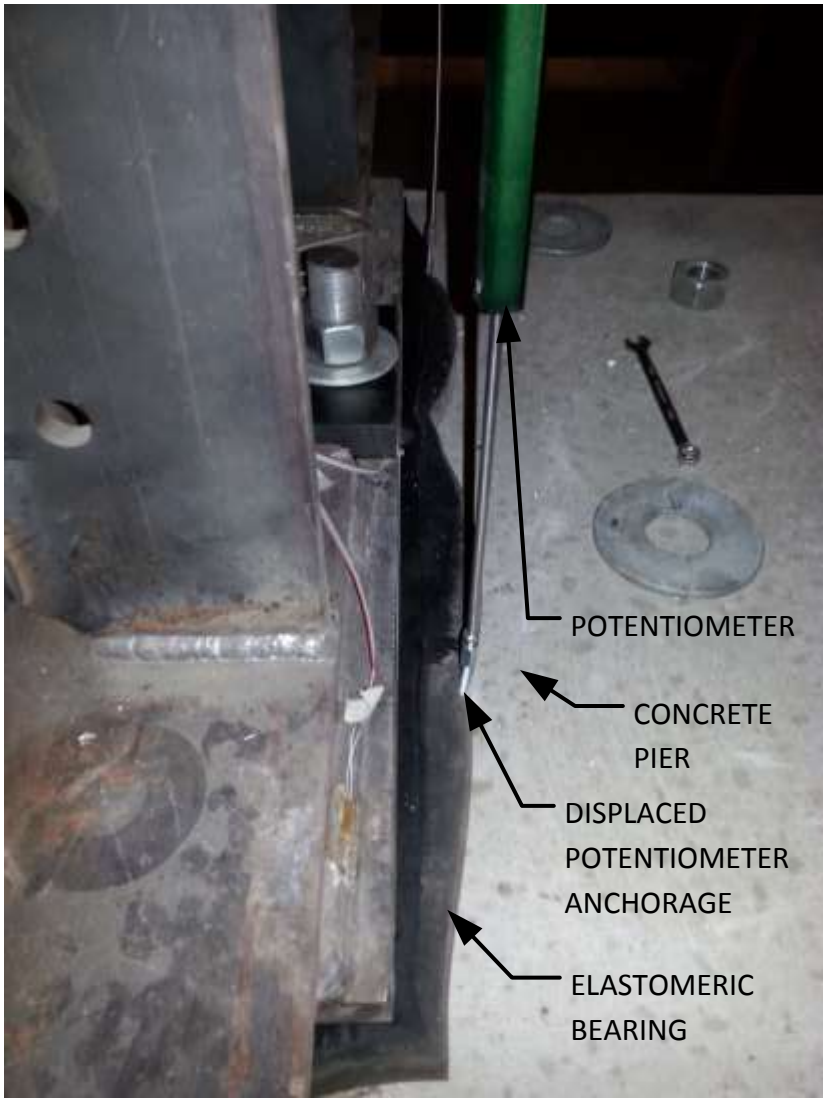

Figure 5.46 Distorted Potentiometer Anchorages - Day 2

The crack pattern in the top of the concrete slab was documented photographically. A representative photo is shown in Figure 5.47 and a plotted diagram is shown in Figure 5.48. The crack pattern was only mapped to within three feet of the load application beams; mapping nearer to the load application beams may not have been reliable due to the localized load effects of the beams. The pattern was as anticipated with the majority of the cracking perpendicular to the direction of stress.

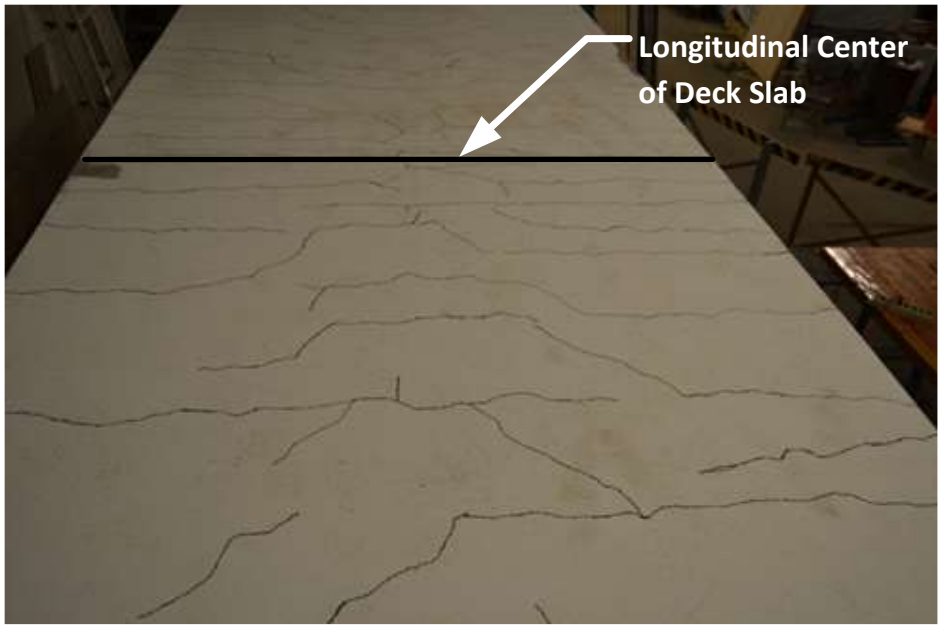

Figure 5.47 Final Crack Pattern in Top of Deck Slab (looking south)

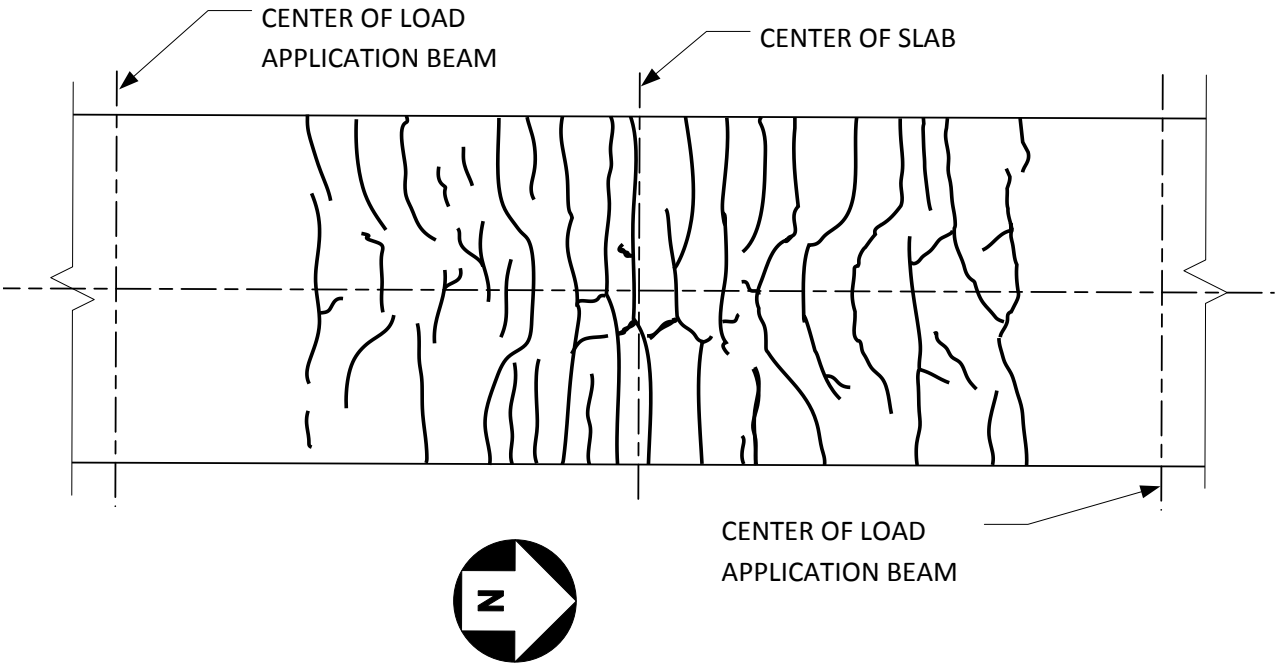

Figure 5.48 Crack Pattern in Top of Deck Slab

5.6 Analysis and Interpretation of Test Results

The test results were analyzed to verify the internal forces/equilibrium of the physical model and for comparison to the hand calculations and to the results of the Abaqus finite element analysis.

5.6.1 Internal Forces and Model Equilibrium

The cross-section of the model at the center was selected for analysis as it was the most heavily instrumented. Casual consideration of the connection would indicate that the largest moments would occur at the center of the connection; however, observing the arrangement of the pier, bearing plates and the locations of the ends of the girders, it became apparent that the maximum moment would be away from the center since the shear is zero at the end of the girder and the girder ends are each three inches from the center of the pier. Based on the Abaqus analysis, the majority of the girder reaction goes into the pier in the first six to 12 inches of bearing; this arrangement of shear actually reduced the moment at the centerline of the connection and also proved to be true in the physical model.

At the end of the Day 1 Test, the theoretical moment was determined to be 1,620 kip-feet at the center of the bridge based on an applied load of 135 kips and a moment arm of 12 feet. The actual moment based on the reinforcing bar forces, shown in Figure 5.25, creating a couple with the sole plate and safety device was determined to be 1,488 kip-feet. On the basis of an applied load of 135 kips and a resultant moment of 1,488 kip-feet, the moment arm was determined to be 11.0 feet, or 12 inches from the centerline of the connection. This result is reasonable as the center of bearing is three inches from the edge of the bearing plate nearest to the face of the pier. This behavior is diagrammed in Figure 5.49.

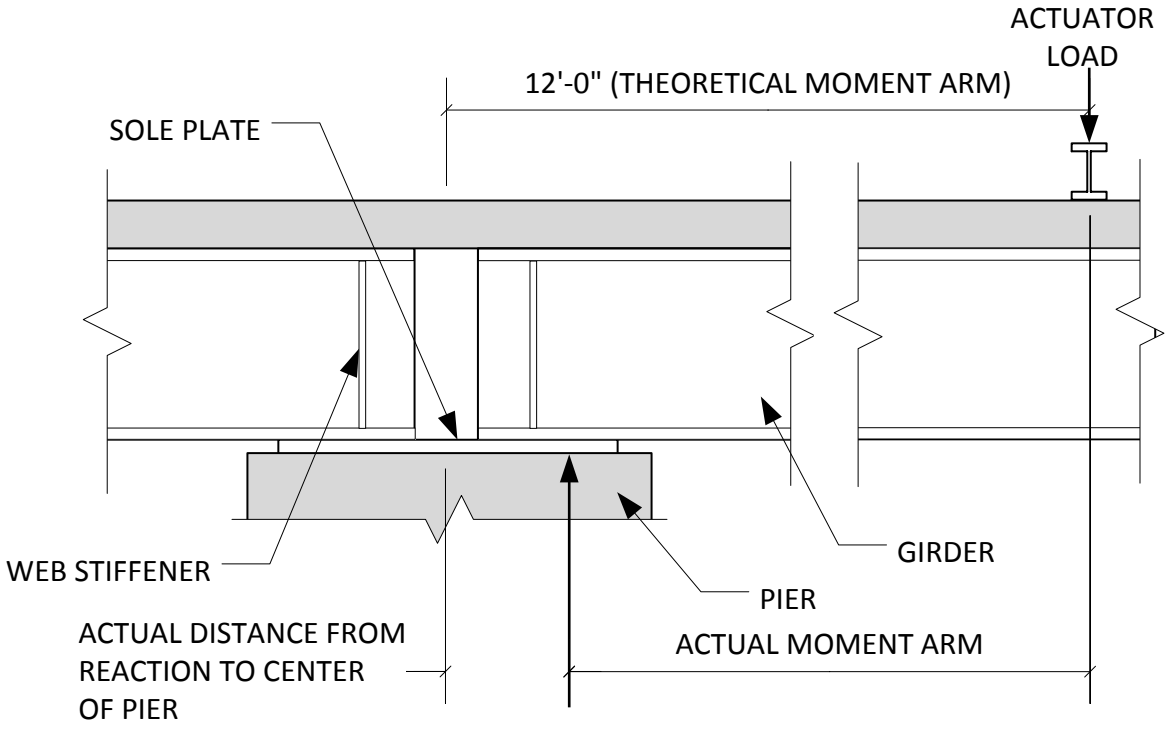

Figure 5.49 Girder Support Behavior

Similar resultant moment behavior to the Day 1 Test was noted in the Day 2 Test and is summarized for both days' tests in Table 5.1. The possible reason for the relative differences in moment arm at the end of Day 1 Test and at the activation of the safety device in the Day 2 Test was the failure of the elastomeric bearing to regain its shape, which may have caused it to more effectively distribute the loads. Also, once the safety device was active, the sole plate was subjected to negative bending, which may have caused the effective reaction location to shift slightly. The locations of the center of bearing also indicate, that although stiffeners are installed to aid in stiffening the web for buckling, it doesn't necessarily mean that the load will go through them; the bearing stiffener in this case is nine inches from the center of the sole plate.

Table 5.1 Location of Resultants for Various Loadings

Event	Theoretical Moment	Actual Moment	Center of Actual Bearing from Center of Sole Plate
End of Day 1 Test Load = 135 kips	1620 kip-feet	1488 kip-feet	15"- 3"= 12"
Activation of Safety Device Day 2 Test	1476 kip-feet	1367 kip-feet	15"- 4.5"= 10.5"
End of Day 2 Test Load = 196.5 kips	2358 kip-feet	2228 kip-feet	15"- 7"= 8"

5.6.2 Deflection and deformation compatibility

The deflections at the ends of the north girder are presented in Table 5.2. The deflections from the test do not correspond well to those calculated by hand nor could they be used for comparison to the actual bridge since it is continuous. Analysis of the deflections indicate that there is a shear component to the displacement, which is reasonable considering that L/d = 3 for the physical model. The actual bridge should not have shear deflections of any significance since the actual L/d > 21. Thus, the deflection values are shown for reference only.

Table 5.2 North Girder End Deflections

Test Day and Event	Recorded Deflection	Deflection Correction for Elastomeric Bearing	Corrected Deflection	Applied Actuator Load
Day 1 – Safety Device Activation	-0.24 inches	-0.09 inches	-0.33 inches	85 kips
Day 1 – End of Test	-0.80 inches	-0.15 inches	-0.95 inches	135 kips
Day 2 – Safety Device Activation	-0.44 inches	-0.12 inches	-0.56 inches	123 kips
Day 2 – End of Test	-1.02 inches	-0.15 inches [(1)]	-1.17 inches	196 kips

[(1)] Estimated since values were unreliable due to excessive lateral deformation of the bearings

5.6.3 Discussion/Conclusions from experimental test

Based on a review of the test results, the following key findings were identified.

For simple-made-continuous bridges in general:

1. The mechanism to transfer the compressive force component of the SMC moment is the most load transfer critical element since the top SMC reinforcing steel doesn't ever become fully stressed.
2. The actual maximum negative moment occurs within the length of the beam on the bearing plate and is less than the theoretical maximum negative moment, which would occur in a fully continuous girder that is considered point supported. Thus, it is slightly conservative to design the simple-made-continuous reinforcing and any transfer plates for the force components of the theoretical maximum negative moment.
3. The shear lag in the slab as indicated by the reinforcing steel forces, concrete strains, and concrete crack pattern was as expected, based upon comparison to test results by others (Farimani M., 2006) for this type of connection.
4. The top SMC reinforcing bars on either side of the center bar each take approximately 8% of the total tension load component of the tensile component of the moment and are, thus, the critical bars for design. This corresponds reasonably well with the Nebraska studies in which similar bars are taking approximately 9% of the total tension load (Azizinamini A., 2005). Thus, the more conservative 9% value will be used herein.

For the CDOT simple-made-continuous bridge in particular:

1. The most load critical element of the connection is the sole plate, as it is not only required to transfer the entire compressive component of the SMC moment, but it is also subjected to a moment due to load eccentricity.
2. The welds of the girder to the sole plate must be increased in size in order to transfer the full compressive component of the SMC moment to the sole plate in accordance with AASHTO requirements (3.3.3 and Table 3.5).
3. The welded connection and the bottom flange of the girder at the weld must also be designed for fatigue considerations, specifically AASHTO fatigue categories E and E', which have stress ranges of 4.5 ksi and 2.6 ksi, respectively.

As an alternative to items 1, 2, and 3, transfer plates flush with the bottom flanges could be installed between the girder flanges as a direct means of compression transfer; these plates could be field adjusted for fit up between the girder ends. This alternative is economical, safe, simple, and not subject to the AASHTO fatigue requirements and will be used in the formulation of the final design equations.

5.6.4 Correlation/Comparison with Abaqus Results

An attempt to verify the Abaqus numerical results with the numerical results of the physical model test was not successful. There was a basic lack of direct correlation of all results from girder end displacements to strains in the reinforcing steel, concrete, and girder steel. The possible reasons for the lack of correlation are many; the major culprits could likely be the concrete damage model, the constraints used between the concrete and the reinforcing and between the concrete and the girder shear connectors. Another important difference was that the elastomeric bearing was not modeled in Abaqus as its extreme displacements would not allow Abaqus to converge and thus, the runs in which it was modeled would abort prematurely. However, the comparison of the overall behavior of the Abaqus model to the physical model did provide some valuable insight into the interpretation of the test results.

The behavior at the sole plate in which the actual component of girder reaction is nearer to front of the pier was clearly indicated in the Abaqus results (Figure 5.50). The location of the bearing stiffener is evident by the flared out, lighter colored sections, which also indicate that the contact forces caused by the stiffeners are significantly lower than those caused by the web. The axial strains in the reinforcing bars are shown in (Figure 5.51) where the effects of the shear lag across the slab are evident. The shear lag in the top SMC reinforcing bars was somewhat similar between the Abaqus model and the physical test (Figure 5.52), although the behavior on either side of the center varied, which was likely due to the concrete in the Abaqus model taking considerably more tension due the concrete damage model used. The shear lag in the top of the slab based on the Abaqus analysis is shown in Figure 5.53; this particular plot was taken from the earlier stages of the analysis prior to the effects of concrete damage became evident.

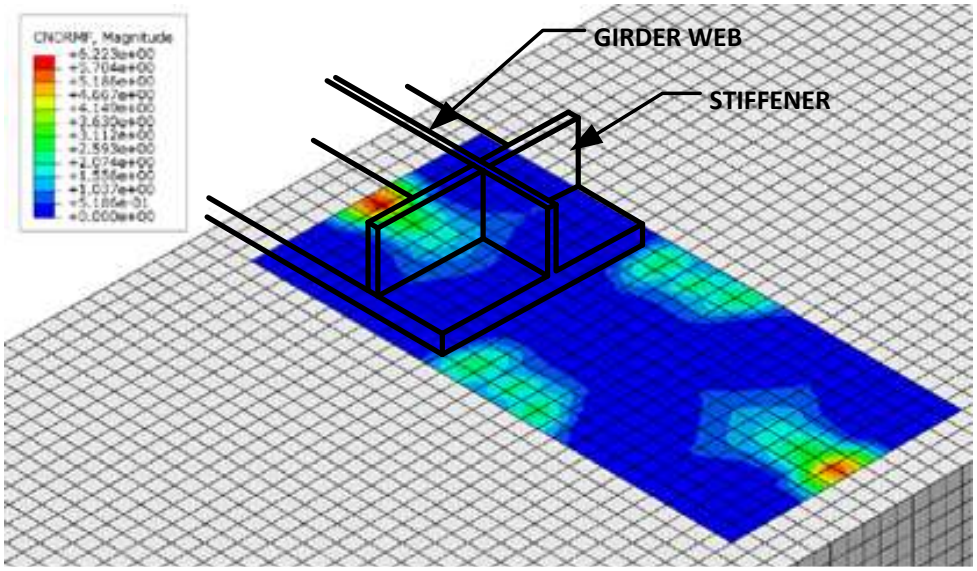

Figure 5.50 Normal Forces on Sole Plate – Abaqus

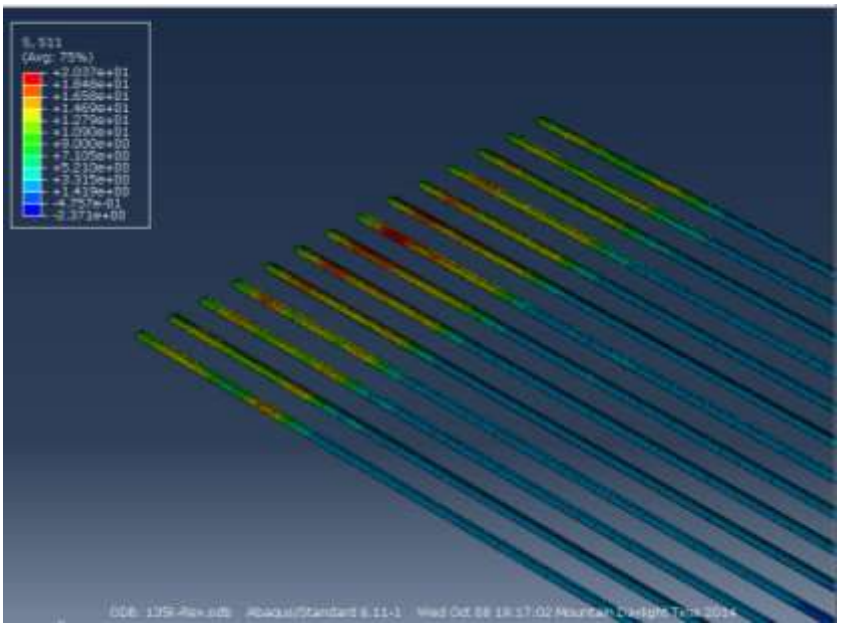

Figure 5.51 Axial Stress in SMC Top Reinforcing Steel

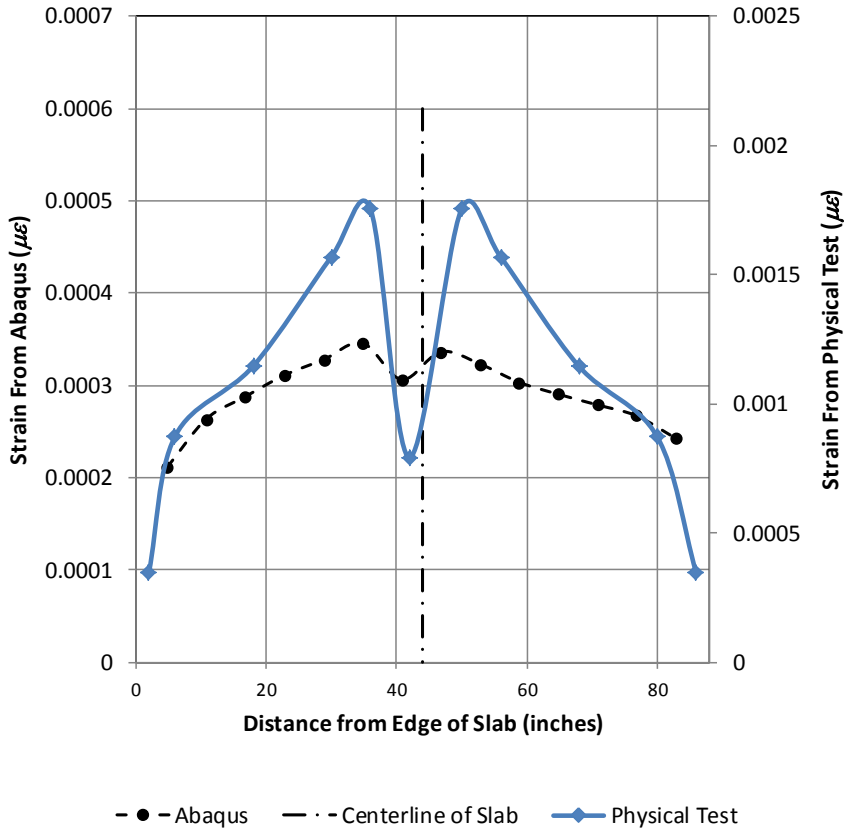

Figure 5.52 Comparison of SMC Reinforcing Strains

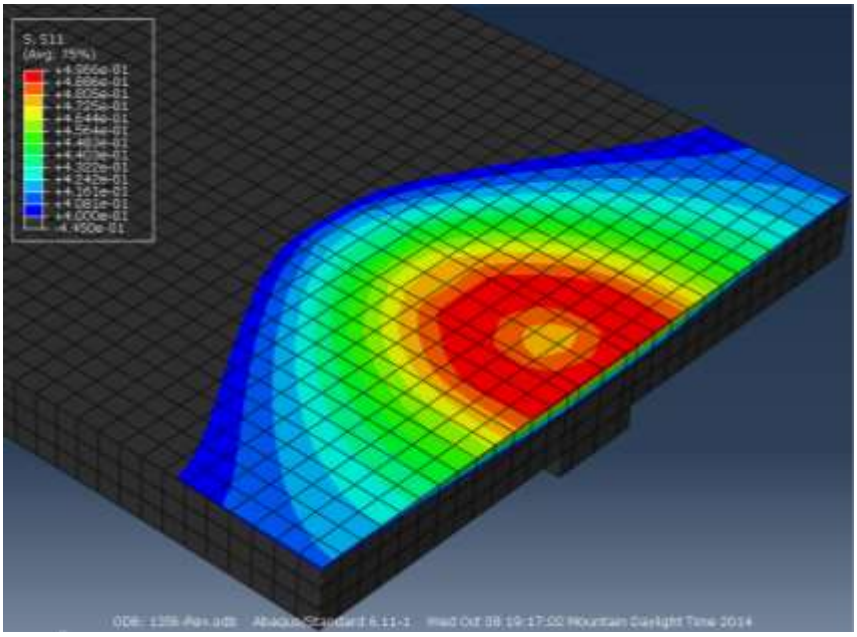

Figure 5.53 Early Shear Lag in Top of Concrete Slab

6. PARAMETRIC STUDY

Following the successful completion of the physical model test, a parametric study was performed to expand the applicability of the study connection. The parametric study consisted of analyzing ranges of girder spans, numbers of spans, girder spacings (slab spans), slab thicknesses, and simple-made-continuous reinforcing arrangements for use in developing design equations for the study connection. The following sections describe the selection of the various design parameters that helped to define the scope of the parametric study, the study methodology, and the results of the study. Design parameters for the study were carefully selected to reflect the practical SMC bridge configurations reviewed and with consideration of the SMC concept under investigation.

6.1 Bridged Roadway Geometry Limitations

The range of girder spans was developed assuming that the bridge would be used to span a roadway. Using CDOT standards for road geometry (CDOT, 2012), which are similar or identical to the standards used by other states' departments of transportation, a set of theoretical roadways to be bridged was assumed, forming the basis for spans to be considered. The applied limitations on the roadway based on CDOT were:

1. Lane width = 12 feet
2. Minimum number of lanes = 2
3. Shoulder width = 8 feet
4. Shoulder on each side of the roadway

Additional geometric restrictions made to keep the study within practical limits were:

1. Maximum number of lanes = 6
2. Distance between the roadway and the bottom of the bridge girder = 18 feet (minimum = 16.5 feet)
3. Two horizontal to one vertical slope on the abutments
4. Space between traffic directions = 6 feet

These limitations are shown diagrammatically in Figure 6.1.

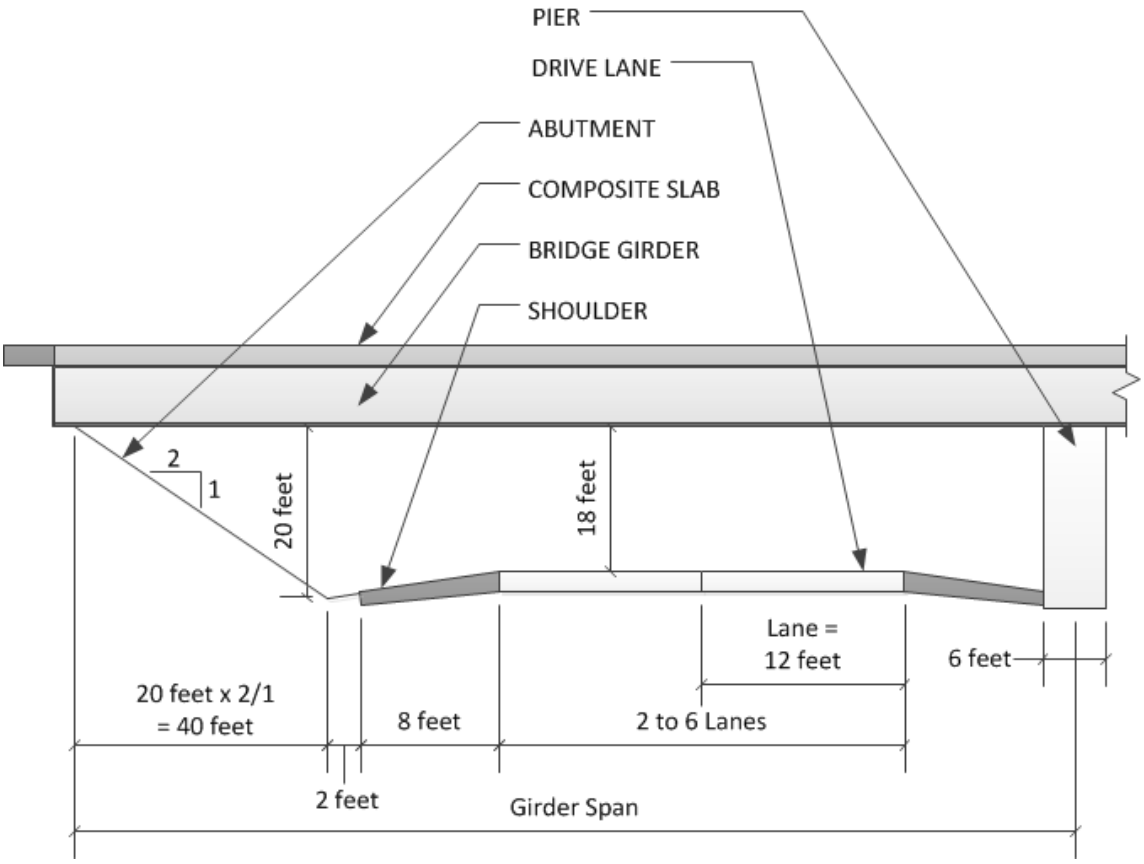

Figure 6.1 Roadway Limitations

Based on the roadway constraints, the range of potential bridge spans was 83 feet to 131 feet. The range selected for the study was set from 80 feet to 140 feet; this range provides for six spans to be considered on 12-foot increments: 80, 92, 104, 116, 128, and 140 feet. The span range of existing SMC bridges varies from 66 feet through 139 feet. The shortest span was for a rebuilt bridge, the next shortest bridge was 78 feet. Thus, using a minimum length of 80 feet to agree with the original study bridge and a maximum length of 140 feet will extend the applicability of a study connection concept to the full range of spans of existing SMC bridges.

6.2 Deck Slab Geometry and Reinforcing

6.2.1 General

The slab span/girder spacing plays an important role in the overall behavior of the bridge structure since the slab span affects the load distribution to the girders as well as the effective flange width of the composite section and limits the amount of SMC reinforcing that may be considered to act with the girder to carry the negative moment at the connection. The slab span, which is also the girder spacing, varied from approximately 7’-4” to 10’-4” on the existing bridges reviewed. This range of slab spans was selected for the parametric study, and the spans were incremented in steps of 4 inches. Slab depths of the SMC bridges reviewed varied from 8 to 9 inches. This same range was used for the parametric study with increments of 1/2 inch. The ranges selected for slab spans and slab depths give slab width/depth ratios in the range of 11 to 16, well below the AASHTO limit of 20, after which, pre-stressing of the slabs is recommended.

6.2.2 AASHTO Limitations

Of the SMC bridges reviewed, the majority of the bridge designs indicated that the slabs were designed using the AASHTO Empirical Design Method, thus the empirical method constraints were used as further limitations of the parametric study.

The Empirical Design Method places specific limitations on minimum slab dimensions and reinforcing steel areas. AASHTO also provides limitations for reinforcing placement relative to the top and the bottom of the slab (clear distances) and spacing requirements between reinforcing bars. The empirical method defined in AASHTO Section 9.7.2 (AASHTO, 2012) specifies guidelines for maximum slab spans of up to 13'-6" clear between girder flanges and a minimum slab thickness of 7 inches. Minimum reinforcing requirements for these slabs are specified as 0.18 $in.^2$/ft. each way for the top reinforcing steel and 0.27 $in.^2$/ft. each way for the bottom reinforcing steel.

The quantity of the top SMC reinforcing bars, which may be placed in the top layer, are functions of the effective slab width, the reinforcing bar size, and the minimum spacing of the reinforcing bars. In accordance with AASHTO section 5.10.3 – Spacing of Reinforcement, "The clear distance between parallel reinforcing bars shall not be less than 1.5 times the nominal diameter of the bar, 1.5 times the maximum size of the coarse aggregate or 1 1/2 in. In effect, these requirements may limit the amount of SMC reinforcing and thus the tension force that can be developed at the top of the connection as part of the tension/compression couple resisting the negative moment.

AASHTO section 5.12.3 specifies minimum reinforcing cover dimensions depending upon the location of the reinforcing, specifically, 2.5 inches clear for top reinforcing and 1.0 inch clear for bottom bars up to No. 11 (Figure 6.2). The clear distances sum to a total of 3.5 inches, which will limit the vertical space available for the SMC reinforcing placement.

Considering that the minimum slab thickness for the empirical method is seven inches and the total of the required clear distances is 3.5 inches, only 3.5 inches (half of the slab thickness) is left available for the placement of four layers of reinforcing. The minimum thickness considered herein, 8 inches, will allow a minimum of 4.5 inches for reinforcing placement. These 4.5 inches of spacing is beneficial in SMC connections because the top reinforcing steel is often larger than the basic top lateral reinforcing in non-SMC bridges.

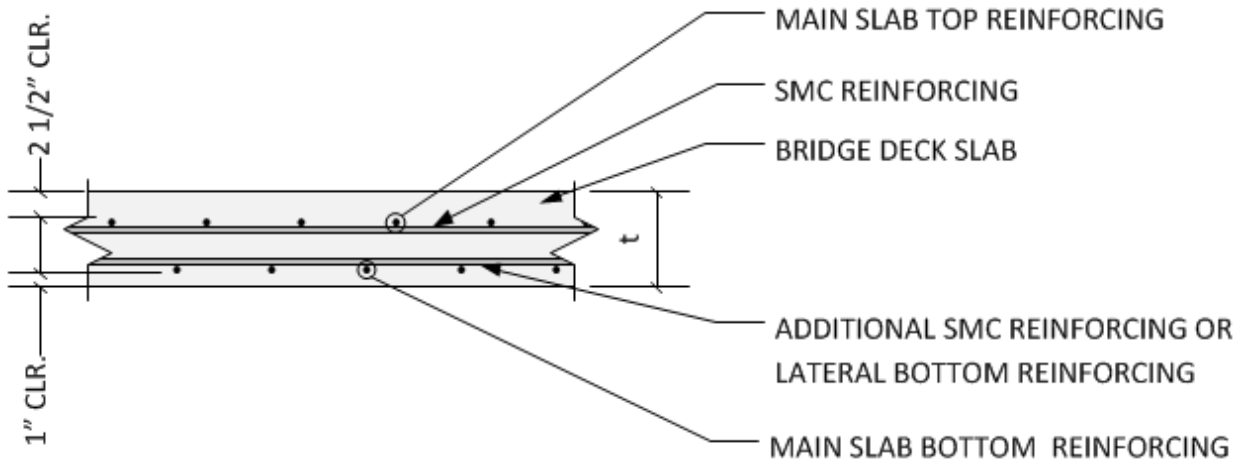

Figure 6.2 Slab Reinforcing Placement

6.3 Girder Selection Criteria

The depth of the bridge girders is critical in determining the composite properties of the positive moment section, the moment arm for the SMC composite properties, and the moment of inertia for deflection calculations. Based on a review of the SMC bridges presently constructed, the ratio of the bridge girder span to nominal girder depth (L/d) varied from 26 to 30; on this basis, an average value of 28 was selected to determine the girder depths for the various bridge spans in this study.

6.3.1 Girder Type Selection

The maximum available standard rolled girder shape is a W44x335 by depth or a W36x800 by weight. Once girders greater than available standard rolled sizes are required, plate girders must be designed. (Also, it is quite possible that plate girders with sections lighter than the standard rolled sizes may be fabricated and have the required section properties. These custom girders may ultimately cost more due to additional fabrication time, and thus, this alternative is beyond the scope of this study.)

Plate girders for required bridge girder depths larger than 44 inches were developed to meet the L/d criteria for spans longer than 104 feet, the limit for a 44-inch deep girder. The plate girder depths range from 48 inches to 60 inches depending upon the span requirement; the plate girder designations and dimensions are given in Appendix E – Plate Girder Dimensions.

6.3.2 Girder Serviceability Criteria

AASHTO has no required limitations on vertical deflections although it does state that when other criteria are not available, the limitation for deflection under vehicular load should be 1/800 of the span. The AASHTO criterion was used for the selection of girders in the parametric study to eliminate girders from consideration that did not meet this requirement. The service load requirement for deflection is AASHTO load combination "Service I," which has the load factors as shown in Table 3.2. The only loads considered in the deflection calculations were the design truck live load and the lane live load; the dead loads of the girders and the slab occur prior to the girders achieving continuity and the girders are typically cambered upward to compensate for these deflections.

6.5 Final Ranges of Parameters

Based on the preceding constraints and criteria, the final ranges of parameters for the study are presented in Table 6.1. The rolled girder sizes are available standard shapes, whereas the plate girder sizes were developed by the author during the analysis. Full information on the dimensional properties of the plate girders are given in Appendix E – Plate Girder Dimensions.

Table 6.1 Span and Spacing Ranges for the Parametric Study

Variable	Range	Increment
Girder Span	80 feet to 140 feet	12 feet
Girder Spacing (Slab span)	7'-4" to 10'-4"	4 inches
Slab Depth	8 inches to 9 inches	1/2 inch
Rolled Girders	W33, W36, W40, W44	Not applicable
Plate Girders	48 inch to 60 inch depths	6 inches

For each particular girder span considered, there are 30 possible configuration combinations to be considered between the various slab depths and girder spacings. As mentioned previously, the girder depths were defined using the ratio of the span to depth of 1/28; the parametric study girder spans and the

corresponding required girder depths are shown in Table 6.2. The plate girders used for girder depths larger than 44 inches in depth were given reference designations of PG1, PG2, etc., for convenience. The range of rolled and plate girder sizes to be analyzed for the varying ranges of slab depths and girder spacings are given in Table 6.2. The first value is the nominal depth and weight of lightest girder in the depth series followed by only the weights of the remaining girders in the series. Also presented in Table 6.2 are the maximum recommended deflections based on L/800. It was likely that the lighter girder sizes may be ruled out by not meeting the deflection criteria, moment capacity, etc.

Table 6.2 Girder Span to Girder Size Table

Span	Girder Sizes Considered	Maximum Deflection
80 feet	W33x118, 130, 141, 152, 169, 201, 221, 241, 263, 291, 381, 354, 387	1.20 inches
92 feet	W40x149, 167, 183, 211, 235, 264, 327, 331, 392, 199, 214, 249, 277, 297, 324, 362	1.38 inches
104 feet	W44x335, 290, 262, 230	1.56 inches
116 feet	PG1, PG2, PG3, PG4, PG5, PG6, PG7, PG8 (48 inch depth)	1.75 inches
128 feet	PG8, PG9, PG10, PG11, PG12, PG13, PG14, PG22 (52 inch depth)	1.92 inches
140 feet	PG15, PG16, PG17, PG18, PG19, PG20, PG21, PG22 (60 inch depth)	2.10 inches

6.6 Analysis Considerations

The parametric study was intended to determine the appropriate girder size from a range of sizes for a particular depth range for bridges from two to eight total girder spans, for varying slab thicknesses and varying slab spans. A sensitivity investigation was performed to compare values of maximum positive and negative moments along the bridge for different numbers of girder spans, since the fewer spans that require analysis, the faster the total processing time. This investigation considered a bridge with 80 foot spans and a bridge with 140-foot spans. The 80-foot span bridge was analyzed with W33x118 girders for each span and the 140-foot span bridge was analyzed with PG23 plate girders for each span. The controlling design moments, which are produced by the AASHTO "Dual Design Truck," are presented in Figure 6.3 for the minimum and maximum spans to be investigated, 80 feet and 140 feet. As the chart shows, for a given span length, the positive moment is constant for all practical purposes for all span quantities. For two span bridges, there is an increase of approximately 10% in the magnitude of the negative moment; for three spans, the negative moment decreases, but increases slightly at four spans and remains virtually constant for more spans. Based on this investigation, the parametric study performed analysis on two bridges, the first with two girder spans to capture the highest negative maximum moments and the second with four girder spans to capture the approximate envelope of maximum positive and negative moments for bridges of three or more spans. It should be noted that very few of the SMC bridges reviewed had less than three girder spans.

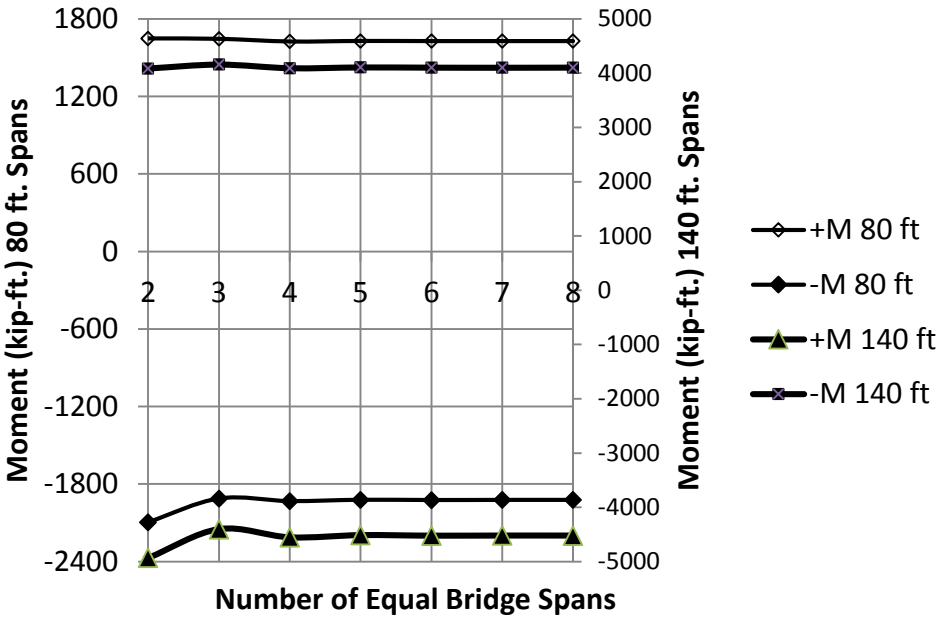

Figure 6.3 Maximum and Minimum Moments vs. Spans (note: moment scales are different)

6.7 Final Truck Load Analysis

Given the ranges of parameters in Section 6.5, it was necessary to analyze each selected bridge span for 10 different girder spacings, each with three possible slab thicknesses. Each slab depth, girder spacing, and girder size resulted in a different axle load distribution factor to calculate the percentage of the axle loads to the girder. Since the original study girder was constructed with a 3-inch deep concrete haunch between the slab and girder, a 3-inch deep haunch was also included in the parametric study analyses. The slab haunch will not only increase the positive moment and negative moment capacity, but it will also increase the composite girder stiffness, thus increasing the axle load distribution factor and, correspondingly, the axle load to the girder. If adjacent girders had different depth haunches, the axle load distribution factor for these girders would be based on their specific haunch depth. While it may be conservative to ignore the slab haunch for the composite properties of the girder, it would be unconservative not to consider the haunch in the calculation of the axle load distribution factor. Along with the axle loads, a uniform lane loading (live load) of 64 psf and a uniform bridge wearing course loading (dead load) of 35 psf were applied.

Each possible girder within the particular span range (as identified in Table 6.2) was evaluated for the following acceptance criteria:

1. Ultimate positive composite moment capacity greater than or equal to the factored applied positive moment
2. Service level maximum downward deflection less than or equal to L/800, where L is in inches

The moving load analysis software discussed in Section 3.3.3 was used to perform the analysis for the various girder and slab combinations. Results of the moving truck load analysis consisted of determining the maximum positive interior moment, the maximum negative SMC moment, and the required composite moment of inertia to meet the Span/800 vehicular load deflection limit for each case. These results were then analyzed and the lightest girder, which met both the positive moment capacity and had sufficient composite beam stiffness to meet the deflection limit, was selected.

Acceptable girders for a bridge with 80-foot girder spans are presented in Table 6.3. The tables for bridges with girder spans from 92 feet through 140 feet in 12-foot increments are provided in Appendix E – Acceptable Bridge Girders.

Table 6.3 Girder Acceptance Table – 80-ft. Span

	Slab Thickness		
Girder Spacing	**8 inches**	**8.5 inches**	**9 inches**
7.33 ft.	W33x152	W33x141	W33x141
7.67 ft.	W33x152	W33x152	W33x152
8.00 ft.	W33x152	W33x152	W33x152
8.33 ft.	W33x169	W33x152	W33x152
8.67 ft.	W33x169	W33x169	W33x169
9.00 ft.	W33x169	W33x169	W33x169
9.33 ft.	W33x169	W33x169	W33x169
9.67 ft.	W33x201	W33x201	W33x169
10.00 ft.	W33x201	W33x201	W33x169
10.33 ft.	W33x201	W33x201	W33x201

The maximum SMC negative moments for the acceptable girders were tabulated for use in the development of the top SMC reinforcing design formulation. The final values for a bridge with 80-foot girder spans are presented in Table 6.4. The tables for bridges with girder spans from 92 feet through 140 feet in 12-foot increments are provided in Appendix F. Maximum SMC Negative Moments.

Table 6.4 Maximum SMC Negative Moments (kip-feet) – 80-ft. Span

	Slab Thickness		
Girder Spacing	**8 inches**	**8.5 inches**	**9 inches**
7.33 ft.	-2020	-2013	-1988
7.67 ft.	-2080	-2074	-2045
8.00 ft.	-2128	-2123	-2093
8.33 ft.	-2190	-2171	-2140
8.67 ft.	-2239	-2241	-2201
9.00 ft.	-2288	-2289	-2248
9.33 ft.	-2336	-2338	-2295
9.67 ft.	-2408	-2400	-2341
10.00 ft.	-2456	-2448	-2388
10.33 ft.	-2504	-2496	-2459

There are several items of note upon review of Table 6.4; first, the SMC negative moments increase with girder spacing. This is logical since an increase in girder spacing will also increase the amount of lane loading and wearing course loading to the girder since both of these are post-composite and thus affect the SMC moment. However, these loads are not the only reason that SMC moments increase; the girder spacing also affects the axle load distribution factor, D_f, (Equation 3), which is due to an increase in the moment of inertia of the composite section as the flange width, which is also one-half of the girder spacing, is increased. The increased girder stiffness will cause it to attract more loading from the design truck axles. Second is the decrease in negative moment for thicker slabs; this is actually because the slab dead load is applied prior to the SMC action becoming effective and therefore does not have an effect on the SMC moment. An additional reason for the decrease is again the axle load distribution factor in which the slab thickness affects the slab stiffness, so a thicker slab is better able to distribute loads to the

adjacent supporting beams and correspondingly decrease both the positive and negative moments due to truck loadings in the SMC condition.

The determination of acceptable girders was based upon the composite slab and girder sections having adequate strength for the positive bridge girder moment and having sufficient stiffness to meet the selected (L/800) deflection criteria. An approximate method for determining the maximum deflections, which in every case occurred in the first span, was developed; this method involved several simplifications in order to be easily used. On the basis of the maximum deflection, a moment of inertia may be determined based on only the span length and maximum moment; the final formulation is given in Equation 7.

$$I_{\min} \geq \frac{800 M_{\max} L}{3452} = 0.24 M_{\max} L \qquad \textbf{Equation 7}$$

Where:

I_{min} = Minimum moment of inertia to achieve $l/800$ deflection limitation in inch^4

M_{max} = Maximum unfactored superimposed load moment in kip-feet

L = Length of the girder span in feet

The moment of inertia formulation was verified using RISA-3D analysis software and found to give acceptable approximations for different span lengths and loading conditions. The calculations for the development of the formula are presented in Appendix G.

The acceptable girders from the parametric study were then used in the development of the SMC connection design methodology presented in Section 7.

7. DESIGN RECOMMENDATIONS FOR FUTURE SMC CONNECTIONS WITH STEEL DIAPHRAGMS

7.1 Preliminary Considerations

In the original study connection, the main elements involved in resisting the SMC moment at the support are the girder bottom flange, the weld to the sole plate, and the sole plate for the compression component and the top SMC and temperature reinforcing bars for the tension component.

As discussed in Section 5.6.3, several elements of the compression transfer mechanism of the study connection as originally designed and tested were cause for concern, specifically the sole plate and the weld of the girder bottom flange to the sole plate. The sole plate failed in yielding at an applied moment of 960 kip-ft and the weld from the girder to the sole plate failed in rupture at an applied moment of 1,440 kip-ft, both of which were well below the required design ultimate moment of 1,782 kip-ft. Both of these elements were crucial to the transfer of the compression component of the maximum internal SMC moment between girders to which the actual study bridge would be subjected. Additionally, the weld between the girder bottom flange and the sole plate was found to be subject to a fatigue stress category E', which has a maximum stress range of 2.6 ksi, well below the actual stress range of approximately 100 ksi. As was also discussed, these concerns may be alleviated through the use of a direct compression transfer plate fitted between the bottom flanges.

A safety device that was used during testing to transfer load in case of weld failure functioned well during the test after both yielding of the sole plate and fracture of the welds of the bottom flange to the sole plate. In order to allow for fit up tolerances in the field, the actual compression transfer plate should consist of two wedge shaped plates as was used in the Tennessee SMC bridges (Appendix A – Current SMC Bridges and Chapman, 2008). These types of plates would allow for both longitudinal and slight angular corrections. The wedge compression plates would subsequently be intermittently field welded to prevent further movement.

This new scheme would not require the welds between the girder bottom flange and the sole plate for axial load transfer since the entire axial load will travel directly through the compression transfer plate. Omitting the extensive welding of the girder to the sole plate would eliminate a significant amount of skilled field labor, but it would also require a new method of lateral restraint to be provided for the girder bottom flange. Several options to provide lateral restraint are:

1. Provide anchor bolts through the sole plate and the bottom girder flanges (Figure 7.1 and Figure 7.2).
2. Provide field welds for only lateral stability between the sides of the flanges and an anchor bolted sole plate (Figure 7.3 and Figure 7.4).
3. Provide welded guide bars on an anchor bolted sole plate with a small space allowance on either side of the girder bottom flange (Figure 7.5 and Figure 7.6).

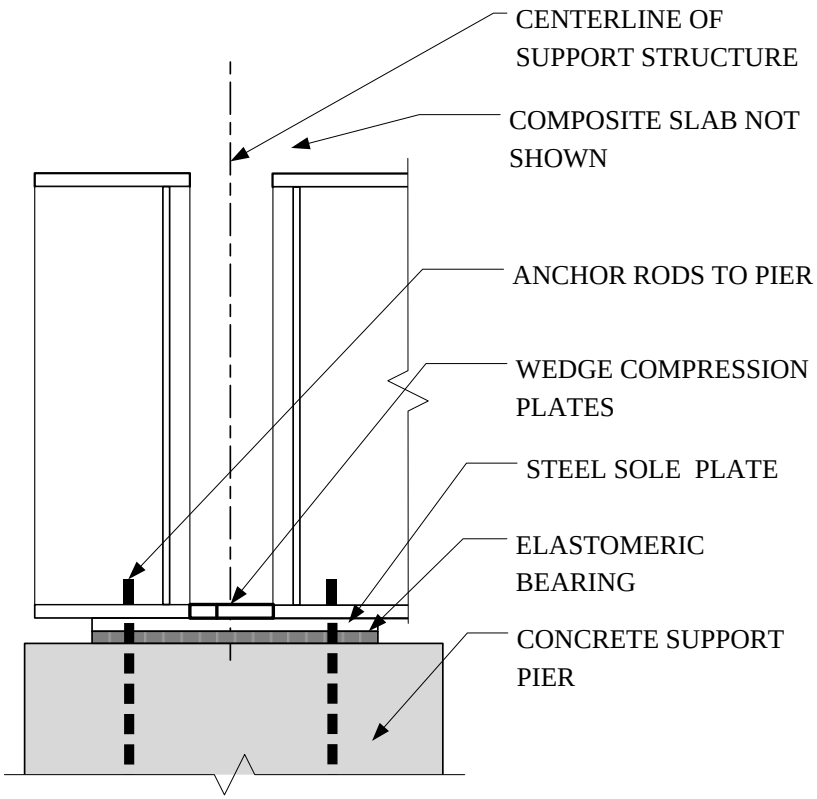

Figure 7.1 SMC Girder Support Detail 1 – Side View

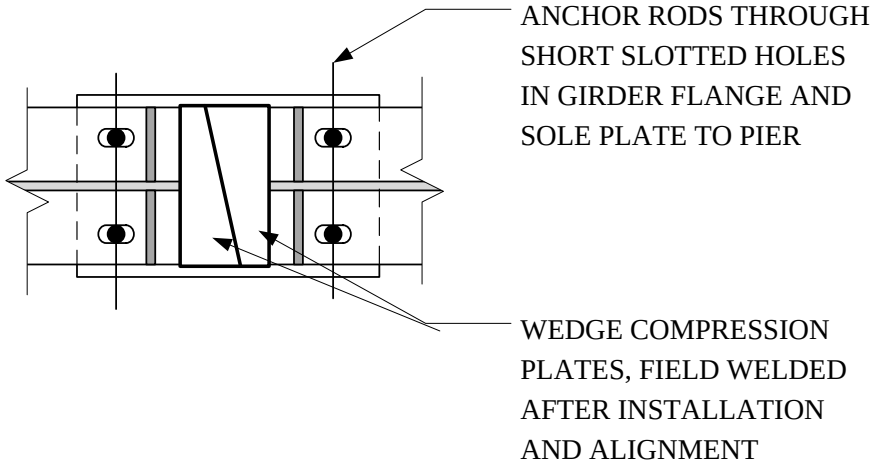

Figure 7.2 SMC Girder Support Detail 1 - Plan View

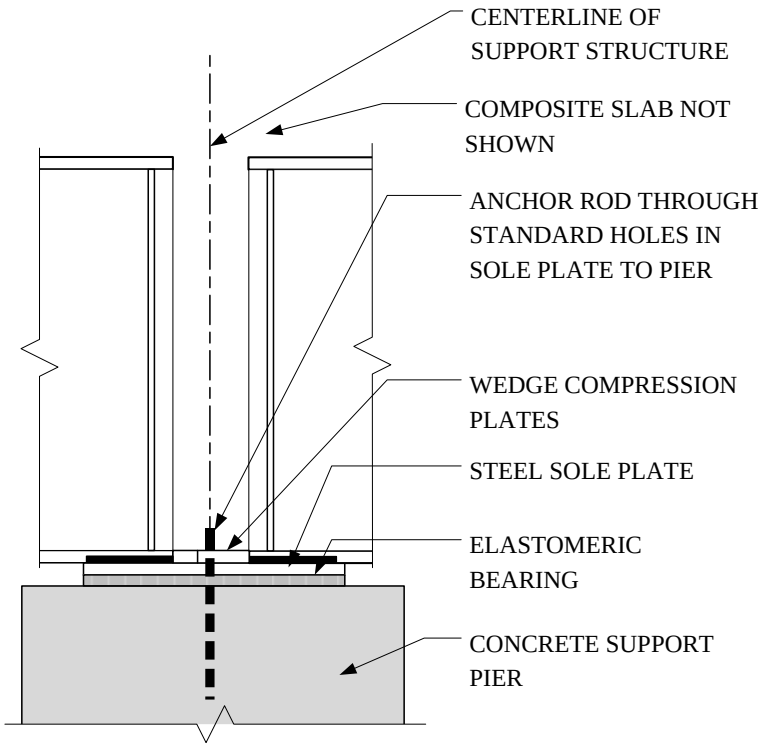

Figure 7.3 SMC Girder Support Detail 2 – Side View

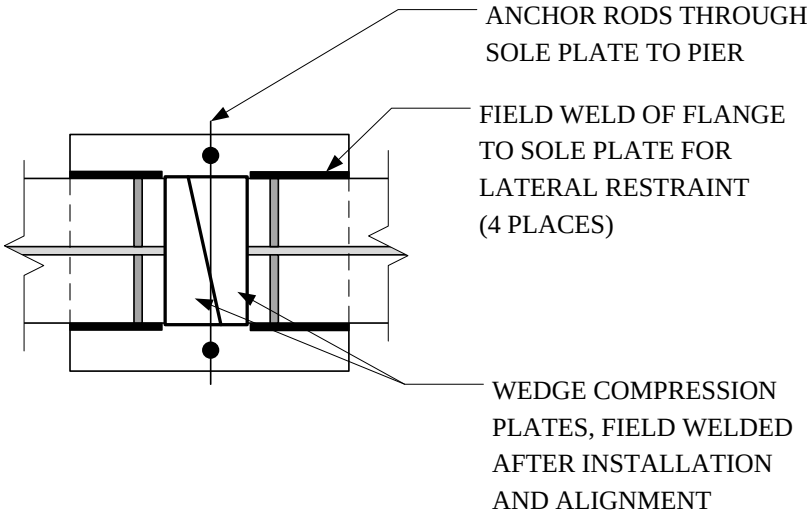

Figure 7.4 SMC Girder Support Detail 2 - Plan View

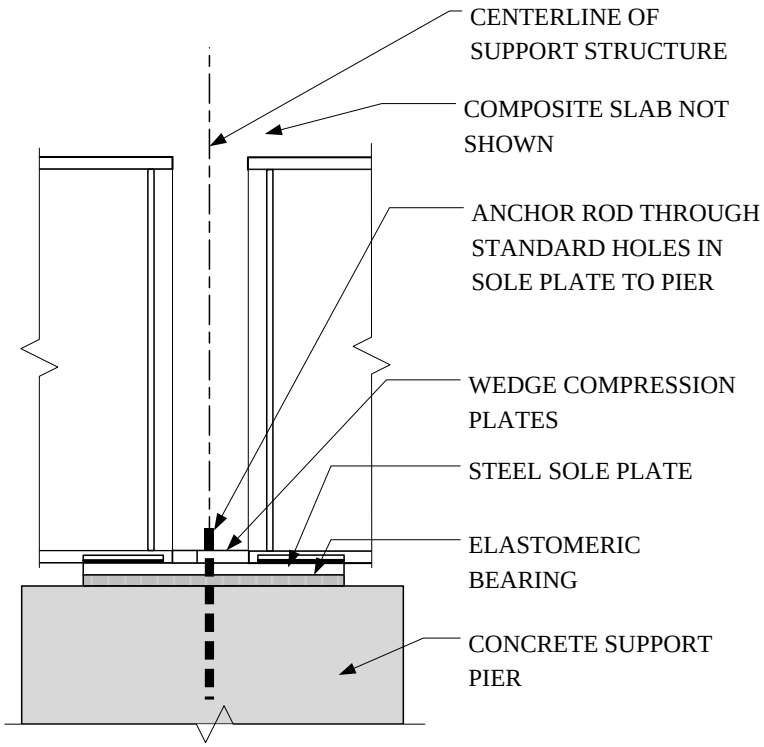

Figure 7.5 SMC Girder Support Detail 3 - Side View

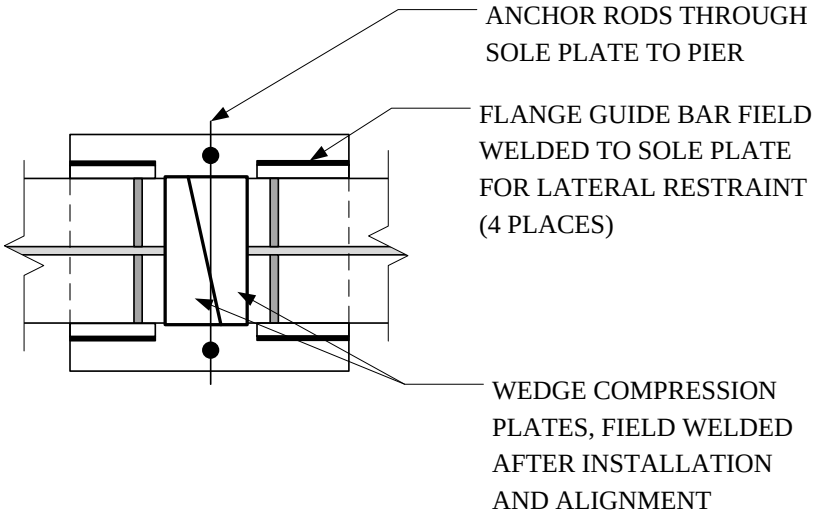

Figure 7.6 SMC Girder Support Detail 3 - Plan View

These three possible modifications involve increasing degrees of complexity and, consequently, construction cost; also, the welds in the second detail could again be subject to fatigue from compression due to bending in the bottom flange. Therefore, the modifications presented in Figure 7.1 and Figure 7.2 will be used in the final connection design strategy.

The wedge transfer plates considered are similar to those used in the Tennessee bridges (Talbot, 2005) and will use the same skew angle of 2.5 degrees between the plates. The design will require the plates to resist the compression load, which will be transferred through direct bearing from the girder bottom flanges. The design will also entail determining the vertical component of the compression force on the skew and designing a partial penetration groove weld for the shear force.

From a review of currently constructed SMC bridges (including the study bridge), all the bridge slabs were reinforced with SMC top reinforcing and top temperature (longitudinal) bars at the same spacing. It's most likely that this was done for convenience and to avoid the possibility of misplacement of bars in the field. This common, combined placement of the slab SMC and temperature bars will be considered in the formulation and evaluation of the tension component of the proposed design equation. Also, as was seen in the evaluation of the shear lag in the SMC reinforcing steel (Figure 5.38), the two sets of bars, SMC, and temperature, immediately on either side of the girder, take a significantly larger share of the tensile load component than the remaining bars.

The final ranges of acceptable girders vs. span and negative moments vs. span were subsequently used in the development of a proposed design equation. These ranges are provided in Table 6.3 in Section 6.7 and Appendix 5 tables, respectively.

7.2 Formulation Development

The basic rationale for the behavior of the connection is the development of an internal couple created by the tension in the simple-made-continuous top reinforcing bars being equal to the compressive component of the bottom flange of the girder. This methodology is not unlike those developed at the University of Nebraska and used in various SMC bridges constructed in Nebraska and elsewhere with the exception that the previous schemes used heavy steel blocks to transfer the compressive component of the couple from the flange and a portion of the weld and encased the entire connection in a concrete diaphragm. The starting point for the design would be the selection of a girder, which has sufficient strength and stiffness in the composite condition to meet the strength and serviceability requirements due to the maximum positive moment in the span; girders meeting these acceptance criteria were determined in Section 6.

A simple and straightforward approach to design the SMC connection is to directly equate the area of the reinforcing steel to the area of the bottom flange of the girder without regard to the difference in the yield stresses and resistance factors between the two. This method is slightly conservative since F_y = 50 ksi for the girder steel and F_y = 60 ksi for the reinforcing steel; however, the resistance factors are ϕ = 1.0 and ϕ = 0.90 for the girder and reinforcing steel, respectively, thus the factored yield stresses are 50 ksi and 54 ksi, respectively. Not only is this method conservative, but will also somewhat equalize the strains of the tension and compression components. Equal or approximately equal strains are a desirable behavior because they will enable more accurate calculation of the section stiffness and thus more accurate determination of girder deflections. Once the area is determined, the next step is to multiply the force developed by the area of steel by the moment arm between the two areas and check the value against the required SMC moment capacity. One point of concern is the considerable increase in the stress in the SMC top bars on either side of the girder; this may be remedied by the inclusion of the temperature bars in the capacity of these bars. Thus, there must be a requirement that the top temperature bars be spaced at the same spacing as the SMC top bars. The same reinforcing bar strain behavior in the bars adjacent to the girder was noted in the physical test results of other SMC bridge researchers as well (Farimani R. S., 2014 and Niroumand, 2009). Also, in this other research, the bridge model's loadings were increased during the experimental test such that the reinforcing bars on either side of the girder yielded, and as the loading was increased the adjacent bars load increased until they yielded, which continued until the bars

at the extents of the slab also yielded. While this is not necessarily a desirable behavior for normal bridge loadings, it does indicate that bridges of this type do have considerable reserve capacity for overload. The final components are the wedge-shaped compression transfer plates, including the weld between the two pieces. Several points to consider are the potential moment induced in the transfer plate if its thickness is greater than the thickness of the bottom flange and the possibility of differences in the yield strengths of the flange and plates. The final modified connection configuration is shown in Figure 7.7.

On the basis of the preceding, the recommended design methodology would proceed as follows:

1. Equate the area of SMC reinforcing to the area of the bottom flange:

$$A_r = A_f = b_f t_f \qquad \textbf{Equation 8}$$

Where:

A_r = required area of SMC reinforcing steel (in.^{2})

A_f = area of girder bottom flange (in.^{2})

b_f = width of bottom flange (in.)

t_f = thickness of bottom flange (in.)

The recommended minimum bar size is #8; smaller bars would require a significantly greater number (over 30%) of bars be placed.

2. Determine the moment arm between the couple based on girder and slab geometry:

$$d_m = d_h + t_s - cl - D_t - \frac{D_{SMC}}{2} + d_G - \frac{t_f}{2} \qquad \textbf{Equation 9}$$

Where:

d_h = depth of haunch (inches)

t_s = thickness of slab (inches)

cl = reinforcing clear distance (inches)

D_t = main (lateral) top reinforcing bar diameter (inches)

D_{SMC} = SMC (longitudinal) reinforcing bar diameter, (inches)

d_G = depth of girder (inches)

t_f = thickness of girder flange (inches)

3. Verify the moment capacity of the section using the area and yield stress of the girder flange:

$$\phi M_n = \phi_f A_f d_m F_{yG} \qquad \textbf{Equation 10}$$

Where:

$\phi_f = 1.0$ Flexure

$M_n =$ Nominal moment capacity (k-in)

$A_f =$ Area of the bottom flange (in.^{2})

$d_m =$ Moment arm between SMC reinforcing and center of bottom flange (in.)

$F_{yG} =$ Yield stress of girder flange (ksi)

4. Design of the wedge compression plates and weld

   a. Cross-sectional area of the wedge plates, A_{pl}:

$$A_{pl} \geq \frac{A_f \phi_f F_{yW}}{\phi_c F_{ypl}} = t_{pl} b_{pl} \qquad \textbf{Equation 11}$$

Where:

$A_f =$ Area of girder bottom flange (in.^{2})

$\phi_f = 1.0$ Flexure

$F_{yW} =$ Yield strength of girder (ksi)

$\phi_c = 0.9$ Axial compression

$F_{ypl} =$ Yield strength of plate (ksi)

$t_{pl} =$ Wedge plate thickness (in.)

$b_{pl} =$ Wedge plate width (in.)

   b. Plate thickness shall match the thickness of the girder flange as closely as possible

c. Check bearing on the plate material from the girder. AASHTO has no specific bearing strength requirements, so these have been taken from the AISC Manual (AISC, 2011).

d.

$$A_p = t_{pl} b_f \geq \frac{\phi_f A_f F_{yW}}{1.8 \phi_p F_{ypl}}$$

Where:

A_p = Bearing area of plate against flange

t_{pl} = Thickness of wedge plate (in.)

b_f = Girder bottom flange width (in.)

$\phi_f = 1.0$ Flexure

A_f = Area of girder bottom flange (in.^{2})

F_{yW} = Yield strength of girder (ksi)

$\phi_p = 0.75$ Bearing

F_{ypl} = Yield strength of plate (ksi)

e. Design of partial penetration groove weld:

$$w_t = \frac{V_W}{0.6 \phi_{e2} F_{exx}} + 0.125 = \text{ Minimum weld size (in.)}$$

Where:

$$w_t = \frac{V_W}{0.6 \phi_{e2} F_{exx}} + 0.125 = \text{ Minimum weld size (in.)}$$

$V_w = A_f F_{yW} \sin(2.5) = 0.044 A_f F_{yW}$ = Shear force between the plates (kips)

$L_w \approx b_{pl}$ = Wedge plate width (in.)

$\phi_{e2} = 0.8$

F_{exx} = Ultimate strength of weld metal (ksi)

5. The SMC reinforcing for the girders must meet two criteria:
   a. The total area of the provided SMC reinforcing steel must equal or exceed the area of the girder bottom flange. This criterion will determine the total number of a specific bar size to be placed at the SMC girder connection within the effective slab width.
   b. A single SMC top bar considered in conjunction with a single top temperature bar must have the factored tensile capacity to resist a factored tensile load of 9% of the total SMC reinforcing tension component. This criterion is based on the results of the physical test for the study connection and review of test results by other investigators (Farimani R. S., 2014) (Niroumand, 2009) and may affect the size of the reinforcing bars used.

The development of these guidelines is given in section 7.3.

Reviewing the equations, it can be seen that once an acceptable girder and SMC reinforcing bar size is selected, all the variables required for the equations are known values.

Not considered in the design equation formulation was the reaction behavior at the support. As was discussed in Section 5.6.1, the actual negative moment at the end of the girder is less than the maximum theoretical centerline of support moment due to the girder reaction not being at the centerline of the pier but actually occurring between 8 and 12 inches away from the centerline of the support. Neglecting this behavior adds a slight conservatism to the design.

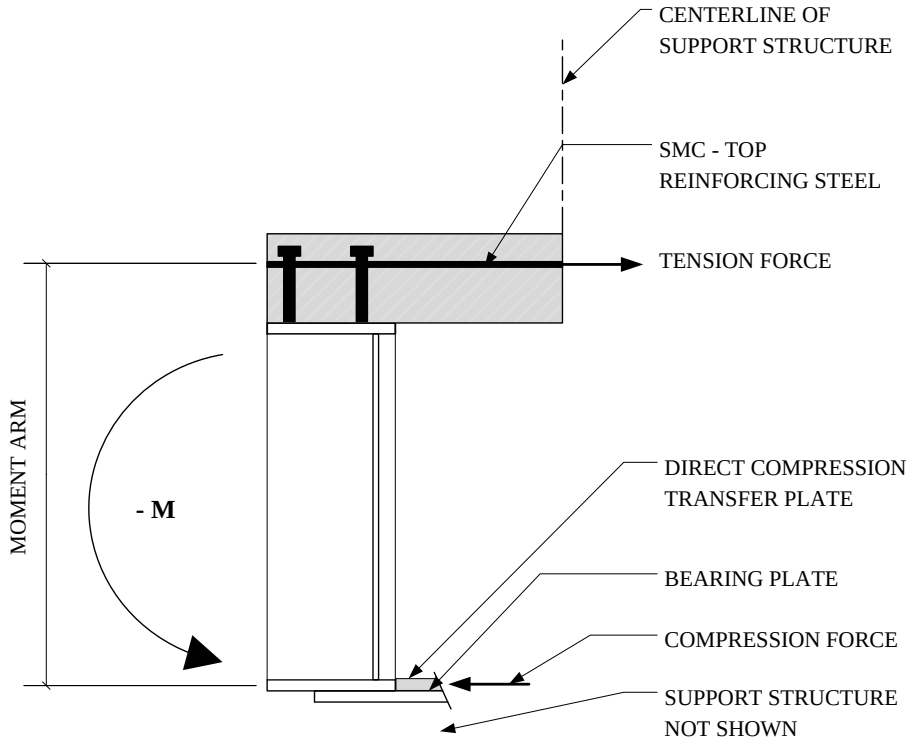

Figure 7.7 SMC Behavior

7.3 Verification/Validation of Design Formulation

To test the proposed design equation, several girders and their corresponding maximum negative moments were compared against the proposed design equation and methodology.

A full example using an 80-foot girder span with a 9-inch thick slab and 9-foot girder spacing and #9 SMC reinforcing bars follows:
From Tables 28 and Table 29 (Section 6.7) the following information is given:

Girder Size: W33x169 $b_f = 11.5$ in., $t_f = 1.22$ in., $d = 33.8$ in.

Negative Moment: M = -2248 k-ft

Calculations for the connection design follow:

Determination of required dimensions:

$A_f = 1.22(11.5) = 14.03 \text{ in.}^2$

$d_h = 3 \text{ in.}$

$t_s = 9 \text{ in.}$

$cl = 2.5 \text{ in.}$

$D_t = 0.625 \text{ in. (\#5 bar)}$

$D_{SMC} = 1.125 \text{ in. (\#9 bar)}$

$d_g = 33.8 \text{ in.}$

$t_f = 1.22 \text{ in.}$

$$d_m = 3 + 9 - 2.5 - 0.625 - \frac{1.125}{2} + 33.8 - \frac{1.22}{2} = 41.5 \text{ in.}$$

Determine SMC bar quantity and spacing:

$A_{\#9} = 1.00 \text{ in.}^2$

$N = 14.03 \text{ in.}^2 / (1 \text{ in.}^2 / \text{bar}) = 14 - \#9 \text{ bars}$

Slab Width = 9.0 ft. = 108 in.

Spacing $= 108 \text{ in.} / 14 \text{ bars} = 7.7 \text{ in./bar;}$ Say $\#9 @ 7\ 1/2$ inches

Verify capacity:

$$\phi M_n = \frac{14.03 \text{ in.}(41.5\text{in.})(50 \text{ ksi})}{12 \text{ in.}/\text{ft.}} = 2425 \text{ kip-ft} > 2248 \text{ kip-ft OK}$$

Design wedge compression transfer plates using F_y =50 ksi plates:

$$A_{pl} \geq \frac{14.03 \text{ in.}^2 (1.0) 50 \text{ ksi}}{0.9(50 \text{ ksi})} = 15.6 \text{ in.}^2$$

Try PL 1 in. x 16 in., $A_{pl} = 16.0 \text{ in.}^2 > 15.6 \text{ in.}^2$, OK

$t_{pl} = 1.0 \text{ in.} \approx 1.06 \text{ in.} = t_f$ OK

$$A_p = 1.0 \text{ in.}(11.6 \text{ in.}) = 11.6 \text{ in.}^2 > \frac{1.0(1.06 \text{ in.})(11.6 \text{ in.})(50 \text{ ksi})}{1.8(0.75)(50 \text{ ksi})} = 9.03 \text{ in.}^2$$

Design weld:

$V_w = 0.044(14.03 \text{ in.}^2)(50 \text{ ksi}) = 30.9 \text{ kips}$

$$w_t = \frac{30.9}{0.6(0.8)(70 \text{ ksi})(16 \text{ in.})} + 0.125 = 0.183 \text{ in. - Use } \frac{1}{4} \text{ in. weld}$$

$$\text{Total weld capacity} = \left(\frac{1}{4} \text{ in.} - \frac{1}{8} \text{ in.} \right)(0.6)(0.8)(70 \text{ ksi})(16 \text{ in.}) = 67.2 \text{ kips} > 30.9 \text{ kips, OK}$$

Verification of area of SMC reinforcing with #5 temperature bars:

$A_{\#9} = 1.00 \text{ in.}^2$, $A_{\#5} = 0.31 \text{ in.}^2$

$A_{total} = 1.31 \text{ in.}^2$

$\phi A_{total} F_y = 0.9(1.31 \text{ in.}^2)(60 \text{ ksi}) = 70.7 \text{ kips}$

Total flange force = $(14.03 \text{ in.}^2)(50 \text{ ksi}) = 702$ kips

Check bar force capacity > 9% of flange force

70.7 kips > 63.2 kips $= 0.09(702 \text{ kips})$, OK

Table 7.1 summarizes the reinforcing design results for the preceding example and several other samples. All of the girder and slab arrangements checked were found to be acceptable, although the capacity of case 2 was slightly under, but within 0.5 % of the required value.

Table 7.1 Sample SMC Reinforcing and Moment Calculations

Case	0	1	2	3	4	5
Girder Span (ft.)	80	92	92	104	116	116
Girder Size	W33x169	W40x183	W40X183	W44x230	PG1	PG1
Slab t (t_s) (in.)	9	8	9	8	8	9
Girder Spacing (ft.)	8	8	9	8	7.67	10
$-M_u$ (k-ft)	**2248**	**2641**	**2770**	**3153**	**3552**	**4134**
b_f (in.)	11.5	11.8	11.8	15.8	24	24
t_f (in.)	1.22	1.2	1.2	1.22	0.75	0.75
A_f ($in.^2$)	14.03	14.16	14.16	19.276	18	18
d_h (in.)	3	3	3	3	3	3
cl (in.)	2.5	2.5	2.5	2.5	2.5	2.5
D_t (in.)	0.625	0.625	0.625	0.625	0.625	0.625
D_{SMC} (in.)	1.125	1.125	1.125	1.125	1.125	1.125
d_G (in.)	33.8	39	39	42.9	48	48
Number of Bars	15	15	15	20	19	19
d_m (in.)	41.5	45.7	46.7	49.6	54.9	55.9
ϕM_n (k-ft)	**2426**	**2697**	**2756**	**3984**	**4120**	**4195**
Status	Adequate	Adequate	Adequate (Within 0.5%)	Adequate	Adequate	Adequate

As was discussed in section 7.2, the SMC reinforcing for the girders must meet an additional criterion besides having a minimum area equal to the girder bottom flange area, which is that the factored strength of one SMC bar combined with the factored strength of one temperature bar must equal or exceed 9% of the total capacity required. This additional criterion is based on the results of the physical test for the

study connection and review of test results by other investigators (Farimani R. S., 2014) (Niroumand, 2009) and may affect the size of the reinforcing bars used.

Thus, the effects of this behavior must also be considered when designing SMC reinforcing. The strain results in the SMC reinforcing bars from the Day 2 test are shown in Figure 7.8, and aside from the jump in curves due to the activation of the safety device, the curves are relatively linear. The physical locations of the individual gages are shown in Figure 5.19. The two most highly stressed reinforcing bars are those located on both sides of the steel girder and are numbers SSL-1 and SSL-2.

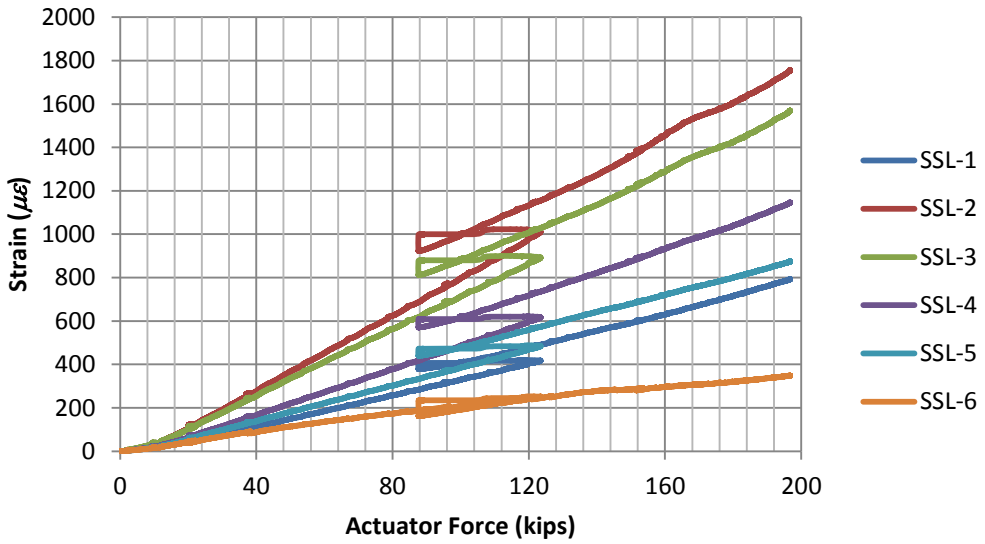

Figure 7.8 Day 2 SMC Reinforcing Strains vs. Actuator Force

In order to account for this effect, the total number of reinforcing bars must be known. The area of reinforcing required based on Equation 8 ($A_r = A_f = b_f t_f$) is 12.3 in^2 for the W33x152 girder, which has an 11.6-in. wide x 1.06-in. deep flange. Using #8 reinforcing bars, which have an area of 0.79 in^2, the total number of bars in the effective flange width must be $12.3/0.79 = 15.6 \approx 16$ bars , which would be spaced at $88/16 = 5.5 \approx 6.0$ inches; coincidentally, this matches the actual test model reinforcing. The tension in each bar adjacent to the girder would be $0.09 \times 2020 \times {}^{12}\!/_{40.35} = 54$ kips (9% of the total tension each). The ultimate capacity of a #8 bar is $\phi F_y A_s = 0.9 \times 60 \times 0.79 = 42.7$ kips, which is less than 54 kips.

A likely reason that the test bridge reinforcing did not yield at the final load, which in effect applied a moment of 2,400 k-ft, was due to #5 temperature bars being adjacent to the #8 SMC bars. There is no reason that these bars may not be considered to act in unison with the SMC reinforcing bars as the SMC reinforcing will aid in reducing shrinkage and the temperature bars will aid in resisting the SMC tension. So considering the adjacent temperature bars, the ultimate capacity of the pair is 66 kips, which when factored is 59.4 kips and is greater than 54 kips.

In order to provide assurance that the reliance on #5 temperature bars to help carry the SMC moment near the girder is reasonable for the full range of girders evaluated, all of the acceptable girders were examined. Checking the combined capacity of the bar adjacent to the girder combined with a #5 temperature bar to 9% of the total SMC tension resulted in a relationship where the size of the main SMC

bar required is a function of the ratio of the area of the girder to the area of the bottom flange. The ratio requirements are presented in Table 7.2. While the table is a reasonable guide, a simple check of the bar capacity is also a very quick and simple calculation.

Table 7.2 Minimum SMC Bar Size based on Girder Area/Flange Area

Minimum SMC Bar Size	**Range of ratios of Girder Area to Flange Area**
#8	$A/A_f>3.5$
#9	$3.5>A/A_f>3.3$
#10	$3.3>A/A_f>3.1$

7.4 Cost Analysis

As a final investigation of the design practicality of using the steel diaphragm SMC connection, the cost of the steel diaphragm-SMC bridge design is compared to a fully continuous bridge and to a concrete diaphragm SMC bridge. Upon first glance, it appears that SMC bridges will be more economical than standard fully continuous bridges; however, other considerations, such as the additional cost of SMC reinforcing, load transfer details, etc., must also be included in the cost analysis. The cost and man-hour comparisons presented herein used data from RS Means, *Open Shop Building Construction Cost Data* (Waier, 2003). This particular edition was selected for ease of cost comparisons with other SMC bridge schemes with documented cost information (i.e., concrete diaphragm designs).

A cost comparison of the SMC scheme proposed herein with the most recent SMC scheme proposed by UN/L and used by NDOR (Azizinamini A., 2014) is presented in Table 7.3. As may be seen, the steel diaphragm results in a cost savings of 8% for the construction of the diaphragms. The spacing between girders on the two bridges differs, but the estimate is performed based on a unit length of diaphragm basis for comparison. The numbers for the concrete bridge considered are the same depth girder as were used in the steel diaphragm bridge, a W33x152.

Table 7.3 Cost Comparison - Concrete vs. Steel Diaphragm

Bridge	Concrete Diaphragm			Steel Diaphragm		
Element	Quantity	Unit Cost	Total Cost	Quantity	Unit Cost	Total Cost
Formwork	57 SFCA	$6.35	$362			
Epoxy Coated Reinforcing Steel	0.08 ton	$2545	$190			
Cast-in-place Concrete	2.85 CY	$85	$242			
Sheet Steel Plate	1.50 cwt	$41.50	$62			
W27x84 Girder				7.33 ft.	$72/ft.	$528
Wedge Plates				31 lb	$72/cwt	$22
Sole Plate Weld				1.33 LF	$12.75/LF	$17
Total			$856			$567
Diaphragm Length	10.33 ft.			7.33 ft.		
Cost/Foot	$83			$77		

A comparison of construction man-hours of the diaphragms is presented in Table 7.4. The proposed scheme requires about 14% of the construction man-hours of the concrete diaphragm scheme used in Nebraska; this means considerably less construction time to erect the steel bridge girders with the

proposed scheme. Considering a burdened man-hour rate of $50/hour, the total cost savings using the proposed SMC concept is nearly 55%/foot. Additionally, NDOR (NDOR, 1996) requires that the concrete diaphragms be cast to only two-thirds of their height and allowed to cure for seven days prior to placing the remainder of the pier and casting the concrete bridge deck. This is a significant detriment to this scheme in that it adds a minimum of seven days to the entire construction schedule. There is no delay required in the proposed steel diaphragm scheme, nor is there such a constraint for conventional fully continuous bridges.

Table 7.4 Construction Man-hour Comparison

Bridge	Concrete Diaphragm			Steel Diaphragm		
Element	Quantity	Man-Hours	Total Hours	Quantity	Man-Hours	Total Hours
Formwork	57 SFCA	0.163/SFCA	9.29			
Reinforcing Steel Placement	0.08 ton	16/ton	1.28			
Cast-in-place Concrete	2.85 CY	1.067/CY	3.044			
Sheet Steel Plate	1	2	2			
W27x84 Girder				7.33 ft.	0.06/ft.	0.5
Install Wedge Plates				2 each	0.25/each	0.5
Weld Wedge Plates				1.33/LF	0.211/LF	0.3
Total			15.6			1.3
Diaphragm Length	10.33 ft.			7.33 ft.		
Hours/Foot	1.5			0.2		

Comparison of cost of the proposed SMC scheme to a fully continuous girder bridge of the same geometry is presented in Table 7.5. Here the savings for the SMC bridge are substantial at 25% less than a fully continuous girder bridge, and this does not include the effects of the shortened construction time, which has positive economic effects to the motorists who must tolerate construction delays.

Table 7.5 Girder Cost Comparison Fully Continuous Bridge to SMC Bridge

Element	Fully Continuous	Steel Diaphragm Simple-Made-Continuous
Steel Unit Cost	$2,500/ton	$2,500/ton
Girder cost	$19,360 each	$14,790
Splice cost (2 every other span)	$4,000 (Azizinamini, 2014)	$0
Epoxy Coated Reinforcing Steel Unit Cost	$1,685/ton	$1,685/ton
SMC Reinforcing cost	N/A	$2,580
Total Cost	$23,360	$17,370
Cost Difference (percent)	25%	

8. RESULTS OF NATIONAL SURVEY

At the request of CDOT, a survey was prepared to investigate how other states are using simple-made-continuous construction. The survey questions were developed by Dr. John van de Lindt and reviewed by the study panel in the early stages of this project before the project was transferred to Drs. Atadero and Chen. The survey was administered using the survey tool available in Google Apps. A list of email addresses for state bridge engineers was obtained from the Subcommittee on Bridges and Structures, which is within the American Association of State Highway and Transportation Officials Standing Committee on Highways. The survey questions were first sent on September 23, 2010. A follow-up email was sent to the same address, or a different address if the state had multiple contacts, on October 22, 2010. The survey responses are summarized below.

Question 1: Approximately what percentage of bridges in service in your state is steel?

Sixteen of the twenty-four states that responded (67%) have fewer than 50% steel bridges in service. Below is the distribution of the responses from the states. The minimum reported is 12% and the maximum is 76%.

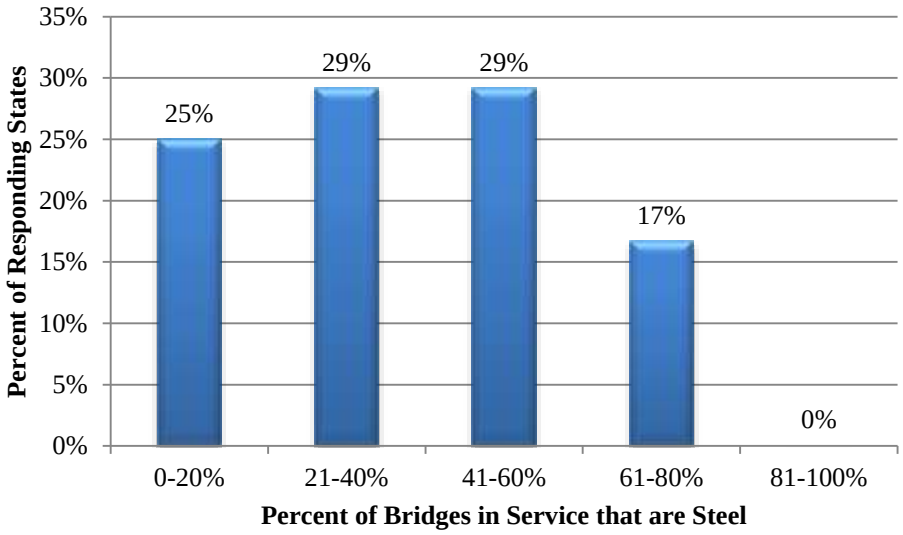

Figure 8.1 Percent of Bridges in Service in Responding States that are Steel

Question 2: Approximately what percentage of bridges designed in your state in the last 10 years is steel?

Over the past 10 years, 63% of states have designed 25% or less of their bridges as steel bridges and 80% of states have designed less than 50% of their bridges as steel bridges. There is a wide range of values from 4% to 90%. The distribution is provided in the figure below.

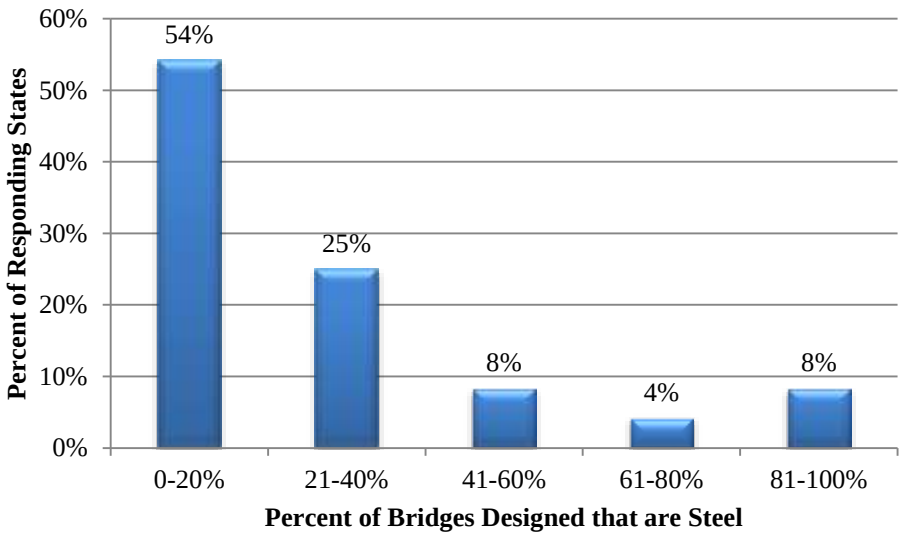

Figure 8.2 Percent of Bridges Designed in Responding States over the Last 10 Years that Are Steel

Question 3: Has your state built any Simple-Made-Continuous (SMC) for live loads bridges?

Twelve of 24 states that responded (50%) have not designed any SMC for live load bridges while 12 (50%) have. Two of the states that said they have not built SMC for live load bridges indicated that they have constructed concrete bridges that are SMC bridges.

Question 4: If you have designed any simple-made-continuous bridges, what is your procedure?

Seven of the 12 states that have made SMC bridges used structural analysis using in-house tools such as a spreadsheet or self-developed software. Two of the states had consultants design the bridges using finite element analysis or their own in-house tools. For the remaining three states that have built SMC bridges, one used university research, one used empirical design with link slabs, and the other was unsure of the procedure used as the SMC bridges were constructed from the late 1950s to the early 1960s.

Question 5: In your professional opinion, which of the following technologies does the AASHTO steel bridge design guide cover?

Twenty-three of the states that responded thought AASHTO covers High Performance Steel and Hybrid Girders well while the other three options, Exterior Post Tensioning (three states), Double Composite Beams (eight states), and FRP Reinforcement and/or Strengthening (one state), were not covered as well by AASHTO.

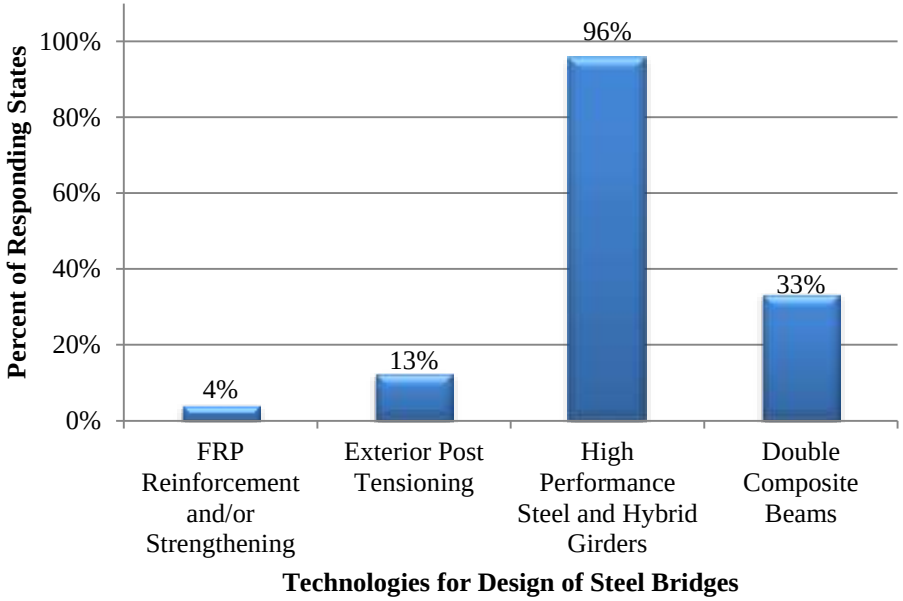

Figure 8.3 Percent of Respondents Indicating Technologies that are addressed by the AASHTO Steel Design Guide

Question 6: Do you think AASHTO should address the simple-made-continuous splice issue, including things like shear lag, beam end rotation, and web crippling?

Sixteen of the 24 states (67%) believe AASHTO should address SMC splice issues while the other eight states did not think this was necessary.

Question 7: Do you feel you have the numerical tools, e.g., finite element analysis or design tools, to design based on your ideas?

Seventeen of the 24 states (71%) felt they have the numerical tools to design while the other seven states felt they did not.

Question 8: Do you have the analysis and design tools to do any of the following?

These results followed a similar trend as Question 5. Twenty-one of the states believe they have the numerical tools to design High Performance Steel and Hybrid Girders while fewer states have numerical tools to design using the other three methods. Two states believed they did not have numerical tools for any of the design methods.

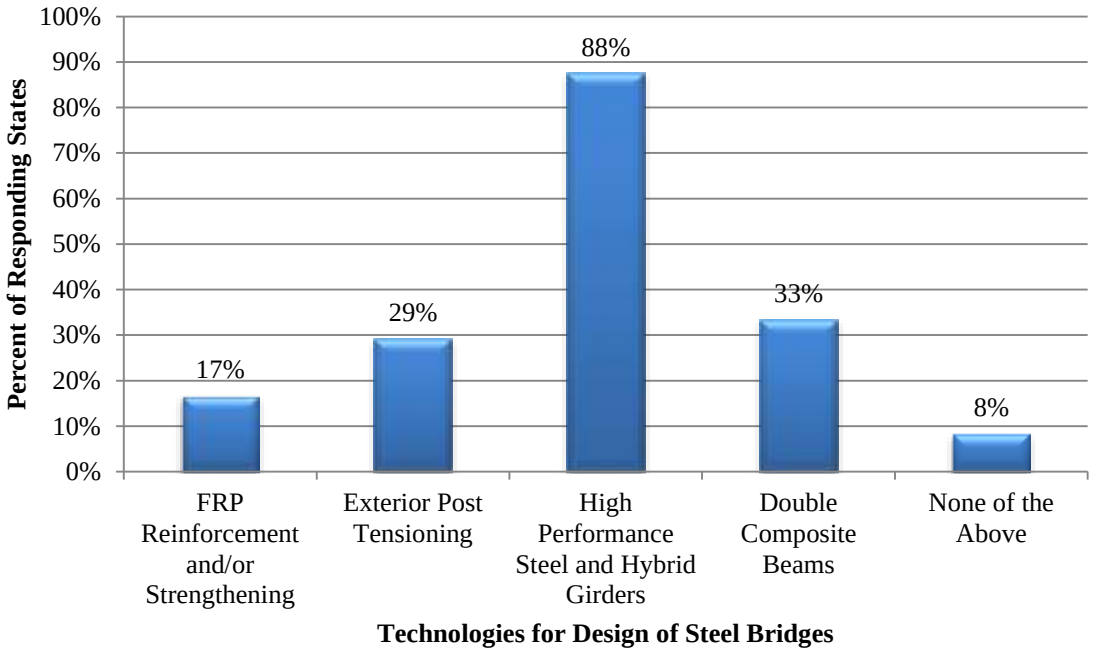

Figure 8.4 Percent of Respondents who had Analysis and Design Tools for Various Steel Bridge Technologies

Question 9: Which of the following techniques do you feel is most developed in engineering practice?

The vast majority (19) of the states selected High Performance Steel and Hybrid Girders as the most developed engineering practice while the other three techniques were only selected by five states. Three states selected double composite beams, one selected FRP Reinforcement and/or strengthening, and one selected Exterior Post Tensioning as the most developed technique in engineering practice.

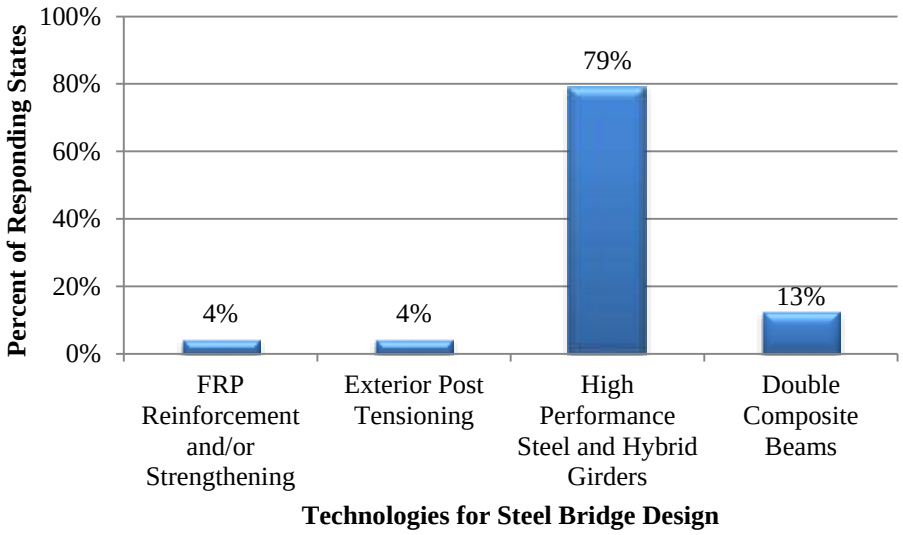

Figure 8.5 Percent of Respondents Indicating Technologies with the Best Developed Design Practice

Question 10: Do you plan to try a SMC design in your state in the next ____ years?

Nineteen of the states that responded (79%) do not plan to design a SMC in the next five years while four states (17%) plan to design an SMC within the next year. The distribution of responses is shown in the figure below.

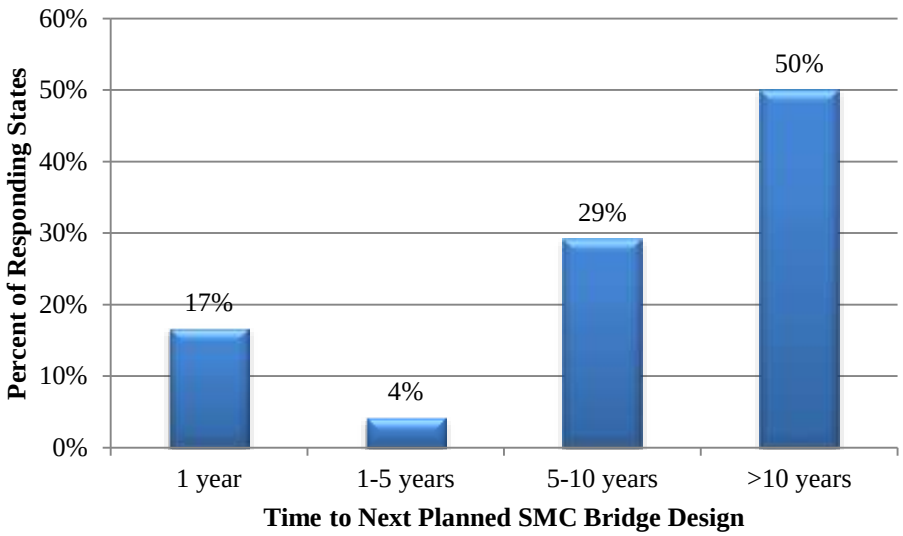

Figure 8.6 Next Planned SMC Design in Responding States

9. CONCLUSION

9.1 Summary and Recommendations

In general, SMC bridges are more economical and safer to construct than fully continuous bridges. Additionally, SMC bridges do not require closure of the bridged roadway for erection of the hung spans nor for connection of the bolted girder continuity splices, which are required for fully continuous bridges. While not a fair comparison, but for completeness, SMC bridges are not only significantly more economical than simple span multi-span bridges, but they don't have the additional maintenance issue of expansion joints at every support. As a matter of fact, very recently an existing simple span bridge was converted to an SMC bridge by replacing the decks and installing SMC reinforcing and compression transfer mechanisms as retrofits (Griffith, 2014).

The original connection selected for study was found to have several weaknesses based upon hand analysis of the connection elements, which were subsequently substantiated by physical testing. Based on these findings, recommendations were made to CDOT to perform corrective actions to the bridge; these actions are described at the end of this section in the implementation section.

The study connection evaluated, developed, and modified herein is unique in that the SMC connection is not embedded in a concrete diaphragm as with other SMC bridges. The study connection is also considerably faster to construct and more economical than other SMC schemes since there is no need to wait for concrete diaphragms to cure and attain strength. The following is a summary of benefits of the proposed connection:

1. More economical than fully continuous bridges and other SMC schemes
2. By being exposed, the girder is allowed to properly weather and thereby develop its protective patina
3. The girder ends and the compression transfer plates are visible for periodic inspection; this is not possible with girders cast into concrete diaphragms
4. No concerns about cracking of a concrete diaphragm at re-entrant corners around the girders
5. A significant savings in construction time (seven days minimum) over concrete diaphragms since there is no need to wait for concrete diaphragms to partially cure

Future designs using the methodology developed by this report can benefit from these advantages.

9.2 Areas for Further Study

The following items are recommendations for future research into SMC schemes for bridges:

1. It is a well-known fact that continuous girders with increased stiffness at the supports attract more negative moment; the reverse should also be true for bridges with decreased stiffness at the supports. Thus, an investigation into the significance of this behavior in the actual continuous beam analysis would be prudent. It should also be investigated whether this behavior is significant enough to be included in analysis of SMC type structures.

2. A value of 9% of the total SMC tension was found to be taken by the SMC reinforcing bars adjacent to the composite girder. Additional research and physical testing is recommended to refine the determination of this value based on the possible variables involved: SMC reinforcing location relative to the girder bottom flange, SMC reinforcing spacing and size, etc.

9.3 Implementation Plan for CDOT

The findings of the connection evaluation described in this report indicate two key implementation steps for CDOT:

1. Inspect and retrofit the existing SMC connections on the S.H. 36 bridge over Box Elder Creek, including:
    a. Inspection of all of the girder bearings specifically looking for those that appear to have failed welds or other signs of distress
    b. Address the connections that appeared distressed immediately by:
        - Measuring the distance between the girder flanges and relative locations of existing bolt holes in relation to the flanges
        - Fabricating and installing safety plates similar to that presented in Figure 2..
        - Carefully grind off failed and partially failed welds that remained.
    c. Address the remaining visually non-distressed connections in accordance with item 2 above.

2. Make use of a modified design procedure for future SMC connection designs.
   This study demonstrated that the use of the SMC connection with steel diaphragms shows promise for construction of steel girder bridges using simple-made-continuous techniques. Chapter 7 of this report provides a detailed approach for connection design that incorporates the findings of this research. Future SMC connections should be designed based on this design procedure in order to avoid the issues present in the existing connections on the Box Elder Creek Bridge.

3. An analysis of the bridge girders as simple spans was performed in the event that more than one connection on a particular span failed and changed the span's behavior from continuous to simple. The composite girder in this condition was found to be adequate for strength requirements, however, it was also found to be significantly deficient in stiffness to meet the AASHTO serviceability (deflection) requirements.

4. The bridge was also analyzed for the CDOT permit truck. Using a full moving load analysis, a maximum negative moment of 2060 kip-ft. was found at the first interior support. Based on the element capacities described in Table 6, if the connection is retrofitted with a load transfer plate between the bottom flanges as described in this report (removing the critical welds and sole plate from the load transfer path), the bridge should be adequate for the permit load.

9.4 Training Plan for Professionals

Section 8 of this report discusses a proposed design process for the future design of SMC connections for steel girder bridges with steel diaphragms. The calculations required in the design process are fairly routine, and it is anticipated that bridge design engineers will be able to design future connections based on the written procedure in Section 8. We do not anticipate a need for significant training, but the study team is very willing to make presentations to interested members of Staff Bridge on the results of this research study and the proposed design process.

REFERENCES

AASHTO. (2012). *AASHTO LRFD BRIDGE DESIGN SPECIFICATIONS.* Washington, DC: American Association of State Highway and Transportation Officials.

AISC. (2011). *Steel Construction Manual.* Chicago: American Institute of Steel Construction.

Azizimanini, A. &. (2004, November 8). "Bridges Made Easy." *Roads & Bridges.*

Azizinamini, A. (2005). *Development of a Steel Bridge System-Simple for Dead Load and Continuous for Live Load, Volumes 1 and 2.* Lincoln: University of Nebraska.

Azizinamini, A. (2014). "Simple for Dead Load - Continuous for Live Load Steel Bridge Systems." *Engineering Journal - American Institute of Steel Construction*, 59-82.

Barber, T. L. (2006, December). "Simple-Made-Continuous Bridges Cuts Costs." *Modern Steel Construction*.

Barker, R. M. (2007). *Design of Highway Bridges: An LRFD Approach.* Hoboken: John Wiley & Sons, Inc.

Barros, M. H. (2002). Elastic degradation and damage in concrete following nonlinear equations and loading function. *Proceedings of the Sixth Conference on Computational Structures Technology* (pp. 255-256). Edinburgh, UK: ICCST.

Carreira, D. J. (1985). "STRESS-STRAIN RELATIONSHIP FOR PLAIN CONCRETE IN COMPRESSION." *Journal of the American Concrete Institute*, 797-804.

CDOT. (2012, July 24). Bridge Design Manual. *CDOT Staff Bridge - Bridge Design Manual*. Denver, CO, USA: CDOT.

Chapman, D. H. (2008). "EVALUATION OF THE DUPONT ACCESS BRIDGE." *Experimental Techniques*, 31-34.

Farimani, M. (2006). "RESISTANCE MECHANISM OF SIMPLE-MADE-CONTINUOUS CONNECTIONS IN STEEL GIRDER BRIDGES." Lincoln: University of Nebraska/Lincoln.

Farimani, R. S. (2014). "Numerical Analysis and Design Provision Development for the Simple for Dead Load - Continuous for Live Load Steel Bridge System." *Engineering Journal - American Institute of Steel Construction*, 109-126.

FHWA. (2005 through 2012). *Annual Materials Report on New BRidge Construction and Bridge Rehabilitation.* Washington, DC: Federal Highway Administration.

Gopalaratnam, V. S. (1985). "Softening Response of Plain Concrete in Direct Tension." *ACI Journal*, 310-323.

Griffith, D. J. (2014). "Existing Simple Steel Spans Made Continuous: A Retrofit Scheme for the I-476 Bridge over the Schuykill River." *Engineering Journal - American Institute of Steel Construction*, 199-208.

Grook. (2010, July 30). *Steel Reinforcement*. Retrieved July 8, 2013, from Grook.net: http://www.grook.net/forum/civil-engineering/construction/steel-reinforcing

ICC. (2012). *ICC0ES Evaluation Report ESR-2856.* Whitier, CA: ICC Evaluation Service.

Javidi, J. A. (2014). "Experimental Investigation, Application and Monitoring of a Simple for Dead Load - Continuous for Live Load Connection for Accelerated Modeular Steel Bridge Construction." *Engineering Journal - American Institute of Steel Construction*, 177 - 198.

Karsan, I. D. (1969). "Behavior of Concrete Under Compressive Loadings." *Journal of the Structural Division, ASCE*, 2543-2563.

Lampe, N. J. (2001). *STEEL GIRDER BRIDGES ENHANCING THE ECONOMY - A THESIS.* Lincoln: University of Nebraska/Lincoln.

Lampe, N. M. (2014). "Development and Experimental Testing of Connections for the Simple for Dead Load - Continuous for Live Load Steel Bridge System." *Engineering Journal - American Institute of Steel Construction*, 83-108.

Lin, M. (2004). *VERIFICATION OF AASHT0-LRFD SPECIFICATIONS LIVE LOAD DISTRIBUTION FACTOR FORMULAS FOR HPS BRIDGES.* Cincinnati: University of Cincinnati.

Lu, Z. H. (2010). "Empirical Stress-Strain Model for Unconfined High-Strength Concrete under Uniaxial Compression." *Journal of Materials in Civil Engineering, ASCE*, 1181-1186.

Lubliner, J. J. (1989). "A PLASTIC-DAMAGE MODEL FOR CONCRETE." *International Journal of Solids and Structures*, 229-326.

Malm, R. (2009). *Predicting shear type crack initiation and growth in concrete with non-linear finite element Method.* Stockholm: Royal Institute of Technology (KTH).

Nakamura, S. Y. (2002). "New technologies of steel/concrete composite bridges." *Journal of Constructional Steel Research*, 99-130.

NDOR. (1996). *Nebraska Bridge Office Policies and Procedures Manual (BOPP).* Omaha: Nebraska Department of Roads.

Nelson. (2011). *2011 Nelson Stud Welding Stud and Ferrule Catalog*. Elyria, Ohio, USA: Nelson Stud Welding, Inc.

Niroumand, S. J. (2009). *RESISTANCE MECHANISM OF SIMPLE-MADE-CONTINUOUS CONNECTIONS IN SKEW AND NON-SKEW STEEL GIRDER BRIDGES USING CONVETIONAL AND ACCELERATED TYPES OF CONSTRUCTION.* Lincoln: University of Nebraska/Lincoln.

NSBA. (2006, September). "Steel Bridge Uses Simple-Span-Made-Continuous Construction." *Modern Steel Construction*.

Ricles, J. M.-W. (2000). *Development and Evaluation of Improved Details for Ductile Welded Unreinforced Connections - Report No. SAC/BD-00/24.* Los Angeles: SAC Joint Venture.

Salmon, C. (2009). *STEEL STRUCTURES Design and Behavior Emphasizing Load and Resistance Factor Design.* Upper Saddle River, NJ: Pearson Prentice-Hall.

Simula. (2011). *ABAQUS Analysis User's Manual (6.11).* Providence, RI: Simula.

Solis, A. J. (2007). *Field Evaluation of a SDL-CLL Steel Bridge in New Mexico*. Las Cruces, New Mexico: New Mexico State University.

Solis, A. V. (2007). *Field Evaluation of a SDL-CLL Steel Bridge in New Mexico.* Las Cruces: New Mexico State University.

Talbot, J. (2005, October). "Simple Made Continuous." *NSBA Steel Bridge News*, pp. 1-5.

Waier, P. R. (2003). *Open Shop Building Construction Cost Data.* Kingston, Mass: R S Means.

Yakel, A. A. (2014). "Field Application Case Studies and Long-Term Monitoring of Bridges Utilizing the Simple for Dead - Continuous for Live Bridge System." *Engineering Journal - American Institute of Steel Construction*, 155 -176.

APPENDIX A. CURRENT SMC BRIDGES

At the time of this writing, at least 10 SMC bridges were found to have been constructed and put into service. Details of these bridges and their SMC connection behavior follow.

State Highway No. 16 over US 85, Fountain, Colorado – February, 2004

Bridge Element/Dimension	Value
Drive Lanes	2
Spans	4
Span Lengths	107'-0", 128'-2",128'-2" and 57'-5"
Girder Spacing	7'-4"
Girder Size/Material	Plate Girder: Top Flange 3/4"x16", Web 1/2"x48", Bottom Flange Ends 3/4"x16", Centers 1 1/8"x16" AASHTO M270 Grade 50
Slab Thickness/Material	9" / f'_c = 4500 psi
Slab Haunch Depth (0 means none)	Min. 1 7/8", Max. 5 3/8"
Wearing Course?/Thickness/Density	None
Comments	

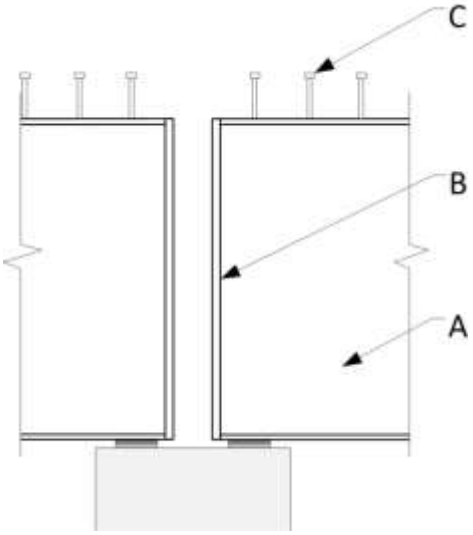

Figure A.1

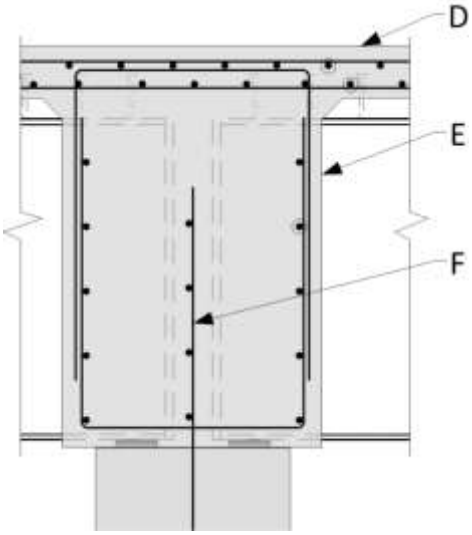

Figure A.2

SMC detail Figure A.1 and Figure A.2:

A = Steel Plate Girder
B = Compression Pl 1 1/4"
C = (3) 7/8" diameter x 7" long headed studs
D = 9" concrete slab reinforced with #6 bars at 8" O.C. top
E = Concrete diaphragm reinforced with #5 longitudinal bars at 10" each side an #5 "U" ties top and bottom at 12" O.C.
F = #9 vertical dowels at 6" O.C. and #5 horizontal bars at 12" O.C.

Notes:
This bridge has more than two spans, thus having the potential of positive moments over one or more of the interior supports.
The beams are placed in pockets in the diaphragms and are not cast into the diaphragms.
The thickness of compression concrete between the end stiffeners of the bridge girders is 6".

State Highway No. 36 over Box Elder Creek, Watkins, Colorado – June, 2005

Bridge Element/Dimension	Value
Drive Lanes	2
Spans	6
Span Lengths	77’-10” Typical
Girder Spacing	7’-4”
Girder Size/Material	W33x152 AASHTO M270 Grade 50W
Slab Thickness/Material	8” / f'_c = 4500 psi
Slab Haunch Depth (0 means none)	3” Minimum
Wearing Course?/Thickness/Density	Asphaltic – 35 psf
Comments	

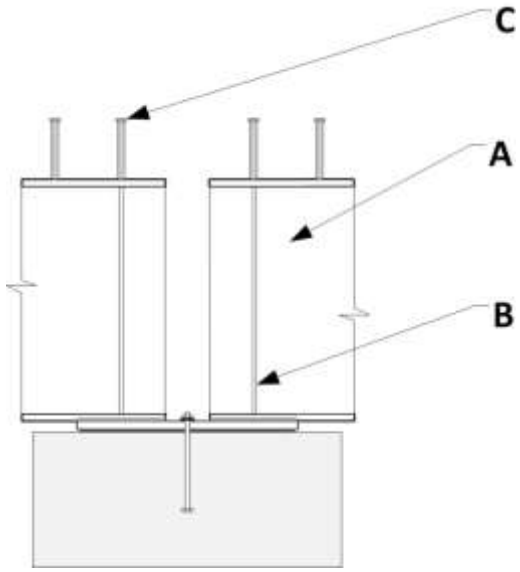

Figure A.3

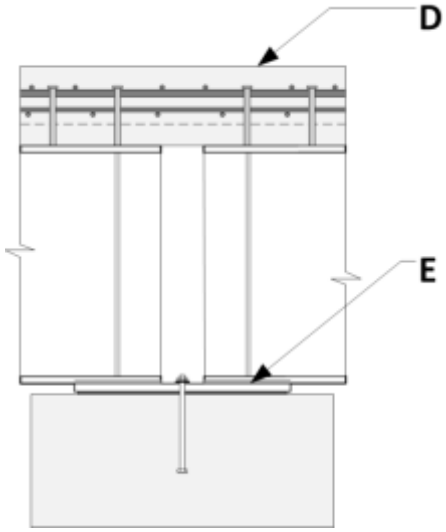

Figure A.4

SMC detail Figure A.3 and Figure A.4:

A = W33x152 girder
B = Plate 1/2" bearing stiffener (diaphragm beam not shown for clarity)
C = (3) 7/8” diameter x 8 3/16” long headed studs
D = 8” concrete slab with #5+#8 bars at 6” O.C. top
E = 5/16” fillet weld x 14” long fillet weld each side of W to1” minimum sole (bearing) plate

Notes:
This bridge has more than two spans, thus having the potential of positive moments over one or more of the interior supports.

This is the only bridge of those reviewed that does not have a concrete diaphragm but rather a steel wide flange diaphragm (not shown), thus leaving the girder ends exposed.

Sprague St. over Interstate 680, Omaha, Nebraska – May, 2003

Bridge Element/Dimension	Value
Drive Lanes	2
Spans	2
Span Lengths	97’-0” Typical
Girder Spacing	10’-4”
Girder Size/Material	W40x249 ASTM A709 Grade 50W
Slab Thickness/Material	8” / f'_c = 4000 psi
Slab Haunch Depth (0 means none)	1”
Wearing Course?/Thickness/Density	None
Comments	

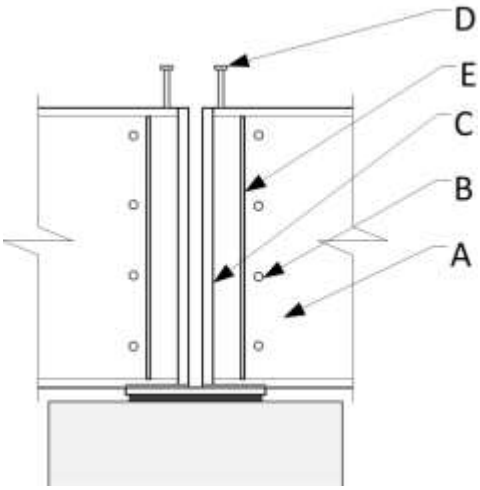

Figure A.5

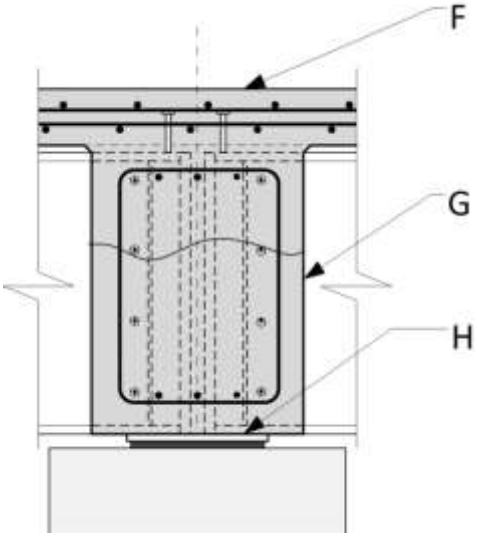

Figure A.6

SMC detail **Error! Reference source not found.** and **Error! Reference source not found.**:

A = W40x249 girder
B = Holes in beam web for longitudinal diaphragm reinforcing bars
C = 1 1/2" x 16” wide compression plate
D = (3) 7/8” diameter x 5” long headed studs
E = Plate 3/8” bearing stiffener
F = 8” concrete slab with #4+#6 bars at 12” O.C. top
G = Reinforced concrete diaphragm; longitudinal side bars are continuous through girder webs
H =5/16” fillet weld x 10” long fillet weld each side of W to1 1/2” sole (bearing) plate

Notes:

This bridge has openings drilled or punched through the girder web at the ends at the abutments in order to make them integral with the abutment concrete. However, there are expansion joints at the abutments which may not perform as anticipated due to the monolithic behavior of the abutment and the girder.

State Highway N-2 over Interstate 80, Hamilton County, Nebraska – November, 2002

SMC detail: Tub (box) girders supported by concrete piers and cast into concrete diaphragms (5000 psi concrete vs. remainder is 4000 psi). The tub girders have a 12'-0" long concrete slab in the bottom for additional compression resistance in the negative moment zone.

Note: While this bridge is unique in that it does not use I-shaped beams, it will not be discussed further since the scope of this work is SMC with I-shaped girders.

US 75 over North Blackbird Creek – Macy, Nebraska – May 2010

Bridge Element/Dimension	Value
Drive Lanes	2
Spans	3
Span Lengths	49'-3", 65'-8", 49'-3"
Girder Spacing	11'-8"
Girder Size/Material	W36x135 Ends, W36x150 Center ASTM A709 Grade 50W
Slab Thickness/Material	8 1/2" / f'_c = 4000 psi
Slab Haunch Depth (0 means none)	1/2" to 13/16"
Wearing Course?/Thickness/Density	None
Comments	

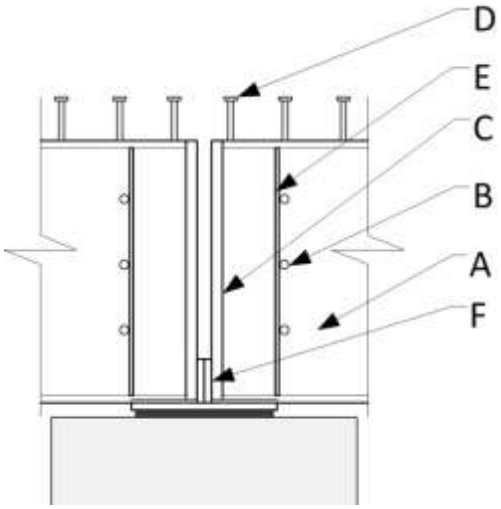

Figure A.7

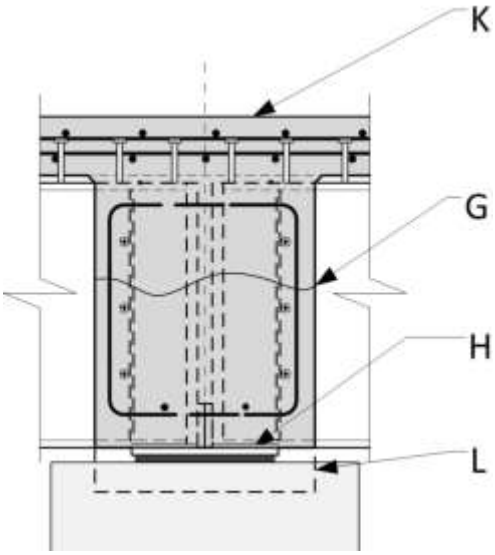

Figure A.8

SMC Detail Figure A.7 and Figure A.8:

A = W36x135 or W36x150 girder
B = Holes in beam web for longitudinal diaphragm reinforcing bars
C = 2" x 12" wide compression plate
D = (3) 7/8" diameter x 5" long headed studs
E = Plate 3/8" bearing stiffener
F = Plate 2"x6"x11.975" beam end plates
G = Reinforced concrete diaphragm; longitudinal side bars are continuous through girder webs
H =5/16" fillet weld x 6" long fillet weld each side of W to1 1/2"x12" wide sole (bearing) plate

K = 8” concrete slab with #8 bars at 12” O.C. top
L = Diaphragm extends down on either side of girder concrete bearing stubs

Notes:
The bottom flange width of both a W36x150 and W36x135 is 12.0”, which is the same as the width of the sole plate, thus, as detailed on the design drawings, the field weld of the Ws to the sole plate would be not be possible to construct.

US 75 over South Blackbird Creek – Macy, Nebraska – May 2010

Bridge Element/Dimension	Value
Drive Lanes	2
Spans	3
Span Lengths	55’-0”, 73’-6”, 55’-0”
Girder Spacing	11’-8”
Girder Size/Material	W36x135 Ends, W36x150 Center ASTM A709 Grade 50W
Slab Thickness/Material	8 1/2” / f'_c = 4000 psi
Slab Haunch Depth (0 means none)	1/2” to 13/16”
Wearing Course?/Thickness/Density	None
Comments	

SMC Detail Figure A.7 and Figure A.8:
This bridge is identical in detailing to the US 75 over North Blackbird Creek bridge with the exception of the girder spans.

New Mexico 187 over Rio Grande River – Arrey/Derry, New Mexico – June, 2004

Bridge Element/Dimension	Value
Drive Lanes	2
Spans	5
Span Lengths	31.75, 32, 32, 32, 31.75 m (104'-2", 105'-0", 105'-0", 105'-0", 104'-2")
Girder Spacing	2.625 m (8'-7")
Girder Size/Material	Plate Girder: Top Flange 22x350 (7/8"x13 3/4"), Web 12x1326(1/2"x52 1/4"), Bottom Flange 22x440(7/8"x17 5/16") AASHTO M270 Fy = 27.6 MPa (50 ksi)
Slab Thickness/Material	0.23 m (9") / f'_c = 27.6 MPa (4000 psi)
Slab Haunch Depth (0 means none)	0.05 m (2")
Wearing Course?/Thickness/Density	None
Comments	Bridge drawings are metric

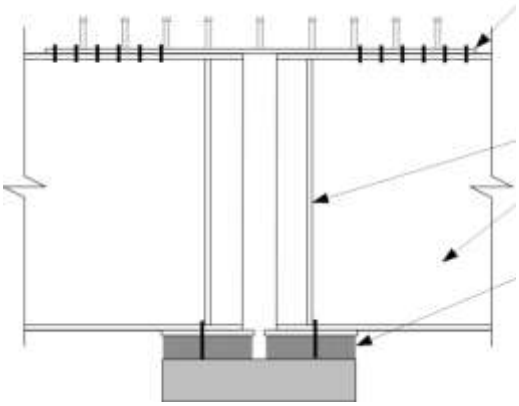

Figure A.9

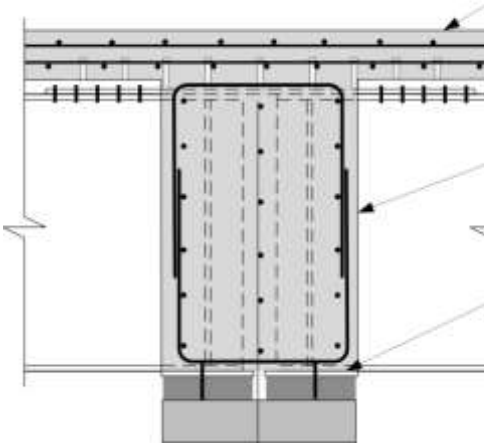

Figure A.10

SMC Detail Figure A.9 and Figure A.10:

A = Plate girder
B = 7/8" Bearing and SMC compression stiffener
C = Elastomeric bearing (no SMC load transfer to pier)
D = Splice plate 7/8" with 9 rows of (3) 7/8" diameter x 5" long headed studs; connected to girder with (8) 7/8" dia. A325-SC bolts each side (see note e)
E = 9" concrete slab with #8 at 6" O.C. top
F = Reinforced concrete diaphragm; center bars are continuous through gap between girders
G = 5/16" fillet weld x 6" long fillet weld each side of plate girder to1 1/2"x13 3/4" wide sole (bearing) plate

Notes:
This is the only set of bridge drawings reviewed that was in metric.
This bridge was discussed in an article in "Steel Bridge News" (Barber, 2006), where the shear connectors were shown as steel channels; whereas the as-built drawings indicate that the shear connectors are headed studs.
For as environmentally friendly as the bridge and all of the surrounding site work was, there is no bike lane on the bridge.
Spans are greater than two, potential for positive moments over supports.
The bolts to connect the splice plate were installed in short slotted holes in the splice plate and standard holes in the top flange of the beam. The nuts were to be "snug" tightened after the concrete was placed, not set. No other notes were provided as further tightening of these nuts to achieve slip critical action. It would seem more appropriate to have put the slots in the girder flange since there is the potential for the bolts to bind in the concrete and move with the slab as it shrinks since they are only snug tight. Also, there is the potential for the bolt heads to crack the slab and slip, thus they could not be tightened.
A possibly better solution would be to have the splice plate with high strength welded threaded studs placed into short slotted holes in the slab.

Ohio S.H. 56 over the Scioto River – Circleville, Ohio – June 2003

Bridge Element/Dimension	Value
Drive Lanes	2 + Pedestrian/Bike
Spans	6
Span Lengths	87.79', 112.58', 112.46', 112.67', 89.87'
Girder Spacing	9'-0"
Girder Size/Material	Girder: Top Flange 7/8"x 18", Web 1/2"x54", Bottom Flange 1 1/2"x18" ASTM A709 Grade 50W
Slab Thickness/Material	8 1/2" / f'_c = 4500 psi
Slab Haunch Depth (0 means none)	1/2" to 13/16"
Wearing Course?/Thickness/Density	1" monolithic concrete (145 psf)
Comments	Galvanized steel stay-in-place slab forms HS-25 and Alt. Military Loading

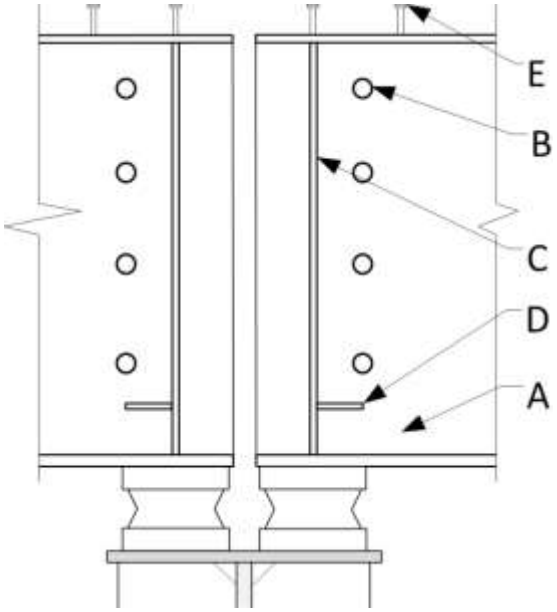

Figure A.11

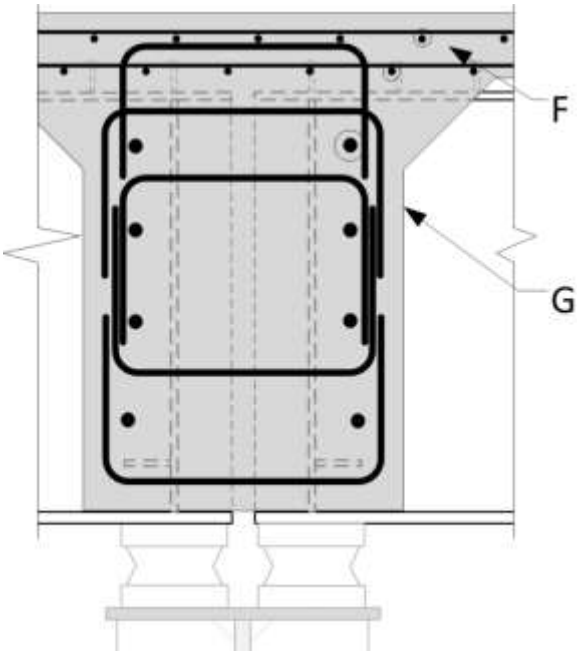

Figure A.12

SMC detail Figure A.11 and Figure A.12:

A = Plate girder
B = Holes in beam web for longitudinal diaphragm reinforcing bars
C = Bearing/SMC compression stiffener plate 7/8"
D = Compression stiffener support stiffener
E = (3) 7/8" diameter x 4" long headed studs
F = 8 1/2" concrete slab reinforced with #8+#4 bars at 9" O.C. top
G = Reinforced concrete diaphragm; longitudinal side bars are continuous through girder webs

Notes:
This bridge is a rebuild and used existing piers and their foundations without modification for loads, although the piers were widened for a wider bridge. Obviously there will be increased loads at the interior supports due to the continuity invoked by the SMC concept.
The bridge has more than two spans, thus having the potential of positive moments over one or more of the interior supports.

Church Ave. over Central Ave., etc., Knox County, Tennessee – January, 2005

Bridge Element/Dimension	Value
Drive Lanes	2 + 1 Pedestrian/Bike + 1 Parking
6	6
Span Lengths	79’-6, 100’-0”, 100’-0”, 100’-0”, 93’-0”, 90’-4”
Girder Spacing	8’-2”
Girder Size/Material	W30x173 ASTM A709 Grade 50W (see notes)
Slab Thickness/Material	8 1/4” / f'_c = 4500 psi (see notes)
Slab Haunch Depth (0 means none)	1 3/4"
Wearing Course?/Thickness/Density	None
Comments	Girder continuity plates connected prior to placement of deck slabs.

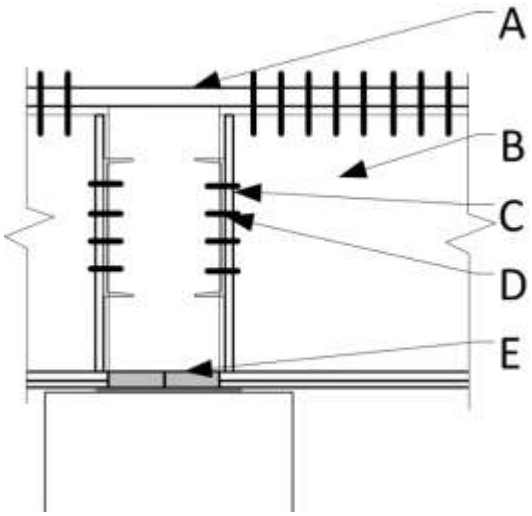

Figure A.13

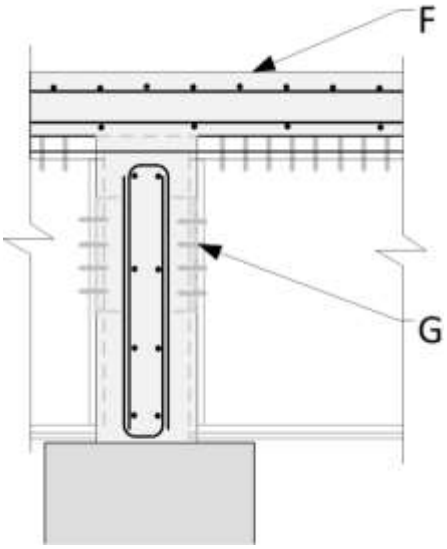

Figure A.14

SMC Detail, Figure A.13 and Figure A.14:

A = Plate girder
B = Bearing stiffener
C = Stabilizer/bracing channel
D = Field welded wedge compression blocks
E = Field bolted splice plate
F = 8 1/4” concrete slab reinforced with #6 bars at 14” O.C. top
G = Reinforced concrete diaphragm

Dupont Access Road over State Route 1, Humphrey's County, Tennessee – 2002

Bridge Element/Dimension	Value
Drive Lanes	2
Spans	2
Span Lengths	87'-0", 76'-0"
Girder Spacing	7'-5"
Girder Size/Material	W33x240 ASTM A709 Gr. 50W
Slab Thickness/Material	8 1/2" / (Material not on drawings provided)
Slab Haunch Depth (0 means none)	4 1/2"
Wearing Course?/Thickness/Density	Wearing course shown on drawings without dimensions or material information.
Comments	Girder continuity plates connected prior to placement of deck slabs.

SMC Detail, Figure A.13 and Figure A.14, except a rolled girder instead of a plate girder.

Massman Drive over Interstate 40, Davidson County, Tennessee – November, 2001

Bridge Element/Dimension	Value
Drive Lanes	2
Spans	2
Span Lengths	138’-6”, 145’-6”
Girder Spacing	9’-9”
Girder Size/Material	Plate Girder: Top Flange 1 1/2"x18” Web 5/8"x60”, Bottom Flange 1 1/2"x18” ASTM A709 Grade 50W
Slab Thickness/Material	8 1/4” / f'_c = 3000 psi (see notes)
Slab Haunch Depth (0 means none)	4 1/2"
Wearing Course?/Thickness/Density	None
Comments	Girder continuity plates connected prior to placement of deck slabs.

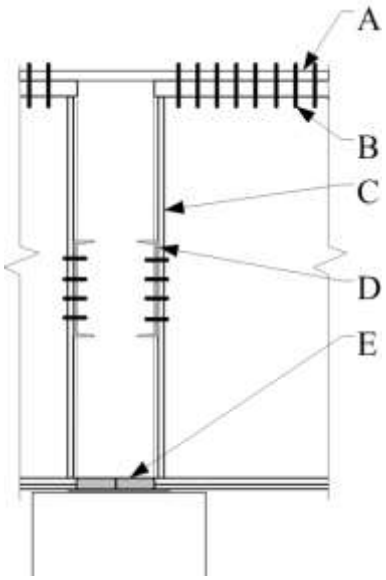

Figure A.15

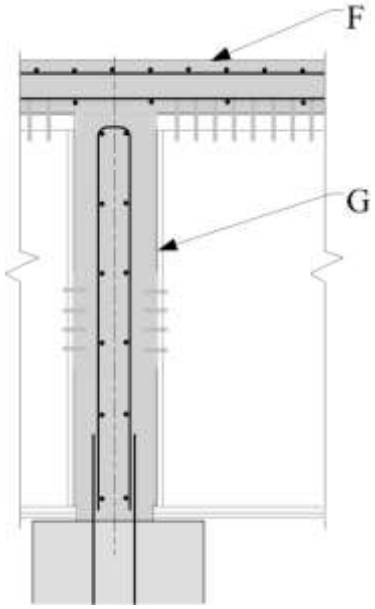

Figure A.16

SMC detail:

A = Plate girder
B = Holes in beam web for longitudinal diaphragm reinforcing bars
C = Bearing/SMC compression stiffener plate 7/8”
D = Compression stiffener support stiffener
E = (3) 7/8” diameter x 4” long headed studs
F = 8 1/2” concrete slab reinforced with #8+#4 bars at 9” O.C. top
G = Reinforced concrete diaphragm; longitudinal side bars are continuous through girder webs

Steel girders with top and bottom splice plates cast into concrete diaphragms over piers. The bottom flanges have welded "wedge" plates between them and the top flanges have bolted top cover plates, additionally, there are full height web stiffeners at the ends of the girders. Girders are plate girders, web = 5/8"x60", top and bottom flanges = 1 ½"x18".
Note: There is an alternative moment splice detail, which shows splice plates on the top and bottom of the top flange; unfortunately, this detail is not constructible since the bottom plate cannot be installed due to the aforementioned web stiffeners. Fortunately, based on review of photos of the bridge it's apparent that the base splice detail was selected. Also, as with the previous Tennessee bridge (Church Ave.), this bridge is simple for only the self-weight of the steel framing.

Notes on bridge information:
Spans are given to centerlines of supports unless noted.

APPENDIX B. HAND CALCULATIONS

The following pages show hand calculations for SMC component behavior for State Highway 36 over Box Elder Creek.

4/13 1/3

Evaluate SH/36 Over Box Elder Creek Connection Behavior

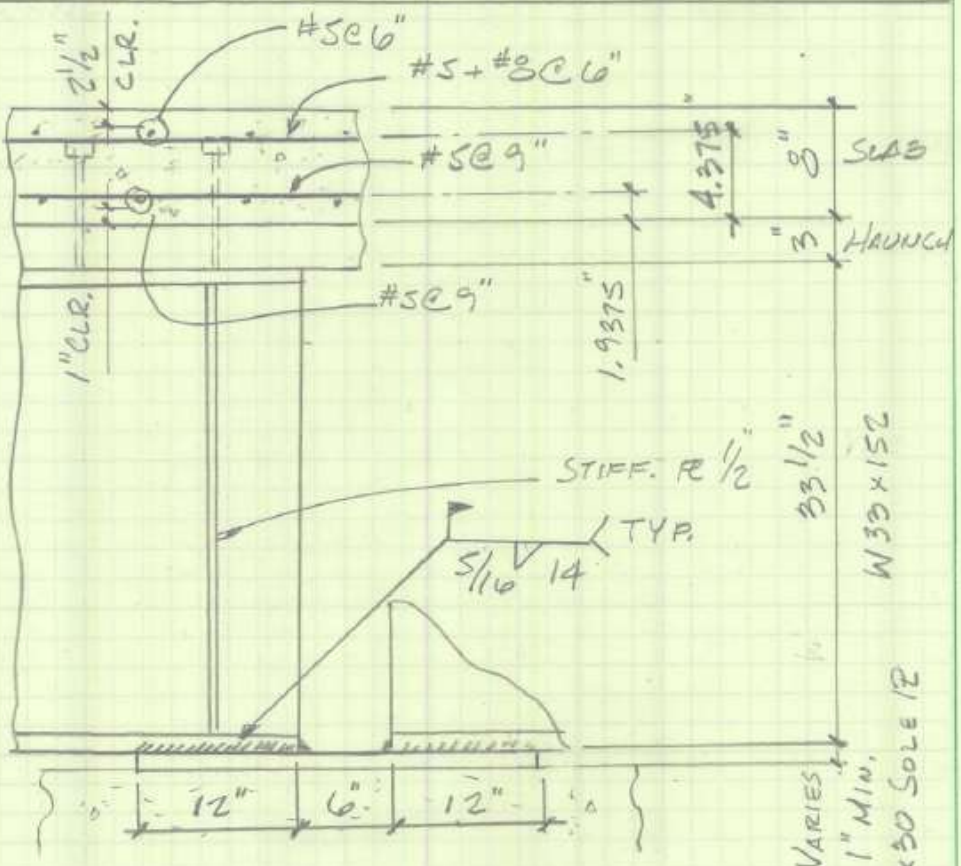

Connection Components / Dimensions

Slab is 7'-4" = 88" wide

Connection Behavior

- Components To Consider

  Sole Plate - Compression
  Welds - Shear
  W33 - Compression & Possible Bending
  #8 + #5 @ 6 - Tension
  #5 @ 9 Bottom - Possible Tension

- **Sole Plate** $A = 1" \times 14" = 14 in^2$ $F_y = 50^{ksi}$ $\phi = 1.0$

  $\phi P_n = 1.0 \times 50^{ksi} \times 14 in^2 = \underline{700^k}$

- **Welds** 5/16 - Eff. Throat $= 0.3125 \times 0.707$
  $= 0.221$ in

  $F_u = 70^{ksi}$ $r_n = 70 \times 0.221 = 15.5^{k/in}$

  $\phi_{long} = 1$ $\phi_{flat} = 0.8$

  $\phi R_n = 2^{welds}\left[12 \times 15.5 \times 1.0^{\phi} + 2 \times 15.5 \times 0.8^{\phi}\right]$

  $= \underline{420.8^k}$

- **W33** Trn Bottom Flg. Only:

  $A_s = 1.060 \times 11.6 = 12.30 in^2$

  $\phi P_n = 12.30 \times 50^{ksi} = \underline{615^k}$

#8 + #5 @ 6" $A_s = 0.79 + 0.31 = 1.10 in^2/6"$

$A_{s\,Total} = 88 \times 1.10/6 = 16.13 in^2$

(88 = Slab Width)

$\phi P_n = 1.0 \times 16.13 \times 70^k = \underline{1129^k}$

- BASED ON PRECEEDING LRFD CAPACITIES, WELDS WILL CONTROL DESIGN:

MOMENT ARM = 33.5 + 3 + 4.375 = 40.88 in
(W33 HAUNCH #8+#5)

ϕM_n = MOMENT ARM × ϕP_n = 40.88 in × 420.8 k / 12 in/ft
= 1433 ft-k

BASED ON ANALYSIS OF WORST CASE LOAD,
M_u = 1782 k-ft > 1433 k-ft
— WELD MAY NOT BE ADEQUATE —
ϕP_n (REQ'D) = 1782 × 12 / 40.88 = 523 k
LESS THAN CAPACITY OF OTHER COMPONENTS ∴ WELD ONLY IS AN ISSUE

APPENDIX C. MODEL CONSTRUCTION DRAWINGS

The following pages present the construction drawings for the full scale model test.

SIMPLE-MADE-CONTINUOUS BRIDGE GIRDER TEST MODEL

STRUCTURAL NOTES:

GENERAL
ALL WORK SHALL BE PERFORMED IN ACCORDANCE WITH ALL APPLICABLE CODES AND STANDARDS, INCLUDING BUT NOT LIMITED TO AASHTO AND OSHA.

CONCRETE
ALL CONCRETE SHALL HAVE A MINIMUM ULTIMATE COMPRESSIVE STRENGTH, f'_c ,OF 4500 PSI AT 28 DAYS.
PROVIDE MIX DESIGN WITH STATISTICAL DATA FOR APPROVAL.
ALL REINFORCING STEEL SHALL BE ASTM A615 GR. 60. PROVIDE MILL CERTIFICATES FOR ALL BARS TO BE PROVIDED.
ALL BARS SHALL BE PROVIDED FULL LENGTH WITHOUT SPLICES.
PROVIDE SHOP DRAWINGS FOR REVIEW AND ACCEPTANCE PRIOR TO FABRICATION OF REINFORCING BARS.

STRUCTURAL STEEL
ALL STRUCTURAL STEEL SHAPES AND PLATES SHALL BE ASTM A992, F_y = 50 ksi. PROVIDE MILL CERTIFICATES FOR ALL STEEL PROVIDED.
ALL STRUCTURAL STEEL RODS SHALL BE ASTM F1554, WITH COMPATIBLE NUTS AND WASHERS AS SHOWN AND REQUIRED.
ALL WELDING SHALL BE PERFORMED IN ACCORDANCE WITH AWS D1.1 USING E70XX ELECTRODES.
HEADED STUDS SHALL BE IN ACCORDANCE WITH ASTM A108.
PROVIDE SHOP DRAWINGS FOR REVIEW AND ACCEPTANCE PRIOR TO FABRICATION OF ALL STRUCTURAL STEEL.

SHORING LUMBER
ALL SHORING LUMBER SHALL BE A MINIMUM OF HEM-FIR NO. 2.

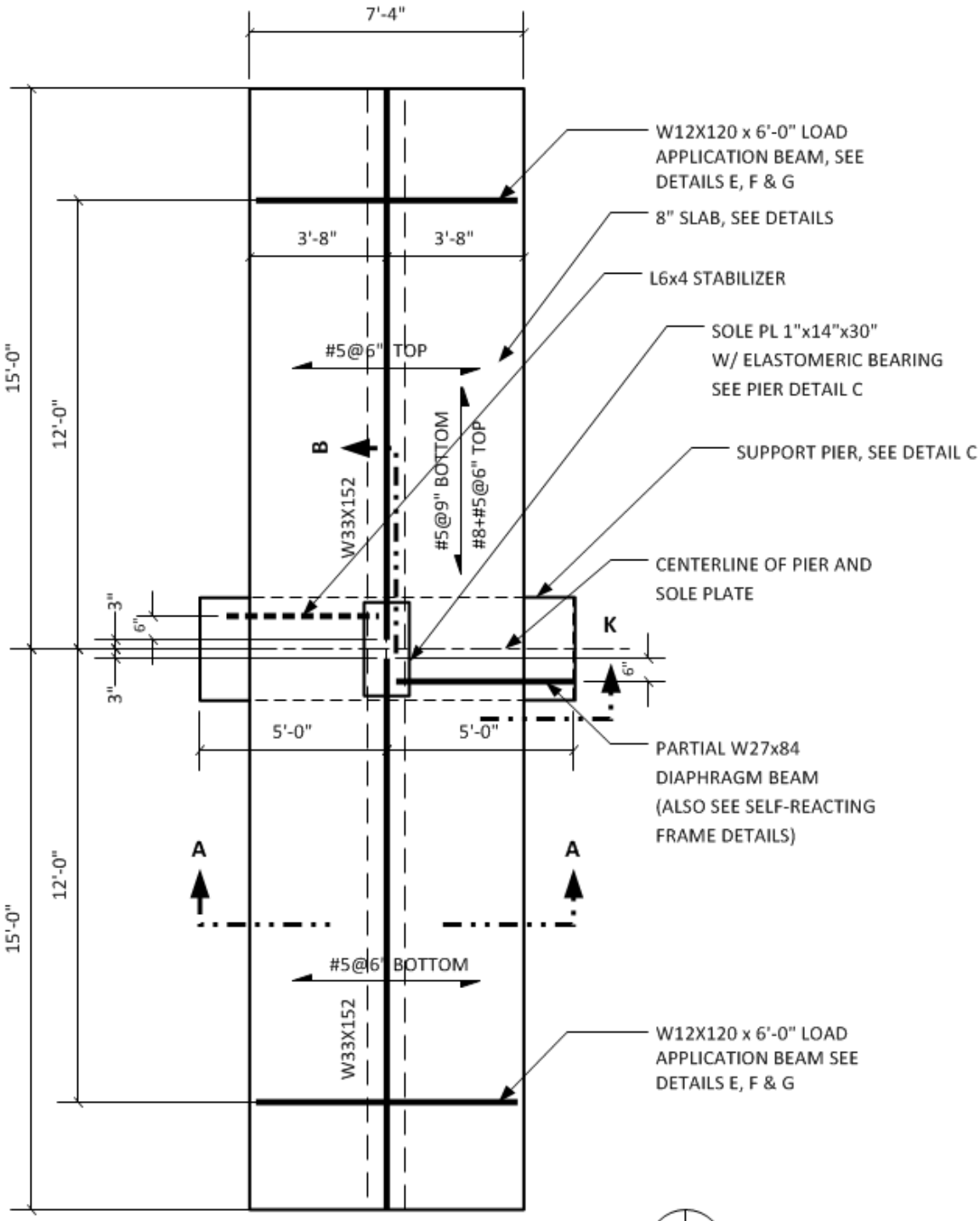

1 FRAMING PLAN

NOTES:

DO NOT INSTALL GIRDER UNTIL CONCRETE PIER HAS ATTAINED DESIGN STRENGTH, 28 DAYS MINIMUM.
SEE SHORING PLAN FOR TEMPORARY SUPPORT DETAILS.

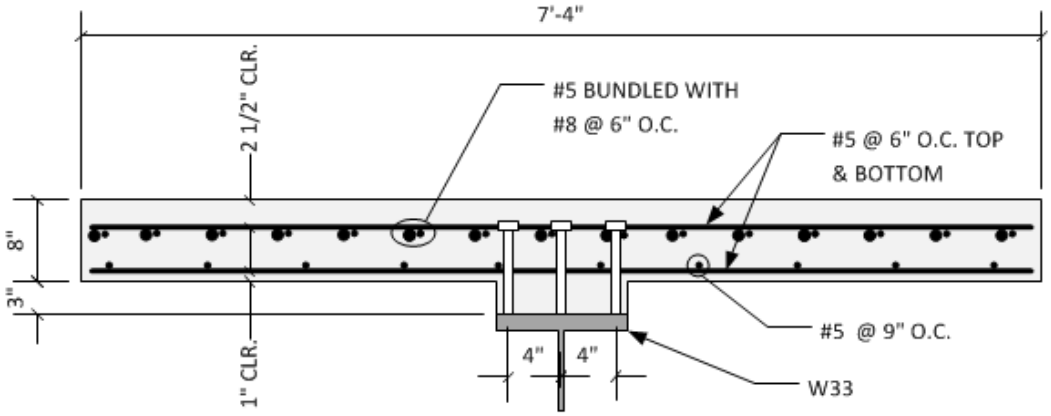

A **SLAB SECTION**

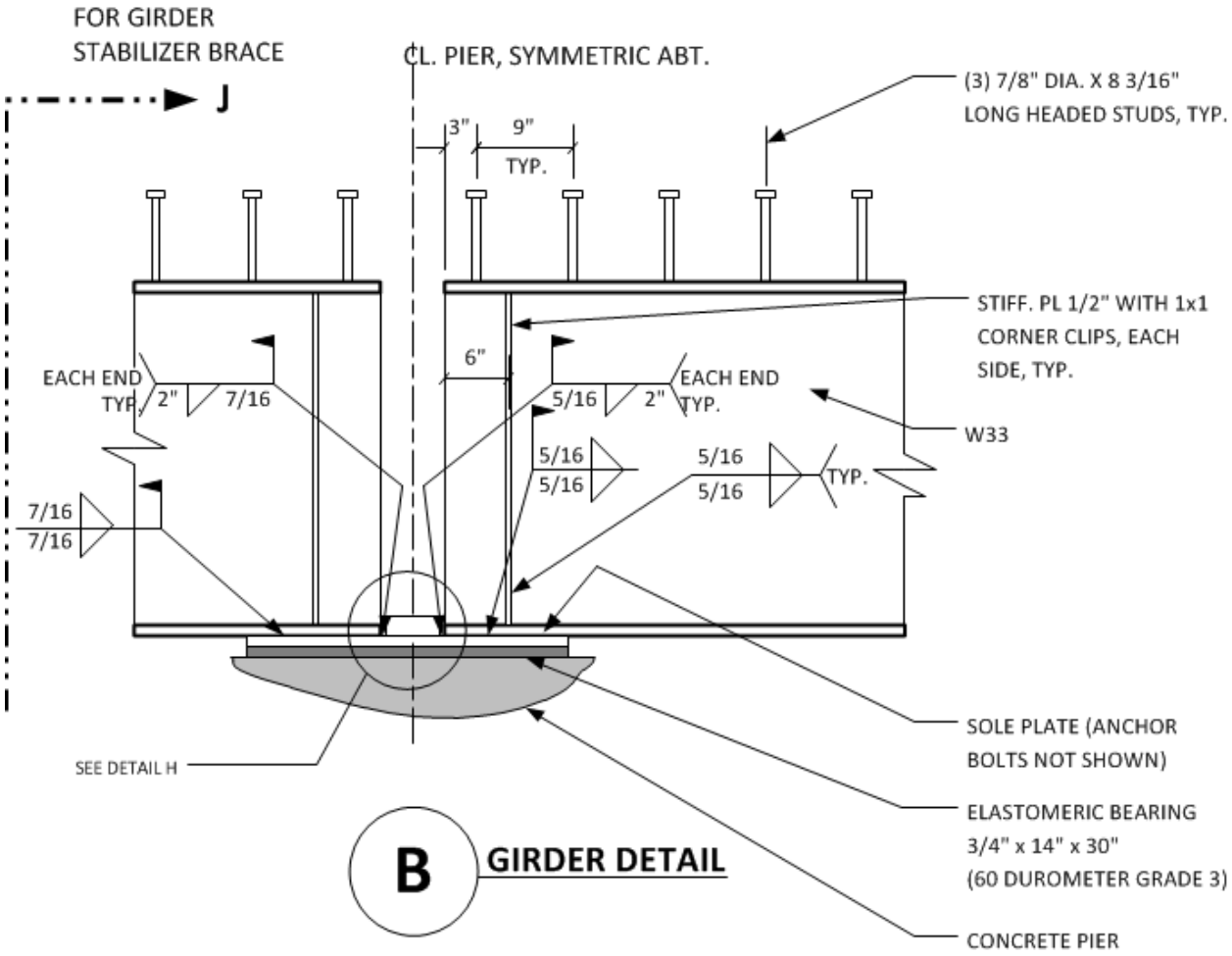

B **GIRDER DETAIL**

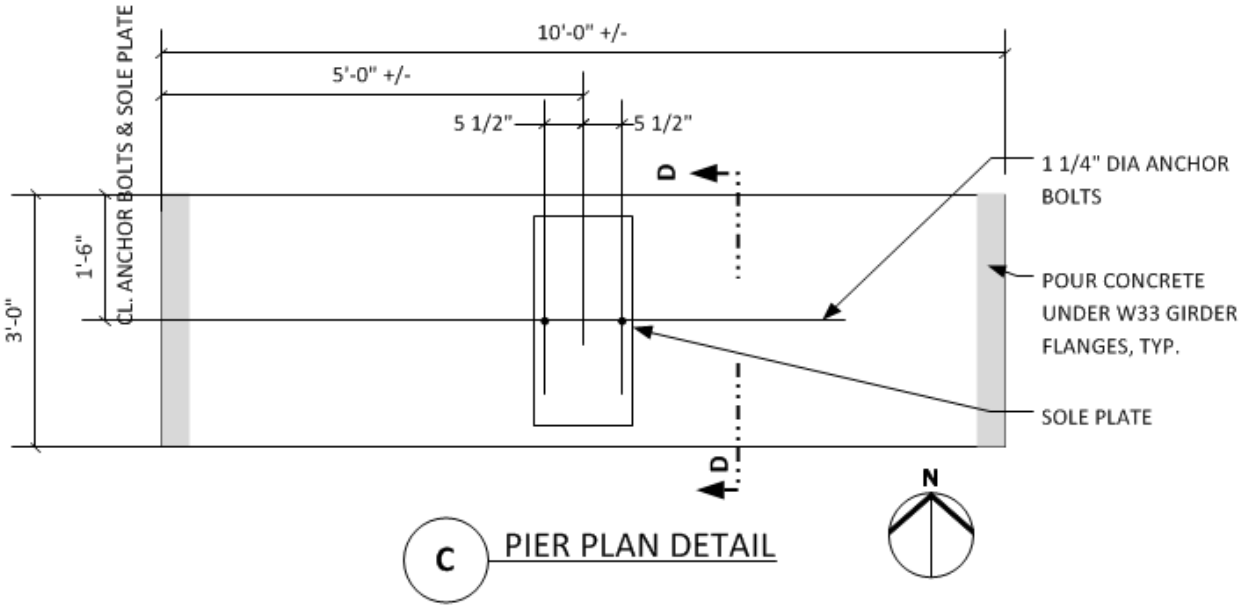

C PIER PLAN DETAIL

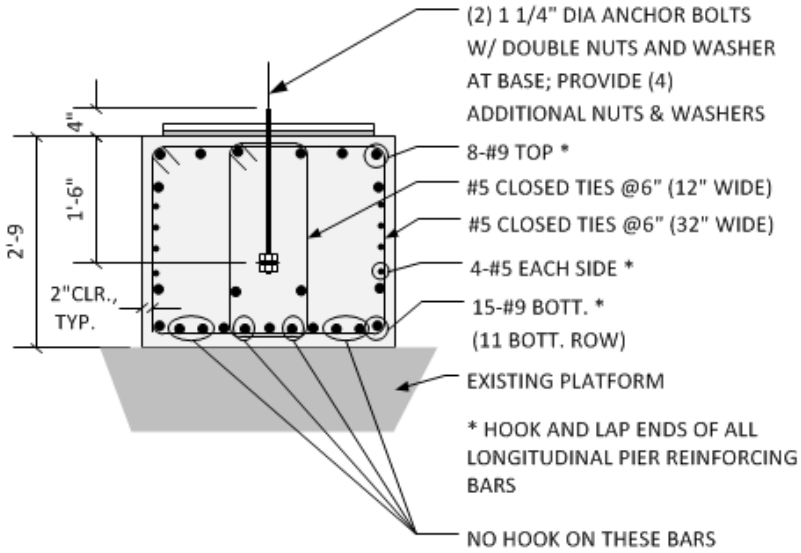

D SECTION AT PIER

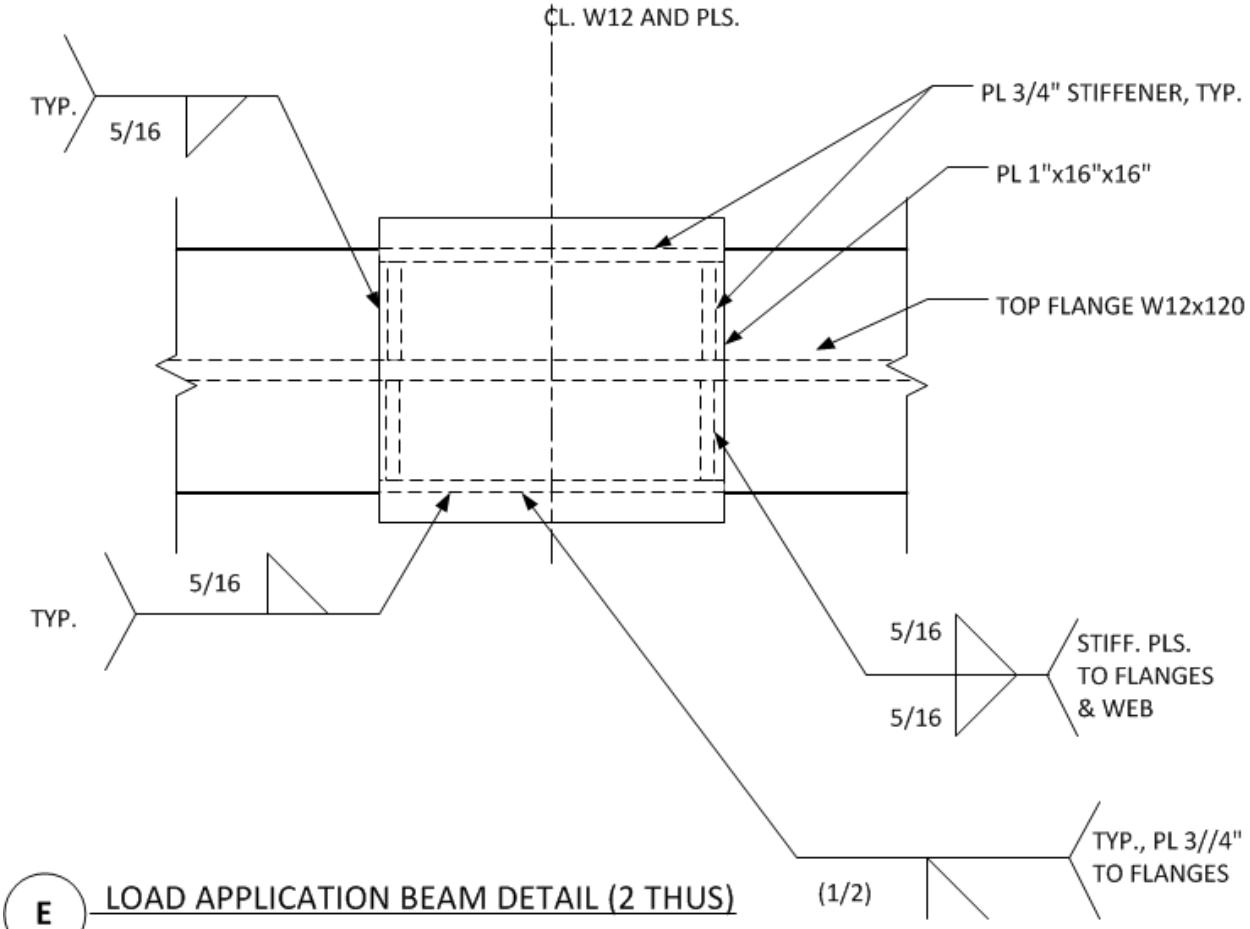

E LOAD APPLICATION BEAM DETAIL (2 THUS)

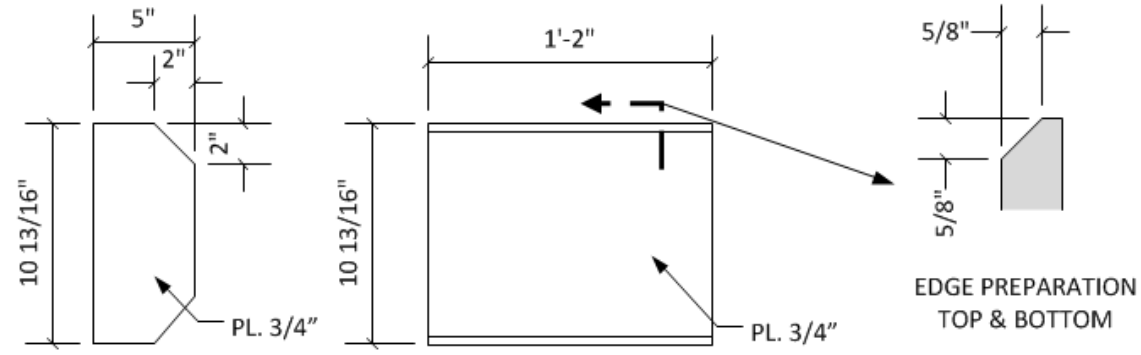

STIFFENER PLATES TO WEB
(4 PER BEAM, 8 TOTAL)

STIFFENER PLATES TO FLANGES
(2 PER BEAM, 4 TOTAL)

F PLATE DETAILS

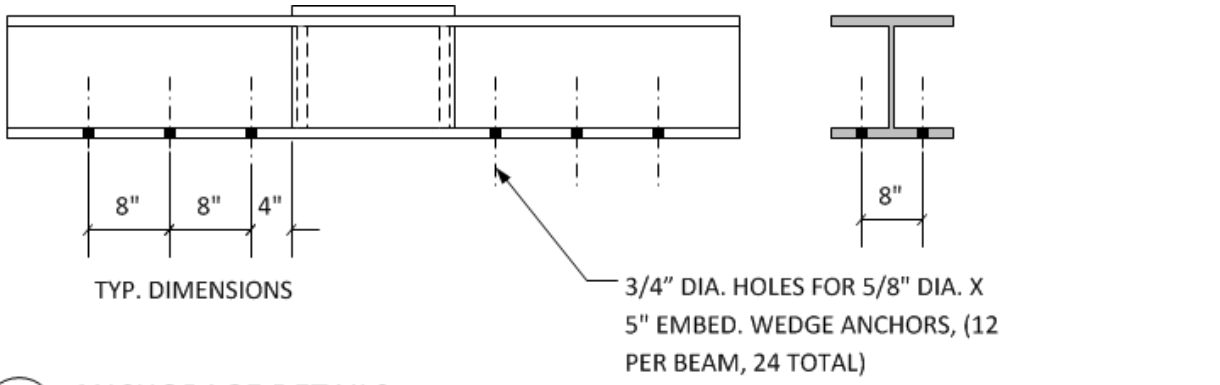

G ANCHORAGE DETAILS

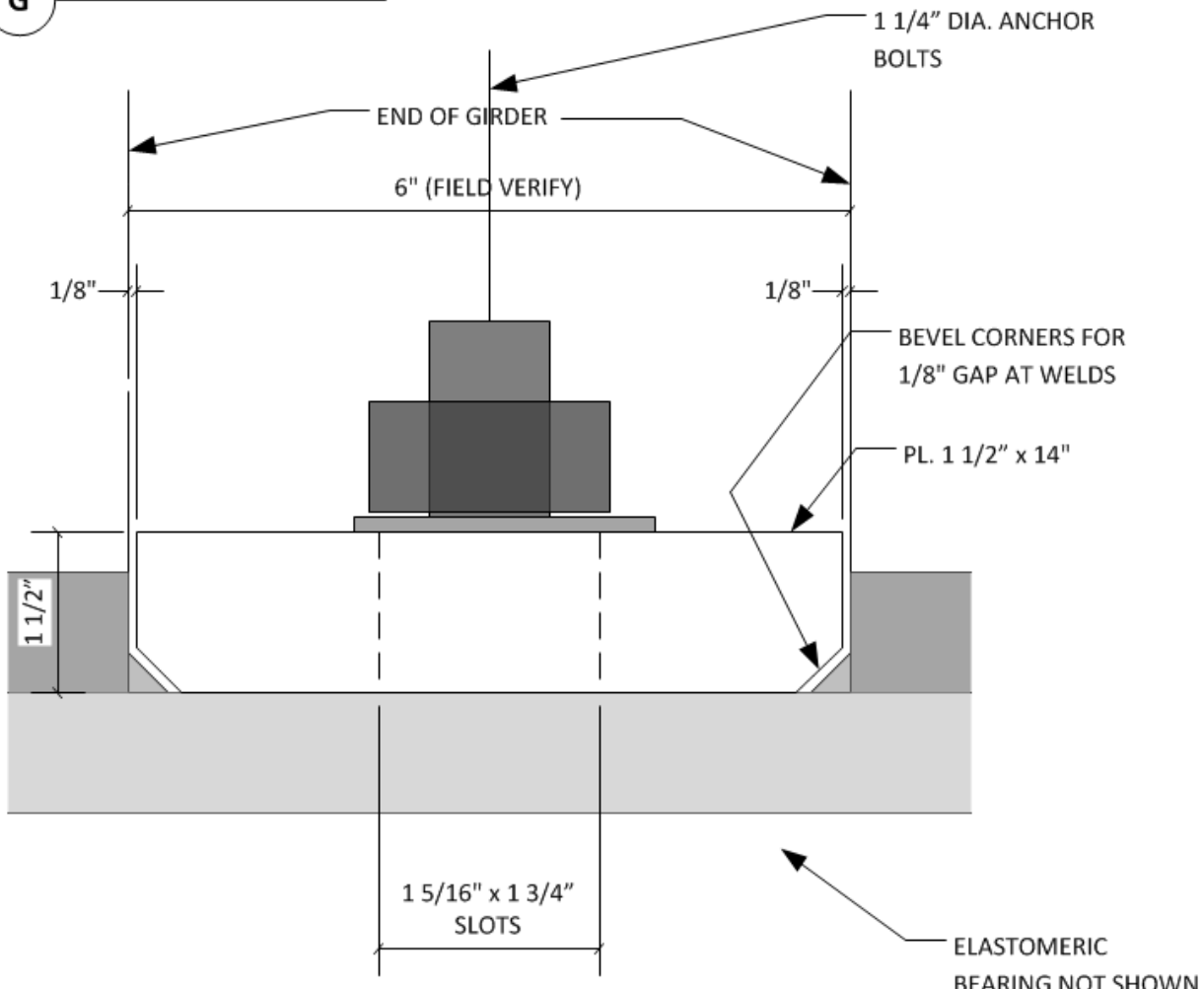

H SPACER PLATE DETAILS

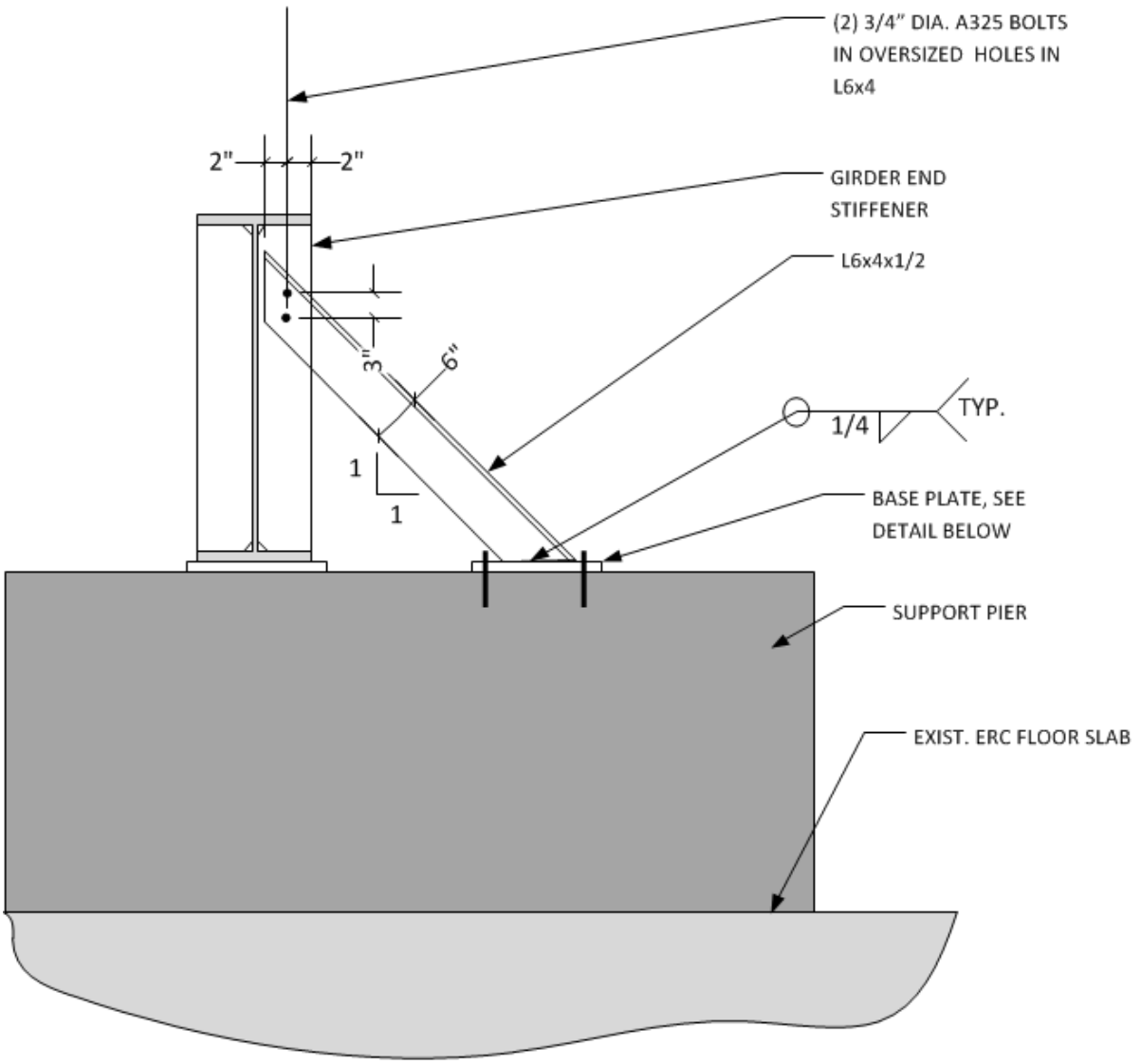

J **GIRDER BRACING SECTION**

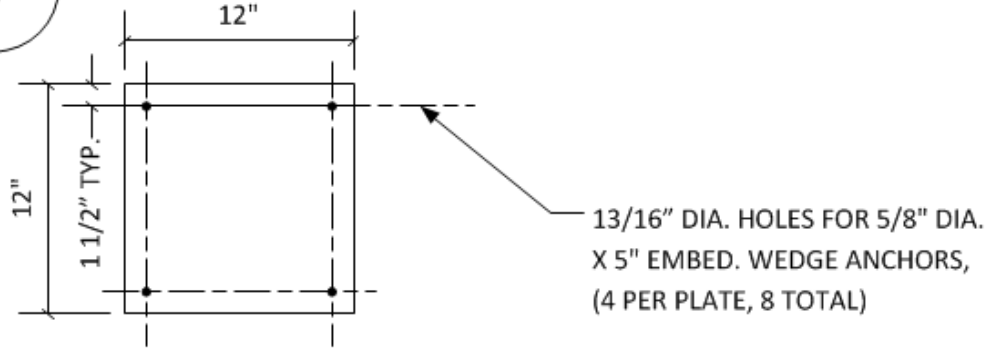

BASE PLATE DETAIL

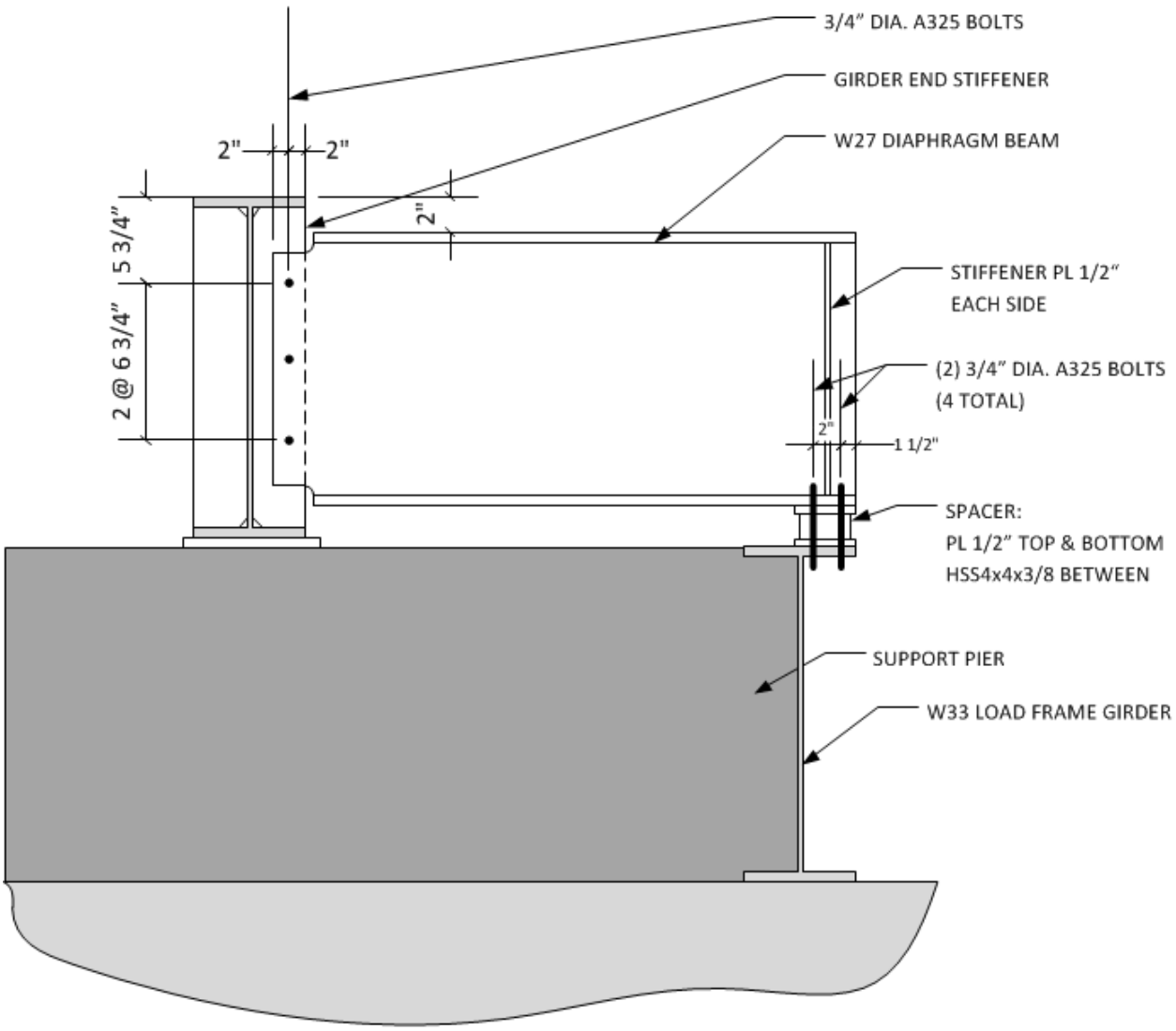

K **GIRDER DIAPHRAGM SECTION**

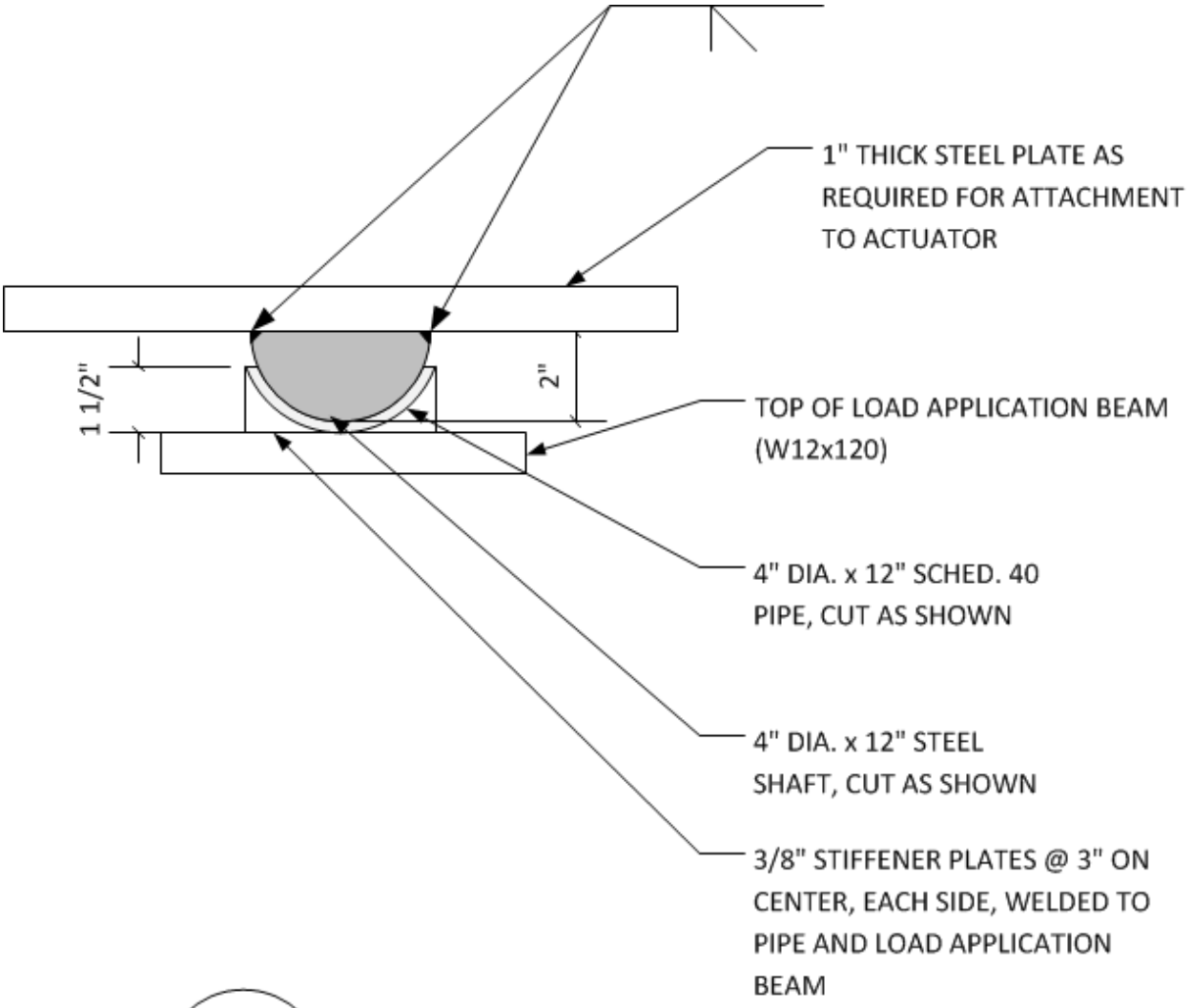

L **NORTH ACTUATOR 'HINGE' DETAIL**

APPENDIX D. PLATE GIRDER DIMENSIONS

Table D.1 Plate Girder Dimensions

Name	d_w	t_f	b_f	t_w	d	A	I_x	Wt./ft.
PG1	46.5	0.75	24	0.625	48	65.1	25331	221
PG2	46.5	0.75	26	0.625	48	68.1	27006	232
PG3	46.25	0.875	28	0.625	48	77.9	32360	265
PG4	46.25	0.875	30	0.625	48	81.4	34304	277
PG5	46.25	0.875	32	0.625	48	84.9	36247	289
PG6	46	1	34	0.625	48	96.8	42628	329
PG7	46	1	36	0.625	48	100.8	44838	343
PG8	50.5	0.75	26	0.625	52	70.6	32319	240
PG9	50.25	0.875	28	0.625	52	80.4	38630	274
PG10	50.25	0.875	30	0.625	52	83.9	40918	286
PG11	50.25	0.875	32	0.625	52	87.4	43205	297
PG12	50	1	34	0.625	52	99.3	50733	338
PG13	50	1	36	0.625	52	103.3	53334	351
PG14	49.75	1.125	38	0.625	52	116.6	61746	397
PG15	52.5	0.75	27	0.625	54	73.3	36249	249
PG16	52.25	0.875	28	0.625	54	81.7	42005	278
PG17	52.25	0.875	30	0.625	54	85.2	44475	290
PG18	52.25	0.875	32	0.625	54	88.7	46945	302
PG19	52	1	34	0.625	54	100.5	55082	342
PG20	52	1	36	0.625	54	104.5	57891	356
PG21	51.75	1.125	38	0.625	54	117.8	66987	401
PG22	51.75	1.125	40	0.625	54	122.3	70132	416
PG23	58.25	0.875	30	0.75	60	96.2	58238	327
PG24	58.25	0.875	31	0.75	60	97.9	59768	333
PG25	58.25	0.875	32	0.75	60	99.7	61297	339
PG26	58	1	33	0.75	60	109.5	69637	373
PG27	58	1	34	0.75	60	111.5	71377	379
PG28	58	1	35	0.75	60	113.5	73118	386
PG29	58	1	36	0.75	60	115.5	74859	393

APPENDIX E. ACCEPTABLE BRIDGE GIRDERS

Table E.1 Girder Acceptance Table - 92 ft. Span

	Slab Thickness		
Girder Spacing	**8 inches**	**8.5 inches**	**9 inches**
7.33 ft.	W40x167	W40x167	W40x167
7.67 ft.	W40x167	W40x167	W40x167
8.00 ft.	W40x183	W40x183	W40x183
8.33 ft.	W40x183	W40x183	W40x183
8.67 ft.	W40x183	W40x183	W40x183
9.00 ft.	W40x183	W40x183	W40x183
9.33 ft.	W40x199	W40x199	W40x183
9.67 ft.	W40x199	W40x199	W40x183
10.00 ft.	W40x199	W40x199	W40x183
10.33 ft.	W40x199	W40x199	W40x183

Table E.2 Girder Acceptance Table - 104 ft. Span

	Slab Thickness		
Girder Spacing	**8 inches**	**8.5 inches**	**9 inches**
7.33 ft.	W44x230	W44x230	W44x290
7.67 ft.	W44x230	W44x230	W44x290
8.00 ft.	W44x230	W44x230	W44x290
8.33 ft.	W44x230	W44x230	W44x290
8.67 ft.	W44x230	W44x230	W44x290
9.00 ft.	W44x230	W44x230	W44x290
9.33 ft.	W44x230	W44x230	W44x335
9.67 ft.	W44x230	W44x262	W44x335
10.00 ft.	W44x230	W44x262	W44x335
10.33 ft.	W44x230	W44x262	W44x335

Table E.3 Girder Acceptance Table - 116 ft. Span

	Slab Thickness		
Girder Spacing	**8 inches**	**8.5 inches**	**9 inches**
7.33 ft.	PG1	PG1	PG1
7.67 ft.	PG1	PG1	PG1
8.00 ft.	PG1	PG1	PG1
8.33 ft.	PG1	PG1	PG1
8.67 ft.	PG1	PG1	PG1
9.00 ft.	PG1	PG1	PG1
9.33 ft.	PG2	PG2	PG2
9.67 ft.	PG2	PG2	PG2
10.00 ft.	PG2	PG2	PG3
10.33 ft.	PG2	PG3	PG3

Table E.4 Girder Acceptance Table - 128 ft. Span

	Slab Thickness		
Girder Spacing	**8 inches**	**8.5 inches**	**9 inches**
7.33 ft.	PG8	PG8	PG8
7.67 ft.	PG8	PG8	PG8
8.00 ft.	PG8	PG8	PG8
8.33 ft.	PG8	PG8	PG9
8.67 ft.	PG9	PG9	PG9
9.00 ft.	PG9	PG9	PG9
9.33 ft.	PG9	PG9	PG9
9.67 ft.	PG9	PG9	PG9
10.00 ft.	PG9	PG9	PG9
10.33 ft.	PG9	PG9	PG9

Table E.5 Girder Acceptance Table - 140 ft. Span

	Slab Thickness		
Girder Spacing	**8 inches**	**8.5 inches**	**9 inches**
7.33 ft.	PG16	PG16	PG16
7.67 ft.	PG16	PG16	PG16
8.00 ft.	PG17	PG17	PG17
8.33 ft.	PG17	PG17	PG17
8.67 ft.	PG18	PG18	PG18
9.00 ft.	PG18	PG18	PG18
9.33 ft.	PG19	PG19	PG18
9.67 ft.	PG19	PG19	PG18
10.00 ft.	PG19	PG19	PG18
10.33 ft.	PG19	PG19	PG18

APPENDIX F. MAXIMUM SMC NEGATIVE MOMENTS

Table F.1 Maximum SMC Negative Moments (kip-feet) - 92 ft. Span

	Slab Thickness		
Girder Spacing	**8 inches**	**8.5 inches**	**9 inches**
7.33 ft.	-2509	-2489	-2470
7.67 ft.	-2569	-2548	-2528
8.00 ft.	-2641	-2619	-2598
8.33 ft.	-2700	-2677	-2656
8.67 ft.	-2759	-2735	-2713
9.00 ft.	-2818	-2792	-2770
9.33 ft.	-2890	-2864	-2827
9.67 ft.	-2948	-2922	-2884
10.00 ft.	-3006	-2979	-2940
10.33 ft.	-3064	-3036	-2996

Table F.2 Maximum SMC Negative Moments (kip-feet) - 104 ft. Span

	Slab Thickness		
Girder Spacing	**8 inches**	**8.5 inches**	**9 inches**
7.33 ft.	-3013	-2989	-3003
7.67 ft.	-3083	-3058	-3072
8.00 ft.	-3153	-3127	-3143
8.33 ft.	-3222	-3195	-3212
8.67 ft.	-3291	-3263	-3280
9.00 ft.	-3359	-3331	-3348
9.33 ft.	-3427	-3398	-3444
9.67 ft.	-3495	-3491	-3512
10.00 ft.	-3562	-3558	-3579
10.33 ft.	-3629	-3625	-3647

Table F.3 Maximum SMC Negative Moments (kip-feet) – 116 ft. Span

	Slab Thickness		
Girder Spacing	**8 inches**	**8.5 inches**	**9 inches**
7.33 ft.	-3473	-3447	-3423
7.67 ft.	-3552	-3524	-3499
8.00 ft.	-3630	-3601	-3575
8.33 ft.	-3707	-3678	-3651
8.67 ft.	-3784	-3754	-3727
9.00 ft.	-3860	-3830	-3801
9.33 ft.	-3946	-3914	-3884
9.67 ft.	-4022	-3989	-3959
10.00 ft.	-4098	-4064	-4060
10.33 ft.	-4173	-4167	-4134

Table F.4 Maximum SMC Negative Moments (kip-feet) - 128 ft. Span

	Slab Thickness		
Girder Spacing	**8 inches**	**8.5 inches**	**9 inches**
7.33 ft.	-3957	-3929	-3902
7.67 ft.	-4044	-4015	-3987
8.00 ft.	-4130	-4100	-4072
8.33 ft.	-4216	-4185	-4180
8.67 ft.	-4327	-4295	-4265
9.00 ft.	-4413	-4380	-4348
9.33 ft.	-4499	-4464	-4432
9.67 ft.	-4584	-4548	-4515
10.00 ft.	-4668	-4631	-4597
10.33 ft.	-4752	-4715	-4680

Table F.5 Maximum SMC Negative Moments (kip-feet) - 140 ft. Span

	Slab Thickness		
Girder Spacing	**8 inches**	**8.5 inches**	**9 inches**
7.33 ft.	-4459	-4428	-4401
7.67 ft.	-4554	-4523	-4494
8.00 ft.	-4657	-4625	-4595
8.33 ft.	-4751	-4718	-4687
8.67 ft.	-4854	-4820	-4788
9.00 ft.	-4948	-4912	-4880
9.33 ft.	-5069	-5032	-4970
9.67 ft.	-5163	-5125	-5062
10.00 ft.	-5256	-5217	-5152
10.33 ft.	-5349	-5309	-5243

APPENDIX G. DEFLECTION EQUATION DEVELOPMENT

1

DEVELOP A SIMPLE METHOD TO DETERMINE I_x REQ'D FOR +M DEFLECTION AS A FUNCTION OF MOMENT (M) IN kip-ft LENGTH (L) IN ft. AND SPAN TO DEFLECTION RATIO OF LENGTH (L) IN INCHES AND RATIO LIMIT $1/N_D$ IN INCH/INCH.

EXAMPLE FOR A UNIFORMLY LOADED SIMPLE BEAM

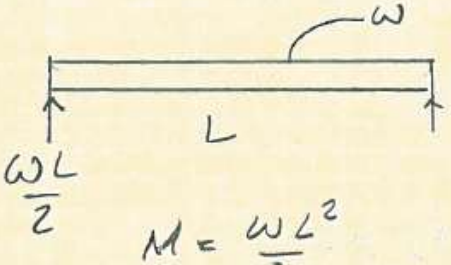

$$M_{MAX} = \frac{WL^2}{8} \text{ (k-ft.)}$$

$$\Delta_{MAX} = \frac{5WL^4}{384EI_x} \text{ (in.)}$$

$$M = \frac{WL^2}{8}$$

$$\Delta_{MAX} = C_1 M = C_1 \times \frac{12WL^2}{8} = \frac{5WL^4}{384EI_x}$$

$$C_1 = \frac{8}{WL^2} \times \frac{5WL^4}{384EI} = \frac{5}{48}\frac{ML^2}{EI_x}$$

$$\Delta_{MAX} = \frac{L}{N_D} \qquad N_D = \text{LIMIT NUMBER } 180, 240, 360, 600, 800 \text{ ETC.}$$

$$\frac{L}{N_D} = \frac{5}{48}\frac{ML^2}{EI_x}$$

WE WANT I_x ∴ $$I_{x\,MIN} = \frac{5}{48}\frac{ML}{E}N_D$$

IN ORDER TO USE L IN ft. AND M IN k-ft., MULTIPLY BY 12^2 AND DIVIDE BY $E = 29{,}000$ ksi (STEEL)

$\therefore I_{x\,MIN} = \dfrac{M L N_D}{1933}$

M IN k-ft
L IN ft
$I_{x\,MIN}$ IN in^4

FOR SIMPLE-SPAN UNIFORMLY LOADED BEAM, $I_{x\,MIN.}$ MAY BE ACCURATELY CALCULATED BASED ON

$$I_{x\,MIN} = \frac{M L N_D}{1933}$$

WHERE M IS MAXIMUM MOMENT (k-ft.)

L IS SPAN (ft.)

$I_{x\,MIN}$ IS MAJOR AXIS MOMENT OF INERTIA (in^4)

N_D = DEFLECTION LIMITATION AS A FUNCTION OF SPAN, i.e., $\Delta_{MAX} = L/N_D$

- THIS PROCEDURE MAY BE REPEATED FOR THE FOLLOWING LOAD CONDITIONS FOR COMPARISON

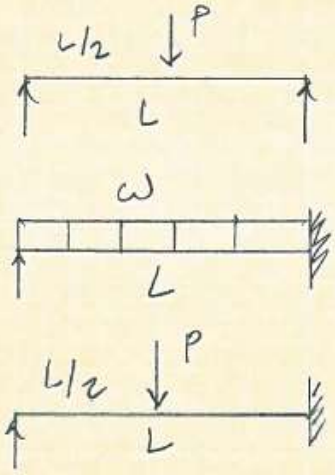

IT'S APPARENT THAT DUE TO INDETERMINACY, THE REQUIRED I_x FOR THESE CONDITIONS WOULD BE LESS THAN THOSE FOR THE CORRESPONDING SIMPLE BEAM CONDITIONS.

Point Loaded Simple Beam

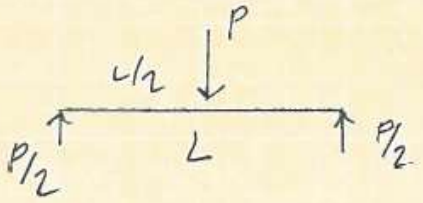

$$M_{MAX} = \frac{PL}{4}$$

$$\Delta = \frac{PL^3}{48EI_x} = \frac{ML^2}{12EI_x} = \frac{L}{N_D}$$

$$\frac{ML}{12EI_x} = \frac{1}{N_D} \quad \therefore \quad I_{x\,MIN.} = \frac{MLN_D}{12} \times \frac{144}{29{,}000}$$

$$\boxed{I_{x\,MIN.} = \frac{MLN_D}{2417}} \quad < \frac{MLN_D}{1933}$$

Fixed-Hinged Beam Look At +M

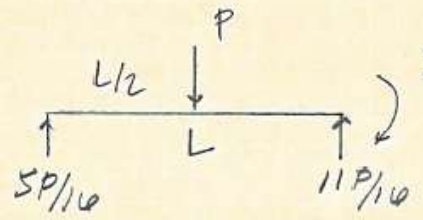

$$\frac{3PL}{16} = -M \qquad +M = \frac{5PL}{32}$$

$$\Delta_P = \frac{7PL^3}{768EI}$$

$$\Delta = \frac{32}{5}\,\frac{7}{768}\,\frac{ML^2}{EI_x} = \frac{L}{N_D} \qquad I_x = \frac{224}{3840} \times \frac{MLN_D}{E}$$

$$\text{At } M_{MAX} = 0.009317\,\frac{PL^3}{EI} \qquad = \frac{MLN_D}{3452} = I_{x\,MIN.}$$

$$\boxed{I_{x\,MIN} = \frac{MLN_D}{3452} \quad M = M_{MAX}}$$

FIXED-HINGED BEAM

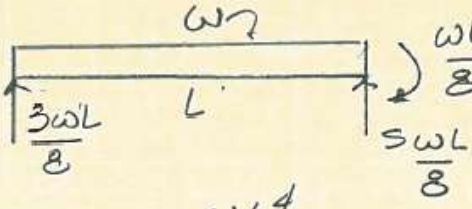

$\frac{WL^2}{8}$ $\quad +M = \frac{9WL^2}{128}$

$$\Delta_{MAX} = \frac{WL^4}{185EI} = \frac{128}{9WL^2} \times \frac{WL^4}{185EI} M$$

$$= \frac{128}{1665} \frac{M}{EI} = \frac{L}{N_D}$$

$$I_{x\,MIN} = \frac{MLN_D}{2620}$$